UNIVERSITÀ DEGLI STUDI DI MILANO

PhD Course in Experimental Medicine

CYCLE XXXIII

Department of Medical Biotechnology and Translational Medicine

PhD thesis

SEARCHING FOR NOVEL MOLECULAR TARGETS IN ASTROCYTES FOR THE TREATMENT OF RETT SYNDROME

Candidate: **Elena ALBIZZATI** (R11955)

Tutor: **Prof. Nicoletta LANDSBERGER**

Supervisor: **Dr. Angelisa FRASCA**

Director: **Prof. Massimo LOCATI**

Academic Year 2019-2020

Abstract

Rett syndrome (RTT) is a rare devastating neurodevelopmental disorder that with an incidence of ~ 1:10,000 represents the most common genetic cause of severe intellectual disability in girls. Mutations in the X-linked methyl-CpG-binding protein 2 (*MECP2*) gene have been reported in over 95% cases of classical forms of RTT. Although initial studies supported a role for MeCP2 exclusively in neurons, recent data indicate a function also in astrocytes, which emerged as critical players involved in RTT pathogenesis through non-cell autonomous effects. Nevertheless, many aspects of RTT astrocyte dysfunctions remain unknown. With this PhD project, we wanted to use different *in vivo* and *in vitro* approaches that could help fill this gap of knowledge, in particular as regards to the effects that RTT astrocytes exert on neuronal health, and the involved molecular mechanisms.

We herein demonstrate that astrocytes in the *Mecp2* null mouse brain show progressive and area-specific alterations in morphology, with cortical areas exhibiting the most affected phenotype compared to the hippocampal cells; no phenotype, instead, is observed in cerebellar astrocytes, at least at early time points. These data, that have been reinforced by *in vitro* studies, represent the first evidence in the RTT field of the importance of considering astrocyte regionality. Considering the link between astrocyte morphogenesis and synaptogenesis, we have further investigated the effects of KO astrocytes on synaptic phenotypes. Our studies highlight a clear defect in synaptic maturation particularly in the *Mecp2* null motor cortex. However, our *in vivo* exploration of synaptic terminals have not permit to find a stringent correlation between astrocyte morphology and synaptic defects probably due to the use of a globally null mouse model. Conversely, by using *in vitro* co-cultures, we have demonstrated for the first time that the lack of *Mecp2* in astrocytes dramatically influences the synaptogenesis of WT neurons, by affecting both pre- and post-synaptic terminals by the release of one or more thermo-labile neurotoxic factors. To identify the involved molecular mechanisms, we have used RNAseq profiling which molecular pathways are activated in wild-type neurons by the paracrine effects triggered by KO astrocytes. Bioinformatic analyses have confirmed that KO astrocytes influence neuronal pathways mainly associated with the pre- and post-synaptic compartments, the mitochondrial functionality and inflammatory responses, therefore suggesting the possibility of an aberrant release of pro-inflammatory molecules. Collectively, the data

presented in this thesis advance our understanding on the pathophysiology of RTT and point astrocytes and their paracrine factors as active players for the synaptic defects observed in RTT. We believe that the identification of the involved factors might reveal novel therapeutic approaches for the treatment of RTT.

Table of Contents

Introduction

1.1 Rett Syndrome

1.1.1 Clinical features

Neurodevelopmental disorders (NDDs) include a wide spectrum of diseases characterized by multifactorial alterations of normal brain development leading to impairments in cognition, communication, behaviour and/or motor skills (*Mullin et al., 2013*).

Frequently, NDDs patients with different monogenic defects manifest phenotypes characterized by a variety of common features. Therefore, an unequivocal distinction using diagnostic criteria can be very challenging. The complexity of this scenario further increases when considering the genes that confer risk for or cause NDDs. Indeed, the list of genetic defects associated with NDDs ranges from large chromosomal deletions to single-nucleotide polymorphism (SNPs). In this context, a correct diagnosis of a specific disorder is extremely relevant to approach a correct therapeutic plan, when possible, rather than promising clinical trials. The evolution of the criteria for diagnosing Rett syndrome is a precise example of the progress in clinical studies of an NDD over 50 years.

Rett syndrome (RTT, MIM 312750) is a rare, devastating and progressive neurodevelopmental disorder which mostly affects females in approximately 1 in 10,000 live births, therefore resulting the second most common cause of intellectual disability in females after Down syndrome (*Gold et al., 2018; Ip et al., 2018*). RTT was originally considered lethal in males (perinatal death) due to its X-linked inheritance, even if we now know that rare cases are documented (*Pitzianti et al., 2019*). Indeed, this pathology is part of the so-called X-linked intellectual disabilities (XLID), which involve alterations of genes encoding for proteins involved in higher brain functions (cognition, learning, memory, etc) such as Fragile X Mental Retardation Protein, Methyl-CpG-Binding Protein 2, Cyclin-Dependent-Kinase-Like 5, Rho GTPases, Cell Adhesion Proteins (*Bassani et al., 2013*).

Despite all the difficulties to univocally identify an NDD, RTT has some peculiarities that make it unique and facilitated the definition of diagnostic criteria through the years. The first time that a physician noticed distinctive symptoms in some of his patients was in 1966 in Vienna. It was the Austrian neuropediatrician Andreas Rett that first reported a series of 22 young female patients with anomalous similarities in almost identical

stereotypic hand movements (*Rett, 1966*). They also featured an early onset of the regression of fine motor and communication skills, cognitive impairments, periodic breathing during wakefulness and gait abnormalities. Dr Rett received no feedback from his colleagues of central Europe until a Swedish child neurologist, Bengt Hagberg, recognized the same symptoms in some of his female patients years later and he finally decided to call this disorder "Rett syndrome" (*Percy, 2016*). In 1983, he published a paper (*Hagberg et al., 1983*) in collaboration with other physicians in which they collected and described the symptoms of about 35 patients from Sweden, France and Portugal. This publication together with the first RTT meeting held in Vienna in 1984 alerted the scientific word, especially in the United States, of the existence of a unique neurodevelopmental disorder. Moreover, this resulted as the first occasion to develop diagnostic criteria; later, these have been re-edited different times up to the last validation proposed in 2010 (*Neul et al., 2010*). Thanks to this progress, we now dispose of simplified consensus criteria to distinct classic and variant forms of RTT (**Table 1.1**). This internal distinction origins from the different course of the symptomatology that in some cases deviates from the 'classic' one, mostly in terms of severity and age of onset (*Chahrour et Zoghbi, 2007*).

Requirement for classic or typical RTT	A period of regression followed by stabilization and recovery: 1. All main and all exclusion criteria 2. Supportive criteria not required although may be present
Requirement for variant or atypical RTT	1. A period of regression followed by stabilization and recovery 2. At least 2 of 4 main criteria and 5 of 11 supportive criteria
Main criteria	1. Partial or complete loss of acquired purposeful hand skills 2. Partial or complete loss of spoken language 3. Dyspraxic gait or inability to ambulate 4. Stereotypic hand movements: hand mouthing, hand wringing/clasping, hand clapping, or finger rubbing
Exclusion criteria	1. Brain injury: peri- or postnatal trauma, neurometabolic disease, or severe infection involving neurological function 2. Grossly abnormal psychomotor development in first 6 months after birth
Supportive criteria for variant RTT	1. Periodic breathing during wakefulness 2. Bruxism while awake 3. Altered sleep pattern 4. Abnormal muscle tone 5. Peripheral vasomotor disturbance 6. Scoliosis/kyphosis 7. Growth failure 8. Small cool/cold hands and/or feet 9. Inappropriate laughing or screaming spells 10. Delayed or diminished response to pain 11. Intense eye communication or "eye pointing"

Table 1.1. Consensus criteria for classic and variant RTT (*Percy, 2016*).

These criteria for the categorization of symptomatology are in the context of an NDD, which means that the distinct features of RTT sequentially progress over time. Indeed, as early as 1985, Hanefeld proposed different “stages” (Stage I to Stage IV) to recapitulate these changes in degrees of severity (*Hanefeld, 1985*; *Chahrour et Zoghbi, 2007*):

- *Stage I*

  Girls with classical RTT appear to develop normally until they reach 6-18 months of age when early signs of the disorder emerge. This stage is characterized by a delay or stagnation of expected developmental milestones and it includes microcephaly, growth arrest, hypotonia.

- *Stage II*

  Patients between 1 and 4 years of age manifest a rapid-developmental regression characterized by the loss of acquired communication skills (language and socialization) and some fine and gross motor skills (Parkinsonian features could be prevalent). Seizures (developed by 60-80% girls) and respiratory abnormalities can also emerge at this stage. In this time period, or sometimes before, the typical hallmark of stereotypical hand movement appears. Due to the similarity with some features of the autism spectrum disorders (ASD), RTT was considered part of them for a long time, until few years ago when the syndrome was removed from that list in the *Diagnostic and Statistical Manual of Mental Disorders* (DSM-V). Patients with autistic-like behaviours can be described as having ASD associated with RTT.

- *Stage III*

  Patients between 5 to 10 years of age enter the so-called pseudostationary stage where they face a stabilization of the phenotypes and girls often increase social awareness with intense eye gaze. They could also reacquire some skills lost in stage II and ameliorate their autistic-like behaviour. Anyway, patients can start suffering from osteopenia, scoliosis, autonomic dysfunction (problems involving the whole gastrointestinal tract), anxiety that carry on for the rest of their life.

- *Stage IV*

  The latest stage is also known as ‘late motor deterioration stage’. Indeed, girls are affected by reduced mobility, muscle weakness, rigidity, spasticity, development of dystonia and hand/foot deformities. Most girls are often wheelchair-bound during teenage years. Cognition, communication, hand skills generally not decline. The

condition can reach a plateau and some patients even survive up to the 6th or 7th decade of life.

As emerged, RTT is a multisystem disease with different comorbidities. Despite a primary involvement of the central nervous system (CNS) with problems in brain growth, stereotypies, epilepsy, periodic breathing, sleep, etc RTT may also affects other systems including growth and nutrition, skeletal and pubertal development, gastrointestinal tract, cardiac system (prolonged QTc) (*Percy, 2016*).

The range of the severity of each symptom is very broad. This was also observed by Hagberg (*Erlandson and Hanefeld, 2005*) that stressed the concept of high variability in the manifestation of the phenotypes, from severe male new-born encephalopathy to female carrier mothers.

We are now aware that the major causes of this variation relate to the type of genetic mutation at the base of RTT in the classical or atypical forms and the pattern of X chromosome inactivation (XCI) (*Chahrour et Zoghbi, 2007*), that will be discussed in the following chapter.

1.1.2 Genetic bases and phenotypic variability of RTT patients

Over 95% of classical RTT cases and over 75% of atypical or variant RTT cases are caused by *de novo* mutations in the X-linked methyl-CpG-binding protein 2 gene (*MECP2;* Xq28; MIM# 300005), resulting the major genetic cause for RTT (*Krishnaraj et al., 2017*). Since 1999, when RTT was associated with *MECP2* mutations for the first time, over 900 unique mutations have been identified within *MECP2*: 518 pathogenic or likely pathogenic, 206 benign or likely pathogenic and 211 Variants Of Unknown Significance (VOUS) (*Amir et al., 1999; Gold et al., 2018*). RettBASE (*http://mecp2.chw.edu.au/mecp2/mecp2_upgrade_proband_list_copy.php*) reports about 3900 females carrying *MECP2* variants and only about 60 cases of male variants (as mentioned, this is mainly due to the severity of the male condition that leads to neonatal encephalopathy) (*Schönewolf-Greulich et al, 2019*).

The prevailing majority of RTT patients presents loss-of-function mutations in *MECP2* with a recurrence (almost 47% of all mutations) of 8 specific missense and nonsense mutations along the different domains of the gene. These hotspots are responsible for

over 60% of all RTT cases (*Gold et al., 2018; Christodoulou and Weaving, 2003; Leonard et al., 2017*) (**Figure 1.1, Table 1.2**).

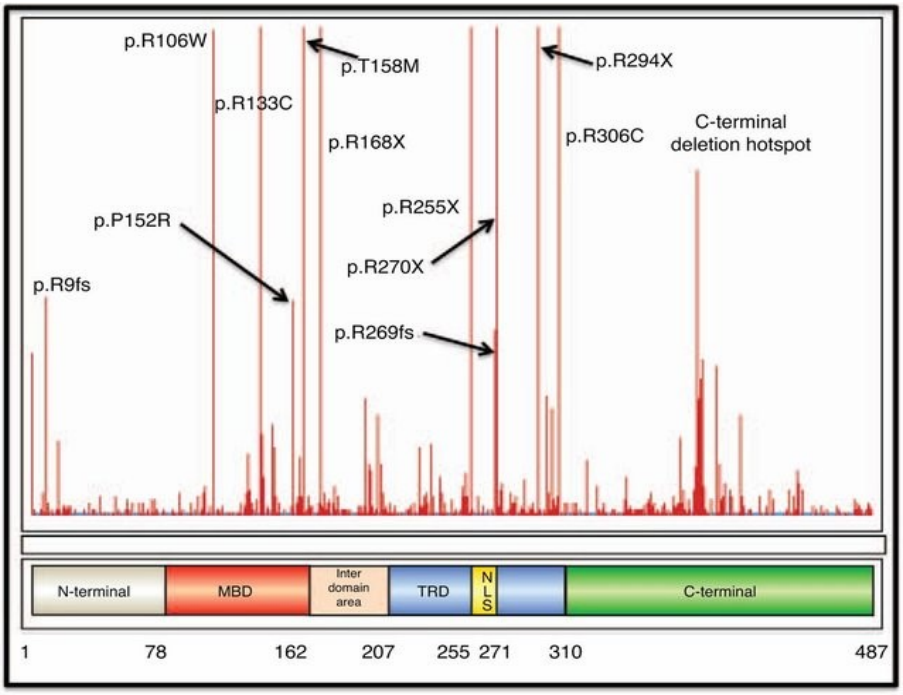

Figure 1.1. Schematic diagram of MeCP2 structure and the distribution of common mutations causing Rett syndrome (*Downs et al., 2014*).

Nucleotide change	Amino acid change	Frequency	Mutation-positive cases (%)
c.473C>T	p.Thr158Met	420	8.74
c.502C>T	p.Arg168*	364	7.57
c.763C>T	p.Arg255*	319	6.64
c.808C>T	p.Arg270*	276	5.74
c.916C>T	p.Arg306Cys	247	5.14
c.880C>T	p.Arg294*	239	4.97
c.397C>T	p.Arg133Cys	217	4.52
c.316C>T	p.Arg106Trp	134	2.79

Table 1.2. Most common *MECP2* mutations (hotspots) seen in patients with RTT (data are derived from RettBASE, updated to April 2021).

Almost any alteration in the translated *MECP2* exons is considered pathogenic, with truncating and missense mutations that constitute the vast majority of mutations (*Gold et al., 2018*). Intronic mutations are less common and a very small part of them was proven to be pathogenic. Variants in the 3' and 5' UTRs consist of an important percentage, but none of them has functional proof of pathogenicity.

The degree of severity of the phenotype depends on different factors. Certainly, the specific molecular variation causing the disease plays a crucial role, as each *MECP2* mutation could differentially impact on the protein function (*Akbarian et al., 2006; Liyanage and Rastegar, 2014*). Interestingly, while truncating mutations often do not lead to the most severe phenotypes, some patients with specific missense mutations can be seriously affected and can display the most severe symptoms, as is the case for the T158M mutation (*Liyanage and Rastegar, 2014; Brown et al., 2016*). Phenotypic variability and differences in clinical manifestations can be also attributed to the pattern of X chromosome inactivation (XCI). Indeed, females with *MECP2* mutations generally go through random XCI, with half of the cells expressing the wild-type allele and the other half the mutant one (so called 'mosaicism'). In some cases, XCI can be substantially skewed toward one of the two X chromosomes, therefore significantly decreasing or increasing the totality of cells expressing the mutant allele (*Vashi and Justice, 2019*). Eventually, modifier genes can also affect symptom severity (*Vashi and Justice, 2019*). Modifier genes are usually defined as genes whose function has phenotypic outcomes on the effect of another gene. Thus, people carrying mutations in modifier genes that suppress RTT phenotype have more alleviate symptoms and more favourable clinical presentation, while individuals carrying mutations in genes that enhance RTT phenotype have more severe symptoms and a more critical case history.

As described so far, the majority of RTT patients display mutations in the *MECP2* gene; however, *MECP2* negative patients count for approximately 5% of classical RTT cases and 25% of atypical RTT cases. These patients might carry mutations in other genes that, therefore, have been associated with RTT. Among these, the most common include (*Gold et al., 2018*):

- the *X-linked cyclin-dependent-kinase-like 5* gene (*CDKL5*; Xp22; MIM# 300203) that was originally considered as a frequent cause of the early-onset seizure variant of RTT. In addition to early and generally intractable epilepsy, common symptoms associated with *CDKL5* mutations are severe intellectual disability, peculiar facial

gestalt and huge motor impairments. However, it was recently published a complete phenotypic assessment of *CDKL5* patients to determine whether they can be considered part of atypical RTT cases. Indeed, an important percentage of individuals carrying *CDKL5* mutation do not meet the accepted diagnostic criteria for RTT. Therefore, since very recently, these patients constitute a separated entity and they belong to another specific disorder: the CDKL5 deficiency disorder (CDD) (*Jakimiec et al., 2020*).

- the *Forkhead box protein G1* gene (*FOXG1*; 14q12; MIM# 164874), a DNA-binding transcription factor containing the fork-head-binding domain, generally associated with the congenital variant of RTT. *FOXG1* encodes for a protein that is essential for early brain development and similarly to *CDKL5*, patients carrying mutations within this gene sometimes display peculiar features (such as agenesis, hypoplasia of the corpus callosum etc) that are not reported in RTT. They are rather ascribed to FOXG1 syndrome (*Pratt et al., 2013*).
- the *Myocyte-specific enhancer factor 2C* (*MEF2C*; 5q14.3; MIM# 600662) was recently proposed in the list of genetic causes of RTT. Many symptoms in patients with *MEFC2* mutations overlap with RTT and it was estimated that almost 2% of people with RTT-like phenotypes carry mutations within this gene. Interestingly, *MEFC2* syndrome is characterized by the prevalence of stereotypic hand movements and patients also show reduced levels of MeCP2 and CDKL5 proteins.

Furthermore, the advent of modern tools to analyse the whole exome (the next-generation sequencing above all) allowed researchers to identify novel genetic causes in Rett patients or patients with Rett-like phenotypes, independent from *MECP2, CDKL5* and *FOXG1* genetic alterations (*Lopes et al., 2016; Wang et al., 2019*). Of note, these *de novo* variants that had already been found in genes implicated in NDDs, include:

TCF4 (*transcription factor 4)*; ZNF238 (*zinc finger protein 238);* EEF1A2 (*Eukaryotic Translation Elongation Factor 1 Alpha 2*); SLC35A2 (*Solute Carrier Family 3 Member 2*); EIF2B2 (*Eukaryotic Translation Initiation Factor 2B Subunit Beta);* SHROOM4 (*Shroom Family Member 4*); STXBP1 (*Syntaxin Binding Protein 1*); SCN8A (*Sodium Voltage-Gated Channel Alpha Subunit 8*); IQSEC2 (*IQ Motif And Sec7 Domain ArfGEF 2);* GABRD (*Gamma-Aminobutyric Acid Type A Receptor Subunit Delta*, the delta subunit of GABA-A receptor); SHANK3 (*SH3 And Multiple Ankyrin Repeat Domains 3*); PTPN4 (*Protein Tyrosine Phosphatase Non-Receptor Type 4);* MFSD8 (*Major*

Facilitator Superfamily Domain Containing 8); KCNQ2 (*Potassium Voltage-Gated Channel Subfamily Q Member 2*); WDR45 (*WD Repeat Domain 45*); SDHA (*Succinate Dehydrogenase Complex Flavoprotein Subunit A*); GRIN1 (*Glutamate Ionotropic Receptor NMDA Type Subunit 1)* and KIF1A (*Kinesin Family Member 1A*). In addition, variants for RTT-like phenotypes were also found in five novel candidate genes for the onset of a NDD (*Lopes et al., 2016*). They include: RHOBTB2 (*Rho Related BTB Domain Containing 2*); SMARCA1 (*SWI/S NF Related, Matrix Associated, Actin Dependent Regulator*); GABBR2 (*Gamma-Aminobutyric Acid Type B Receptor Subunit 2*); EIF4G1 (*Eukaryotic Translation Initiation Factor 4 Gamma 1*) and HTT (*Huntingtin*).

Despite the extent of the genetic causes at the base of RTT, the gene of election for the study of the pathophysiology of this NDD still remains *MECP2*, since, as already mentioned, the vast majority of RTT cases (classic and atypical) derives from its *de novo* mutations.

1.1.3 *MECP2* gene: structure, expression and functions

MeCP2 is a nuclear protein considered one of the most important epigenetic readers and a key regulator of gene expression. Indeed, it was the first component of the Methyl Binding Protein (MBP) family to be recognized thanks to its ability to bind DNA with at least one symmetrically methylated CpG-dinucleotide (*Guy et al., 2011*). Its importance is highlighted by the transversal presence among all vertebrates, with a high conservation of amino acidic sequences in mammals (the ones of humans and mice are identical for the 95%) (*Guy et al., 2011*). The *MECP2* gene spans ~ 76kb in the long arm of the X-chromosome (Xq28) and displays higher levels of complexity respect to other nuclear proteins. Indeed, it has a considerable extension of its 3'UTR, one of the longest known in the human genome, and several polyadenylation signals that generate transcripts of different length with various expression patterns (*Singh et al., 2008*). *MECP2* consists of three introns and four exons that, due to alternative splicing, encode for two alternative isoforms: MeCP2_e1 and MeCP2_e2. They differ in their N-terminal regions: isoform e1 has a section with 21 aminoacidic residues combining for an acid pI, whilst isoform e2 has only 9 residues in the same section which confer it a basic pI (**Figure 1.2**).

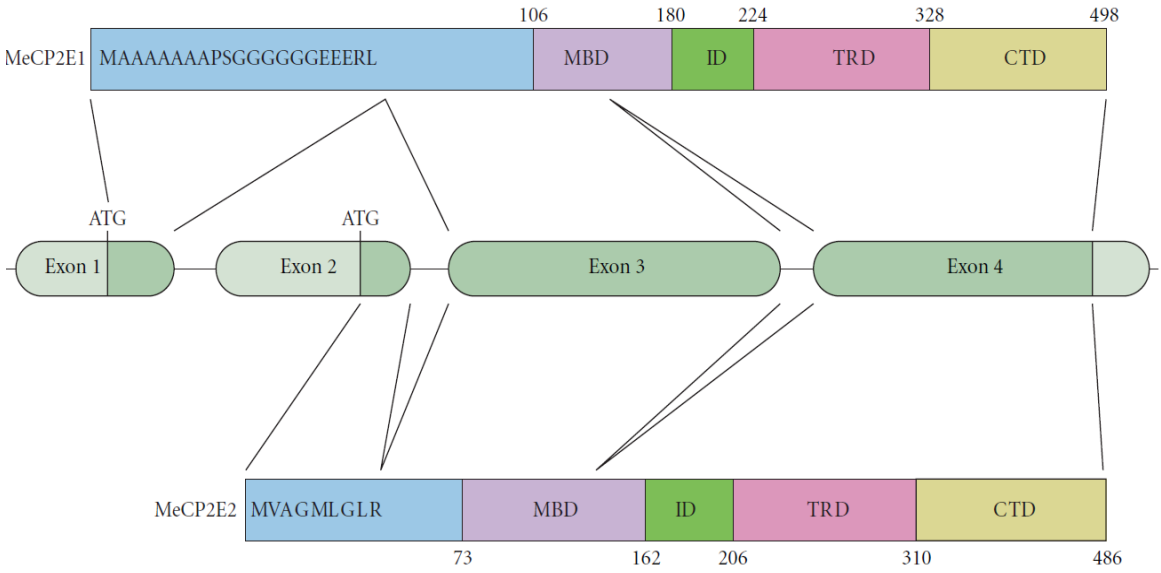

Figure 1.2. *MECP2* gene and protein isoforms. Schematic illustration of the *MECP2* gene structure and the different domains of the two protein isoforms, MeCP2_e1 and MeCP2_e2 (*Zachariah and Rastegar, 2012*)**.**

The most abundant isoform in mouse and human brains is the e1 isoform (10 times more expressed than e2) (*Singh et al., 2008*). At cellular level, both isoforms accumulate on the highly methylated pericentromeric heterochromatic regions of murine nuclei highlighting these foci; generally, in all cells their distribution on chromatin correlates with DNA methylation (*Skene et al, 2010*). Of note, even if it was recently demonstrated that both variants present unique interacting protein partners and a specific regulation of different sets of genes (*Martinez de Paz et al., 2019*), the most relevant isoform studied in the context of RTT is the e1 considering its sole relevance for the manifestation of symptoms (*Itoh et al., 2012; Yasui et al, 2014*).

The protein (**Figure 1.2**) is a polypeptide of 486 (MeCP2_e2) or 498 (MeCP2_e1) residues and it consists of five distinct functional domains (*Hite et al., 2009; Adkins et al., 2011; Gulmez Karaca et al., 2019*):

- the N-terminal domain (NTD);
- the methyl-CpG-binding domain (MBD);
- the intervening domain (ID);
- the transcriptional repressor domain (TRD) or NCoR/SMRT (nuclear receptor co-repressor/silencing mediator of retinoic acid and thyroid hormone receptor) interacting domain (NID);

- the C-terminal domain, which can be subdivided into domain α and β (CTD α and β).

Furthermore, MeCP2 disposes of a nuclear localisation signal (NLS) within the TRD, that allows its nuclear localization, two strong PET sequences, usually correlated with rapid proteolytic degradation (*Bedogni et al., 2014*), two highly conserved AT-hooks, that can bend DNA at specific AT-rich sites (*Baker et al., 2013*), and a highly conserved stretch of histidines in the C-terminus (*Lombardi et al., 2015*). Due to the link with DNA methylation and gene silencing, most of the studies focused on the two main functional domains: the MBD and the TRD. The other domains were subsequently defined by biophysical and protease digestion experiments (*Adkins et al., 2011*). It was demonstrated over the years that also these MeCP2 domains play important roles, being involved in methyl-independent DNA interaction or in regulative events of post transcriptional modifications. For example, the ID enhances the affinity of the MBD for DNA and offers an independent site of interaction with the nucleic acid (*Claveria-Gimeno et al., 2017*), the CTDs are necessary for the association with proteins regulating chromatin structure and the CTDβ contains a WW binding domain involved in splicing factor interactions (*Adkins et al., 2011*).

Another remarkable peculiarity of MeCP2 protein consists in its folding, that contributes to its multifunctional versatility. Indeed, its known tertiary structure is composed of 4% α-helices, 21% β-sheets and 13% β-turns, whilst the remaining ~ 60% is represented by unstructured regions. Therefore, this protein is one of the so-called intrinsically disordered proteins (IDPs). These include a list of thousands of proteins (almost 30% of the ones encoded in the human genome) that are partially or completely devoid of a stable structure and that can acquire specific structures depending on partners. These flexible regions have been linked to large number of functions, including DNA interactions. Besides, the ability of structural rearrangement allows destructured proteins to make the necessary allosteric changes required for binding and/or regulating their partners (*Hite et al., 2009; Liyanage and Rastegar, 2014*). Interestingly, many key mutations associated with RTT are located right inside these regions.

Regarding the expression profile of Mecp2 in the adult mice, the protein levels are high in the brain, lung and spleen, lower in heart and kidney and barely detectable in liver, stomach and small intestine (*Shahbazian et al., 2002*). Focusing on the brain, while transcript levels are high during embryogenesis but postnatally decrease, the protein

levels are low during embryogenesis and increase postnatally following neuronal maturation. Interestingly, these high levels of expression are maintained throughout adulthood, reflecting the importance in supporting neuronal functions besides development (*Zachariah and Rastegar, 2012*).

The absence of a correlation between protein and RNA levels suggests tissue-specific regulation of translation. Another important characteristic of the adult mouse brain is that Mecp2 presents a different spatial expression depending on the area. Indeed, the protein is more expressed in the cortex and cerebellum rather than in the olfactory bulb, striatum, hippocampus, thalamus or brain stem (*Zachariah et al., 2012*). Of note, in all mammals, MeCP2 also exhibits a heterogenous pattern of expression depending on the stage of cerebral development. In particular, in human and mouse brains, MeCP2 expression correlates with the ontology of the CNS. At first, it appears in structures like spinal cord, brainstem and thalamus and lastly in neurons of the more superficial layers of the cerebral cortex (*Shahbazian et al., 2002; Zoghbi, 2003*; *Zachariah and Rastegar, 2012)*. At the cellular level, Mecp2 is predominantly expressed in neurons (14 million copies of MeCP2 per neuron), but lower levels are detectable also in glia (10-30 times less) (*Maezawa et al., 2009; Skene et al., 2010*).

Despite the theoretical molecular weight of MeCP2 protein is 53 kDa, it is normally detected at 73 kDa by Western blot analysis (*Liyanage and Rastegar, 2014)*. *Post-translational modifications* (PTMs) probably contribute to this phenomenon. PTMs of MeCP2 include phosphorylation, ubiquitination, SUMOylation, acetylation, methylation and O-glycosylation (*Liyanage and Rastegar, 2014; Cheng et al., 2014; Bellini et al., 2014*). These modifications alter the protein structure and change its ability to physically interact with other components or partners, leading to variations in protein localization, signal transduction and functions (*Beltrao et al., 2012*). Therefore, together with the highly disorganized structure, PTMs may generate and justify MeCP2 functional versatility (*Bellini et al., 2014*). Phosphorylation of MeCP2 is the most characterized among the different PTMs. It has implications in neuronal activity-dependent transcriptional regulation and modulates the interactions with other proteins (*Adkins et al., 2011; Bellini et al., 2014*). This is the case for the two firstly characterized phosphorylation sites, occurring on serine 421 and serine 80. While phosphorylation of S421 is induced by neuronal activity and the associated influx of calcium (*Zhou et al., 2006*), S80 phosphorylation is negatively regulated by neuronal activation *(Tao et al., 2009)*. This suggested that the equilibrium of phosphorylation at these sites could

promote the transition from resting to depolarized state of a neuron (*Adkins et al., 2011*). Importantly, S421 phosphorylation has been proposed to decrease the association of MeCP2 to specific targets, such as the *Bdnf* promoter, while S80 phosphorylation was proposed to increase the affinity of MeCP2 for specific euchromatic targets (*Zhou et al., 2006; Tao et al., 2009*). Of note, the activity-dependent phosphorylation of MeCP2 occurs on several different residues of cultured neurons and allows to modify associations with cofactors (*Gonzales et al., 2012; Ebert et al., 2013*). The T308 phosphorylation abolishes the interaction of MeCP2 with its corepressors. Lastly, our group demonstrated that the phosphorylation of MeCP2 at S164 is dynamically regulated during neuronal maturation and it is strictly needed for correct neuronal morphology (*Stefanelli et al, 2016*). Available data on PTMs different from phosphorylation are still very limited. In particular, sumoylation of lysine 233 allows Mecp2 recruitment of HDAC1/2 complexes and mutations at this residue abolish the silencing properties of Mecp2 in primary cortical neurons (*Cheng et al., 2014*). Moreover, K233 mutations also impact excitatory synaptogenesis both *in vitro* and *in vivo*, thus highlighting the importance of a correct SUMOylation at this site.

MeCP2 functions (**Figure 1.3**):

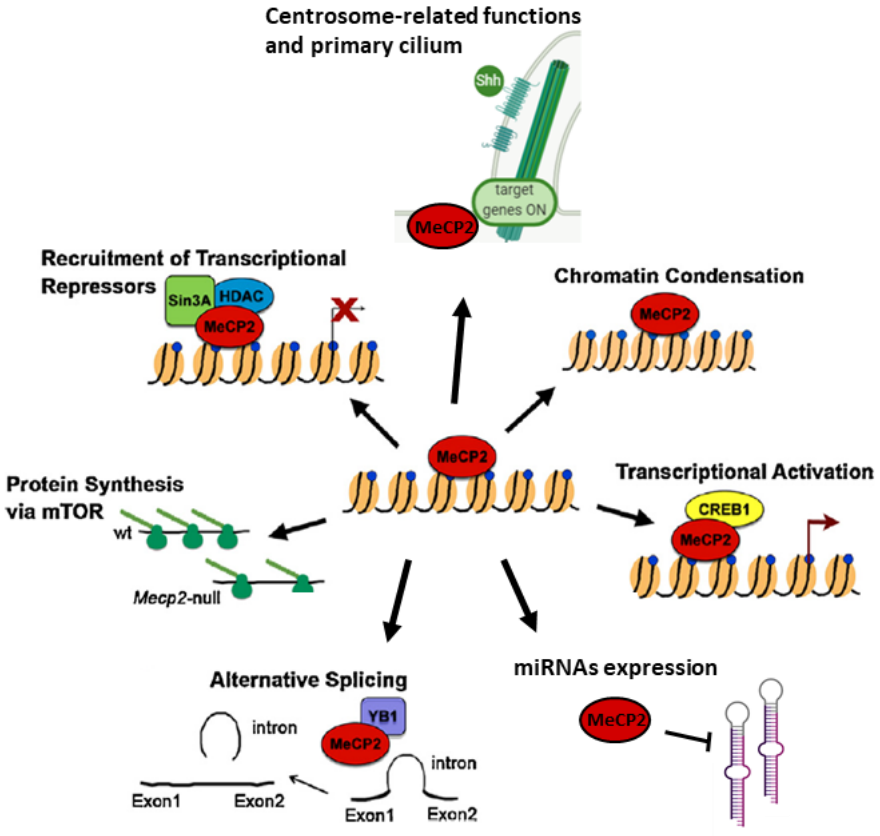

Figure 1.3. Schematic representation of MeCP2 functions (adapted from *Bedogni et al., 2014*).

- *MeCP2 and transcriptional regulation*

  MeCP2 mainly acts as a *transcriptional repressor* linking two epigenetic repressive mechanisms that are DNA methylation and histone deacetylation, through two specific domains of the protein: the MBD and the TRD.

  The MBD is a 63 residues domain that allows MeCP2 to selectively bind methylated DNA. In particular, recent ChIP studies have suggested a preferential association of MeCP2 with methylated cytosines belonging to CpG or CpA dinucleotides (*Nan et al., 1998; Mellén et al., 2012; Kinde et al., 2015; Ip et al., 2018*). The interaction with mCA is very interesting because these methylated dinucleotides accumulate throughout development and are abundant in post mitotic neurons, where, as stated, Mecp2 reaches its maximal levels. A model proposed for the presence of MeCP2 at both mCG and mCA sites of some genes suggests the need of a strong repression for a correct regulation of brain maturation (*Stroud et al., 2017*).

  In parallel, the TRD domain, that alone can repress transcription, interacts with HDAC-containing complexes further repressing transcription (*Zachariah and Rastegar, 2012; Liyanage and Rastegar, 2014*). A tangible demonstration for the direct binding of the TRD with co-repressor complexes was recently provided by the resolution of the cocrystal structure of the MeCP2 NID and TBLR1, a component of the NCoR/SMRT co-repressor complex (*Kruusvee et al., 2017*). This result is very relevant because the majority of RTT missense mutations in the TRD disrupts the binding of MeCP2 with that multi-subunit complex (*Lyst et al., 2013*). The subunits include: NCoR1 (and/or SMRT), Histone Deacetylase 3 (HDAC3), G Protein Pathway Suppressor 2 (GPS2) and Transducing beta-like 1 (TBL1) and/or its paralog TBL1 Related (TBLR1). Other proteins have been found to directly bind MeCP2 permitting the recruitment on methylated DNA of different transcriptional repression complexes, such as Ski (Sloan-Kettering Institute) and SnoN (Ski novel) (*Tecalco-Cruz et al., 2018*). The link between MeCP2 and transcriptional regulation was additionally reinforced over the years by the identification of several interacting partners that are chromatin remodelling complexes, such as Brahma (*Harikrishnan et al., 2005*), CoREST and LANA and a H3K9 histone methyltransferase (*Bedogni et al., 2014*). Interestingly, MeCP2 also interacts with the transcription regulating helicase ATRX, extremely important for the formation of higher-order chromatin loops (*Nan et al., 2007*).

The repressive effects of MeCP2 are genome wide and they positively correlate with the state of DNA methylation within gene bodies, whose density is particularly enriched in long genes (>100 kb) (*Gabel et al., 2015*). Therefore, it has been proposed that MeCP2 deficient brains manifest a length-dependent increase in gene expression. To support this, it was shown that populations of long genes are selectively expressed in the *Mecp2* null brain and decreasing the expression of these long genes ameliorates null-neurons dysfunctions. However, this bias towards long genes regulation is still under debate for the reliability of the statistical analyses (*Raman et al., 2018*).

Beyond this repressive role, recent studies proposed that MeCP2 can also act as a *transcriptional activator* and, therefore, that its transcriptional regulatory role depends on its protein partners. Indeed, while exploring gene expression patterns of mice presenting *Mecp2* dysfunctions, it was found that Mecp2 associates with the cAMP-responsive element-binding protein1 (CREB1) on an active but not a repressed form of the same gene (*Chahrour et al., 2008*). It was even proposed that MeCP2 could positively regulate a subset of neuronal genes through its NID, as this domain recruits HDAC3 to deacetylate the transcription factor Forkhead box protein O3 (FOXO3), thus promoting transcription (*Nott et al., 2016*). However, these studies proposing MeCP2 as a transcriptional activator rather than just a repressor remain to be further supported.

Apart from a leading role in transcriptional regulation of methylated DNA regions, several other functions have been attributed to Mecp2 (*Cheng and Qiu, 2014*) as summarized below.

- *MeCP2 modulates chromatin structure in neurons*

  In mature neurons MeCP2 is one of the major DNA binding proteins and its involvement in the control of global architecture of chromatin is not surprising (*Skene et al, 2010*). Since the early studies on the ability of the TRD to bind corepressor complexes, the repressor activity of MeCP2 was in fact connected to chromatin compaction. Indeed, it was proved that *in vitro* MeCP2 can substitute itself to histone H1 (*Nan et al., 1997*) and can stabilize linker DNA through its CTD, mimicking H1 association (*Chandler et al., 1999*). Moreover, at a high molar ratio to nucleosomes, MeCP2 mediates the formation of a novel highly compacted chromatin structure (*Georgel et al., 2003*). In line with these findings, *Mecp2*-null brains show a general

increase in histone acetylation and a compensatory raise of H1 levels, outlining the effect on global genomic architecture (*Skene et al, 2010*).

- *MeCP2 and RNA splicing*

  Studies of co-immunoprecipitation revealed that MeCP2 directly interacts with several RNA-binding proteins and spicing factors, such as the Y box-binding protein 1 (YB-1) (*Young et al., 2005*), a conserved RNA-binding protein that is involved in RNA splicing, and the spliceosome-associated protein PRPF3 (*Long et al., 2011*). Recent experiments on *Mecp2*-null rat brain, mouse primary neurons and human cell lines proved that several MeCP2-associated proteins are involved in mRNA splicing (*Cheng et al., 2017*). Furthermore, in *Mecp2* deficient cultured cortical neurons there is a widespread alteration of mRNA alternative splicing.

- *MeCP2 and microRNAs*

  Considering that transcripts of protein-coding genes account for only a very small part of all transcripts in the genome, it was interesting to investigate the influence of MeCP2 in regulating the expression of non-coding RNAs, in particular microRNAs (miRNAs). miRNAs are abundant in the nervous system and can modulate gene expression post-transcriptionally to influence different aspects critical for developmental processes, as neurogenesis, cell fate determination, synaptic plasticity and brain maturation (*Jobe et al., 2012; Cheng and Qiu, 2014; Ip et al., 2018*). As expected, Mecp2 does regulate miRNAs expression, suggesting the ability of this protein to globally modulate genome transcription, independently from the RNA type. In details, Mecp2 controls the expression of miR-137 (which is involved in neuronal proliferation and differentiation) (*Szulwach et al., 2010*) and represses the transcription of other primary miRNAs (pri-miRNAs) binding the associated methylated promoter (*Ip et al., 2018*). Moreover, Mecp2 can directly inhibit the expression of miRNAs by blocking their pri-miRNA processing (*Cheng et al., 2014*). Indeed, in animal models of RTT, the deletion of *Mecp2* disrupts the expression of a wide spectrum of miRNAs, therefore probably contributing to disturbances of brain development and maturation. Accordingly, miRNAs have been reported to be dysregulated in the total brain, hippocampus, cortex, cerebellum of *Mecp2*-null mice as well as in *Mecp2*-deficient neuronal cultures and neuronal cultures and cerebral organoids derived from RTT iPSCs (*Ip et al., 2018*). Lastly, miRNAs can regulate *MECP2* expression. miR-200a and miR302c control *MECP2* long 3' UTR transcript during *in vitro* differentiation of human embryonic stem cells

(hESCs) (*Rodrigues et al., 2016*), leading to mRNA destabilization and translational silencing. Moreover, in cultured rat cortical neurons, miR-130a, that inhibits neurite outgrowth and reduces dendritic spine density and complexity, targets *Mecp2*, downregulating its expression during important steps of neuronal maturation (*Zhang et al., 2016*). This suggests the existence of a possible feedback mechanism to regulate neuronal development.

- *MeCP2 and protein synthesis*

  The correlation between MeCP2 and the regulation of protein synthesis emerged during investigations on the regulatory pathway of protein synthesis of AKT/mTOR, which is crucial for synaptic organization and whose dysfunctions were already linked to different NDDs (*Ricciardi et al., 2011*). Indeed, it was demonstrated that in cortical neurons of *Mecp2*-null brains, phosphorylation of ribosomal protein S6 (rpS6), an important target of mTOR pathway, is severely impaired just before the manifestation of severe symptoms. To support this, general dysfunctions of the AKT/mTOR pathway and defects of protein synthesis in null brains were further proved.

- *MeCP2 and centrosome-related functions*

  Our laboratory has recently attributed a novel centrosomal role to MeCP2. Indeed, we found that MeCP2 phosphorylated at Tyr-120 is enriched at the centrosome, both in dividing and postmitotic cells and its deficiency causes aberrant spindle geometry, defects in cell proliferation, prolonged mitosis and defects in microtubule nucleation (*Bergo et al., 2015*). The relevance of this new function of Mecp2 has been further investigated considering the link of the centrosome to the primary cilium (*Frasca et al., 2020*). Primary cilium represents a non-motile protruding organelle which grows from the basal body, a centrosome-derived structure, in almost every quiescent or differentiated mammalian cell, including neurons (*Guemez-Gamboa et al., 2014*). Primary cilia are “sensory antennae” involved in a wide variety of physiological processes including neuronal differentiation, migration and maturation (*Pala et al., 2017; Park et al., 2019*). Dysfunctions in their assembly or signalling lead to several disorders generally called “ciliopathies” (*Valente et al., 2014*) that share many clinical features with RTT (*Kyle et al., 2018*). As proved by *Frasca et al.*, I have contributed to demonstrate that MeCP2 deficiency affects ciliogenesis both *in vitro* and *in vivo*. Consequently, the cilium related Sonic Hedgehog pathway, which is essential for brain development and functioning, is impaired. Microtubule

instability participates in these phenotypes that can be rescued through HDAC6 inhibition, together with neuronal morphology and synaptic functionality (*Frasca and Spiombi et al., 2020*). Altogether these data pinpoint the relevance of this novel function of MeCP2.

As emerged from this chapter, MeCP2 functions as a versatile protein, mainly affecting gene expression. However, we still lack a full comprehension of the contribution and relevance of the above-mentioned roles to the pathophysiology of Rett syndrome and/or other neurological disorders.

1.1.4 Animal models for the study of RTT

One of the crucial points for studying a molecular mechanism, a specific pathology, or a therapeutic approach is to select the most informative model species (*Ericsson et al., 2013*). In the case of RTT, the first thing to consider is that MeCP2 protein is expressed in all vertebrates, whilst is absent in non-vertebrate genetic model organisms, including Drosophila or the worm *C. elegans* (*Hendrich and Tweedie, 2003*). Furthermore, this disorder exhibits peculiar characteristics (the late onset and the complexity of symptomatology above all) and its progression needs to be followed at different stages of development. Therefore, the animal model of election has been represented over the years by rodents (almost all mice, with exception of few rats (*Jin et al., 2008; Wu et al., 2016*)), with several lines generated for the different investigation queries. Few zebrafish and Drosophila models exist, and they have been developed to investigate specific RTT-causing mutations or genetic modifiers of *MECP2* (*Cukier et al., 2008; Pietri et al., 2013*).

Mouse models	Description
***Mecp2* null mouse models**	
Mecp2$^{tm1.1Bird}$	Exon 3 and 4 deletion. *Mecp2* expression and function are abolished *(Guy et al., 2001; Cobolli Gigli et al., 2016)*
Mecp2$^{tm1.1Jae}$	Exon 3 deletion. *Mecp2* expression and function are abolished (*Chen et al., 2001*)
Other *Mecp2* mutant mice	
Mecp2$^{308/y}$	Introduction of a premature STOP codon in exon 4. Truncated MeCP2 protein with residual unknown function (*Shahbazian et al, 2002*)

Mouse models	Description
RTT-causing mutations mouse models	
Mecp2^{R168X}	Premature STOP codon at amino acid 168 (*Schaevitz et al., 2013*)
Mecp2^{R133C}	Missense mutation that produces mutant *Mecp2* protein (*Brown et al., 2016*)
Mecp2^{Y120D}	Knock-in mutation that leads to a more accessible and transcriptionally active chromatin structure (*Gandaglia et al., 2019*)
Mecp2^{T158M}	Knock-in mutation that disrupts protein stability (*Brown et al., 2016*)
***Mecp2* conditional-mutant mice**	
Nestin-cre knockout	Brain-specific deletion (*Guy et al., 2001; Chen et al., 2001*)
Sim 1-cre knockout	Selective deletion in neurons of hypothalamus and amygdala (*Fyffe et al., 2008*)
TH-cre knockout	Selective deletion in dopaminergic and noradrenergic neurons (*Lindeberg et al., 2004; Samaco et al., 2009*)
CamKII-cre knockout	Forebrain-specific deletion (*Gemelli et al., 2006*)
Pet1-cre knockout	Selective deletion in serotonergic neurons (*Fyffe et al., 2008*)
Viaat-cre knockout	Selective deletion in GABAergic neurons (*Chao et al., 2010*)
Mecp2$^{loxJ/y}$*/cre-ER*	Induction of *Mecp2* loss at specific postnatal stages (*Nguyen et al., 2012*)
***Mecp2* mouse models of phenotypic rescue**	
Mecp2$^{lox\text{-}Stop/y}$/cre-ER	Activation of *Mecp2* gene in *Mecp2*$^{lox\text{-}Stop/y}$ mouse model by Tamoxifen injections (*Guy et al., 2007*)
Mecp2^{Stop}*-hGFAPcreT2*	Selective re-expression of *Mecp2* gene in astrocytes in *Mecp2* null mouse model by Tamoxifen injections (*Lioy et al., 2011*)

Table 1.3. Summary list of mouse models for the study of Rett described in the chapter.

Among the first mouse models generated for studying RTT, the *Mecp2*-null lines derived from two independent laboratories in 2001 are still the most popular animal models used. One is the *Mecp2*$^{tm1.1Bird}$ mouse line or “Bird strain” which lacks any *Mecp2* product (exon 3-4 deletion) (*Guy et al., 2001*); the other is the *Mecp2*$^{tm1.1Jae}$ line or “Jaenisch strain” which expresses only small fragments of the protein (exon 3 deletion) (*Chen et al., 2001*). Both strains recapitulate RTT symptoms and share similar phenotypes. Therefore, they are suitable for studying the mechanistic basis of

the disease or testing the efficacy of treatments in pre-clinical trials (*Vashi and Justice, 2019*). Of note, in this section of the chapter we are only referring to RTT mouse models carrying global (rather than cell specific) *Mecp2* null alleles, on the original genetic background (C57BL/6 for the Bird strain, mixed C57BL/6 and BALB/c for the Jaenisch). Regarding the most relevant model for the clinic, female *Mecp2*-mutant mice are certainly preferred as RTT is predominantly a female pathology. However, these heterozygous mice present complicated problems of phenotypic variability due to the pattern of XCI. In accordance with their heterozygosity, *Mecp2*$^{-/+}$ female mice exhibit milder symptoms than males. Generally, they develop overt RTT-like features at 4-6 months of age (therefore, apparently later than RTT girls) and they typically exhibit a normal life span. Since hemizygous males are sterile, heterozygous females are needed to maintain the colony (*Guy et al., 2001; Chen et al., 2001*). Due to these disadvantages that may hinder the needs of some research investigations, the majority of RTT studies have been and still are carried out on hemizygous *Mecp2*-null male mice. In fact, they show a more pronounced phenotype and an earlier onset of overt symptoms that generally arise after 4 weeks of age and develop quickly (*Vashi and Justice, 2019*). Lifespan is severely shortened in null males (they rarely live longer than 3 months) and prior to death they often display severe hypoactivity, kyphosis, disheveled fur and severe weight loss (*Kats et al., 2012*). As for RTT patients, the most profound symptoms of these *Mecp2*-null lines are gross motor abnormalities, that include reduced mobility, impaired balance and motor coordination, ataxic gait, impaired limb and postural reflexes, and spontaneous tremors (*Guy et al., 2001; Chen et al., 2001*). While girls replace a purposeful use of hands with stereotypical hand movements, these mice develop an uncontrolled clasping of their hindlimbs (*Kats et al., 2012*). Of note, *Mecp2*$^{tm1.1Jae}$ null mice show an excessive and repetitive grooming that might represent a form of motor stereotypy (*Sterns et al., 2007*). From the morphological point of view, both humans and null mice exhibit reduced brain volume and neuronal hypotrophy (*Chahrour and Zoghbi, 2007*). Neurological regression and loss of speech are two characteristic traits of RTT patient behaviour; this is not a measurable feature in mice, anyway they were reported to have learning deficits (*Moretti et al., 2006*). Indeed, they exhibit an impairment in contextual fear conditioning (*Sterns et al., 2007*) (a test of associative learning and memory), in object recognition (*Sterns et al., 2007*), and in motor-cerebellar learning (*Kats et al., 2012*). Similar to RTT girls that typically manifest increased anxiety, *Mecp2*-null mice display heightened

anxiety levels respect to wild types (*Adachi et al., 2009*). On the contrary, while young RTT patients show social avoidance, null mice exhibit an increased sociability, with more time exploring unfamiliar mice (*Vashi and Justice, 2019*). As humans, these mice manifest important metabolic disturbances (including neurometabolites, increased serum cholesterol and triglycerides, abnormal mitochondrial structure, increased oxidative stress), breathing irregularities, cardiac abnormalities (prolongation of the corrected QT interval) and seizures (*Kats et al., 2012; Vashi and Justice, 2019*). Interestingly, null mice present abnormalities in ultrasonic vocalization when separated from their mothers at early postnatal stage (*Picker et al., 2006*). To summarize, these *Mecp2*-null mouse models share a broad spectrum of phenotypes with human RTT patients, thus resulting excellent models to study the pathology.

However, *Mecp2* null mice do not represent the best molecular model of the human pathology; indeed, most RTT patients carry pathogenic mutations causing a hypomorphic or unstable MeCP2 protein rather than the complete absence of it. For this reason, several mouse lines were subsequently generated mimicking human RTT-causing mutations (missense or early truncating point mutations). These mice have been fundamental for understanding the correlation of the mutation with the severity of symptoms or exploring the molecular consequences of the specific mutation. To mention some of the most relevant, the mouse line mimicking the hotspot T158M has a life span of almost 13 weeks and a manifestation of very severe symptoms while the mouse model of the R133C missense mutation shows a much milder phenotype; functional studies allowed to correlate the T158M phenotype with a decreased affinity for DNA together with protein instability (*Brown et al., 2016*). Both male and female mice carrying the early truncating *Mecp2* R168X nonsense mutation mirror many features of the null mice, like impaired motor and cognitive functions (*Schaevitz et al., 2013*). Nevertheless, they manifest also unique phenotypic features; indeed, *Mecp2*$^{R168X/+}$ females are characterized by later motor symptom onset, normal anxiety-like behaviour and higher rate of susceptibility to severe seizures. This emphasizes the importance of choosing the best model for studying specific features of the disease or assess potential therapeutics. Another interesting model is the KI mouse with the human mutation Y120D (localized in the MBD) (*Gandaglia et al., 2019*). These mice develop a severe RTT-like phenotype quite similar to the nulls; however, molecular studies aimed at defining the chromatin consequences of these mutations revealed that the two mice diverge at this level. Indeed, while the presence of the Mecp2 Y120D

protein, that manifests a decreased affinity for DNA, leads to a more accessible and transcriptionally active chromatin structure, the total absence of Mecp2 determines a more closed and transcriptionally inert structure. These studies suggested for the first time that the molecular consequences of different *Mecp2* alleles might be quite different. A further model that provided *in vivo* evidence of *Mecp2* importance in the regulation of chromatin architecture is represented by the *Mecp2*$^{308/y}$ mice, that carries a truncating mutation (codon 308>C-terminal truncation) and display elevated levels of histone H3 acetylation (*Shahbazian et al, 2002*).

One of the turning points that allowed to correlate the aetiology of RTT with the dysfunction of *Mecp2* in specific tissues, brain regions or cell types was certainly the development of different conditional KO mice. To test whether the effects of *Mecp2* loss are brain specific, the conditional *Mecp2* allele was combined with the *nestin*-Cre transgene both in the Bird and the Jaenisch strains as Nestin is selectively expressed from ~ E12 in neuronal precursors, that will originate neurons and glia cells. In both cases, the phenotype of mice with the CNS-specific deletion of *Mecp2* was almost indistinguishable from that of null mice (*Guy et al., 2001; Chen et al., 2001*). These findings indicated that the major features of the null phenotype were probably due to the absence of *Mecp2* in neuronal and/or glial cells rather than in peripheral tissues. These results were then confirmed in a mouse model in which *Mecp2* was selectively silenced in peripheral tissues but prenatally reactivated at normal levels within the CNS (*Ross et al., 2016*). These mice exhibited a normal survival and the absence of RTT-like signs, although the authors do not exclude that a subset of less extreme phenotypes may be peripheral in origin. Many more *Mecp2* conditional-mutant mice have been engineered through the years to selectively silence *Mecp2* in different brain area or neuronal subtypes such as in the hypothalamus and amygdala (*Fyffe et al., 2008*), dopaminergic and noradrenergic neurons (*Lindeberg et al., 2004; Samaco et al., 2009*), forebrain neurons (*Gemelli et al., 2006*), serotoninergic neurons (*Fyffe et al., 2008*) and GABAergic neurons (*Chao et al., 2010*). Interestingly, each mouse model shows a peculiar phenotype with characteristic features, highlighting the importance of *Mecp2* expression in all those types of neurons for a fine regulation of specific neuronal circuits.

Importantly, a conditional KO mouse allowed us also to prove that neuronal dysfunctions are not the only cause of RTT symptoms. As mentioned before, Mecp2 is abundantly expressed in neurons but also in glial cells even if at much lower levels.

Astrocytes, one of the most abundant glial population of the CNS, express Mecp2 and play a fundamental role in brain functioning (astrocyte functions will be treated later on, in dedicated chapters). Therefore, a conditional KO mouse was developed to investigate the astrocytic contribution to RTT. *Mecp2*-floxed mice were crossed with a glial-specific *GFAP*-Cre transgene permitting to demonstrate that the specific ablation of *Mecp2* from glia could induce some RTT-like symptoms, including decreased body weight, hindlimb clasping and irregular breathing (*Lioy et al., 2011*).

Eventually, conditional mice were used to selectively delete *Mecp2* at different post-natal stages; importantly, in any case the late ablation of the RTT gene led to the onset of RTT-like symptoms and premature death (*Luikenhuis et al., 2004; McGraw et al., 2011; Cheval et al., 2012; Nguyen et al., 2012*) suggesting that *Mecp2* is fundamental for both the development and the maintenance of adult brain functions.

Since the early efforts for a cure for RTT, a prominent question always concerned whether there was the possibility of reverting the phenotype. Indeed, a recurrent observation that derived from the study of post-mortem RTT brains and of different mouse models was that they do no exhibit neuronal death or sings of neurodegeneration, though impairments of brain functions are present (*Vashi and Justice, 2019*). To explore the possibility of repairing *Mecp2*-deficient brains an *Mecp2* mouse line with a transcriptional STOP cassette flanked by *lox*P sites was generated (*Guy et al., 2007*). These mice were crossed with mice ubiquitously expressing a Cre-ER transgene, allowing *Mecp2* silencing until the injection of tamoxifen. After the onset of the typical RTT-like phenotype, tamoxifen was administrated in order to obtain a gradual and physiological reactivation of the endogenous *Mecp2* (of note, a sudden widespread activation led to toxicity). This restoration remarkably reversed general poor conditions including inertia, gait, hind-limb clasping, tremor, breathing abnormalities and LTP defects, and normalized the lifespan of adult mice. Heterozygous females were also used in this study demonstrating that also their late-onset neurological symptoms are reversible. Therefore, this study is considered a milestone because it raised the possibility of pursuing a cure for symptom reversal also in humans. Subsequent experiments confirmed these findings in other female mouse models of RTT; indeed, a systemic delivery of Mecp2 significantly stabilized or reversed their symptoms (*Garg et al., 2013*). Of relevance for our study, it was also proved that the selective re-expression of *Mecp2* in astrocytes of otherwise null mice significantly improves locomotion and anxiety levels, restores respiratory abnormalities

and greatly prolongs lifespan (*Lioy et al., 2011*). In addition, Mecp2 expressing astrocytes exert a non-cell autonomous positive effect on null neurons *in vivo*, as they restore dendritic morphology and the levels of excitatory glutamate transporter (VGlut1) (further details in chapter 1.2.7).

It is well known that phenotypic outcomes in transgenic mice vastly depend on their genetic background and, therefore, on their specific set of modifier genes. There are inherent differences between strains in basic biological parameters and strain selection is one of the most important considerations in mouse modelling (*Ericsson et al., 2013*). As mentioned before, the original Bird strain was produced on a C57BL/6 background while the Jaenisch strain was developed using a mixed genetic background (129, C57BL/6 and BALB/c). Considering the C57BL/6 *Mecp2*$^{tm1.1Bird}$ strain, which is the most widely used mouse model for RTT, breeding these animals is very challenging (*Jugloff et al., 2006*). Since *Mecp2* null mice are sterile heterozygous females are necessary to maintain the colony. In addition, a peculiarity of BL/6 heterozygous females is that they frequently cannibalize their small litters and take less care of their progeny along with colony aging. Different suggestions about housing methods have been indicated through the years to facilitate the management of the colony (*Garg et al., 2013*), however they are often not sufficient for efficient basic and translational studies. For these reasons, our research group in the past years transferred the *Mecp2*$^{tm1.1Bird}$ genetic modification on the outbred CD1 (ICR) genetic background (*Cobolli Gigli et al., 2016*). This allowed us to prove that CD1 mice, that recapitulate most of the measurable outcomes of the BL/6 background at behavioural, cellular and molecular level, dramatically simplify the management of the colony. Indeed, these mice produce large litters, with very low frequency of cannibalism and show a clearly increased robustness, therefore facilitating and speeding up our studies.

However, it is correct to remind that possibly because of the outbred genotype and the slightly milder phenotype, studies on CD1 null mice might require few more animals to obtain significant data.

1.1.5 Neurobiological alterations following MeCP2 dysfunctions

Since neurological defects are the leading cause of the development of RTT symptoms, lots of efforts have been employed to characterize structural and molecular

alterations in the CNS. This chapter will describe neuropathological changes and neurophysiological abnormalities of synaptic circuits caused by MeCP2 deficiency.

From a morphologic point of view, RTT patients show a 12-34% reduction of their brain weight and volume, mostly pronounced in the prefrontal, posterior frontal, and anterior temporal regions (*Armstrong et al., 2005*). MRI data further corroborated these observations, indicating selective reductions of dorsal parietal grey matter, and preservation of occipital cortex as basic neuroanatomic features of RTT (*Carter et al., 2008*). Besides, a preferential reduction of the anterior frontal lobe was suggested to correlate with clinical severity. Together with reduced brain size and the absence of neurodegenerative events (*Chahrour and Zoghbi, 2007*), histological analyses revealed characteristic features in RTT patients such as decreased cellular size with increased cell density (*Baumann et al., 1995*), decreased dendritic complexity (*Belichenko et al., 1994*; *Armstrong et al., 2005*) and spine density (*Belichenko et al., 1994; Chapleau et al., 2009*). These changes appear area-specific; indeed, they have been observed in the motor, frontal, and inferior temporal cortices but not in the visual cortex and hippocampus; further, they have been identified within definite layers of the same cortical area (*Armstrong et al., 1995*). Nevertheless, it is unclear from human sample analyses to what extent these alterations caused by MeCP2 dysfunction can contribute to the pathology and/or if they are an emergent feature of long-term illness.

In view of unveiling this pathogenic aspect, several mouse models have been studied and characterized. Consistent with post-mortem brains that suggest RTT as a disorder involving region-specific alterations of neuronal morphology and synaptic maturation, investigations on mice confirmed these aspects. Indeed, both *Mecp2*-null lines manifest a decrease in brain weight (9-13%), volume of the cortex (7-11%), hippocampus (8%) and cerebellum (8-12%) (*Belichenko et al., 2008*). Detailed measurements were also performed within areas of major interest for RTT pathogenesis and they revealed that null mice exhibit an arrest of the increase in cortical thickness of both somatosensory and motor cortices after 4 weeks of age (*Fukuda et al., 2005*). Further studies in the barrel field cortex, a model for cortical development and activity-dependent plasticity in mice (*Inan and Crair, 2007*), documented the presence of analogous somatosensory deficits. The cross-sectional area of the barrel field of null mice is significantly decreased already at P10 (*Moroto et al., 2013*), and the decrement progresses with time; the volume reduction has been confirmed in *Mecp2*-het mice at 2 and 7 weeks of age (*Smith et al., 2019*). Moreover,

null mice display a higher density of neurons in layers II/III of the cortex (*Fukuda et al., 2005*) and in the hippocampus of different models of *Mecp2* (*Chapleau et al., 2009*; *Jentarra et al., 2010*). This suggested that, similarly to RTT patients, the reduction of brain volume could be promoted by a decreased complexity and size of neurons (*Gulmez-Karaca et al., 2019*). Indeed, over the past few years, it was demonstrated that *Mecp2* alterations impact fundamental aspects of neuronal maturation, morphology and synaptogenesis (**Figure 1.4**), leading to reductions in neuronal soma size, dendritic arborization, postsynaptic density protein 95 (PSD95) and spine density, together with abnormal spine morphology (*Tropea et al., 2009; Fukuda et al., 2005; Smrt et al., 2007; Xu et al., 2014*).

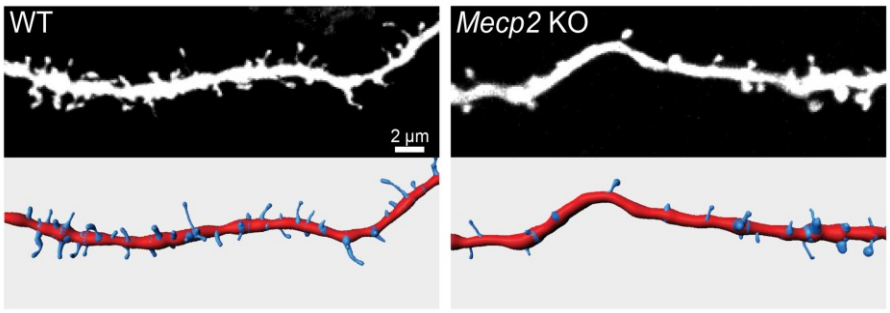

Figure 1.4. Dendritic spine dysgenesis in apical dendritic segments of CA1 pyramidal neurons (DIV11) of *Mecp2* KO mice, and their correspondent reconstructions (*Xu et al., 2014*).

Since neuronal morphology correlates with the architecture of the whole brain and probably impacts on RTT clinical symptoms, it was thoroughly investigated in different *Mecp2* mouse models along development proving that it is intrinsically variable and strictly dependent on age, cell type and *Mecp2* mutation (*Wang et al., 2013*). Just to describe some aspects of this variability, the dendritic complexity of layer V pyramidal neurons is reduced in the somatosensory cortex of null mice at P30 and even more at P60. On the contrary, these neurons are not affected in the *Mecp2*$^{T158A/y}$ mice at P30 while they manifest defects limited to the basal dendritic arbour in symptomatic mice at P90 (*Wang et al., 2013*). In addition, the hippocampus of null mice reveals important dendritic and synaptic morphology changes at already 3 weeks of age, together with a dysregulation of glutamatergic receptors and a reduction in excitatory synapses number, while no change in the hippocampal CA1 neurons was described for the *Mecp2*$^{T158A/y}$ mice at any age (*Wang et al., 2013*). Therefore, the possibility to use

dendritic morphology as measurable outcome for testing the therapeutic potential of a treatment for RTT should carefully evaluate the considered brain area and mouse model.

The neurobiological studies described so far were generally performed in adult or juvenile humans and mice. Given the increasing evidence of the importance of *Mecp2* throughout all the steps of brain development (including the regulation of neurogenesis, cellular differentiation and neuronal migration), researchers started to investigate MeCP2-related dysfunctions present in former time windows (*Ip et al., 2018)*. Clinical studies revealed that RTT patients manifest neurological alterations already in the first months of life, through atypical general movements and impaired speech-language capacities (*Marschik et al., 2013*). Mouse models allowed to deeply explore these aspects confirming that RTT phenotypes are already detectable during neurogenesis and synaptic circuits development. Accordingly, our group demonstrated that *Mecp2* is expressed in the embryonic neocortex affecting its transcriptional profile. In particular, the lack of *Mecp2* during early neuronal maturation increases the expression of neuroprogenitors genes, while it downregulates genes typical of mature neurons, ionic channels, and glutamatergic receptors (*Bedogni et al., 2016*). Consequently, already at DIV3, *Mecp2*-null cultured neurons exhibit morphological alterations and reduced responsiveness to stimuli. Similarly, neurons derived from RTT human iPCs show defects related to neuronal maturation (*Kim et al., 2011*).

In accordance with the aforementioned phenotypes, *Mecp2* deficiency in mice causes alterations in neuronal excitability and defects in experience-dependent plasticity such as altered neuronal connectivity and disrupted excitatory/inhibitory balance (*Ip et al., 2018*). In line with the regional and temporal specificity of neuropathological features, also neuronal circuit deficits appear region-specific. Indeed, cortical somatosensory neurons of *Mecp2* null slices exhibit an overall reduced excitation that progress in time with the increase of symptoms in mice (*Dani et al., 2005*). Similarly, *in vivo* whole-cell recordings of visually evoked responses in V1 pyramidal neurons lacking *Mecp2* revealed decreased excitatory and inhibitory conductances (*Banerjee et al., 2016*), thus confirming circuit-wide changes in cortical processing. On the contrary, acute slices of the CA3 hippocampal region from symptomatic null mice indicated a shift towards hyperexcitation (*Calfa et al., 2015*). This hyperactive hippocampal network was associated with reduced expression of GABA-A receptors and increased expression of GluA1 subunits, that are components of AMPA receptors. Synaptic

hyperexcitability was also described in brainstem areas including locus coeruleus (*Taneja et al, 2009*), ventrolateral medulla (*Abdala et al., 2010; Medrihan et al., 2008*); and nucleus solitarius (*Kron et al., 2012*). These region-specific changes in synaptic activities of null mice were indirectly supported by the analysis of the expression of the immediately early gene *Fos* that resulted downregulated in various cortical regions of the forebrain circuit including the prelimbic cortex, infralimbic cortex, retro-splenial cortex, motor cortex and nucleus accumbens, whilst upregulated in the hindbrain (*Kim et al., 2012*). Interestingly, activation of the medial prefrontal cortex improves neurobehavioral outcomes (such as conditioned fear responses and respiratory phenotype), together with the recovery of Fos expression in the nucleus of the solitary tract, which is a brainstem nuclei fundamental for respiratory circuits (*Howell et al., 2017*).

All in all, this data indicate that MeCP2 plays a fundamental role in the activity-dependent feedback mechanisms required to establish and maintain brain circuits throughout neuronal maturation and life (*Nelson and Valakh, 2015*).

1.1.6 MeCP2 molecular targets involved in RTT pathogenesis

Despite the advances in the characterization of neurological alterations due to MeCP2 dysfunction, only few target genes have been directly related to the pathogenesis of RTT (*Faundez et al., 2019*).

Genome-wide expression studies have been conducted mainly on brain samples derived from different *Mecp2* mouse models. Most of them were null mice, whilst few were knock-in or *Mecp2* overexpressing (Tg) models (for a complete list of mouse models see *Krishnaraj et al., 2019*). In accordance with the region-specificity of the disease, studies were performed also on individual brain regions and their isolated cells. Available transcriptomic data span from whole brain, cortex, visual cortex, cerebellum, hippocampus, and amygdala together with analyses of cells sorted from the forebrain, hypothalamus, striatum (*Krishnaraj et al., 2019*). Gene expression profiles have also been evaluated in embryonic cortical neurons and excitatory/inhibitory cortical neurons from adult mice (*Bedogni et al., 2016; Vacca et al., 2016; Johnson et al., 2017*). Probably because of the complexity of the disorder that, as already stated, involves multiple neurotransmitter systems, cellular populations, and distinct cerebral area, these analyses did not lead to a concordant list

of dysregulated genes (*Zachariah and Rastegar, 2012; Krishnaraj et al., 2019*). One of the few exceptions is represented by the Brain-Derived Neurotrophic Factor (*BDNF*) gene, that functionally interacts with *MECP2* and its pathological reduction directly correlates with the presence of some RTT-like features. BDNF regulation is both important and paradoxical. While Mecp2 represses *Bdnf* transcription (*Wade et al, 2004*), its mRNA and protein levels in *Mecp2*-null mice are downregulated (*Sun and Wu., 2006*). Although the involved mechanisms are still not fully understood, it is generally assumed that the overall reduced neuronal activity featured by the MeCP2 deficient brain contributes to this downregulation (*Xu et al., 2014*). To support this direct link, *Bdnf* overexpression in null mice rescues a subset of RTT-like phenotypes (*Chang et al., 2006; Wang et al., 2006*).

These heterogeneous results suggested the possible value of analysing gene pathways (gene sets) in order to identify the most affected aspects of brain functioning instead of searching for single deregulated genes, that could be even misleading. This allowed to correlate *Mecp2* alterations to important biological mechanisms and cellular functions strictly related to RTT pathogenesis, including lipid metabolism, mitochondrial activity, neuronal migration, neuronal maturation, and synaptic functions (*Krishnaraj et al., 2019*). For example, *Mecp2* null cerebella exhibit altered expression of genes involved in synaptic plasticity and transmission, neuronal migration, learning and behaviour modulation, dendrite development (*Jordan et al., 2007*). In addition, analyses performed on different neuronal types lacking *Mecp2* indicated perturbations in genes involved in cellular adhesion and communication, neuronal connectivity, glutamate and glutathione metabolism, abnormal neuronal excitatory and inhibitory activity (*Sugino et al., 2014; Ehrhart et al., 2016*). Our group identified an overall delayed maturation in embryonic null cortical neurons linked with a decreased expression of ionic channels, glutamatergic receptors and genes involved in cerebral cortex development (*Bedogni et al., 2016*). Of note, several dysfunctions have been also found in astrocytes (*Yasui et al., 2013; Delepine et al., 2015*) (chapter 1.2.7).

Considering the importance of post-transcriptional regulation, proteomic profiling is usually considered a challenging but useful method to validate gene expression results. So far, three important proteomic studies have been conducted in *Mecp2* mouse models: in the cortex of P60 null mice (*Pacheco et al., 2017*), in the olfactory and epithelium bulb of null mice at 2 and 4 weeks of age (*Matarazzo and Ronnett 2004*) and in the plasma of symptomatic heterozygous *Mecp2*^{308} females (*Cortelazzo et al.,*

2017). Although all studies confirmed the presence of several alterations, only *Pacheco et al*. integrated transcriptomic and proteomic datasets derived from the same samples. As a matter of facts, they revealed that within the cortex of adult null mice there is a significant dysregulation of 35 gene-protein "hits", belonging to pathways involved in synaptic functions, neurotransmission, neuronal morphology and development (*Pacheco et al., 2017*). One of these "hits" is represented by the FKBP prolyl isomerase 5 (*FKBP5*), a gene that modulates glucocorticoid sensitivity and is implicated in stress and mood disorders in humans (*Klengel and Binder, 2015*). This gene was already found dysregulated in many other transcriptomic studies (*Krishnaraj et al., 2019)*. Of great relevance for this thesis, these null mice also manifest a significant disruption of glia markers (specifically those related to apoptosis, morphology, and reactivity of astrocytes) together with abnormal brain myelination (*Pacheco et al., 2017*).

1.1.7 Therapeutic approaches and clinical trials

Nowadays, RTT treatments are purely symptomatic and aimed at ameliorating secondary phenotypes, as no specific cure is currently available. The difficulty of medical management is accentuated by the presence of several comorbidities that require a multidisciplinary approach (*Gold et al., 2017*). However, solutions usually offer to patients a better quality of life and longer lifespan.

To date, therapeutic approaches can be divided into two main categories (*Vashi and Justice, 2019*) (**Figure 1.5**):

- Affecting downstream targets of MeCP2
- Directly restoring *MECP2 gene*/functions

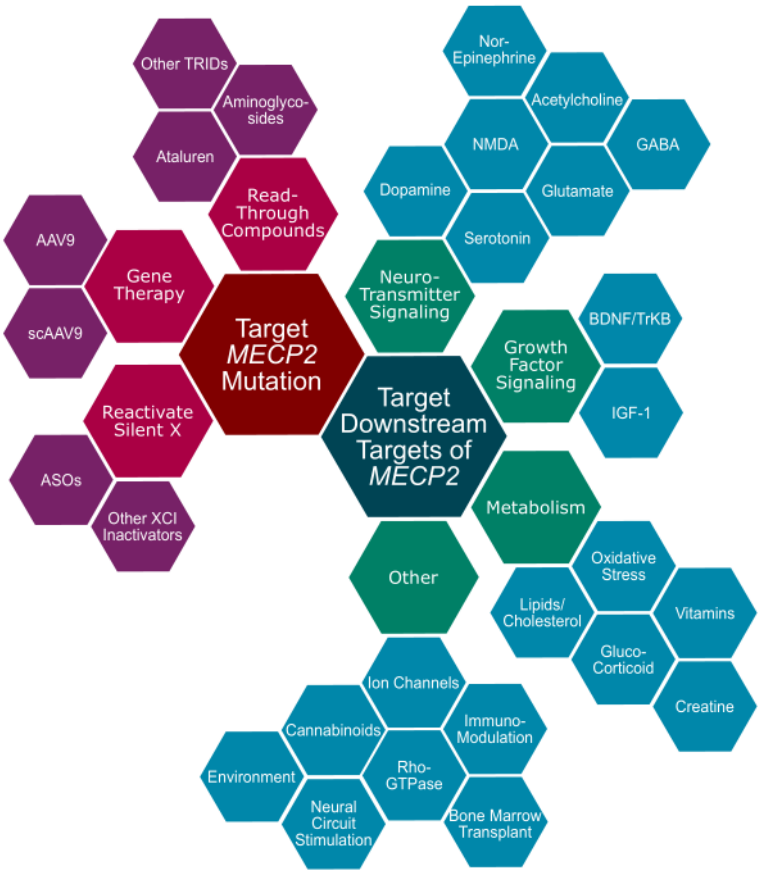

Figure 1.5. Available treatment options for RTT (*Vashi and Justice, 2019*).

Affecting downstream targets of MeCP2

So far several preclinical trials have tested the capacity of different molecules to ameliorate symptoms in *Mecp2*-mutant mice and, since 1966, over 25 clinical trials have been initiated to evaluate whether therapies could improve motor, cognitive and autonomous dysfunctions of patients (*Ehinger et al., 2018*).

Pharmacological strategies generally aim to restore main perturbed aspects of RTT such as neurotransmitter signalling, growth factor signalling and metabolism.

The idea of treatments targeting neurotransmitter signalling derives from the well-proved alteration of multiple synaptic circuits in *Mecp2* mouse models (chapter 1.1.5), such as the dopaminergic, serotoninergic, noradrenergic, glutamatergic, and GABAergic systems (*Vashi and Justice, 2019*). Indeed, desipramine, which is an inhibitor of norepinephrine reuptake, improves breathing abnormalities and apneas of mutant mice (*Roux et al., 2007; Zanella et al., 2008*). However, no clinical improvement was noticed following a trial on RTT patients.

Another drug that ameliorates breathing irregularities in mice is Sarizotan (*Abdala et al., 2014*), a serotonin 1a agonist and dopamine D2-like receptor, that is currently tested in clinics for its efficacy in improving respiratory symptoms.

Acting as NMDA receptor agonist, also ketamine has been tested in pre-clinical trials with the attempt to improve the imbalance of neuronal activity in *Mecp2*-deficient brains (*Kron et al., 2012; Patrizi et al., 2016*). Ketamine increases cortical activity while decreasing hyperexcitability of brainstem network even at low doses, thus improving motor and breathing abnormalities of mice. Clinical trials are currently ongoing to assess ketamine safety.

A second important set of treatments targets growth factor signalling. As mentioned in previous chapter, BDNF is one of the few targets of *MECP2* to be directly involved in some aspects of the pathogenesis of RTT. Unfortunately, direct administration of this neurotrophin to patients is not possible as BDNF cannot cross the blood-brain barrier (BBB) (*Pardridge, 2007*). There is a molecule, a sphingosine-1 phosphate analogue named fingolimod (FTY720), that increases BDNF levels and improves motor deficits in mice (*Deogracias et al., 2012*), whose efficacy and safety are currently under investigation in clinics.

Similarly to BDNF, Insulin-like growth factor-1 (IGF-1) activates a cascade of signalling involved in neuronal survival, outgrowth, and synapse formation (*D' Ercole et al., 1996*); however, IGF-1 can cross the BBB. Preclinical studies demonstrated that this growth factor remarkably improves a wide spectrum of RTT-like symptoms (*Tropea et al., 2009*), while Trofinetide, a synthetic analogue, passed phase 2 clinical trial with promising results (*Deacon et al., 2015*) and a phase III is currently at the recruitment step.

Metabolic defects include another large group of promising targets for RTT patients, as girls manifest perturbed lipid metabolism, altered cholesterol homeostasis and mitochondrial abnormalities (*Vashi and Justice, 2019*). Statins effectively ameliorated motor symptoms and lifespan of *Mecp2*-mutant mice (*Buchovecky et al., 2013*) and clinical trials are evaluating their efficacy and safety in humans.

Considering the defects in mitochondrial energy production and the presence of markers of oxidative stress *(De Felice et al., 2014),* supplementation of intermediates such as anaplerotic substances was a strategy proposed to restore this pathway. It was demonstrated that feeding mice with a diet rich in anaplerotic triheptanoin improves mitochondrial dysfunctions and motor RTT-like phenotypes (*Roe et al., 2002;*

Mochel et al., 2005). Accordingly to these encouraging results, two clinical trials are ongoing. Recent studies indicated that also oral administration of polyunsaturated fatty acids (PUFAs) adjusts cellular redox imbalance in RTT patients, together with an improvement of the redox-related cardiac alterations (*Signorini et al., 2014; Maffei et al., 2014*).

Although many of these strategies aimed at affecting downstream targets of MeCP2 present a reasonable hope of success in clinics, they are limited by the capacity to ameliorate only a subset of symptoms. Therefore, their putative efficacy will have to consider the concomitant prescription of more than one treatment. Further, it is important to recall that most molecules efficacious in preclinical studies fail when passing to clinical trials (*Vashi and Justice, 2019*).

Directly restoring MECP2 gene/functions

Direct restoration of *MECP2* gene/function probably represents the most difficult but efficient approach to treat RTT. Two main strategies are currently considered: gene therapy and X chromosome reactivation.

Gene therapy is considered the first-choice strategy for treating RTT. The idea behind this approach consists in introducing a healthy copy of *MECP2* into neural cells. Viral vector-mediated gene transfer has been already successfully used in basic research as well as in proof of concept studies for the reversal of RTT-like symptoms in mice (*Fagiolini et al., 2020*). The spectrum of viral vectors available for therapeutic intervention is very broad and the choice should consider the characteristics of the disorder (*Lundstrom, 2018*). In the case of RTT, the vector must cross the BBB, transduce many cells, and maintain a stable and long-term expression of the gene (*Vashi and Justice, 2019*). Then, of course, the vector must be able to restore MeCP2 activity in unhealthy cells while avoiding a MeCP2 duplication-like phenotype (*Van Esch et al., 2005*; *Lombardi et al., 2015*). Considering all these requirements, various preclinical trials have already been carried out using different adeno-associated viral (AAVs) vectors, engineered through time to be more brain-specific and efficient in rescuing RTT-like phenotypes (*Garg et al., 2013; Matagne et al., 2017; Sinnett et al., 2017; Gadalla et al., 2017; Tillotson et al., 2017*). This AAV vector-mediated *MECP2* transfer significantly extended the lifespan of RTT mouse models and reversed (or delayed) some typical features. However, it proved that MeCP2 overexpression in liver is highly toxic, therefore further complicating the process of scaling the dosage for

humans, one of the most delicate steps of gene therapy. Indeed, it is well established that systemic administration of too high doses of AAV9 causes severe liver and neuronal toxicity in non-human primates (*Hinderer et al., 2018*). Ongoing scientific efforts aim to improve the design of viral vectors and to increase *MECP2* gene therapy efficacy, while a *MECP2* gene therapy clinical trial, testing AVXS-201, is already pending for approval from U.S. Food and Drug Administration (*Fagiolini et al., 2020*).
Another powerful approach for restoring *MECP2* might be represented by genome editing. Accordingly, a team of researchers has recently developed a CRISPR/Cas9-mediated system able to efficiently targeting and correcting specific *MECP2* mutations in human RTT iPSCs (*Le et al., 2019*).
A different approach for directly restoring *MECP2* is based on the idea of reactivating the silent healthy X chromosome (X_i). Indeed, RTT girls are heterozygous mosaics for *MECP2* mutation, and each cell contains a normal copy of *MECP2,* whether expressed or not (*Vacca et al., 2016*). The major complications of this strategy derive from the activation of all the other genes on the sex chromosome, whose physiological dosage is very important. Ideally, X_i reactivation for RTT should be able to target only *MECP2*, or few neighbour sequences. Although this approach is still in its early phase, some studies have already revealed valuable pharmacological targets affecting *MECP2* reactivation within the X_i (*Vashi and Justice, 2019; Fagiolini et al., 2020*). Similarly, it has been demonstrated that the inhibition of specific genes can reactivate *Mecp2* in RTT neurons and in cerebral cortical neurons of adult mice (*Sripathy et al., 2017; Przanowsky et al., 2018*).

1.2 Astrocytes: from physiology to brain disorders

1.2.1 Astrogenesis and the basis of astrocyte heterogeneity

Astrocytes are one of the most abundant class of glial cells in the brain (20-40% of all neuroglia in human CNS) and since their first description by Rudolf Virchow in 1846, they have been associated with multiple functions vital to CNS physiology and neuronal plasticity (*Allen and Barres, 2009; Verkhratsky and Nedergaard, 2018*). The traditional view that astroglial cells have a passive role in maintaining neuronal proper functioning is outdated as recent discoveries indicate a primary role in information

processing. This close relationship between neurons and astrocytes originates very early in embryonic development and continues throughout adulthood.

Astrogenesis

During development, neurons and astrocytes are generated by the same cellular progenitors which are represented by a distinct population of neural stem cells (NSCs), the so-called radial glia (RG) (*Kanski et al., 2014*). In mammals, neurogenesis precedes gliogenesis (with astrogenesis prior to oligogenesis) and each step of differentiation involves a complex interplay of both intrinsic and extrinsic cellular signals that act on NSCs or precursor cells (*Takouda et al., 2017*). Therefore, a tight regulation from neurogenesis to astrogenesis is critical for the generation of a balanced number of each cell type and proper synaptic circuit activity. Most of the current knowledge comes from studies on the development of the mouse neocortex (**Figure 1.6**) (*Miyata et al., 2010*).

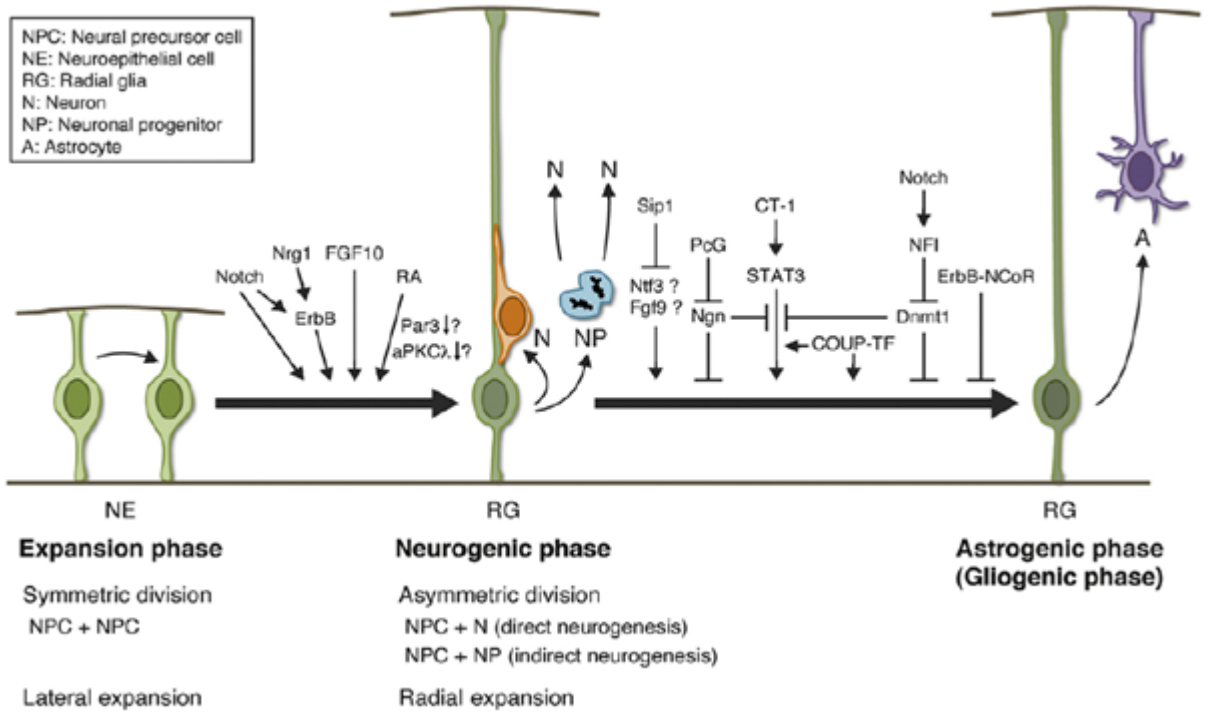

Figure 1.6. Regulation of the gliogenic switch in the mouse neocortex: from neurogenesis to astrogenesis (*Miyata et al., 2010*).

The first step is represented by the ‘expansion phase’ which in mouse starts at early stages of embryogenesis (from ~ E8.5 to E11.5), when most NSCs divide symmetrically to generate other neuroepithelial cells (NEs), that expand their own pool. After this lateral expansion that strictly regulates the amplitude of the cortical surface, the ‘neurogenic phase’ begins and NEs turn into radial glia cells (RGs) (at ~ E14.5), therefore, initiating their commitments. At this stage, RGs switch to asymmetric division to generate neurons (directly or indirectly) and the neocortex mainly expands radially. In the late-gestation and perinatal periods (from E16.5 to the first postnatal days), RGs shift into the ‘gliogenic phase’ and acquire the ability to directly differentiate into astrocytes and oligodendrocytes or to generate intermediate progenitors. Newborn astrocytes are crucial for proper neuronal development since they regulate the development of synapses (*Eroglu and Barres, 2010*).

As emerged, a correct balance between suppressors and activators of astrogenesis plays a fundamental role in determining the fate of the whole brain development and a highly complex array of regulated factors is necessary to modulate astrogenesis inhibition and activation. Since gliogenic factors are already present at early embryonic stages, the JAK/STAT pathway, that represents the canonical pathway mediating astrocytic gene activation, must be silenced (*Uemura et al., 2002; Derouet et al., 2004*). In line with this, during neurogenesis the transcription factor STAT3 and its p300/CBP co-activator complex are impeded from executing their functions at astrocytic promoters (*Kanski et al., 2014*). One of the most important competences that RGs acquire to switch from neurogenesis to astrogenesis, indeed, is the removal of inhibitory epigenetic signals from the *Glial Fibrillar Acidic Protein (GFAP*) promoter, thus allowing precursor cells to originate astrocytes (*Kanski et al,2014*; *Hirabayashi et al., 2009; Namihira et al., 2009; Wilczynska et al., 2009; Cebolla and Vallejo, 2006; Tchieu et al., 2019; Irmady et al., 2011*) (**Figure 1.7**).

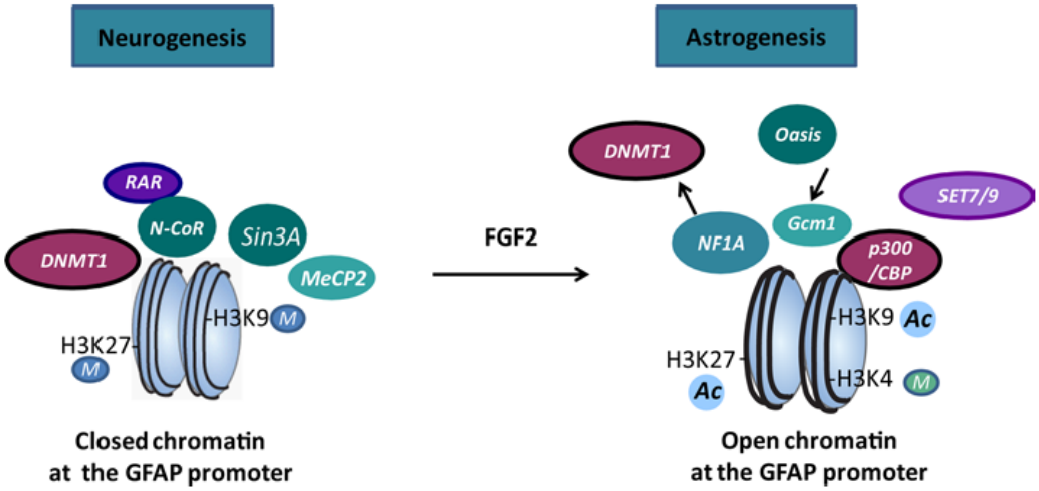

Figure 1.7. Epigenetic remodelling of GFAP promoter (*Kanski et al., 2014*).

As well as for GFAP, several transcription factors promote the onset of astrogenesis by directly or indirectly changing the epigenetic state of other genes crucial for astrocyte specification (*Naka et al. 2008; Namihira et al. 2009; Kang et al. 2012; Nagao et al. 2016*). Of note, astrocyte differentiation is also a response to cytokines secreted by newly generated neurons (*Kanski et al., 2014*).

Once newborn astrocytes are generated in the developing brain, they must maintain their own identity. Therefore, repression of neuronal genes represents a critical point. The key player of neuronal gene repression in astrocytes is considered the Repressor Element 1-Silencing Transcription factor (REST). It was demonstrated that REST targets and inhibits proneuronal genes at the onset of astrogenesis (*Abrajano et al., 2009*) through epigenetic mechanisms (*Huang et al., 1999*). Moreover, in differentiated astrocytes, REST is bound to neuronal gene promoters, like β-III-tubulin, thus blocking their transcription (*Kohyama et al., 2010*). Astrocyte specification is further characterized by the expression of individual markers of the astrocyte lineage; this induction occurs while they are migrating in the CNS to colonize their final destinations in the parenchyma. Three of the mostly used markers to demarcate astrocytic precursors in developmental studies include: GLutamate ASpartate Transporter (GLAST), Fatty Acid Binding Protein 7 (FABP7 / BLBP) and Fibroblast Growth Factor Receptor 3 (FGFR3) (*Shibata et al., 1997; Owada et al., 2008; Liu et al., 2010; Pringle et al., 2003*). GLAST is a functionally active glutamate transporter in astrocytes (chapter 1.2.3), whose expression starts with astrogenesis (*Deneen et al., 2006*). It is considered the most specific marker of astrocyte precursors especially in the spinal

cord, whilst FABP7/BLBP and FGFR3 are expressed also during neurogenesis (*Anthony et al., 2004; Pringle et al., 2003*). Currently, researchers are searching for novel markers able to uniquely distinguish astrocyte progenitors without labelling oligodendrocytes (as they share the same precursors), or able to predict the astrocytic fate.

The bases of astrocyte heterogeneity

Much effort has been spent on identifying specific signals that astrocytes receive during gliogenesis to differentiate and migrate to their final location in the CNS (*Molofsky and Deneen, 2015*). Besides, researchers started also to investigate whether progenitors of astrocytes are a homogeneous or heterogeneous population of cells. Indeed, it was evident that mature astrocytes exhibit a wide range of morphological, molecular and functional differences among populations located in distinct or even within the same region of the adult brain (*Haim and Rowitch, 2017*) (chapter 1.2.2). This high heterogeneity was supposed to have a specific developmental derivation. Indeed, regionally committed RGs would explain the reason why astrocytes still maintain embryonic positional information into adulthood (such as different transcription profiles) and even after injury (*Molofsky and Deneen, 2015; Bayraktar al., 2015*).

In possible good accordance with this model, it is already known that although NEs and RGs appear as a homogeneous population of cells dividing along the ventricles, they are regionally specialized and produce distinct subtypes of neurons (*Campbell et al., 2003; Puelles and Rubenstein 2003*). This diversification among pools of progenitors is established by cell-extrinsic positional signals, such as dorsal BMPs and ventral Sonic Hedgehog (Shh), together with a fine regulation of transcriptional factors. Studies on the earliest stages of development demonstrated that the major domains of RGs along the dorsoventral axis of the forebrain can be divided into distinct areas: the pallium (cortex), the lateral and medial ganglionic eminences, and the septum (*Bayraktar al., 2015)*. Each domain produces different layers of projection neurons with distinct identities (*Campbell et al., 2003; Wonders and Anderson 2006; Flames et al.2007*), within specific spatiotemporal boundaries (*Bayraktar al., 2015*). Therefore, similar mechanisms of patterning programs were proposed to influence astrocytes diversification from glial precursors to maturation (**Figure 1.8**).

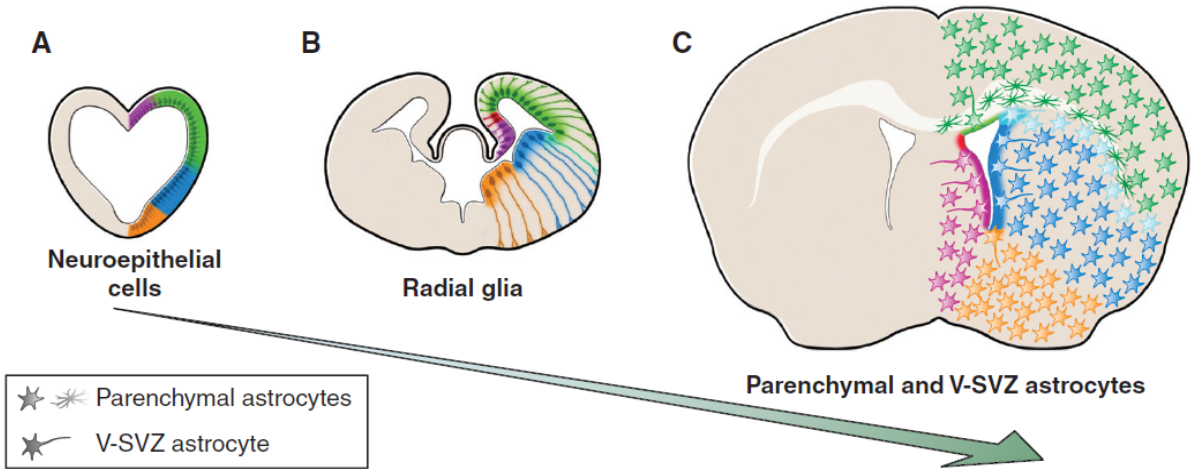

Figure 1.8. Representation of the developmental origins of the heterogeneity of adult parenchymal and ventricular-subventricular zone (V-SVZ) astrocytes. NEs and RGs of the developing forebrain organize in domains: the pallium (green), lateral ganglionic eminence (blue), medial ganglionic eminence (orange), and septum (purple). They generate adult V-SVZ NSCs along lateral ventricles and parenchymal astrocytes that retain positional information signals to control the progeny they originate during proliferation (Figure adapted from *Bayraktar al., 2015*).

One crucial point was understanding whether astrocyte diversity is intrinsically encoded by domain-specific cues or it is driven by neuronal signals. In support to astrocyte independent programming, it was demonstrated that isolated human embryonic stem cells can adopt anterior or posterior identity and generate astrocytes with correspondent regional individuality (*Krencik et al., 2011*). Similarly, astrocytes derived from ventral and dorsal parts of the spinal cord retain their specific features in culture even in the absence of neurons (*Molofsky et al., 2014*), suggesting that information provided by progenitor patterns are sufficient for astrocytes to maintain their own identity.

All in all, these observations indicate that intrinsic mechanisms in astrocytes do generate distinct subtypes of populations that depends on the different regional domain of derivation. In addition, *in vivo* clonal analyses in mice recently confirmed that cerebellar astrocyte heterogeneity derives from a well-defined spatiotemporal program of RG subsets, which dispose of distinct fate potentials (*Cerrato et al., 2018*).

Nevertheless, several experiments demonstrated that also neuronal activity plays a role in determining astrocytic heterogeneity and in programming their responsiveness to local stimuli. Multiple neuronal signals from distinct microenvironments (including the expression of ion channels, membrane transporters and receptors) can trigger intracellular changes in astrocytes that specify their identity (*Haim and Rowitch, 2017*). Both *in vitro* and *in vivo* studies showed how neuronal activity regulates the expression of astrocytic markers, such as glutamate transporters, gap junction proteins, neuropeptide receptors (*Perego et al., 2000; Koulakoff et al., 2008; Genoud et al., 2006*). To give a noteworthy example, the release of Shh by Purkinje neurons determines the unique identity of the two astrocytic subpopulations living in the cerebellum, the Bergman glia and the velate protoplasmic astrocytes (*Farmer et al., 2016*). Therefore, even distinct classes of neuronal cells can direct the expression profile of astrocytes to obtain a specific phenotype.

In accordance with this, the different astrocyte subpopulations populating the mouse neocortex are distributed in patterns dependent on cortical organization. Indeed, cortical astrocytes exhibit morphological and molecular differences depending on neuronal layers (*Lanjakornsiripan et al., 2018*). This layer-specific organization, once established during early postnatal development, mostly persists in adulthood (*Bayraktar et al., 2020*). Neuronal factors do regulate the formation of this astrocyte layer distribution, as post-mitotic L4-specific neuron identity is necessary for the generation of superficial-layer astrocyte identity. The inversion of radial glial polarity and neuronal layers causes in turn an inversion of deep-layer astrocyte identity, with an aberrant location of upper-layer astrocytes across cortical depth. Taken as a whole, these results indicate that layer-dependent neuronal cues are crucial for directing the development of astrocytic cortical layers as well.

1.2.2 Astrocyte populations

How to identify different astrocyte populations

Morphology represents a fundamental characteristic that allows to distinguish astrocyte populations from each other and from other cells of the CNS. The first study that highlighted the extraordinary heterogeneity of astroglial cells and the complexity of their networks dates back to the 19th century, when Camillo Golgi studied neural cells using his silver-chromate staining technique (*Golgi C., 1870*). The word itself

astrocyte (from the Greek equivalent '*star-like cell'*) was introduced in 1895 by von Lenhossék to indicate the peculiar shape of a subtype of glial cells respect to other parenchymal glia 'spongiocytes' (*Lenhossék M., 1895*). Finally, the use of the term *astrocytes* for denoting all parenchymal neuroglia was proposed by Santiago Ramon y Cajal in the early 1900s. He developed an astroglia-specific gold and mercury chloride-sublimate staining technique to label GFAP positive cells and noticed substantial differences in their structure depending on the brain region considered (*Garcia-Marin et al., 2007*). Indeed, astrocyte morphology is tightly associated with their origin and regional function (*Bayraktar al., 2015; Verkhratsky and Nedergaard, 2018)*.

The molecular machinery that controls all different shapeshifts from the cylindrical RGs to the great complexity of mature astrocytes is not completely understood yet. One of the key reasons for this lack of knowledge is the limit of pursuing exhaustive mechanistic studies *in vitro.* Indeed, astrocytes cultures in serum-enriched cultures acquire a polygonal morphology which is far away from the *in vivo* arborization (*McCarthy and de Vellis, 1980*). Moreover, they maintain an immature transcriptional profile with respect to astrocytes matured in living brains (*Foo et al., 2011*). Of course, astrocyte morphogenesis and cytoskeletal organization of stellate astrocytes are the products of an interplay among microtubules, intermediate filaments, and actin cytoskeleton (*Schiweck et al., 2018*). Indeed, mature astrocytes dispose of denser microtubule networks within their main processes than immature cells (*Peters and Vaughn, 1967; Eom et al, 2011*). Similarly, proteins of the intermediate filament group finely change their expression along with maturation and constitute the major components of the main processes (*Bushong et al., 2002*). While astrocyte progenitors express vimentin, nestin and synemin, the mature and differentiated astrocytes express only GFAP and vimentin as essential subunits for polymerization (*Sultana et al., 2000*). The last group of structural proteins that regulate astrocyte morphology is represented by the actin cytoskeleton, that is controlled by Rho GTPases. *In vitro* experiments indicated that the shapeshift towards stars-like cells is promoted by the increase in the Rac1 activity (that remodel contractile fibers into branched actin arrays) and by the inhibition of the ROCK-RhoA-axis (*Schiweck et al., 2018; Zeug et al., 2018).* Lastly, connexin 30 (Cx30), one of the two main astroglial subunits of the gap-junctions expressed postnatally (chapter 1.2.3), regulates *in situ* the extension and ramification of astrocytic processes (*Ghézali et al., 2018*). Indeed, Cx30 sets the orientation of the

astrocyte protrusion through modulation of the laminin/β1 integrinCdc42 polarity pathway.

One of the major difficulties in characterizing astrocyte populations is the lack of unique markers labelling all cells of a specific lineage. As a matter of fact, the great heterogeneity of astrocytes appears to be constructed on a combinatorial expression of the same molecules, with relative concentrations that vary depending on brain region and astrocyte subtypes (*Emsley and Macklis, 2006*; *Verkhratsky and Nedergaard, 2018*). However, many techniques have been refined over the years and new tools have been developed to overcome these limitations.

GFAP has been the most used marker in the last 50 years (*Eng et al., 1971; Uyeda et al., 1972*). It is a protein which counts of 10 different isoforms formed by alternative splicing of which GFAPα is the canonical one, while the functions of the others are still under study (*Moeton et al., 2016*). As previously described, GFAP is a structural protein that belongs to the large family of intermediate filaments. The pattern of GFAP staining is peculiar as it follows regional heterogeneity and development. Therefore, only a fraction of astrocytes is labelled by GFAP *in vivo* (*Walz, 2000*). In particular, the largest subpopulations expressing this marker are located within the juvenile hippocampus (almost 80% of astrocytes are GFAP positive) (*Bushong et al., 2002; Ogata et al., 2002*) and in the cerebellum, with all Bergmann glia immunoreactive for it (*Ango et al., 2008; Nolte et al., 2001*). On the contrary, most of healthy astrocytes in other brain regions are poorly stained with anti-GFAP antibodies (85% of cortical astrocytes are negative for GFAP), unless very sensitive techniques are used (*Walz and Lang, 1998; Kimelberg et al., 2004*). Indeed, GFAP expression is pathologically upregulated in the whole brain after a switch into reactive astroglia, such as in the presence of a brain injury or inflammation (*Brahmachari et al., 2006*). GFAP immunolabelling still represents a very useful tool to perform morphological studies as it marks the major processes of astrocyte cytoskeleton and it allows to reconstruct their arbour (*Connor and Berkowitz, 1985*). Parameters that can be obtained include GFAP expression changes and intracellular distribution, astrocytic shape, number and length of processes, branch point numbers and branching complexity (Sholl analysis) (*Zeug et al., 2018*). Of note, peripheral and perisynaptic thicker processes remain unstained (*Reichenbach et al., 2010; Simard et al., 2003*). Another important marker to characterize astrocytes in the CNS both under physiological and pathological conditions is represented by the glycoprotein S100β, which acts as a calcium binding

protein (*Donato et al., 2013*). Even if S100β stains more astrocytes than GFAP in general, its cell specificity is much lower (*Steiner et al., 2007*). Moreover, S100β labels the nuclei, the cytoplasm, and the fine processes of astrocytes but not the major processes, resulting inappropriate for morphological characterizations when used alone (**Figure 1.9**).

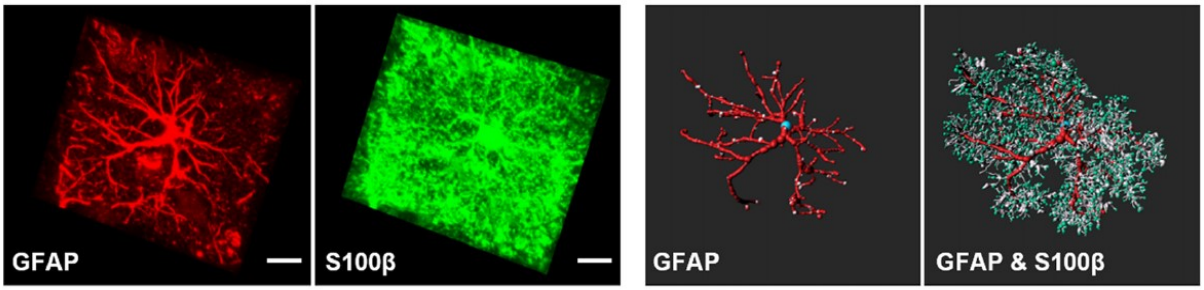

Figure 1.9. *in vivo* study of astrocyte morphology. Example of a Z-projection acquired with a confocal microscope (left) of a cortical protoplasmic rat astrocyte (P14) stained for GFAP (red) and S100B (green). The 3D reconstruction highlights the labelling of main processes by GFAP, whilst S100β refines the myriads of fine positive processes (*Schiweck et al., 2018*).

Other common astrocytic markers are the key enzyme of foliate metabolism ALdehyde DeHydrogenase 1 family member L1 (ALDH1L1), the glutamate transporters EAAT-1 (GLAST) and EAAT-2 (GLT-1), the Glutamine Synthetase (GS) enzyme, the water channel Aquaporin 4 (AQP4) and the connexins Cx30 and Cx43. Notably, they are mainly retained in the cytoplasm, they show punctate pattern along processes and they are often concentrated in the fine perisynaptic processes (the endfeet) (*Cahoy et al., 2008; Waller et al., 2016; Yang et al., 2011; Verkhratsky and Nedergaard, 2018*). Therefore, none alone can be used for complete morphological characterizations. To overcome this, new molecular tools were exploited and several genetically encoded markers have been generated to perform detailed morphological examinations *in vivo*. Currently, the most used approach is represented by the engineering of different mouse models to express probes under the control of astrocyte-specific promoters (i.e. GFAP, ALDH1L1, GLAST) to enhance a fluorescent signal in the whole cell. A notable example is represented by the generation of transgenic mice in which astrocytes express an enhanced GFP (EGFP) under the control of the mouse or human GFAP promoters to label protoplasmic, fibrous or reactive astrocytes (*Nolte et al., 2001*;

Suzuki et al., 2003) (**Figure 1.10**). This staining results an ideal source to perform volumetric analyses and 3D reconstructions (*Emsley and Macklis, 2008*).

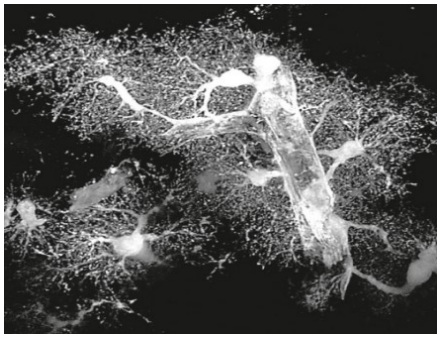

Figure 1.10. EGFP-expressing mouse cortical protoplasmic astrocytes around a blood vessel. Figure adapted from *Verkhratsky and Nedergaard, 2018*.

Of note, in parallel with the refinement of labelling techniques to obtain a precise three-dimensional characterization, methods for image acquisition and data analysis have been improved. Modern microscopy systems (such as serial section confocal and electron microscopy, STED, super-resolution, two-photon microscopy etc.) and the combined use of softwares for mathematical reconstructions allowed to overcome the diffraction limits of the conventional light microscopy (*Zeug et al., 2018; Yu et al., 2020*). Astrocyte heterogeneity might be investigated also analyzing the transcriptional profile, providing that the specific developmental stage is considered. Indeed, as expected, the expression of astrocytic genes changes along with maturation. A paradigmatic example is given by a study carried in the mouse cortex and reporting that immature astrocytes (P7-8) highly express genes involved in cell proliferation and development that are not astrocyte-specific; mature astrocytes (P17-30), instead, express genes typical of their differentiation, including those specifying secreted proteins crucial for synaptic plasticity and circuit functioning (*Cahoy et al., 2008*). An additional element to consider is that the number of astrocytes in the murine brain increases 6-8 times during the first three postnatal weeks (*Bandeira et al., 2009*), so astroglial cells coexist with their precursors in the developing cortex at multiple developmental stages (*Ge et al., 2012*). Moreover, the timing of proliferation and maturation of region-specific populations is different and follows brain development (*Molofsky and Deneen, 2015*). For example, cerebellar astrocytes are one of the last astroglial population to mature as this cerebral area fully develops at P30 (*Fleming et al., 2013; Marazziti et al., 2013*). Researchers dispose of several online databases of astrocyte transcriptomes and proteomes from various mouse brain regions and developmental stages (*Yu et al., 2020*). Nevertheless, an exhaustive molecular characterization of each population of

mature astrocytes is still in progress (*Verkhratsky and Nedergaard, 2018*). Past genomic comparisons performed among astrocytic populations expressing 'classic' markers such as GFAP, GLT-1 or ALDH1L1 (*Lovatt et al., 2007; Yang et al., 2011*) did not show significant difference as they are co-expressed by most astrocytes (*Verkhratsky and Nedergaard, 2018*). Unbiased single-cell transcriptomics might permit to bypass the observed obstacles. Indeed, this approach has already been successfully used in adult mouse cortex and hippocampus revealing the presence of five unique and spatially clustered molecular astrocytic groups, that also exhibit distinct Ca^{2+} transient properties (*Batiuk et al., 2020*).

Main astrocyte populations in the mammalian brain

To date, astrocytes have been classified into different populations with distinct morphologies and functions. Herein I will mention only the most important, at least for this thesis.

- PROTOPLASMIC ASTROCYTES

Protoplasmic astrocytes represent the major astrocyte population in the grey matter of brain and spinal cord. In rodents, they are characterized by a small round soma from which 5 – 10 primary processes depart and branch to form a highly elaborated arborization (they can be polarized in one direction). They end with very thick processes, which origin the typical spongiform appearance (*Oberheim Bush and Nedergaard, 2017; Verkhratsky and Nedergaard, 2018*). The overall morphology of protoplasmic astrocytes differs between and within different anatomical structures. For example, while in the CA1 hippocampal region they can be fusiform, elongated and spherical (*Bushong et al., 2002; Nixdorf-Bergweiler et al., 1994*), several other shapes are observed in the rest of the brain (*Emsley and Macklis, 2008; Olude et al., 2015*). Both in rodents and humans, protoplasmic astrocytes are organized into territorial domains with a minimal overlap, which is confined to the finest processes of the adjacent cells only (*Bushong et al., 2002; Ogata and Kosaka, 2002; Oberheim et al., 2009; Freeman, 2010*). These short and ultra-thick processes (perisynaptic processes are in range of 100-200 nm) are the main reason of the great morphological plasticity (*Heller and Rusakov, 2015*) (further details in chapter 1.2.3). Moreover, at least one process per astrocyte contacts a blood vessel and forms a perivascular endfeet (*Verkhratsky and Nedergaard, 2018*). Remarkably, it was calculated that a single

protoplasmic astrocyte in the rodent cortex contacts 4-8 neurons, surrounds almost 300-600 neuronal dendrites and encompasses an average of 100,000 synapses within its domain (*Halassa et al., 2007; Oberheim et al., 2006; Oberheim et al., 2009*). Of note, human protoplasmic astrocytes are much more complex (nearly by a 16.5-fold increase in volume), they send on average 37.5 main GFAP-positive processes in multiple directions, and a single cell can provide cover for up to one million of synapses (*Oberheim et al., 2009*).

- VELATE ASTROCYTES

Velate astrocytes represent a variation of protoplasmic astrocytes and are found in regions of the brain densely packed with neurons (i.e. olfactory bulb or granular layers of cerebellar cortex) (*Chan-Palay et al., 1972*). These cells are characterized by a small soma and quite short processes with a high surface-volume ratio. In the cerebellum they form a sort of envelopes of vellum around groups of granule neurons and glomeruli, probably to isolate different synaptic structures and fibers (*Buffo and Rossi, 2013; Hoogland and Kuhn, 2010; Kita et al., 2013*).

- FIBROUS ASTROCYTES

These astrocytes populate the white matter of both the brain and spinal cord, the optic nerve, and the nerve fiber layer of the retina (*Verkhratsky and Nedergaard, 2018*). The soma of fibrous astroglia is organized in rows between axons and the main processes project far away radially, following the direction of the axon bundles (*Lundgaard et al., 2014; Oberheim et al., 2009*). Unlike the protoplasmic, fibrous astrocytes dispose of much fewer terminal fine processes; moreover, they overlap, reflecting the absence of the characteristic domain organization of the protoplasmic cells. Given the presence of myelinated axons, the processes of fibrous astrocytes send several perivascular or subpial endfeet that contact the nodes of Ranvier. Thus, they provide metabolic support to surrounding cells, but they have no role in modulating synaptic activity due to morphological limitations (*Butt et al., 1994; Oberheim Bush and Nedergaard, 2017*).

- RADIAL GLIA (only in embryogenesis)

As already mentioned, radial glia defines the group of cells involved in astrogenesis and development. They are the bipolar cells that extend through the thickness of the neural tube and that are considered universal neural precursor cells (*Verkhratsky and Nedergaard, 2018)*.

- RADIAL ASTROCYTES

Radial astrocytes indicate a multifaced group of cells within different regions of the adult mammalian brain that have in common a radial-like morphology. They perform very different functions, which are invariably associated with their local homeostasis (*Verkhratsky and Nedergaard, 2018*). Among the most important, we find the cerebellar radial astrocytes, also referred as Bergmann glia. These cells located in the Purkinje cell layer have small bodies and extend three to six processes to the pia, which in turn send highly elaborated branches to cover synapses at the terminals of granule neurons. A single Bergmann glia can contact up to 8,000 synapses and it was estimated that in rodents a single Purkinje neuron is surrounded by 8 Bergmann glial cells, whose processes form a 'tunnel' around the dendritic arborisation (*Grosche et al., 1999; Grosche et al., 2002*).

1.2.3 The functions of astrocytes and their roles at synaptic level

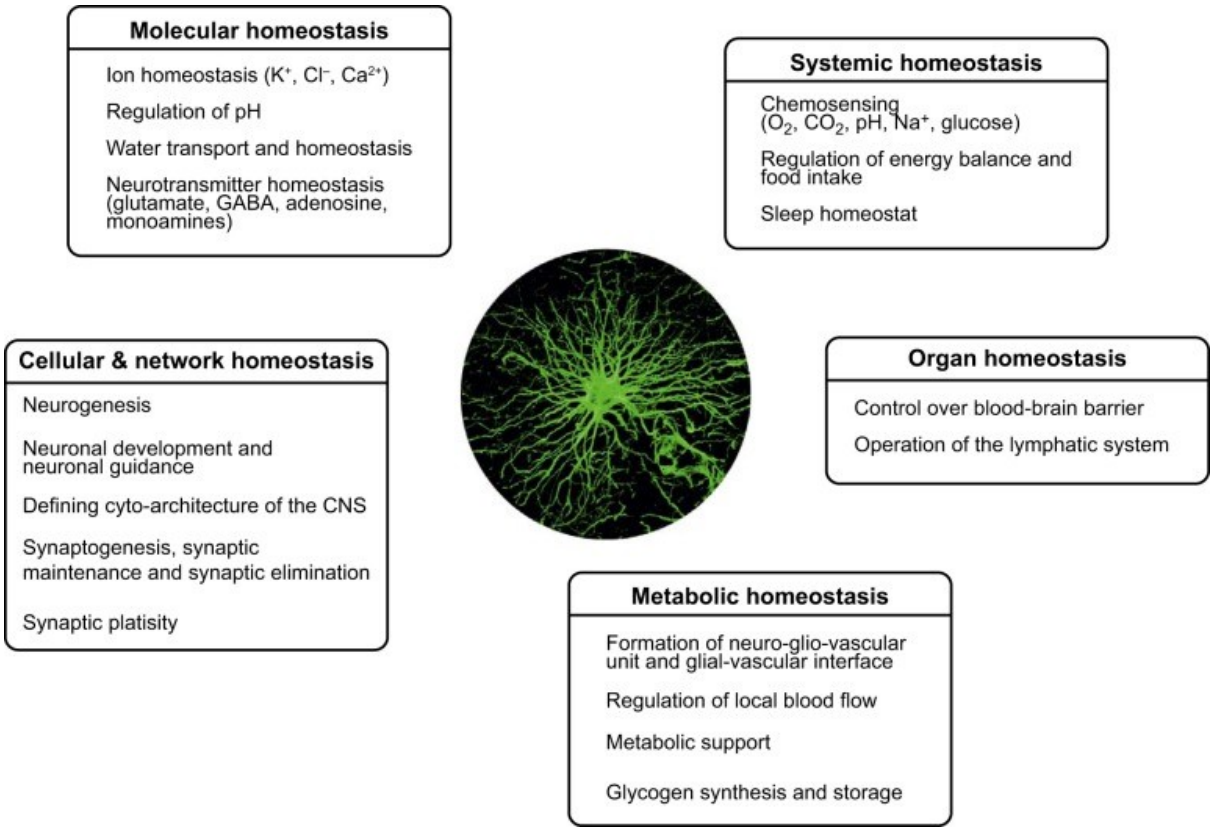

Figure 1.11. Schematic representation of the astrocytic functions characterized so far in the healthy brain (*Verkhratsky and Nedergaard, 2018*)

Although heterogeneity confers distinct characteristics to each population (chapter 1.2.2), astrocytes play crucial roles within the CNS that can be summarized in the concept of maintaining homeostasis at multiple levels of organization (*Verkhratsky and Nedergaard, 2018*) (**Figure 1.11**).

Of note, astroglial cells drastically change in response to immune attack, chronic neurodegenerative diseases, or acute trauma into the so-called 'reactive state'. This implies morphological, transcriptional and functional modifications of astrocytes that, depending on the initiating injury, can lead to different reactive phenotypes, with specific properties (*Liddelow and Barres, 2017*). For a long time, they have been divided into the A1 neuroinflammatory reactive state, usually considered harmful (e.g. it is destructive for synapses), and the ischemia induced A2 reactive state, which was considered helpful or reparative (A2 astrocytes express many neurotrophic factors to promote neuronal survival, growth and repair). However, it was recently published a consensus statement that pinpoints astrocyte reactivity as a complex phenomenon far away from simple binary phenotypes and, instead, characterized by multiple states that can be adopted based on the context (*Escartin et al., 2021*).

Astrocytes exploit all their functions through intra and inter-cellular crosstalks with adjacent astrocytes or other cell types, respectively (*Hu et al., 2016)*. Indeed, they represent active communication elements in the CNS that reuptake and release a wide variety of regulatory signals in multiple networks. Astrocytes can form different functional structures that are listed below.

- Gap junctions (GJs), through the coupling of hemichannels formed by connexins (Cxs). In particular, the two main connexins, Cx30 and Cx43, couple different astrocytes together to allow rapid intracellular exchanges of different small molecules such as ions and metabolites (*Xing et al., 2019*). Of note, Cxs functions extend beyond GJ communication. Indeed, gap junction channels can be also expressed unpaired on astrocyte membrane to provide adhesion with other cells or allow the release of gliotransmitters (*Theis et al., 2005*; *Elias et al., 2007*).
- The blood-brain barrier, through astrocytic projections (endfeet) that surround the endothelial cells of brain vessels. This allows biochemical support (uptake of oxygen and glucose above all) and regulation of cerebral blood flow in the brain (*Howarth, 2014*)
- The 'tripartite synapse', through the physical enwrapping of pre- and post-synapses by astrocytic processes. This term conceptualizes the reciprocal influence and

bidirectional communication between astrocytes and neurons (*Perea and Araque, 2009*). Astrocytes exchange information with neurons to modulate the structure and function of both excitatory and inhibitory synapses (chapter 1.2.4 and 1.2.5) while, contextually, synaptic activity regulates astroglial cells' responses (*Farhy-Tselnicker and Allen, 2018*). However, this concept has been recently refined introducing the term 'multipartite synapse' indicating a functional structure that comprehend processes of the nearest microglial cells and the extracellular matrix (ECM) present in the synaptic cleft (*Verkhratsky and Nedergaard, 2018*).

In this chapter, I will discuss the astrocytic contribute to maintain the synaptic homeostasis. Then, I will consider which molecules are released by astrocytes ('gliotransmitters') to control neuronal functions (chapter 1.2.4). Because of its relevance for my thesis, I will also dedicate an independent chapter to astrocytes and synaptogenesis (1.2.5).

Astrocytes control synaptic homeostasis through their processes, that dispose of unique morphological features to enwrap synapses and express specific proteins to keep ions and neurotransmitters at physiological levels.

In the CNS, half of all synapses are covered by astrocytic terminal extensions protruding from peripheral processes, that are also known as Peripheral Astroglial Processes (PAPs) (*Derouiche, 2003; Derouiche et al., 2002*; *Reichenbach et al., 2010*). Astrocytes cover a variable percentage of local synapses depending on the brain region and the neuronal sub-type. For example, PAPs enwrap 29-56% of excitatory synapses in the neocortex (*Bernardinelli et al., 2014),* while this percentage can increase up to 90% for the synapses located in layer IV of the somatosensory cortex (*Bernardinelli et al., 2014*), for the large mushroom spines and perforated synapses positioned in the hippocampus (*Witcher et al., 2007*), and for the synapses formed by climbing fibers of Bergmann glial cells around Purkinje neurons within the cerebellum (*Grosche et al., 1999*; *Xu-Friedman et al., 2001*). Moreover, astrocytic processes totally cover and isolate whole synaptic glomeruli of the olfactory bulb, sensory thalamus or cerebellar cortex (*Reichenbach et al., 2010*). PAPs membrane represent ~ 80% of the total cell surface area of astrocytes but they contribute only to a minor fraction of the astrocytic volume (~ 4-10%) (*Grosche et al., 2002*). Indeed, they are extremely thin, with an average diameter ranging from less than 100 nm to a maximum of 200 nm (*Reichenbach et al., 2010*); this characteristic is extremely relevant to allow astrocytic processes to reach and control single synapses.

Interestingly, PAPs generally lack organelles (*Peters et al., 1991; Reichenbach et al., 2010*), with sporadic exceptions for small spherical mitochondria (*Derouiche et al., 2015*), but they dispose of rapid filopodial movements, which allow fine rearrangements in response to environmental stimuli (*Hirrlinger et al., 2004*; *Lavialle et al., 2011; Genoud et al., 2006*; *Bellesi et al., 2015*). In accordance with their adaptability, it was recently demonstrated that local translation does occurs in PAPs and that the pool of mRNAs at the synaptic interface is highly specific and changes depending on brain status or neuronal activity (*Mazaré et al., 2020*). The repertoire includes genes involved in iron homeostasis, translation, cell cycle and cytoskeleton, that together allow astrocytes to regulate the volume of synaptic cleft and control the availability of ions, neurotransmitters and transporters.

The balance of ions within the nervous system is crucial for proper regulation of neuronal excitability and circuit functioning. Astrocytes control these aspects by expressing several ion channels and transporters according to astrocytic subtype and brain region (*Olsen et al., 2015*; *Hu et al., 2016*). They include channels for the regulation of the influx-efflux of potassium, chloride, extracellular calcium and the ones committed to the regulation of pH. Besides this, astrocytes are essential for the rapid cerebral turnover of neurotransmitters necessary to maintain synaptic transmission and avoid excitotoxicity. Indeed, they are the major responsible for removing glutamate from the synaptic cleft, therefore blocking the excitatory signal and preventing the spillover to adjacent synapses (*Marcaggi and Attwell, 2004; Tzingounis and Wadiche, 2007)*. Almost 80% of extracellular glutamate of the whole brain is recovered by astrocytes using the specific excitatory amino acid transporters GLAST1 (glutamate-aspartate transporter 1) (*Storck et al., 1992*) and GLT-1 (glutamate transporter 1) (*Pines et al., 1992*). Moreover, astrocytes ensure new replenishment of glutamate to neurons as they dispose of unique enzymes. Indeed, thanks to the pyruvate carboxylase, they are the sole *de novo* synthesizers of glutamate from glucose in the CNS (*Hertz et al., 1999; Schousboe et al., 2014*), and they exclusively express Glutamine Synthetase (GS), an enzyme involved in glutamate turnover (*Norenberg and Martinez-Hernandez, 1979*) (**Figure 1.12**).

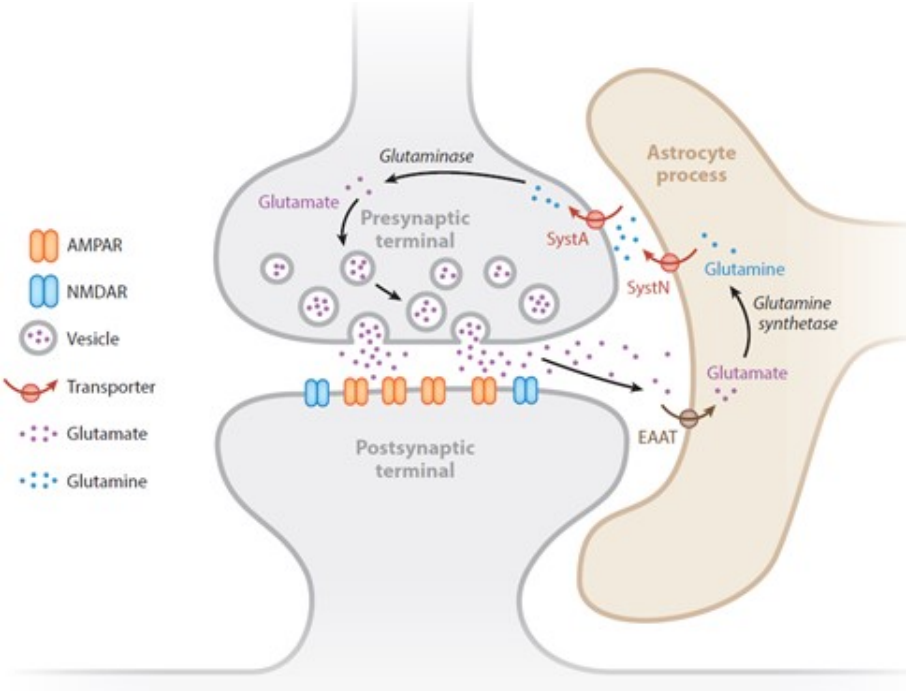

Figure 1.12. The glutamate-glutamine cycle regulated by astrocytes at the perisynaptic level (*NJ Allen, 2014*).

GS detoxifies the ammonium accumulated in the brain during neuronal activity (*Cooper and Plum, 1987; Marcaggi et el., 2004*) and catalyzes the conversion of glutamate into glutamine, that is in turn internalized by neurons to reobtain glutamate in excitatory neurons or further converted into GABA in inhibitory neurons ('glutamine-glutamate (GABA) shuttle' (*Broer and Brookes, 2001; Hertz, 2013*)). Hence, glutamate homeostasis also affects inhibitory neurotransmission. In line with their role of maintaining homeostasis, astrocytes also directly remove extracellular GABA through the specific GABA transporters (GATs) GAT-1 and GAT-3 (*Mederos and Perea, 2018*), therefore affecting GABAergic transmission and enhancing synaptic depression (*Boddum et al., 2016; Yu et al., 2018*).

Lastly, astrocytes finely regulate synaptic transmissions by removing and inactivating adenosine and monoamines (*Lovatt et al., 2012*; *Studer et al., 2006*; *Hertz et al., 2004*; *Kintner et al., 2007; Riederer, 1987; Saura et al., 1992*, *Hansson, 1985; Karhuenen et al., 1995)*.

1.2.4 Gliotransmitters and synaptic transmission

Besides regulating the levels of extra-cellular ions and neurotransmitters through clearance mechanisms, perisynaptic astrocytes can, contextually, release different neuroactive substances to modulate neuronal activity. Indeed, astrocytes are highly secretory cells and different families of astrocyte-secreted substances have been identified so far (*Petrelli and Bezzi, 2015*). These molecules are the so-called 'gliotransmitters', which are secreted by astrocytes with distinct molecular mechanisms including diffusion through membrane channels, translocation via plasmalemmal transporters and vesicular exocytosis (*Araque et al., 2014; Haydon and Carmignoto, 2006; Perea et al., 2009; Volterra and Meldolesi, 2005; Zorec et al., 2016*). The specific signals responsible for gliotransmitters release are still object of great debate and controversy (*Bazargani and Attwell, 2016; Savtchouk and Volterra, 2018; Durkee and Araque, 2019*). Pre-synaptic neurotransmitters generate transient elevations of calcium concentration in fine processes that trigger the release, but this is not the sole mechanism. Indeed, activated microglia and proinflammatory molecules can also initiate astrocytic secretion (e.g. TNFα, chemotactic cytokines, prostaglandins, etc.) (*Agulhon et al., 2012*). Therefore, gliotransmission is a complex phenomenon consisting of several forms, probably non mutually exclusive, that requires in-depth investigations to be fully understood.

Based on current knowledge, gliotransmitters can be divided into 'established' and 'emerging' substances (full list in *Petrelli and Bezzi, 2015*). Herein, I will only report the most relevant for the context of my thesis.

The 'emerging' category consists of neuroactive substances released on timescales ranging from milliseconds to minutes that can directly regulate synaptic transmission and plasticity (*Petrelli and Bezzi, 2015*). They include neurotransmitters and neuromodulators.

Astrocytes release several neurotransmitters into the CNS that either directly regulate neurons or act through surrounding cells to modulate excitatory and inhibitory transmission. The enhancement of synaptic activity is mainly supported by the release of glutamate, that modulates ionotropic and metabotropic receptors on both neurons and other glial cells (*Bezzi et al., 1998; Parpura et al., 1994*; *Araque et a., 1998; Bezzi et al., 2004; Angulo et al., 2004; Jourdain et al., 2007; Min and Nevian, 2012; Martin et al., 2015*). Another key player involved in the positive regulation of basal synaptic

transmission is represented by ATP, which is released by astrocytes in the extracellular space via exocytosis and hydrolysed to adenosine (*Hines and Haydon, 2014*). This secreted molecule acts on pre-synaptic A_{2A} receptors, excitatory P2X receptors or triggers pleiotropic effects on neurons and glial cells via P_2Y receptors (*Gourine et al., 2010; Pascual et al., 2005*). On the other hand, astrocytes enhance inhibitory transmission by secreting GABA, which modulates $GABA_A$ and $GABA_B$ receptors (*Lee et al., 2010; Jo et al., 2014*), and glycine (*Eulenburg et al., 2010).* Lastly, astrocytes mediate synaptic development and function thought Neuropeptide Y (*Prada et al., 2011*). In addition to neurotransmitters, astroglial cells also release neuromodulators; in particular, the secretion of D-Serine, a co-agonist of N-methyl-D-aspartate (NMDA) receptors, is critical for the formation of LTP in hippocampal Schaffer collateral-pyramidal neurons (*Martineau et al., 2013; Henneberger et al., 2010; Fossat et al., 2012; Martineau et al., 2014; Mothet et al., 2005; Pan et al., 2015).*

The 'established' substances are molecules that are released on timescales that range from minutes to days, and that regulate metabolism, energy supply (as well as cerebral blood flow), inflammation and synaptogenesis. They include metabolic substrates, lipids, eicosanoids, inflammatory factors, growth factors and synaptogenic molecules (chapter 1.2.5).

Glycogen is the main energy store in the brain and is found almost exclusively in astrocytes (*Bak et al., 2018*). Its metabolism is essential to support several physiological processes, including those dependent on lactate and glucose levels (*Barros and Deitmer 2010*). Through glycogen breakdown, indeed, astrocytes produce and release L-lactate, which is a powerful source of energy for neurons (*Kasparov, 2016*), and it is fundamental for maintaining synaptic strength (LTP), modulating synaptic plasticity, triggering the learning-induced mRNA translation in excitatory/inhibitory neurons, and releasing norepinephrine in locus coeruleus neurons (*Suzuki et al., 2011; Tang et al., 2014; Yang et al., 2014; Descalzi et al., 2019; Calì et al., 2019*). Moreover, glycogen breakdown allows astrocytes also to produce glucose, which is the main source of energy for the mammalian brains. At synaptic level, glucose sustains glutamatergic transmission and maintains neurotransmitter homeostasis (*Bak et al., 2006*; *Rouach et al., 2008*).

Apart from metabolic substrates, astrocytes can take advantage from their lipid metabolism to control synaptic transmission. In fact, they release sphingosine and its metabolite sphingosine 1-phosphate (S1P), which are lipid mediators that stimulate

excitatory transmission by controlling pre-synaptic glutamate exocytosis (*Sato et al., 2007*). In detail, sphingosine directly enhances vesicle release through the formation of SNARE fusion complexes (*Darios et al., 2009*), while S1P promotes neurotransmission targeting Synapsin I, a presynaptic protein that controls the availability of synaptic vesicles for exocytosis (*Riganti et al., 2016*).

Another class of astrocyte-secreted molecules involved in the control of synaptic activity, cerebral blood flow and inflammatory response is represented by eicosanoids. They include mediators such as arachidonic acid, prostaglandins, epoxyeicosatrienoic acid and 20-yhdroxyeicosatetraenoic acid (20-HETE) (*Bezzi et al., 1998; Mulligan and MacVicar, 2004; Zonta et al., 2003*). Curiously, even an inflammatory factor such as Tumor Necrosis Factor α (TNFα), is involved in the homeostatic activity-dependent regulation of synaptic connectivity, when supplied by astrocytes at the synaptic level (*Beattie et al., 2002; Stellwagen and Malenka, 2006*).

Lastly, astrocytes release various neurotrophins both during development and in adulthood to modulate synaptic development and functions (*Poyhonen et al., 2019*). Of note, astroglial cells are the main recipient of neuron-derived BDNF in its mature form (*Stahlberg et al., 2018*), whose release regulates synaptic formation (*Bergami et al., 2008; Gomez-Casati et al., 2010*), neuronal morphology and synaptic plasticity (*Pins et al., 2019*).

As emerged, astroglial cells control synaptic activity and modulate different circuits through the release of several gliotransmitters (*Perea et al., 2009; Mederos et al., 2018*). Notably, the secretion of these molecules depends on the inputs received but also on the ability of astrocytes to decipher CNS needs and context. Indeed, on the one hand, astrocytes can directly propagate excitatory synaptic transmission in response to glutamatergic activation. This triggers the release of different neurotransmitters such as glutamate, D-serine and ATP (or adenosine), that in turn bind to different pre- and post-synaptic receptors to support the propagation of excitatory signaling (e.g. the enhancement of short- and long-term glutamatergic synaptic plasticity) (*Jourdain et al., 2007; Bonansco et al., 2011; Panatier et al., 2011; Perea and Araque, 2007; Henneberger et al., 2010*).

On the other hand, astrocytes enhance or inhibit excitation by deciphering signals from inhibitory circuits. As a matter of fact, they can decode the frequency and the duration of the different networks of interneurons and positively or negatively regulate the excitatory synaptic transmission in an activity and time- dependent manner (*Perea et*

al., 2016; Bartos et al., 2007; Kullmann, 2011; *Covelo & Araque, 2018; Deemyad et al., 2018; Matos et al., 2018; Perea et al., 2016*). Therefore, a defective or aberrant release of gliotransmitters causes alterations in signal propagation, driving an unbalanced E/I ratio at the circuit level that affects the whole brain health.

1.2.5 Astrocytes and synaptogenesis

In good accordance with their importance for homeostasis and brain activity, astrocytes actively regulate synapse formation since the earliest steps of development. This discovery dates back at least 20 years ago, when it was observed for the first time that synapse formation coincides with the appearance of astrocytes (*Correa-Gillieron & Cavalcante,1999*). Moreover, the main periods of synaptogenesis (second and third postnatal weeks in mice) only occur after the maturation and differentiation of astrocytes (*Freeman, 2010*). To date, we know that astrocytes can selectively control the type of synapse to form on a neuron during the refinement of neuronal circuits. Astrocyte-derived signals, indeed, can regulate the formation, functional maturation, and refinement of glutamatergic (*Ullian et al., 2001*), GABAergic (*Elmariah et al., 2005; Hughes et al., 2010*), glycinergic (*Cuevas et al., 2005*) and cholinergic (*Reddy et al., 2003*) synapses. Several factors are involved and the responsiveness of neurons is closely related to their developmental stage (*N.J. Allen, 2014; Chung et al., 2015*). In the early stages, physical contact between astroglial cells and neurons is a critical permissive first step to induce synapse formation. Then, neurons undergo a developmental switch that makes them responsive to soluble synaptogenic signals from astrocytes (*Ullian et al., 2001; Hama et al., 2004; Barker et al., 2008*).

- *Synapse formation and maintenance*

Most of the secreted molecules identified so far are involved in the regulation of glutamatergic synapse formation (**Figure 1.13**), however some factors cooperate to balance the inhibitory transmission (*NJ Allen, 2014*).

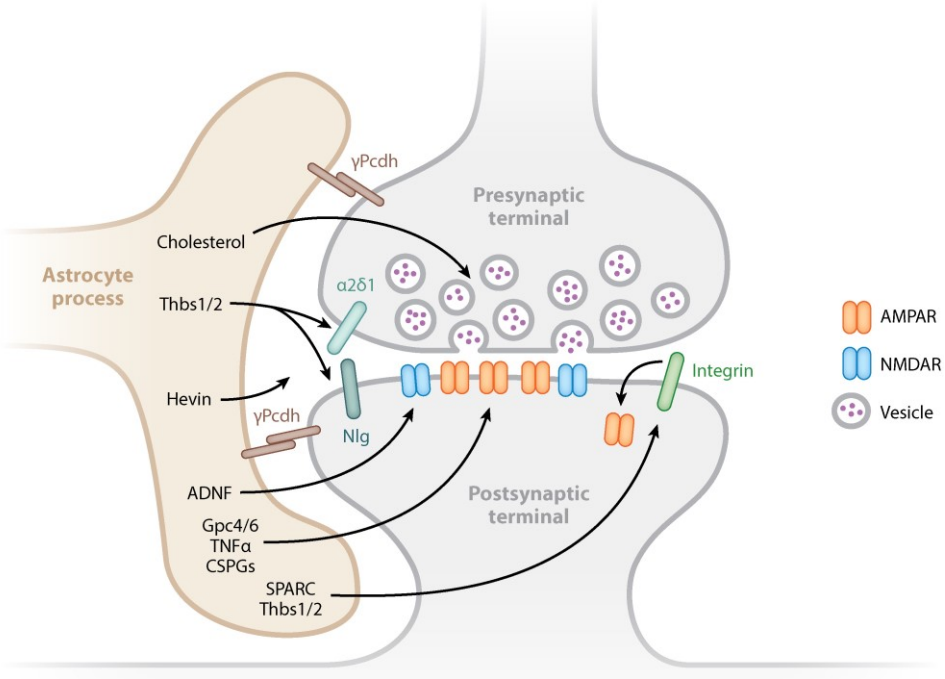

Figure 1.13. Astrocytic pathways that regulate glutamatergic synapse formation (*NJ Allen, 2014*).

The first synaptogenic molecule to be identified was cholesterol, a lipid synthesized by astrocytes in the CNS and secreted in complex with ApoE in order to be internalized by neurons (*Goritz et al., 2005; Mauch et al., 2001*). Cholesterol increases the number of vesicles at pre-synaptic terminals and the probability of their release, thus enhancing presynaptic function. Mouse models with alterations in lipid synthesis, indeed, show impairments in cholesterol release from astrocytes, with decreased number of presynaptic vesicles and defective synaptic development (*Deijk et al., 2017*).

Other astrocyte-secreted molecules include Thrombospondins (TSPs), oligomeric multidomain glycoproteins that represent one of the major synaptogenic factors present in the Astrocyte Conditioned Medium (ACM) (*Christopherson et al., 2005; Richer and Eroglu, 2014*). There are five different TSPs in mammals and they are all capable of inducing synaptogenesis, however the most characterized isoforms are: TSP1 and -2, that are mainly expressed by protoplasmic astrocytes, and TSP4 which is mainly expressed by astrocytes that originate from the SVZ and fibrous astrocytes (*Eroglu, 2009; Benner et al., 2013*). Removing TSPs from ACM eliminates the majority of its synaptogenic activity and TSP1/2 double KO mice develop fewer cortical excitatory synapses. Furthermore, in the mouse cortex, TSPs are highly expressed by

immature astrocytes during the first week of postnatal development (a period that corresponds to the initiation of excitatory synapse formation) (*Christopherson et al., 2005*), whereas TSPs levels in adult mice are low and increase only after injury. TPSs are able to rearrange actin cytoskeleton, cell migration and cell attachment through several extracellular proteins and cell surface receptors. The major synaptogenic neuronal receptor for TSPs is represented by the pre-synaptic calcium channel subunit α2δ1 (Cacna2d1) (*Eroglu, 2009*), that is bound by all TSPs isoforms. Of note, TSP1 also interacts with the postsynaptic adhesion protein neuroligin 1 to accelerate excitatory synapse formation (*Xu et al., 2010*).

Recently, Hevin (or SPARC-like 1), that belongs to the Secreted Protein Acidic Rich in Cysteine (SPARC) family of protein, was included in the list of synaptogenic proteins secreted by astrocytes (*Kucukdereli et al., 2011*). Hevin is highly expressed by developing and mature astrocytes in the brain and has been shown to localize at synaptic clefts (*Johnston et al. 1990; Lively and Brown 2008*) where it regulates thalamocortical glutamatergic synapse formation by bridging two neuronal cell adhesion molecules: presynaptic neurexin-1alpha (NRX1a) with postsynaptic neuroligin-1B (NL1B), (*Singh et al., 2016*). In addition, Hevin recruits NL1 and NL1-associated proteins such as PSD95 and NMDA receptor subunits to synapses. Interestingly, Hevin is not able to exert its full activity when present within the ACM. This observation allowed to discover a further astrocyte-secreted protein, SPARC, that is highly homologous to Hevin and specifically antagonizes its synaptogenic function (*Kucukdereli et al. 2011*). In addition, SPARC decreases the number of AMPA receptors at post-synaptic terminals (*Jones et al., 2011*), prevents the maturation of cholinergic presynaptic terminals and triggers a program of synapse elimination (*Albrecht et al., 2012; Lopez-Murcia et al., 2015*). All in all, the opposing actions of Hevin and SPARC control the rate and extent of synapse formation and maturation in the CNS. Of note, while astrocytes express Hevin throughout all adulthood, SPARC expression in highly reduced in the adult CNS.

Other astrocyte-derived molecules that are necessary and sufficient to promote excitatory post-synaptic maturation and activity are the matricellular proteins glypican 4 (Gpc4) and 6 (Gpc6) (*Allen et al., 2012*). They both increase the surface level and clustering of the GluA1 subunit of the AMPA glutamate receptor (AMPAR) at post-synapses. Gpc4 and 6 are expressed *in vivo* in the developing CNS (pointing towards a role in synapse initiation) but while Gpc4 is enriched in the hippocampus, Gpc6 is

mainly expressed in the cerebellum. Moreover, they exhibit a divergent expression pattern in the cortex during development, with Gpc6 enriched in the upper cortical layers where VGlut1 synapses are present. The synaptogenic mechanism of Gpcs involves the interaction with presynaptic RPTPδ and RPTPδ receptors, which induces the secretion of the AMPAR clustering factor Neuronal Pentraxin 1 and promotes synapse formation (*Farhy-Tselnicker et al., 2017*). In support of the importance of the role of Gpcs at postsynaptic level, *Gpc4* KO mice show defective synapse formation, decreased amplitude of excitatory synaptic currents in the developing hippocampus and reduced recruitment of AMPARs to synapses (*Allen et al., 2012*).

Further secreted-factors that positively regulate excitatory postsynaptic receptors include:

- Tumor necrosis factor 1 alpha (TNFα), that increases AMPAR levels at existing synapses and decreases $GABA_A$ receptors at inhibitory synapses, leading to overall increased neuronal activity. It is also involved in the homeostatic scaling to maintain neuronal network activity (chapter 1.2.4) (*Beattie et al., 2002; Stellwagen et al., 2005; Stellwagen and Malenka, 2006*).
- Wingless/Wnt, that induce the clustering of glutamate receptors when secreted by astrocytes (*Ciani et al., 2011; Kerr et al., 2014*).
- Chondroitin sulfate proteoglycans (CSPGs), that stabilize the surface AMPARs (*Pyka et al., 2011*).
- Activity-dependent neurotrophic factor (ADNF), that increases synaptic NMDA glutamate receptors (NMDARs) (*Blondel et al., 2000*).

Of note, the heterogeneity that characterizes astrocytic populations also influences their synaptogenic potential (*Buosi et al., 2018*). Indeed, the ACMs of astrocytes derived from distinct brain regions differentially affect excitatory synaptic maturation. Interestingly, heterotypical co-cultures show comparable results to co-cultures in which neurons and astrocytes derive from the same brain area.

Besides a crucial role in controlling excitatory synapses formation, astrocytes can directly stimulate the formation and functional maturation of inhibitory GABAergic synapses. The list of secreted factors that regulate $GABA_A$ receptor recruitment to synapses, however, is less defined. However, usually the astrocytic factors that induce excitatory synapse formation usually do not induce the inhibitory one; thus, astrocytes release a pool of different signals to dictate the class of synapse to form (*Huges et al., 2010*).

Nevertheless, an exception is represented by the Transforming Growth Factor beta-1 (TGF-β1), a secreted protein of the TGF superfamily that promotes the formation of both excitatory and inhibitory synapses in cultured mouse cortical neurons and *in vivo* (*Diniz et al., 2012*; *Diniz et al., 2014*). The increase of excitatory activity is mainly mediated by D-serine, a co-agonist of the NMDA receptor, whose levels are induced by TGF-β1. Moreover, TGF-β1 overexpression in mice increases hippocampal levels of AMPA and NMDA receptor subunits, thus promoting excitatory synapse formation (*Sultan et al., 2015*; *Bae et al., 2011*). On the other hand, TGF-β1 can trigger signaling mechanisms involving the phosphorylation of CAMKII at Thr286 and occurring via NMDA activity to induce inhibitory synaptogenesis (*Diniz et al., 2014*). In addition, TGF-β1 increases the level of two important components of inhibitory post-synapses: Neuroligin 2(NL2) and Gephyrin/NL2 clustering (*Diniz et al., 2014*).

Contextually with soluble factors, astrocytes physically interact with neurons to control synapse formation and function. A noteworthy example is represented by the astrocytic expression of Neuronal Cell Adhesion Molecule (NRCAM) in the mouse cortex that allows astroglial processes to contact neuronal NRCAM coupled to gephyrin at inhibitory post-synapses (*Takano et al., 2020*). Loss of astrocytic NRCAM significantly decreases the number and function of inhibitory synapses, with little effect on excitation.

In accordance with this, astrocytes express several Cell Adhesion Molecules (CAMs) to regulate synapses through physical contact (*Hillen et al, 2018*). CAMs allow astrocytes to be closed to neurons through a configuration promoted by axon guidance molecules. Proteins such as tenascin-C, ephrins and SynCAM (*Jones and Bouvier, 2014; Filosa et al., 2009; Frei and Stoeckli, 2014*) affect the actin-mediated cytoskeleton of growth cones and direct astrocyte processes towards dendrites of nascent synapses (*Bashaw and Klein, 2010; Dent et al., 2011; Missler et al., 2012; O'Donnell et al., 2009*). After the alignment of newly formed pre- and post-synaptic sites, CAMs strengthen their contact providing adhesiveness and cytoskeleton remodelling (*Siddiqui and Craig, 2011*). Moreover, CAMs support synaptic plasticity and functional specification (*Wit and Ghosh, 2016; Missler et al., 2012*). Several CAM families exist (**Figure 1.14**) and they all share different extracellular domains, including multiple tandem repeats, that confer a greater repertoire of interactions (*Missler et al., 2012*).

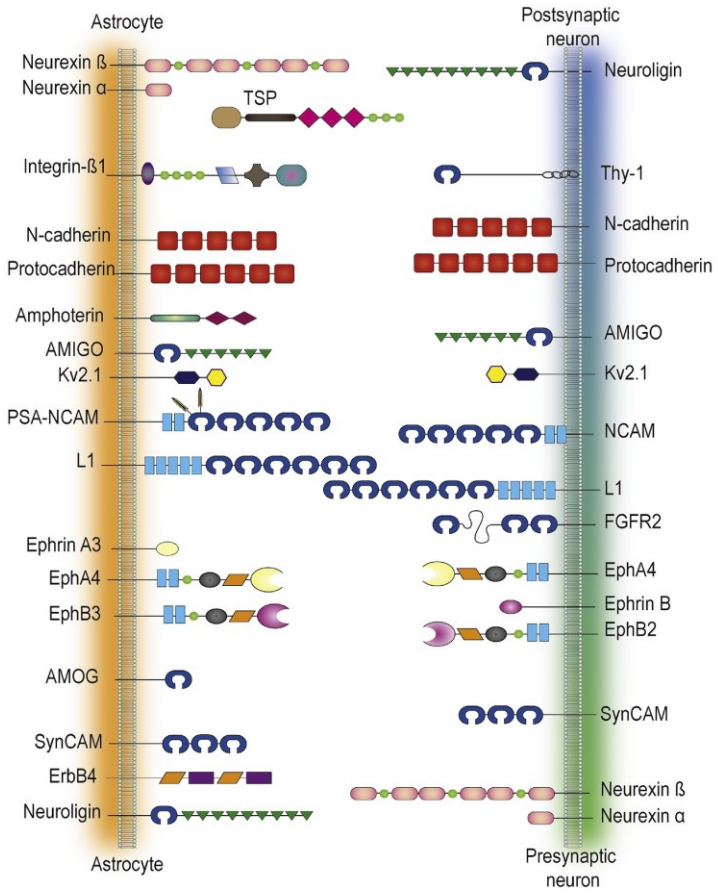

Figure 1.14. CAMs within the astrocytic membrane and their pre-/post-synaptic interaction partners (Figure adapted from *Hillen et al, 2018*).

Astrocytes and the elimination of synapses

During all developmental stages and adulthood, synapses need to be dynamic structures that undergo rapid formation and elimination to balance neural circuits. Moreover, synaptic networks must be plastic structures that respond to sensory experiences during learning and memory formation (*Chung et al., 2015*). Astrocytes participate in these processes by mediating synapse elimination through direct or indirect mechanisms. Regarding the indirect pathway, TGF-β secreted by astrocytes initiates C1q mRNA expression via the corresponding TGFBR2 receptor (*Bialas and Stevens, 2013*). This mediates the microglial-dependent elimination of synapses, as C1q/C3-coated synapses are recognized and engulfed by microglia cells through C3R-mediated phagocytosis (*Schafer et al., 2012*).

In addition to this, astrocytes themselves express a broad spectrum of genes implicated in engulfment and phagocytosis. In fact, they express two main phagocytic

receptors: Multiple EGF Like Domains 10 (MEGF10) and MER Proto-Oncogene Tyrosine Kinase (MERTK) (*Chung et al., 2015*). MERTK acts together with two other TAM receptors (TYRO3 and AXL) and in collaboration with the integrin pathway to regulate the downstream targets of phagocytosis (*Wu et al., 2005*). The second pathway, on the other hand, involves MEGF10, GULP and ABCA1, which participate in the recognition and engulfment of cellular debris (*Zhou et al., 2001; MacDonald et al., 2006; Yu et al., 2008*). In line with this, it was recently found that astrocytes in the CA1 region of the adult mouse hippocampus play a major role in the neuronal-activity-dependent elimination of excitatory synapses (*Lee et al., 2020*). Mice lacking the MEGF10 receptor, in fact, show a decrease in phagocytosis that leads to an excessive accumulation of functionally compromised synapses.

1.2.6 The role of astrocytes in RTT

Astrocytes as emergent therapeutic targets in intellectual disabilities

To date, most of the therapeutic strategies designed for the treatment of neurological disorders have been targeted at non-specific cells or neuronal pathways. However, this neuro-centric view has been recently challenged including glial cells in the list of new potential targets. In accordance with their crucial role in maintaining brain homeostasis, it is not surprisingly that astrocytes play central roles in the pathogenesis of multiple brain diseases. Of relevance, astroglial dysfunctions are deeply involved in intellectual disabilities (IDs), a peculiar group of neurodevelopmental disorders including RTT (*Molofsky et al., 2012*). Modern techniques of gene expression analysis unveiled that about 70% of genes causing IDs are expressed not only in neurons but also in astrocytes (*Zeisel et al., 2015; Zhang et al., 2014; Lelieveld et al., 2016*; *Blanco-Suarez et al., 2016*). These ID-related genes usually encode proteins critical for the regulation of dendritic spine morphogenesis, synaptic activity and neural circuit development (*Dierssen and Ramakers, 2006; Gatto and Broadie, 2010*). As a matter of facts, astroglial cells in IDs exhibit several dysfunctions that influence their ability to sense and uptake neurotransmitters, support neuronal maturation, regulate synaptic networks and maintain brain homeostasis (*Cresto et al., 2019; Simhal et al., 2019*) (**Figure 1.15**). The molecular mechanisms leading to neuronal dysfunctions are still unclear, although evidence suggests that secreted factors are involved. Certainly, astrocytic alterations influence neuronal development and contribute to worsening the

pathogenic features of synaptopathies. Therefore, targeting deregulated astrocytic pathways in IDs is considered an effective and innovative therapeutic strategy.

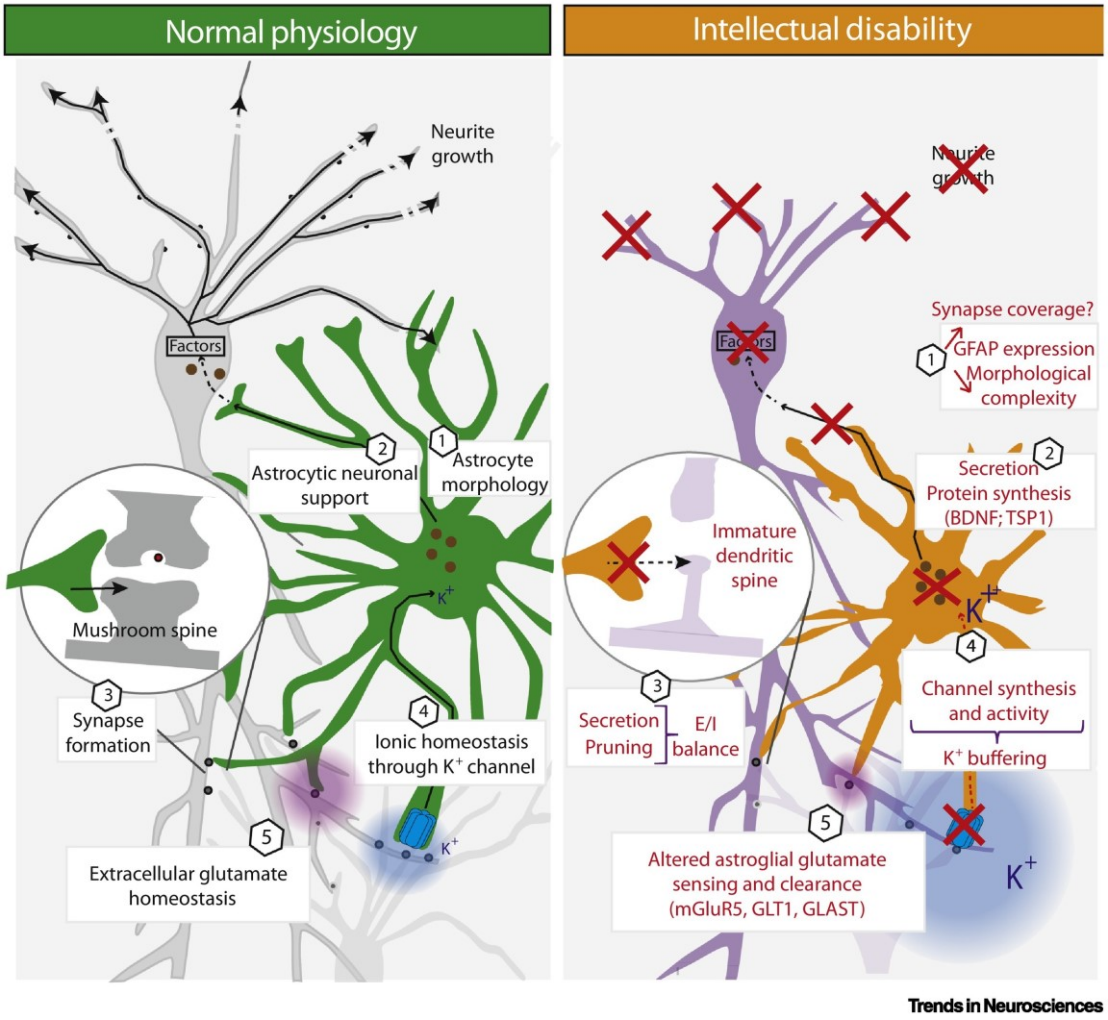

Figure 1.15. Astrocytes and the tripartite synapse: a comparison between normal physiology and the context of intellectual disabilities (*Cresto et al., 2019*).

Astrocytes and RTT

Over the past 12 years, several experiments have attributed an important role to astroglial cells in the pathogenesis of RTT (*Jin et al., 2017; Kahanovitch et al., 2019; Sharma et al., 2018*). It was observed, indeed, that *Mecp2* deficient astrocytes exhibit multiple dysfunctions that alter neuronal development and synaptic transmission.

First evidence of the involvement of astrocytes in RTT dates back to 2009, when *Ballas* reported that *Mecp2* is also expressed in astroglial cells and *Mecp2* KO astrocytes do not well support neuronal growth (*Ballas et a., 2009*). In details, they showed that culturing WT hippocampal neurons with *Mecp2* deficient cortical astrocytes for at least

6 days leads to aberrant dendritic morphology, that get worse over time. Neurons do not develop fine processes and have fewer long dendrites, together with an abnormal concentration of MAP2 in the soma. The same phenotype was obtained treating neurons with mutant cortical ACM, thus suggesting the involvement of secreted factors. Of relevance, dendritic defects were also present when mimicking a heterozygous mutation of the ACM (1:1 mixture of ACM and neuronal maintenance medium), implying that the secretion of aberrant factors could be involved in non-cell autonomous alterations in RTT patients. In support of these results on primary mouse cultures, the detrimental effect of mutant astrocytes on neurons was also confirmed by differentiating astrocytes from 3 different isogenic induced pluripotent stem cells (iPSCs) lines of RTT patients (V247X, R294X and R306C mutations) (*Williams et al., 2014*). Both in contact co-cultures and ACM treatments, indeed, showed that human RTT mutant astrocytes influence the morphology and function (lower average frequency of the miniature excitatory postsynaptic currents (mEPSC) of WT mouse hippocampal neurons via non cell-autonomous mechanisms. Despite a reduction in synaptic transmission, authors did not observe a decrease in the density of excitatory synapses by IF of pre- and post-synaptic markers (vGlut1 and PSD95) after 8 days of co-culture.

In good accordance with these studies, *Maezawa* reported that KO astrocytes exhibit an altered phenotype consisting of abnormal growth, defective regulation of BDNF, different release of pro-inflammatory cytokines (TNFα, IL-1β, IL-6), altered p38MAPK activity and abnormal neuronal dendritic induction (*Maezawa et al., 2009*). Interestingly, this aberrant astrocytic state caused by *Mecp2* deficiency is progressively spread in WT astrocytes via a non-cell autonomous mechanism involving gap junctions.

On the other hand, mutant neurons can revert their defective morphology when supported by WT ACM, highlighting the possibility to target astrocytes for therapeutic purposes (*Ballas et al., 2009; Williams et al., 2014*). To corroborate these results, *Mecp2* was selectively reactivated in astrocytes of *Mecp2* null mice, significantly improving their locomotion, anxiety levels, respiratory abnormalities and lifespan (chapter 1.1.4) (*Lioy et el., 2012*). Of note, this phenotypic rescue is at least in part sustained by a non-cell-autonomous positive effect on mutant neurons, as they reacquire normal dendritic morphology and restore physiological levels of VGlut1 in neuronal cell bodies of the medulla oblungata. Further, conditional mice have permitted

to demonstrate that *Mecp2* expression in astrocytes is crucial for the maintenance of astroglial properties at any developmental stage. Indeed, the selective postnatal deletion of *Mecp2* from astrocytes either in youth or adulthood leads to the progression of RTT-like symptoms in mice together with the onset of astrocytic defects. In details, depletion from a late juvenile stage (5 weeks of age) leads to shorter and less complex ramified processes of hippocampal astrocytes in the CA1 area of adult mice (*Nguyen et al., 2012*), while the deletion from adult mice is sufficient to alter their respiratory CO_2 response, resulting in a dramatic attenuation of the hypercapnic ventilatory response (HCVR) (*Garg et al., 2015*).

To decipher the molecular mechanisms underlying the aforementioned phenotypes, several transcriptional studies have been carried out on *Mecp2* null astrocytes. Experiments on primary cultured astrocytes from *Mecp2*$^{tm1.1Bird/+}$ mice revealed a higher expression of astrocyte-specific genes such as *Gfap* and *S100b* compared to WT, along with an abnormal response of genes involved in glutamate clearance (GLT-1, GLAST, GS) (*Okabe et al., 2012*). Despite an increase of *Gfap* expression was also reported in RTT brains (*Colantuoni et al., 2001*), RTT astrocytes do not reveal a classical reactive phenotype. Deeper investigations are required to assess whether the RTT brain features a predisposition to altered inflammatory responses. A more comprehensive *in vitro* study of primary cultures from null mice revealed 118 differentially regulated genes in null cortical astrocytes and proposed a unique set of genes responsive to *Mecp2* (*Yasui et al., 2013*). Similarly, microarray expression data of *Mecp2*$^{308/y}$ cultured cortical astrocytes reported the alteration of 257 genes, generally involved in major cellular functions, including cell-cell communication and cellular development (*Delépine et al., 2015*). Authors suggested as possible contributors to the non-cell autonomous effect on neurons two secreted proteins and one transcription factor: Chromogranin B (*Chgb*), Lipocalin 2 (*Lcn2*) and Nuclear receptor subfamily 2 group F member 2 (*Nr2f2*), respectively (*Ferreira et al., 2013; Landén et al., 1999; Marksteiner et al., 2000; Diaz-Vera et a., 2010*; *Okamura et al., 2009; Lyst et al., 2013*). Curiously, transcriptional studies from *Yasui's* and *Delepine's* laboratories displayed very limited overlap. This could be related to the use of different mouse models and different number of astrocyte cell divisions *in vitro*, or to the presence of fetal bovine serum (FBS) in astrocyte cultures, with inter-vendor and inter-batch inconsistencies contributing to the variability, as suggested by *Pacheco et al.*.

For these reasons, the expression profile of null astrocyte was also evaluated in various null and knock down models of RTT (chapter 1.1.4). A multi-omics study of the adult *Mecp2*$^{tm1.1Jae/y}$ KO cortex (P60) reported the alteration of 46 astrocyte-specific genes associated with astrocyte maturation and morphology (*Pacheco et al.*, 2017), together with decreased levels of astrocytic proteins involved in apoptosis.

As extensively discussed in chapter 1.2.2, cytoskeleton organization is a critical aspect for astrocytes to develop a correct shape, which in turn allows these cells to properly exploit their functions. Therefore, several research groups investigated whether *Mecp2* loss could affect astrocyte maturation and structural rearrangements in RTT models. *Mecp2* null cultured cortical astrocytes do not exhibit difference in growth rate (*Okabe et al., 2012*) and iPSCs from RTT patients manifest a rate of differentiation into astrocytes similar to controls (*Yasui et al, 2017*). However, primary astrocyte cultures from either *Mecp2*$^{308/y}$ or *Mecp2*$^{tm1.1Bird/y}$ mice exhibit an enhanced rate of microtubule (MT) polymerization (*Nectoux et al., 2012*), that might influence remodelling of the cytoskeleton and cellular shape. The decreased expression of stathmin-like 2 (STMN2), a protein affecting the assembly and dynamics of microtubules, might be involved in the observed phenotype. Further, *Mecp2* deficient astrocytes and human *MECP2* p.Arg294* iPSC-derived astrocytes exhibit an altered microtubule-dependent vesicle transport (*Delépine et al., 2016*); the administration of a microtubule stabilizer (Epothilone D) restore the phenotype *in vitro* and low doses partially reverse the impaired exploratory behaviour of *Mecp2*$^{308/y}$ male mice. Furthermore, activation of brain RhoGTPases (a group on enzymes that induces dynamic changes in microtubule organization and impact astrocyte morphology (chapter 1.2.2) by a single intracerebroventricular (ICV) injection of bacterial Cytotoxic Necrotizing Factor 1 (CNF1) revert astrocyte atrophy and markedly improves the behavioural phenotype of *Mecp2*$^{308/y}$ mice (*De Filippis et al., 2012*).

Mecp2 deficiency in astrocytes also impacts their ability of maintaining homeostasis at the synaptic level, as KO astrocytes manifest an altered regulation of ion and neurotransmitters. In fact, as already mentioned, KO cultured astrocytes show higher glutamate clearance due to impairments in the downregulation of GLT-1 and GLAST (*Okabe et al., 2012*). Moreover, astrocytes from RTT animal models manifest alterations in the expression of the inwardly-rectifying potassium channel Kir 4.1, (*Kahanovitch et al., 2018*). Even in this case, we dispose of conflicting data probably because of intrinsic differences within experiments and regional heterogeneity. Indeed,

one study performed on 3 to 6 weeks old *Mecp2*$^{tm1.1Bird}$ male mice reported an increase of *Kir4.1* in the locus coeruleus (*Zhang et al., 2011*). Conversely, other experiments carried out using *Mecp2*$^{tm1.1Jae}$ male mice at P50 described decreased transcription of *Kir4.1* in the cortex, midbrain, brainstem, hippocampus and cerebellum (*Kahanovitch et al., 2018*). Moreover, Kir4.1 protein level in these mice is significantly lower in the cortex at P10, P21 and P50.

Astroglia cells also play a fundamental role in supporting brain metabolism. Therefore, different studies investigated mitochondria functionality and lactate production in RTT astrocytes. Primary astrocytes from *Mecp2*$^{tm1.1Bird/y}$ mice have more mitochondria, though their shape and membrane potential are not altered (*Bebensee et al., 2017*). Moreover, depletion of *Mecp2* in cultured rat astrocytes leads to elevated expression of proteins of the mitochondrial respiratory chain together with lower activity of complexes II/III and increased levels of reactive oxygen species (ROS) (*Dave et al., 2019*). Lastly, brain slices from *Mecp2*$^{tm1.1Bird/y}$ mice at pre-symptomatic stages exhibit an increased oxidation (*Grosser et al., 2012*). Taken together, these data confirm the presence of impairments in mitochondrial activity and aberrant redox homeostasis in KO astrocytes.

Regarding the role of astrocytes in the 'lactate shuttle' to supply energy to neurons, evidence suggested that this function is preserved in RTT. Indeed, no change in lactate was detected in RTT patients (*Nielsen et al., 1993*) and studies on astrocytes of the medulla oblungata and cortex from *Mecp2*$^{tm1.1Bird}$ and *Mecp2*$^{tm1.1Jtc}$ mice reported no alteration in tonic or hypoxia-induced release of this metabolite (*Turkovsky et al., 2015*).

Eventually, astrocytes are master regulators of synaptic transmission and actively control the E/I balance of brain circuits (chapter 1.2.4). *Rakela* demonstrated that the expression of *Mecp2* in astrocytes (and not in neurons) in brain slices of *Mecp2*$^{tm1.1Bird}$ female mice at P10 is the sole requirement of the astrocyte-mediated modulation of neuronal signaling (*Rakela et al., 2018*). Authors, indeed, reported a perturbed excitatory communication exclusively when stimulating KO astrocytes and recording WT neurons.

Moreover, RTT astrocytes present an abnormal spontaneous intracellular calcium activity *in vitro* (RTT iPSC) and *in vivo (Dong et al., 2018).* This phenotype has been associated with calcium overload in the endoplasmic reticulum (ER) caused by the increased expression of Transient Receptor Potential Cation Channel Subfamily C

Member 4 (TRPC4). These impaired calcium dynamics cause an excessive activation of extra-synaptic NMDA receptors (eNMDARs) in neurons and consequently increased network excitability in null mice.

Recently, *Dong et al.* also proved that *Mecp2* KO astrocytes impair tonic inhibition in hippocampal CA1 pyramidal neurons of *Mecp2*$^{tm1.1jae}$ mice at 8-10 weeks of age (*Dong et al., 2020*). The decrease of extracellular GABA level in the hippocampus of null mice is related to the increase of the astrocytic GABA transporter 3 (GAT3) and its inwardly currents. As a matter of facts, the phenotype can be rescued by pharmacological blockage of GAT3, that normalizes tonic inhibition and decreases CA1 pyramidal neurons excitability.

All in all this experimental evidence indicates that loss of *Mecp2* in astrocytes causes cell-autonomous alterations, which in turn affects neuronal maturation, synaptic signaling and brain homeostasis.

Aims of the thesis

The importance of *Mecp2* expression in astrocytes for brain development has been largely documented in the past years. It emerged that *Mecp2*-deficient astrocytes show transcriptional alterations that affect their ability to support several aspects of neuronal growth, from dendritic morphology to synaptic transmission. Nonetheless, deregulated molecular pathways in *Mecp2* KO astrocytes and their role through non-cell autonomous effects on neurons and in RTT pathogenesis remain largely unknown. Furthermore, it remains unknown whether *Mecp2* influences astrocytes differently according to their regional heterogeneity. This characterization might support the identification of region-specific morphological, molecular and functional alterations. Filling these gaps of knowledge and possibly identifying altered pathways in *Mecp2*-deficient astrocytes with a potential therapeutic value for RTT represented the main goals of this thesis. To fulfil these aims, firstly, we characterized astrocyte morphology in *Mecp2* KO mouse brains with respect to brain area and progression of symptoms. Indeed, astrocytic shape could be indicative of a pathological state that also mirror a functional alteration. Then, considering the importance of astrocyte morphology for synaptogenesis and synaptic dysfunctions in RTT, we focused on the study of excitatory synapses both *in vivo* and *in vitro*. We made an extent use of primary co-cultures in order to isolate the astroglial-neuron crosstalk and dissect the consequences that *Mecp2* deficiency in astrocytes exert on neuronal synaptogenesis. Having demonstrated the involvement of cytotoxic secreted factors we have used transcriptomic approaches to postulate the involved molecular mechanisms.

Materials and methods

2.1 Animals

2.1.1 Animal care

The Mecp2$^{tm1.1Bird}$ mouse strain was originally purchased from the Jackson Laboratories and then backcrossed and maintained on a clean CD1 background (*Cobolli Gigli et al, 2016*). These mice recapitulate the typical phenotype of C57BL/6 mice, with the advantage of having a larger progeny and minor risk of litter cannibalization (chapter 1.1.4).
To perform *ex vivo* analyses, WT and *Mecp2* null mice at P20, P40 and P70, heterozygous female mice at P180, and the corresponding WT littermates were used. Animals were sacrificed by rapid decapitation or by transcardial perfusion depending on experimental needs. Mice were housed in a temperature- and humidity-controlled environment in a 12-h light/12-h dark cycle with food and water ad libitum. All procedures were performed in accordance with the European Union Communities Council Directive (2010/63/EU) and Italian laws (D.L.26/2014). Protocols were approved by the Italian Council on Animal Care in accordance with the Italian law (Italian Government decree No. 210/2017).

2.1.2 Genotyping of genetically-modified mice

Mouse genotype was determined by Polymerase Chain Reaction (PCR) protocol on genomic DNA purified from tails or mouse paws in case of embryos.

- *DNA extraction*

Tissues were dissociated with "*Phire animal tissue direct PCR kit*" (Thermo Scientific) to rapidly extract DNA from samples used in primary cultures, while other animals were genotyped at P15-20 following an overnight (O/N) protocol.

DNA extraction for embryos and P2 mice:
Each sample (mouse paw or tail) was incubated with a mix of 20 µL (19.5 µL Dilution Buffer + 0.5 µL DNARelease Additive from "*Phire animal tissue direct PCR kit*") for 4 minutes at room temperature (RT). Then, the reaction was stopped at 98°C for 2 minutes and supernatant was directly used for DNA quantification.

DNA extraction for P15-P20 mice:

Each sample was dissociated in Tail lysis buffer + proteinase K (0.5 mg/mL) at 55°C O/N and centrifuged (13,000 rpm, 6 minutes, RT) to remove any debris. Then, 450 µL of 100% isopropanol was added to the supernatants and DNA was precipitated (13,000 rpm, 5 minutes, RT). Pellets were washed with 150 µL of 70% EtOH and precipitated (13,000 rpm, 5 minutes, 4°C). EtOH was discarded, pellets were dried at RT and resuspended in 150 µL H_2O (DNAsi and RNAsi-free) for DNA quantification.

DNA was quantified with a spectrophotometer (NanoDrop, ThermoFisher) prior to amplification. The reaction requires 100 ng DNA / sample; therefore, if necessary, sample concentrations were diluted to obtain an adequate quantity in 1 µL of solution.

- *PCR and gel electrophoresis*

Reaction mix for one sample (Final volume = 20 µL) (**Table 2.1**):

Reagents	Concentration	Final volume
H_2O	-	12.6 µL
Xtra RTL GL Reaction Buffer	5 X	4 µL
dNTPs	10 µM	0.4 µL
Reverse primer	20 µM	0.5 µL
Forward primer (WT allele)	20 µM	0.5 µL
Forward primer (null allele)	20 µM	0.5 µL
XtraTaq Pol RTL	5 U/µL	0.5 µL
DNA	100 ng	1 µL

Table 2.1. PCR reaction mix for *Mecp2* mutant mice genotyping.

Negative controls (19 µL reaction mix + 1 µL H_2O) and positive controls (19 µL reaction mix + 1 µL DNA of a heterozygous mouse) were always included. PCR cycles (**Table 2.2**):

Step	Temperature	Time
Heat lid	110°C	-
Denaturation	95.0° C	2 minutes
Start loop		35 X

denaturation	95.0 C	30 seconds
annealing	59.0° C	30 seconds
extension	72.0° C	30 seconds
Close loop		
Final extension	72.0° C	5 minutes
Hold	4°C	∞

Table 2.2. PCR cycles for *Mecp2* mutant mice genotyping.

PCR products were resolved by electrophoresis run in 2% agarose gel stained with SYBR safe 1:20,000 (110V, 40 minutes run in TAE1X buffer). Bands were visualized using a UV transilluminator (Essential V6 imaging platform, UVITEC, Cambridge). WT mice present a band of 411 bp, while *Mecp2* KO mice present a band of 458 bp (primers were designed to amplify the deletion cassette). Heterozygous mice exhibit both bands, one for each allele (**Figure 2.1**).

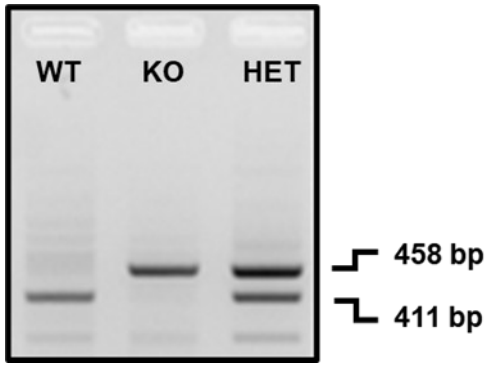

Figure 2.1. Representative electrophoresis run of PCR products from WT, *Mecp2* KO and heterozygous animals.

Materials

- 2-Propanol, SIGMA, cod. 33539
- Agarose LE, GENESPIN, cod. STS-AG500
- Deoxynucleotide Set, 100 mM, SIGMA, cod. DNTP100A
- Ethylenediaminetetraacetic acid (EDTA), SIGMA, cod. EDS
- Ethanol (EtOH), SIGMA, cod. 32221
- Glacial acetic acid, SIGMA, cod. A6283

- NaCl, SIGMA, cod. S9888
- Nuclease-Free Water, SIGMA, cod. W4502
- Phire animal tissue direct PCR kit, Thermo Scientific, cod. F140WH
- Proteinase K, GENESPIN, cod. STS-OK500
- Sodium dodecyl sulfate (SDS), SIGMA, cod. L3771
- SYBR Safe DNA Gel Stain, Thermo Scientific, cod. S33102
- Trizma base, SIGMA, cod. 93352
- Xtra RTL GL Reaction Buffer, GENESPIN, cod. XSTS-T5XRTL GL
- Xtra Taq Pol, GENESPIN, cod. XSTS-T5XRTL GL

Primers for BIRD mice genotype:

- common reverse primer: 5'-CCACCCTCCAGTTTGGTTTA-3'
- forward primer for wild-type allele: 5'-GACTGAAGTTACAGATGGTTGTG-3'
- forward primer for null allele: 5'-ACCTAGCCTGCCTGTACTTT-3'

Solutions

- Tail lysis buffer (Final volume = 250 mL):

Reagents	Starting concentration	Final Volume
dH_2O	-	Up to 250 mL
Tris pH8	1 M	25 mL
EDTA	0.5 M	2.5 mL
SDS	10%	5 mL
NaCl	5 M	10 mL

- TAE (Tris-acetate-EDTA) buffer 10X (Final volume = 1 L):

Reagents	Starting concentration	Final Volume
dH_2O	-	Up to 1 L
Trizma base	stock	48.4 gr
Glacial acetic acid	stock	11.4 mL
EDTA pH8	0.5 M	20 mL

2.2 Primary cultures

2.2.1 Primary cultures of cortical neurons

The day of vaginal plug was considered E0.5 and primary cortical neurons were prepared from WT and *Mecp2* null mouse embryos at E15.5. Embryos were sacrificed by decapitation and brains were removed under a microscope and immersed in ice-cold Hank's Buffered Salt Solution (HBSS). Meninges were removed, and cerebral cortex was rapidly dissected and maintained in cold HBSS until tissue dissociation. Tissues were washed in HBSS, incubated with 0.25% trypsin/EDTA for 7 min at 37°C and the digestion was blocked with 10% FBS in DMEM High Glucose. Then, cortices were accurately washed and mechanically dissociated by pipetting in neuron culture medium (see below). Cell count was performed with an automated cell counter by using Trypan blue (Countess Automated Cell Counter, ThermoFisher). Depending on experimental needs, neurons were seeded on poly-D-lysine (0.1 mg/mL)-coated plates, poly-D-lysine-coated glass coverslips (Neuvitro) or directly on astrocytes.

2.2.2 Primary cultures of cortical, hippocampal and cerebellar astrocytes

Primary astrocyte cultures were prepared from cerebral tissue of P2 WT and *Mecp2* null mice. Mice were decapitated and brain was removed. Meninges were carefully dissected and, depending on the experiment, cortices, hippocampi or cerebella were isolated and immersed in HBSS containing 10 mM HEPES and 4 mM $NaHCO_3$. Tissues were then incubated in 0.25% trypsin/EDTA for 30 min at 37°C, mechanically dissociated in astrocyte culture medium (see below) and filtered through cell strainers of 40 µm pore size to obtain a single cell suspension. The resulting cells were centrifuged at 1,500 g for 7 min, re-suspended in culture medium, and plated in poly-D-lysine (15 µg/mL)-coated 75 cm^2 flasks. At DIV4, flasks were shaked in astrocyte culture medium containing 10 mM HEPES at 200 rpm for 6 h at 37°C to eliminate residual microglia, and the medium was replaced with fresh culture medium. Cells were incubated in a humidified incubator at 37°C and 5% CO2 and culture medium was refreshed every 4 days. After astrocytes reached confluence (DIV12-DIV15), they were detached by 0.25% trypsin/EDTA in HBSS and manually counted in a Bürker chamber.

Depending on experimental needs, they were seeded on poly-D-lysine (15 µg/mL)-coated plates, poly-D-lysine (1 mg/mL)-coated glass coverslips or transwell membrane inserts (Corning).
When astrocytes were cultured alone for morphological characterization *in vitro*, they were seeded at the density of 20,000 cells/well. In all other cases, they were seeded as follows.

2.2.3 Astrocyte-neuron co-cultures

Both in contact and transwell-based co-culture systems were set up.

In contact co-cultures

Astrocytes (30,000 cells) were seeded on glass coverslips or directly in 24-well dishes. After 2-4 days, neurons were seeded on the top of astrocyte monolayers, at low density, corresponding to 10,000 cells/well for the analysis of synaptic phenotype and 5,000 cells/well for morphological analysis.
Cells were cultured with 5% FBS co-culture medium (see below) the first 48 hours, then it was replaced by 2.5 % FBS co-culture medium, which was maintained for the entire duration of the experiment. When neurons were fixed at DIV14, cultures were filled with fresh medium at DIV7 for a third of the original volume.

Transwell co-cultures

Astrocytes were seeded in astrocyte culture medium on PET membrane cell culture inserts (Corning) at a density of 8,000 cells/insert for immunofluorescence analyses in 24-well dishes or 150,000 cells/insert for RNA-Seq and sphingolipids analyses in 6-well dishes. After 4 days, neurons were seeded in neuron culture medium, respectively on PDL coated coverslips in 24-well dishes at a density of 40,000 cells/well or in 6-well dishes at a density of 200,000 cells/well (for sphingolipids analysis 2.5 % FBS co-culture medium was used).
After neurons attached to coverslips or wells (~ 2 hours), inserts with astrocytes were carefully transferred to neuron-containing plates and maintained for the entire duration of the experiment. For immunofluorescence and sphingolipid analyses astrocytes were maintained in their culture medium, while for RNA-Seq analysis medium within the inserts was replaced by neuron culture medium to avoid FBS contamination. When

neurons were collected at DIV14, cultures were filled with fresh medium at DIV7 for a third of the original volume.

2.2.4 Co-culture with Astrocyte Conditioned Medium (ACM)

Astrocytes were seeded in 6-well dishes at a density of 100,000 cells/well. At 90 % confluence, *astrocyte culture medium* was replaced by serum-free medium for conditioning. In details, after a rapid wash to remove cell debris and serum-containing medium, cells were incubated in 2 mL/well of serum-free medium for 1 hour and 30 minutes to remove astrocyte-secreted FBS. Then, ACM was collected after 48 hours and immediately centrifuged at 1,200 rpm for 5 minutes at 4 °C to remove cellular debris. Protease inhibitor was added to all supernatants (1:1,000) and samples were stored at -80°C. The day of the treatment, ACM was heated at 37°C in a water bath and added to neurons (1:1 respect to neuron culture medium). Protein denaturation of the ACM was performed by boiling samples at 95°C for 5 minutes.

Materials

- Hanks' balanced salt solution (HBSS), SIGMA, cod. H6648
- Trypsin-EDTA (0,25%) phenol red, ThermoFisher, cod. 25200-056
- Dulbecco's Modified Eagle's Medium (DMEM), high glucose, pyruvate, ThermoFisher, cod. 41966029
- Ham's F-10 Nutrient mix, ThermoFisher, cod. 31550023
- Neurobasal medium, ThermoFisher, cod. 21103049
- L-Glutamine solution, ThermoFisher, cod. G7513
- Penicillin-Streptomycin, ThermoFisher, cod. P0781
- B27 Supplement (50X), serum free, ThermoFisher, cod. 17504044
- Fetal Bovine Serum (FBS), qualified, heat inactivated, E.U.-approved, South America Origin, GIBCO (ThermoFisher), cod. 10500064 GIBCO, Lot: 08G2082K
- Poly-D-lysine hydrobromide 100MG, SIGMA, cod. P7886
- Coverslips PDL coated, NEUVITRO, cod. GG-12-PDL
- HEPES solution 1 M, pH 7.0-7.6, sterile-filtered, SIGMA, cod. H0887
- Protease Inhibitor Cocktail, SIGMA, cod. P8340
- Falcon® Permeable Support for 6-well Plate with 0.4 µm Transparent PET Membrane, CORNING, cod. 353090
- ThinCert™ Cell Culture Inserts 24 Well plates, tc, sterile, translucent membrane (PET), pore diameter: 0,4 µm, Greiner Bio-One, cod. 662640
- Sodium bicarbonate ($NaHCO_3$), SIGMA, cod. S6014

Culture mediums

- Neuron culture medium (Final volume = 100 mL)

	Final concentration	Final Volume
Neurobasal medium	-	Up to 100 mL
B27 supplement 50X	2 %	2 mL
Pen/Strep	1 %	1 mL
L-Glutamine	1 %	1 mL

- Astrocyte culture medium (Final volume = 100 mL)

	Final concentration	Final Volume
DMEM HG, pyruvate	-	44.5 mL
Ham's F-10	-	44.5 mL
FBS	10 %	10 mL
Pen/Strep	1 %	1 mL

- Co-culture medium for first 0-48 hours (Final volume = 100 mL)

	Final concentration	Final Volume
Neurobasal medium	-	91 mL
B27 supplement 50X	2 %	2 mL
Pen/Strep	1 %	1 mL
L-Glutamine	1 %	1 mL
FBS	5 %	5 mL

- Co-culture medium after 48 hours (Final volume = 100 mL)

	Final concentration	Final Volume
Neurobasal medium	-	93.5 mL
B27 supplement 50X	2 %	2 mL
Pen/Strep	1 %	1 mL
L-Glutamine	1 %	1 mL
FBS	2.5 %	2.5 mL

2.3 Immunofluorescence

2.3.1 Immunofluorescence on cellular cultures for astrocyte morphology, neuronal morphology and synaptic markers

- *Cells fixation*

Astrocytes (DIV15-20) seeded on glass coverslips for morphology characterization were fixed with 4% paraformaldehyde in PBS for 15 min at RT, then washed three times with PBS and stored in PBS-Sodium azide 0.1% at 4°C. For neuronal morphology and synaptic puncta analysis, neurons (DIV 7 and DIV12-14) were fixed for 8 min with 4% paraformaldehyde dissolved in PBS with 10% sucrose, then washed three times with PBS and stored in PBS-Sodium azide 0.1% at 4°C.

- *Immunostaining for astrocyte morphology* (GFAP) / *neuronal morphology* (MAP2) / *synaptic markers* (Synapsin 1 / 2; Shank2)

After a wash in PBS to remove sodium azide, cells were permeabilized in PBS – Triton X-100 0.2% for 3 minutes on ice. Then, cells were washed in PBS – BSA 0.2% and blocked in PBS – BSA 4% for 15 minutes. Incubation with primary antibodies in incubation solution (PBS – BSA 0.2%) was performed overnight at 4°C.
The following primary antibodies were used: mouse anti-GFAP (1:1,000), rabbit anti-MAP2 (1:1,000), chicken anti-SYNAPSIN1/2 (1:500), mouse anti-SHANK2 (1:300).
After washing in PBS – BSA 0.2%, cells were incubated with the specific Alexa Fluor 488/568/647 secondary antibodies (1:500) in PBS – BSA 0.2% for 1 hour in the dark. Cells were washed several times in incubation solution (at least 8 washes of 5 minutes). DNA was stained with DAPI solution (1:1,000 in PBS) following a 10-minute incubation and cells were washed in PBS. Lastly, glass coverslips were mounted on microscope slides with Fluoromount Aqueous Mounting Medium and stored at 4°C until image acquisition.

2.3.2 Immunofluorescence on brain sections for astrocyte morphology and synaptic markers

- *Transcardial perfusion, brain collection and cryostat sectioning*

Mice were anesthetized by intraperitoneal injections of Avertin (250 mg/Kg) and transcardially perfused with 4% paraformaldehyde in PBS. Brains were post-fixed 1 hour and 30 minutes at 4°C and slowly dehydrated in a solution of PBS – sucrose 30% at 4°C (~ 48h). Then, samples were frozen in *n*-pentane at – 30 / - 40°C for 3 minutes and stored at - 80°C. Sectioning was performed with a cryostat (LEICA CM1860). Each brain was embedded by PolyFreeze Tissue Freezing Medium, coronal or sagittal sections of 40 µm were immediately collected in PBS-sodium azide 0.1% and stored at 4°C. Three sections per animal were selected for the experiment. Coronal section were used for the analysis in the cortex and hippocampus, whereas sagittal section were selected for the analysis in the cerebellum.

- *Immunostaining for astrocyte morphology* (GFAP)

A protocol of antigen retrieval was applied before performing immunofluorescence. Free-floating sections were transferred into a pre-heated solution (80°C) of sodium citrate buffer 10 mM, pH6 for 8 minutes. Samples were cooled to RT and then rinsed in PBS before free-floating immunostaining. They were kept on ice and in gentle shaking for the entire duration of the immunostaining. Firstly, sections were permeabilized in PBS – Triton 0.4% for 30 minutes and blocked in PBS – FBS 4% - Triton X-100 0.1% for 15 minutes. Incubation with mouse anti-GFAP (1:3,500) primary antibody was performed in blocking solution overnight at 4°C. Then, sections were washed and incubated with Alexa Fluor anti-mouse 488-conjugated secondary antibody (1:500) in blocking solution for 1 hour in the dark. After several washes in blocking solution (at least 5 washes of 5 minutes), DNA was stained with DAPI solution (1:1,000 in PBS) following a 10-minute incubation and sections were washed in PBS. Lastly, they were mounted on microscope slides with Fluoromount Aqueous Mounting Medium and stored at 4°C until image acquisition.

- *Immunostaining for synaptic markers* (Synapsin1/2; PSD95)

Free-floating sections were kept in gentle shaking for the entire duration of the immunostaining. Firstly, sections were rinsed in PBS and then blocked in PBS – Horse

serum 10% - Triton X-100 0.5% for 1 hour. Incubation with chicken anti-Synapsin1/2 (1:500) and rabbit anti-PSD95 (1:300) primary antibodies was performed in incubation solution (PBS – Horse Serum 3% - Triton X-100 0.5%) overnight at 4°C. Then, sections were washed and incubated with Alexa Fluor anti-chicken 488 (1:500) and anti-rabbit 568 (1:500) secondary antibodies in incubation solution for 1 hour and 30 minutes in the dark. After several washes in incubation solution (at least 6 washes of 10 minutes), DNA was stained with DAPI solution (1:1,000 in PBS) following a 10-minute incubation and sections were washed in PBS. Lastly, sections were mounted on microscope slides with Fluoromount Aqueous Mounting Medium and stored at 4°C until image acquisition.

Materials

- 2,2,2-Tribromoethanol, SIGMA, cod. T48402
- 2-Methyl-1-butanol, SIGMA, cod. 15246-3
- Bovine Serum Albumin (BSA), SIGMA, cod. A3059
- Citric acid, SIGMA, cod. C0759
- Coverslip 24 x 50 mm, Menzel-Glaser
- di-Sodium hydrogen phosphate, SIGMA, cod. 1065660500
- Fetal Bovine Serum (FBS), qualified, heat inactivated, E.U.-approved, South America Origin, GIBCO (ThermoFisher), cod. 10500064 GIBCO, Lot: 08G2082K
- Fluoromount Aqueous Mounting Medium, SIGMA, cod. F4680
- Horse Serum, SIGMA, cod. H0146
- Microscope slides, Thermo Scientific, cod. AFAA000001##12E
- *n*-Pentane 99% RE, Carlo Erba, cod. 528993
- Paraformaldehyde, SIGMA, cod. P6148
- PolyFreeze Tissue Freezing Medium, SIGMA, cod. SHH0026
- Potassium phosphate monobasic, SIGMA, cod. V000225
- Sodium azide, SIGMA, cod. S2002
- Sodium chloride, SIGMA, S9888
- Sodium citrate, SIGMA, cod. W302600
- Sodium hydroxide, SIGMA, cod. 221465
- Sucrose, SIGMA, cod. S9378
- Triton X-100, SIGMA, cod. T8787

Antibodies

- GFAP cloneGA5, Merck Millipore, MAB 3402
- MAP2 (D5G1), Cell Signaling, cod. 8707
- PSD95, ThermoFisher Invitrogen, Rabbit, COD. 516900
- SHANK2, Synaptic Systems, Mouse, COD.
- SYNAPSIN1/2, Synaptic Systems, Chicken, COD. 106006
- DAPI Solution (1 mg/mL), ThermoFisher, cod. 62248

- Donkey anti-Mouse IgG (H+L) Highly Cross-Adsorbed Secondary Antibody, Alexa Fluor 488, ThermoFisher, cod. A21202
- Donkey anti-Mouse IgG (H+L) Highly Cross-Adsorbed Secondary Antibody, Alexa Fluor 568, ThermoFisher, cod. A10037
- Donkey anti-Rabbit IgG (H+L) Highly Cross-Adsorbed Secondary Antibody, Alexa Fluor 647, ThermoFisher, cod. A31573
- Goat anti-Chicken IgG (H+L), Secondary Antibody, Alexa Fluor 488, ThermoFisher, cod.A32931
- Goat anti-Rabbit IgG (H+L) Secondary Antibody, Alexa Fluor 568, ThermoFisher, cod. A11036

Solutions

- Pfa 4% (Final volume = 1 L)

  For 1 L of 4% Paraformaldehyde, 40 g of paraformaldehyde powder were added to 800 mL pre-heated PBS solution (approximately 60 °C) on a stir plate in a ventilated hood. Once the paraformaldehyde was dissolved, the volume of the solution was adjusted to 1 L with 1X PBS, cooled and filtered.

- Avertin

  A stock of 100% avertin was prepared by mixing 5 g of 2,2,2-tribromoethyl alcohol with 10 ml of tert-amyl alcohol. pH adjusted to 6.7.

- Phosphate-Buffered Saline (PBS) 10X (Final volume = 1 L)

Reagents	Final quantities
dH_2O	Up to 1 L
Na_2HPO_4	14.4 g
KH_2PO_4	2.4 g
NaCl	80 g
KCl	2 g

- Sodium citrate buffer 0.1 M, pH6 (Final volume = 500 mL). pH adjusted to 6 with NaOH.

Reagents	Final quantities
dH_2O	Up to 500 mL
Sodium Citrate dihydrate	6.022 g
Citric acid	5.671 g

2.4 Microscope acquisition and image analysis

2.4.1 Astrocyte morphology: characterization *in vitro*

Images of GFAP-labelled astrocytes were randomly acquired for each biological sample using an epi-fluorescence microscope by Nikon (Eclipse N*i* U) with a Plan Fluor 40x DIC M N2 objective in green (GFAP) and blue (DAPI) channels. To characterize the complexity of their shape we used the Shape Index formula (*Matsutani and Yamamoto, 1997*):

$$(\text{Perimeter}^2/\text{Area}) - 4 * \pi$$

Single astrocytes were analysed with Fiji-ImageJ (**Figure 2.2 A, B**). Firstly, to measure area and perimeter of each cell, we adjusted the contrast and brightness of the green (GFAP) channel to clearly visualize all astrocytic contours and we applied the sharpen filter to better unveil intermediate filaments on the edges (**Figure 2.2 A**). Then, images were binarized and by highlighting the perimeter by the *Wand (tracing) tool,* we used the *Fill holes* tool to fill the selection (**Figure 2.2 B**)**.** Lastly, to calculate the perimeter and area of the astrocyte we used the *Analyze Particles* tool.

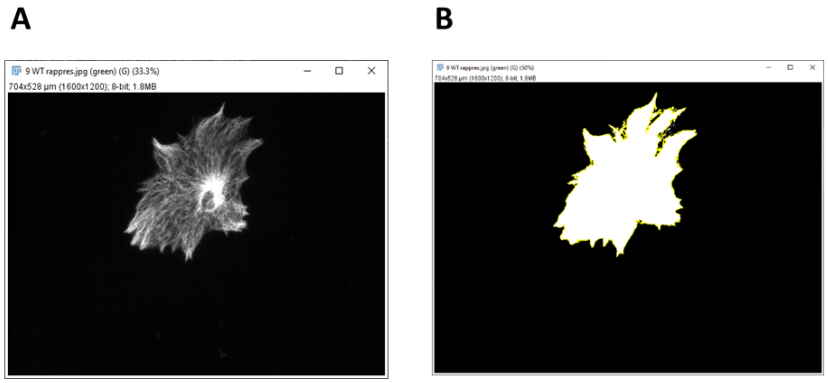

Figure 2.2. An astrocyte in the original green channel (**A**) and its binary mask (**B**) obtained after different passages with ImageJ software, that allowed to clearly delineated cell contours.

2.4.2 Astrocyte morphology: characterization *in vivo*

Z-stacks images (212.13 × 212.13 μm^2, 1,024 × 1,024-pixel resolution, 16-bit grayscale depth) were acquired at a Nikon Ti2 Microscope equipped with an A1+ laser scanning confocal system and a Plan Apo λ 60x oil-immersion objective, using a step size of 0.5 µm. For each dataset, images were acquired in two channels (Laser Wavelength for DAPI: 409.1 nm; Laser Wavelength for GFAP: 487.5 nm) and parameters were maintained constant within same experiments (offset background, digital gain, laser intensity, pinhole size, scanning speed, digital zoom, scan direction, line average mode).

Then, we manually reconstructed the GFAP-stained structure of each astrocyte using *Simple Neurite Tracer* (SNT) plugin of Fiji-ImageJ software (*Tavares et al., 2017*). We performed morphological analyses to study the complexity of astrocytic shape, the total length of processes and their number (**Figure 2.3 A-E**). In details:

A) Astrocytes (at least 3 per brain section) were identified by their typical GFAP-positive bushy shape, with thicker processes around a single DAPI-stained nucleus. The other selection criteria applied to include an astrocyte in the analysis was that the main structure did not present truncated processes (**Figure 2.3 A**)
B) Using SNT, all GFAP-positive processes were traced, starting from the ones departing from the soma (**Figure 2.3 B**)
C) Once the reconstruction was completed, all the paths located in different stacks were skeletonized ('Path Manager'- Analyze - Skeletonize) and unified in a single image (Image – Stacks – Z project – Max intensity) (**Figure 2.3 C**)
D) Data about total length of processes and their total number were obtained from 'Path Manager' window ('Path Manager' – Analyze - Measurements – Measure Paths) (**Figure 2.3 D**)
E) To investigate the complexity of astrocytic arbour, Sholl analysis was performed on the binary skeleton. Circles spaced by 4 µm and centered on astrocyte nuclei were used. The number of intersections between processes and the concentric circles were counted by ImageJ plugin "*Sholl analysis*" (*Abramoff, Megalhaes & Ram, 2004*) (**Figure 2.3 E**)

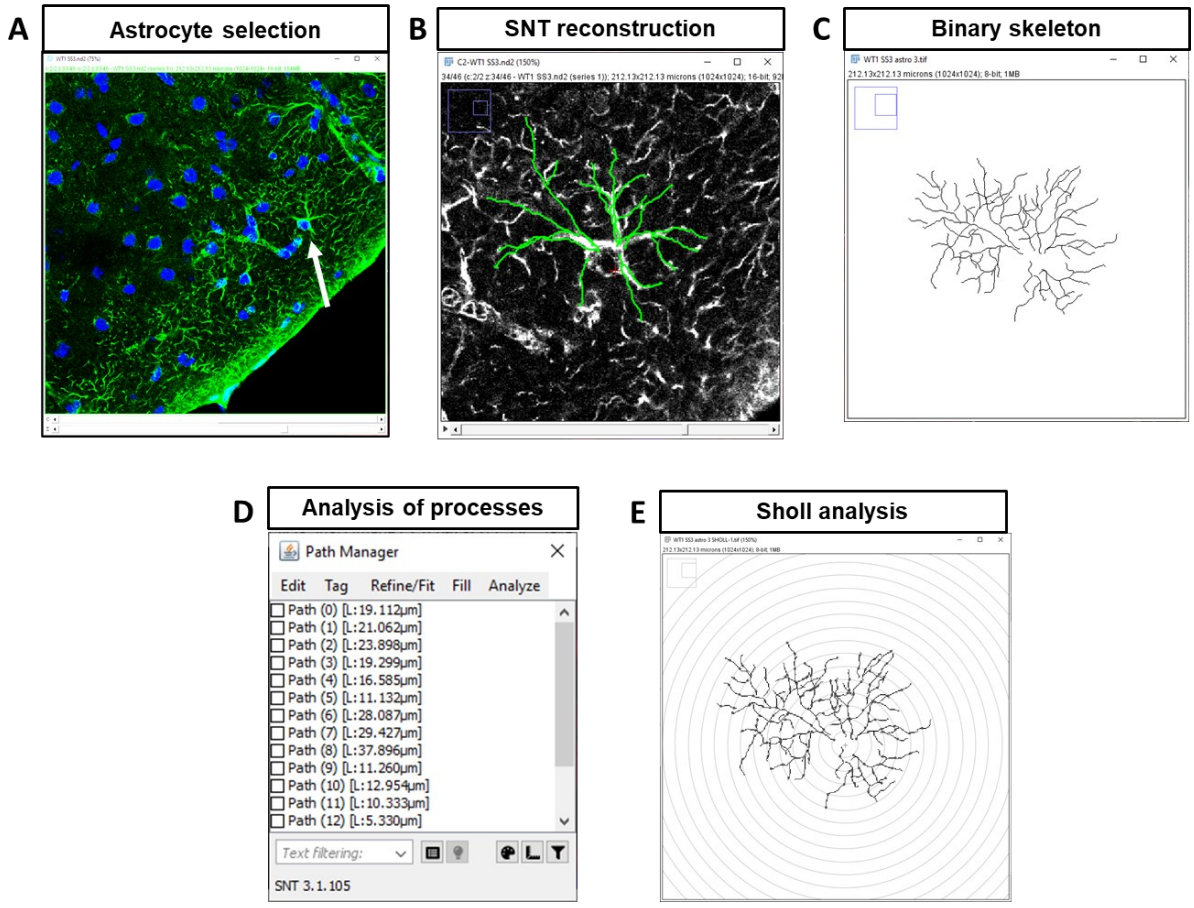

Figure 2.3. Workflow for GFAP-positive processes reconstruction across z-stacks with SNT plugin provided by Fiji-ImageJ software. **A**) Astrocyte selection from brain sections: the white arrow indicates a cell suitable for 3D reconstruction. **B, C**) SNT manual reconstruction of processes along all Z-stacks (**B**) and their binary rendering (**C**). **D, E**) Data obtained from the reconstructed arbour included total length and number of processes (**D**) and the complexity of cell shape (Sholl analysis (**E**).

Bergmann glia

Since Bergmann glia exhibits a completely different morphology, analyses were performed counting the number of GFAP-positive radial processes in 100 µm of molecular layer (*Belozor et al., 2019*) by Fiji-ImageJ software (**Figure 2.4 A-C**). In details:

A) Sub-stacks of 20 contiguous stacks (corresponding to 10 µm of brain section) were extrapolated from images (Image – Stacks – Tools – Make Sub-stacks) and Max projections were obtained (Image – Stacks – Z project – Max intensity) (**Figure 2.4 A**).

B) A threshold was applied to include all GFAP-labelled processes and images were binarized (**Figure 2.4 B**).

C) A line of 100 µm was traced in the centre of each molecular layer and parallel to granular layer. The intensity plot profile of the line was calculated (**Figure 2.4 C**) and data were tabulated in Excel (Microsoft Corporation) to automatically count the number of processes. Intensity values > 200 appearing in at least 2 consecutive cells were counted.

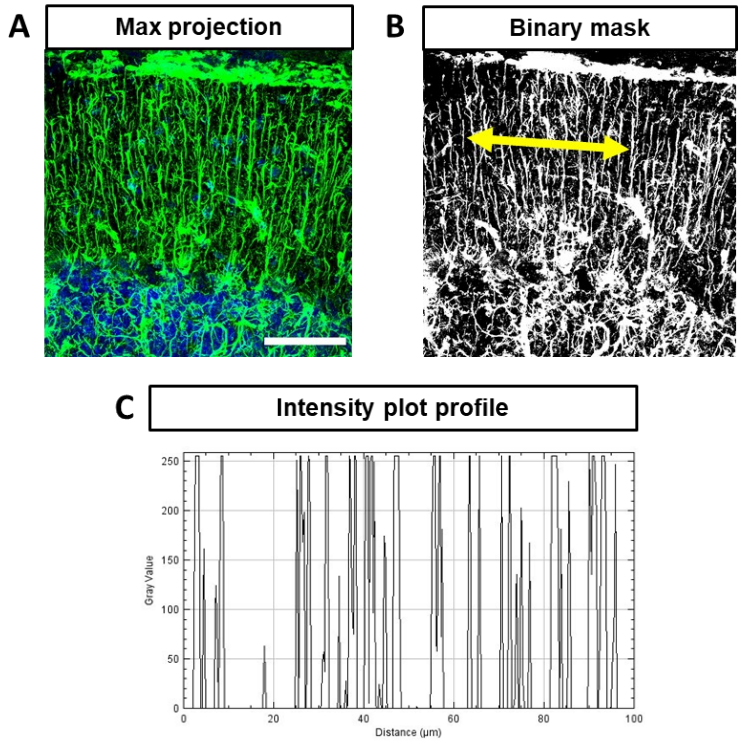

Figure 2.4. Workflow for Bergman glia GFAP-positive processes analysis. **A**) Representative Max projection image of a sub-stack with radial glia processes in the molecular layer (GFAP: green) and nuclei in the granular layer (DAPI: blue). **B**) Binarized image with a yellow double-headed arrow depicting the 100 µm of section analysed. **C**) Intensity plot profile of the traced line (100 µm).

2.4.3 Analysis of neuronal morphology *in vitro*

Single MAP2-stained neurons were randomly acquired at epi-fluorescence microscopes by Nikon (Nikon Eclipse T*i* for DIV7 and Eclipse N*i* U for DIV14) equipped with a Plan Apo λ 20x objective in green (DIV7) or red (DIV14) channel. To characterize

neuronal morphology we performed different analyses with Fiji-ImageJ software. We used "*Sholl analysis*" plugin (*Abramoff, Megalhaes & Ram, 2004*) to study the complexity of the dendritic arbour, and *NeuronJ* plugin (*Meijering et al., 2004*) to characterize the length and number of dendrites (**Figure 2.5 A-D**). Since both plugins need binary masks to work properly, first step consisted of selecting single neurons to design their skeletons (**Figure 2.5 A**). Then, we manually traced all dendrites labelled with MAP2 with Photoshop (Adobe Photoshop CS. 2004. Berkeley, CA: Peachpit Press.) and binarized the images obtained (**Figure 2.5 B**). Finally, we characterized dendritic arborization by performing Sholl analysis on the masks using a radius step size of 10 µm (**Figure 2.5 C**). The same reconstructed arbours were used to analyse the lengths of dendrites (total length and maximal length) and their number by *NeuronJ* (**Figure 2.5 D**). Lastly, we also investigated whether different culturing conditions could affect the percentage of neurons with apical dendrites (polarized neurons). To calculate it, we used the following formula (*Bay et al., 2014*):

Length of the longest dendrite / Total dendritic length

When the result is > 2, the neuron is considered polarized.

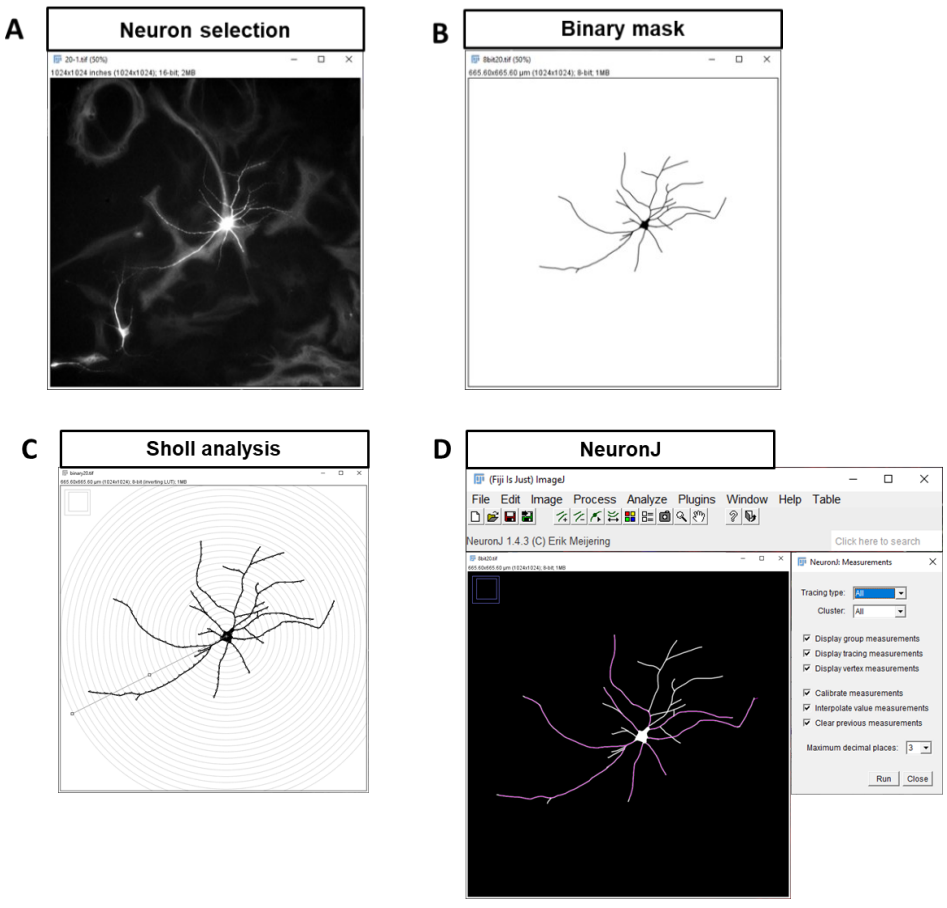

Figure 2.5. Workflow for MAP2-positive dendrites reconstruction by Fiji-ImageJ software. **A**) Representative image of a MAP2-stained neuron (DIV7) analysed. **B**) Binary mask of the dendric arbour manually traced and binarized. **C**) Sholl analysis performed with *Sholl analysis tool* by Fiji. **D**) *NeuronJ* interface with traced dendrites.

2.4.4 Synaptic markers *in vitro*: single puncta analysis and colocalization

Z-stacks images (127.28 × 127.28 μm^2, 1,024 × 1,024-pixel resolution, 16-bit grayscale depth) were acquired at a Nikon Ti2 Microscope equipped with an A1+ laser scanning confocal system and a SR Apo TIRF 100x oil-immersion objective, using a step size of 0.3 µm. For each dataset, images were acquired in four channels (Laser Wavelength for DAPI: 409.1 nm; Laser Wavelength for Synapsin1/2: 487.5 nm; Laser Wavelength for Shank2: 560.5 nm; Laser Wavelength for MAP2: 635.5 nm) and parameters were maintained constant within same experiments (offset background, digital gain, laser intensity, pinhole size, scanning speed, digital zoom, scan direction, line average mode).

Single puncta analysis

To evaluate the density and area of Synapsin1/2 and Shank2 puncta we analyzed single channels (green and red) by Fiji-ImageJ software (**Figure 2.6 A-C**). In details:

A) Max projections were obtained from Z-stacks images (Image – Stacks – Z project – Max intensity) (**Figure 2.6 A**).
B) By fixing a threshold for each channel acquired, that was maintained constant within the same experiment, images were binarized and segmented with *Watershed* tool to eventually separate joined puncta (**Figure 2.6 B**).
C) ROIs (20 x 4 µm) were manually selected on 3 primary branches/neuron and puncta were analysed by *Analyze particles* tool. Only puncta with a minimum size of 0.16 μm^2 were counted (*Fantuzzo et al., 2017*) (**Figure 2.6 C**). Average number of puncta and their area/neuron was used for statistical analyses.

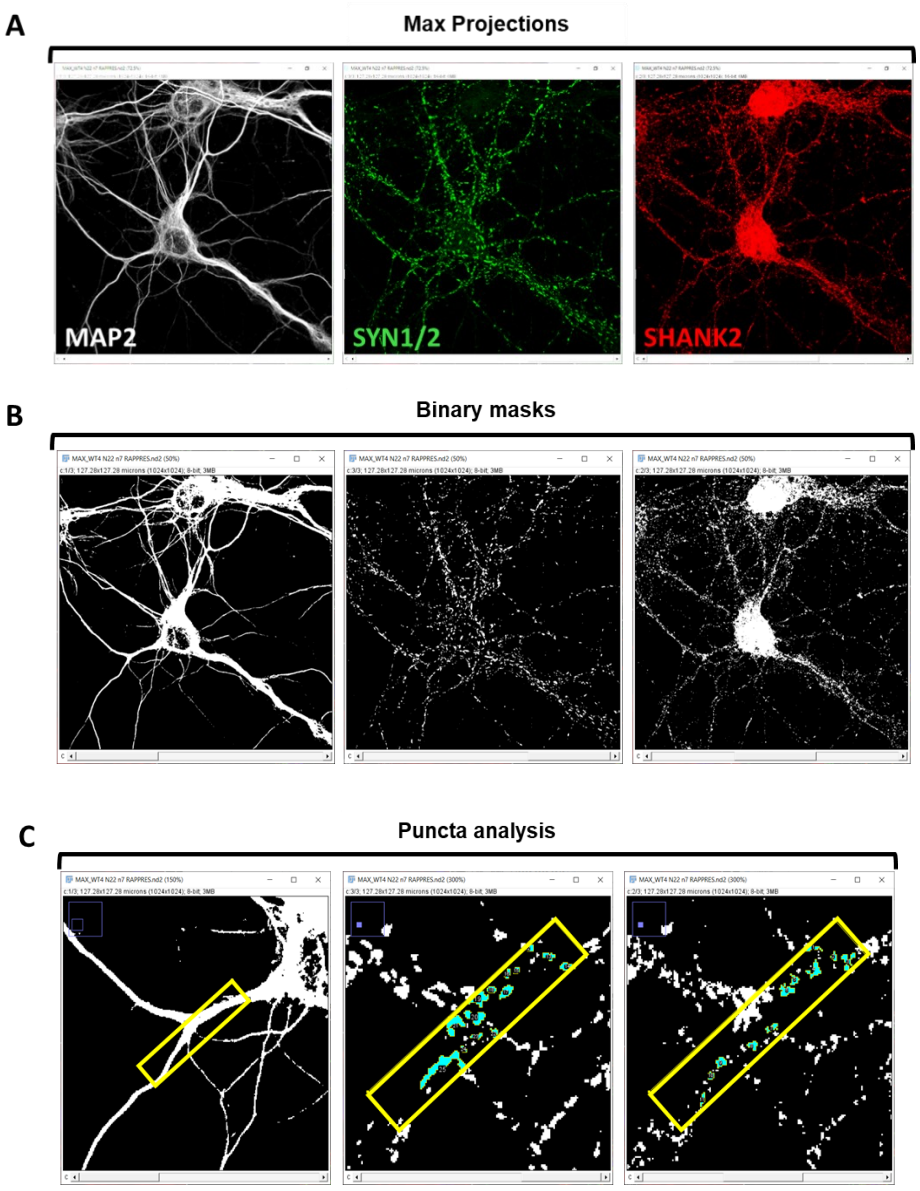

Figure 2.6. Workflow for Synapsin1/2 and Shank2 puncta analysis by Fiji-ImageJ software. **A**) Representative Max projection images of a neuron stained for MAP2 (white), Synapsin1/2 (green) and Shank2 (red). **B**) Binary mask of each channel. **C**) Puncta analysis performed with *Analyze particles* by Fiji. Yellow selection on MAP2 (left) depicts a ROI (20 µm x 4 µm) on a primary dendrite; the two enlarged selections indicate the puncta detected (light blue) in green and red channels.

Colocalization analysis

To assess puncta colocalization of pre- and post-synaptic markers, Fiji-ImageJ Plugin *Colocalization* was run on each Z-stack image acquired (**Figure 2.7 A-C**). In details:

A) Z-stacks in green (Synapsin1/2) and red (Shank2) channels were analysed using the same threshold parameters set for single puncta (**Figure 2.7 A**).

B) The plugin *Colocalization* produced binary images (8-bit) of colocalized puncta for each stack, that were merged to obtain a Max projection (**Figure 2.7 B**).

C) Max projection of MAP2 channel was merged to the one of colocalized puncta. Then, ROIs (20 x 4 µm) were manually selected on 3 primary branches/neuron and puncta were analysed by *Analyze particles* tool. Only puncta with a minimum size of 0.1 µm^2 were counted (**Figure 2.7 C**). Average number of puncta/neuron was used for statistical analyses.

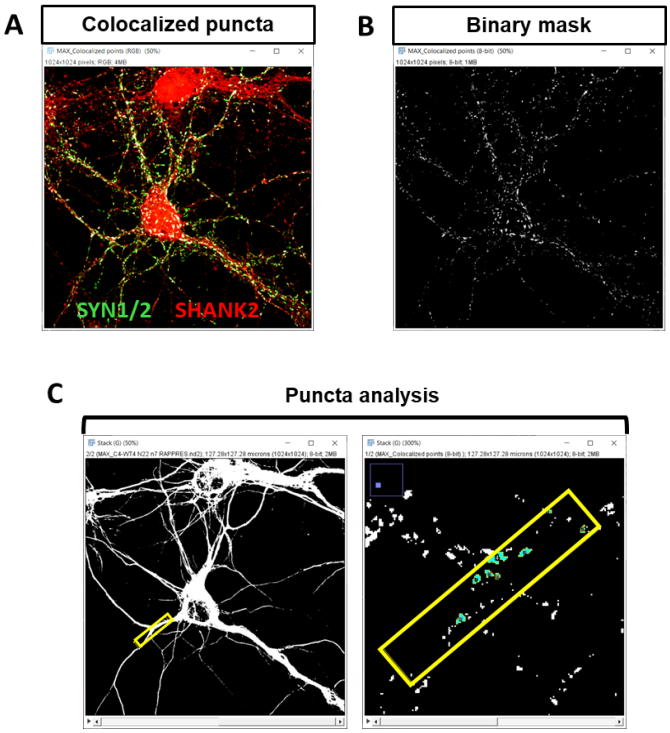

Figure 2.7. Workflow for Synapsin1/2 and Shank2 colocalization analysis with *Colocalization* plugin by Fiji-ImageJ software. **A**) Representative Max projection image of a neuron stained for Synapsin1/2 (green) and Shank2 (red) with colocalized puncta (white). **B**) Binary mask of the Max projection of colocalized puncta. **C**) Puncta analysis performed with *Analyze particles* by Fiji. Yellow selection on MAP2 depicts a ROI (20 µm x 4 µm) on a primary dendrite; the enlarged selection indicates the colocalized puncta counted (light blue).

2.4.5 Synaptic markers *in vivo*: single puncta analysis and colocalization

Z-stacks images (127.28 × 127.28 μm^2, 1,024 × 1,024-pixel resolution, 16-bit grayscale depth) were acquired at a Nikon Ti2 Microscope equipped with an A1+ laser scanning confocal system and a SR Apo TIRF 100x oil-immersion objective, using a step size of 0.3 µm. A minimum of 15 stacks/image were acquired. For each dataset, images were acquired in three channels (Laser Wavelength for DAPI: 409.1 nm; Laser Wavelength for Synapsin1/2: 487.5 nm; Laser Wavelength for PSD95: 560.5 nm) and parameters were maintained constant within same experiments (offset background, digital gain, laser intensity, pinhole size, scanning speed, digital zoom, scan direction, line average mode).

Analysis of single puncta, their volume and their colocalization across Z-stacks were performed with Arivis 4D Vision software (Arivis, AG, München, Germany), that allowed a 3D rendering of the immunostaining (**Figure 2.8 A-D**). In details:

A) *Attenuation correction* plugin by Fiji-ImageJ software was run on all Z-stacks images to correct fluorescence intensity decrease with depth in stacks (**Figure 2.8 A**).

B) Then, a specific pipeline was created to process, segmentate and obtain the number of puncta and their reconstructed volume with Arivis. For each single analysis, the pipeline consisted of following steps:

- Selection of 15 contiguous stacks (when stacks were n >15).
- Denoising, to eliminate the background.
- Filter size, to establish size exclusion criterion of the signals detected.
- Segmentation (Blob Finder), to extrapolate puncta from each channel.
- Compartmentalization, to give hierarchy and define the interactions between all compartments identified (i.e. overlaps). It was fundamental to set the percentage of coverage of Synapsin1/2 over PSD95 that defined colocalization.

To analyse different fields of the same brain section and reduce any internal variability (i.e. presence of nuclei or blood vessels, antibody permeability, etc.), 6 ROIs (30 µm x 30 µm) were designed and manually drag in the desired position of the section (**Figure 2.8 B-D**). To do this, we wrote a python script to create the sub-volumes boxes matrix. Synapsin1/2 and PSD95 puncta were analysed for each box and average values of their number and volume were used for statistical analyses.

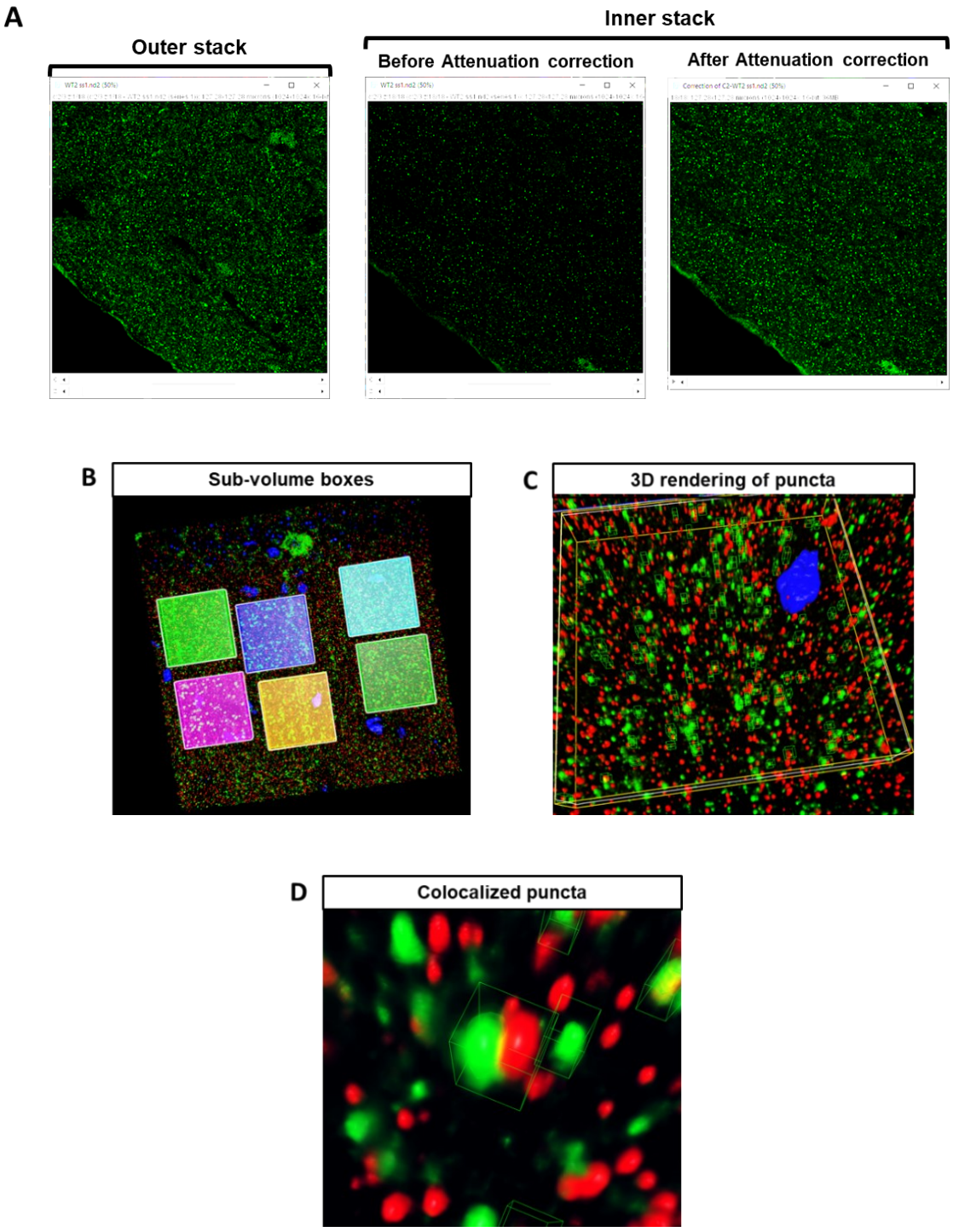

Figure 2.8. Workflow for Synapsin1/2 and PSD95 puncta analysis of brain sections. **A**) Representative 2D images (green channel) of inner stacks before and after *Attenuation correction* processing by Fiji-ImageJ. The plugin allows to correct fluorescence intensity decrease respect to a reference stack (outer stack). **B-D**) Images representing crucial steps of the pipeline run by Arivis software: creation of 6 different sub-volume boxes within the section (**B**), 3D rendering of pre- and post- synaptic markers in one box (**C**), detection of colocalized puncta (**D**).

2.5 Gene expression analysis

2.5.1 RNA extraction from cell cultures

After a rapid wash in D-PBS to remove any cell debris, total RNA was extracted from neurons (DIV 14) using PureZOL (1 mL/10 cm^2). Samples were incubated for 5 minutes at RT and 100% chloroform was added 1:5 (200 µL/1 mL PureZOL). Then, samples were manually inverted to gently mix the phenol:chloroform mixture and following 2 minutes of incubation at RT they were centrifuged (12,000 g, 15 minutes, 4°C) to separate aqueous and organic phases. The upper aqueous phase was collected and RNA was precipitated with 100% isopropanol 1:2 (500 µL /1 mL PureZOL) and 10 µg/sample of glycogen for 48 hours at -20 °C. RNA was centrifuged (12,000 g, 10 minutes, 4 °C), pellets were washed in 70 % EtOH (500 µL /sample) and re-precipitated (7,500 g, 10 minutes, 4 °C). To remove genomic DNA, DNase was directly added to dried pellets (20 µL of a mix composed of: 17 µL H_2O RNAsi-free + 2 µL buffer + 1 µL DNase amplification grade) and incubated at 37°C for 15 minutes in a dry bath. RNA extraction was repeated adding 80 µL PureZOL / sample, following the exact protocol and proportions of the volumes mentioned above, until pellet precipitation in 70% EtOH. At this step, RNA was completely dried at RT, resuspended in 12 µL H_2O RNAsi-free and stored at – 80°C.

2.5.2 RNA quality assessment

Integrity of the total RNA extracted from samples was assessed using Agilent 2100 Bioanalyzer using the *RNA 600 Nano Reagent*. Samples were previously quantified using a spectrophotometer (NanoDrop, ThermoFisher) and concentrations were eventually diluted to obtain an adequate quantity in 1 µL of solution.

Bioanalyzer uses microfluidics/capillary electrophoresis to analyse nucleic acids. It compares the fluorescence of the sample, to which an RNA-specific dye has been added, with that of a standard. High quality total RNA presents two distinct bands for 28S and 18S subunits, with a ratio of 2:1, respectively, in the electropherograms (**Figure 2.9**). Agilent 2100 Bioanalyzer software (Expert 2100 software) uses an algorithm to calculate the RNA Integrity Number (RIN), that ranges from 0 (totally degraded RNA) to 10 (completely intact RNA). All RIN values were >9.

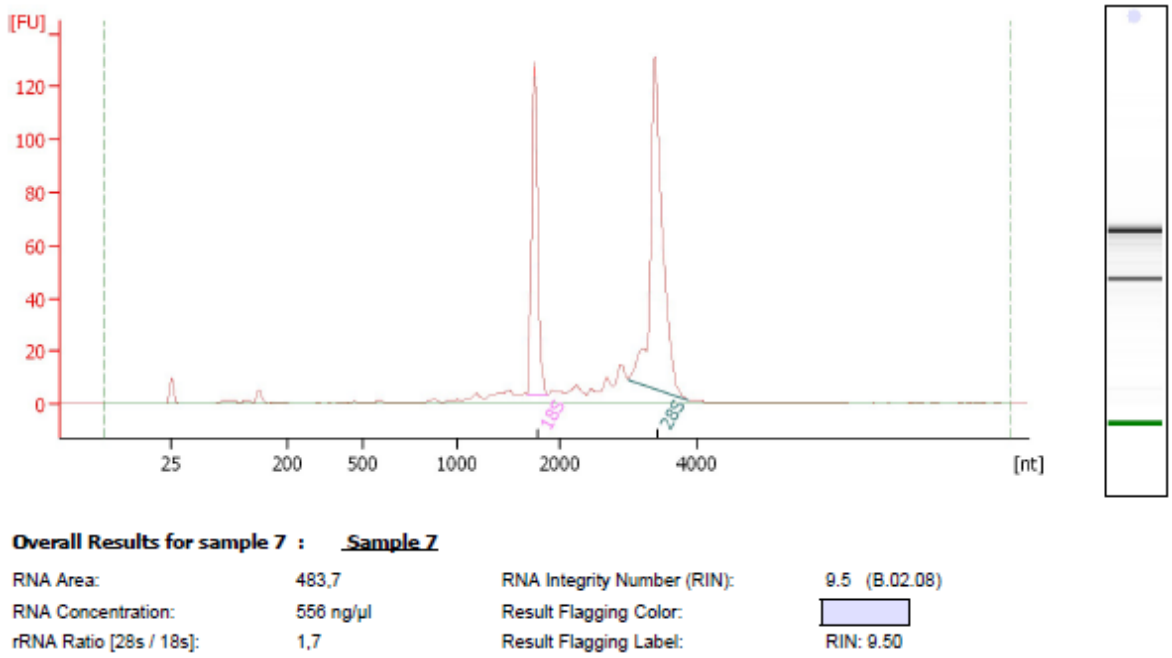

Figure 2.9. Representative electropherogram of a run with Agilent 2100 Bioanalyzer. The software calculates RNA concentration and quality (RIN).

2.5.3 RNA-Seq analysis

RNA-Seq analysis was performed in collaboration with the Functional Genomic Lab, Department of Biotechnology, at the University of Verona, as follows:

RNA quality control was performed on the 20 RNA samples after shipment. RNA purity was measured using a NanoDrop Spectrophotometer, while RNA integrity was assessed using the RNA 6000 Nano Kit on a Bioanalyzer (Agilent Technologies). All samples showed an RNA integrity number (RIN) >9. RNA samples were quantified using the Qubit RNA BR Assay Kit (Thermo Fisher Scientific).

RNA-seq libraries were generated using the TruSeq stranded mRNA kit (Illumina) from 400ng of RNA samples, after poly(A) capture and according to manufacturer's instructions.

Library quality control. Quality and size of RNAseq libraries were assessed by capillary electrophoretic analysis with the Agilent 4200 Tape station (Agilent). Libraries were quantified by real-time PCR against a standard curve with the KAPA Library Quantification Kit (KapaBiosystems, Wilmington, MA, USA).

Sequencing. Libraries were pooled at equimolar concentration and sequenced on a NovaSeq6000 (Illumina) generating >20 million fragments in 150PE mode for each sample.

Sequencing data quality control and filtering (Figure 2.10). Quality of reads was assessed using FastQC software (http://www.bioinformatics.babraham.ac.uk/projects/fastqc/); a QC report is included for each sample in the result folder. Sequencing read trimming and quality control. Quality of reads was assessed using FastQC software (http://www.bioinformatics.babraham.ac.uk/projects/fastqc/). Starting from raw FASTQ files, reads with more than 10% of undetermined bases or more than 50 bases with a quality score <7 were discarded. Reads were then clipped from adapter sequences using Scythe software (v0.991) (https://github.com/vsbuffalo/scythe), and low-quality ends (Q score <20 on a 10-nt window) were trimmed with Sickle (v1.33) (https://github.com/vsbuffalo/sickle). Filtered reads were aligned to the Human reference genome GRCh38 (Ensembl release 99) using STAR (v2.7.6a) with default

parameters and --quantMode TranscriptomeSAM option that output alignments translated into transcript coordinates. After reads mapping, the distribution of reads across known gene features, such as exons (CDS, 5'UTR, 3'UTR), introns and intergenic regions was verified using the script read_distribution.py provided by RSeQC package (v3.0.1).

Transcriptome quantification and differential expression analysis (Figure 2.10). Read counts on genes were quantified using RSEM (v.1.3.3). Genes-level abundance, estimated counts and gene length obtained with RSEM were summarized into a matrix using the R package tximport (v1.12.3) and subsequently the differential expression analysis was performed with DESeq2(v1.24.0). To generate more accurate Log2 FoldChange estimates, the shrinkage of the Log2 FoldChange was performed applying the apelglm method.

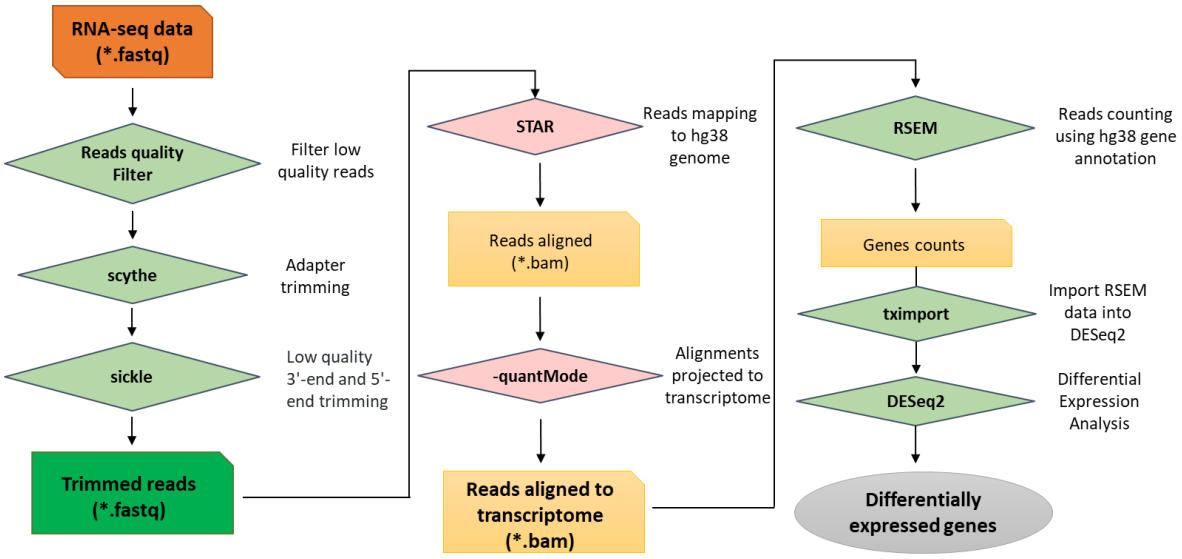

Figure 2.10. RNA-Seq analysis pipeline.

Analyses were performed for the following 3 comparison groups:

1. WT neurons co-cultured with WT astrocytes *versus* WT neurons cultured alone (WT *versus* CTRL)
2. WT neurons co-cultured with *Mecp2* KO astrocytes *versus* WT neurons cultured alone (KO *versus* CTRL)

3. WT neurons co-cultured with *Mecp2* KO astrocytes *versus* WT neurons co-cultured with WT astrocytes (KO *versus* WT).

Gene Ontology (GO) enrichment analysis was performed using clusterProfiler**,** an R Package for comparing biological themes among gene clusters (*Yu et al., 2011*) (Bioconductor version: Release (3.12)). The function *simplify* has been used to remove redundancy of enriched GO terms. Differentially expressed genes (DEGs) with p.adjust<0.1 were included in the analysis, that were performed on all the 3 comparison groups. FDR adjusted p-value (q-value) <0.05 was used as a threshold and GO terms fulfilling this condition were defined as significantly enriched.

GSEA—Gene Set Enrichment Analysis (GSEA) (*Subramanian et al., 2005*)(version 4.1.0, the Broad Institute of MIT and Harvard; https://www.gsea-msigdb.org/gsea/downloads.jsp) was performed on shrunken, log-normalized exonic fold changes from DESeq2 between WT neurons cultured with *Mecp2* KO astrocytes and WT neurons cultured with WT astrocytes RNA-Seq data. GSEA calculated a gene set Enrichment Score (ES) that analyzed genes were enriched in the biological signal conduction on the MsigDB 7.2 (Molecular Signatures Database; https://www.gsea-msigdb.org/gsea/msigdb). Background was set to all expressed genes in this study and 1,000 permutations were set to generate a null distribution for enrichment score in the hallmark gene sets and functional annotation gene sets. The gene sets database used for enrichment analysis were 'c5.go.bp.v7.2.symbols.gmt', 'c5.go.cc.v7.2.symbols.gmt', 'c5.go.mf.v7.2.symbols.gmt' and FDR < 0.1 was defined as the cut-off criteria for significance.

Materials

- PureZOL RNA isolation Reagent, Bio-Rad, cod. 7326890
- Chloroform, SIGMA, cod. 372978
- 2-Propanol, SIGMA, cod. 33539
- Ethanol, SIGMA, cod. 32221
- Nuclease-Free Water, SIGMA, cod. W4502
- DNase I Amplification Grade, SIGMA, cod. AMPD1
- RNA 600 Nano Reagent, AGILENT, cod. 5067-1511

2.6 Sphingolipids

2.6.1 Evaluation of the cell sphingolipid pattern

Neurons (DIV14) or astrocytes in the different experimental conditions were analysed for their lipid content after feeding with [1-^{3}H]-sphingosine to label cell sphingolipids.
Radioactive sphingosine is solubilized in the complete culturing medium at the stock concentration of 216 nM (specific radioactivity 1.06 Ci/ mmol).
In the experimental condition A, neurons and astrocytes were fed with an appropriate volume of ^{3}H-sphingosine stock solution in order to obtain a final concentration of 36 nM. Co-culture in presence of radioactive sphingosine was maintained for 8 days without changing the medium.
In the experimental condition B, astrocytes were fed with ^{3}H-sphingosine as described above for 24 hours. After that the culture medium was substituted and cells maintained in culture for other 24 hours before to starting the following 8 days of co-culture with WT neurons.
At the end of the co-culture, in both the experimental conditions astrocytes and neurons were harvested lysed in water containing protease inhibitors, sonicated and subjected to DC protein assay (Biorad).
To perform lipid analysis, cell lysates were lyophilized overnight using a Freeze Dryer (Labconco Freezone).
After lyophilisation, total lipids were extracted resuspending the pellets in 50 µl H_2O, 500 µl of methanol and 1 ml of chloroform. After each addition samples were vortexed, sonicated in a water bath sonicator for 1 minute, and mixed for 10 minutes at RT in a ThermoMixer® (Eppendorf). Samples were then centrifuged at 13000 x g for 10 minutes at 4°C. The obtained surnatant is transferred to another 2 ml Eppendorf tube while the pellet is subjected to a second lipid extraction as previously described. The surnatant obtained is added to the previous one forming the total lipid extract (TLE).
Aliquots of TLE were counted by liquid scintillator to determine the amount of radioactivity.
Lipids of TLE were separated by HPTLC loading the same amount of radioactivity for each sample and separated using the solvent system chloroform: methanol: $CaCl_2$ 0.2%, 50: 42: 11 (v: v: v). Radioactive lipids were detected and quantified by digital autoradiography performed with a Beta-Imager ^{T}Racer instrument (BioSpace).

Identification of lipids after separation was assessed by co-migration with authentic radioactive lipid standards. The radioactivity associated with individual lipids was determined with M3 Vision software.

2.6.2 Evaluation of the sphingolipids released in the astrocytes extracellular milieu

Astrocytes were seeded on 100 mm dishes at a density of 800,000 cells/dish and maintained in culture with *astrocyte culture medium* until 90% confluence (DIV13). At this time, WT and KO astrocytes were fed with ^{3}H-sphingosine as described above for 2 hours. After that, the culture medium was substituted and cells maintained in culture for other 72 hours. At the end of the incubation the medium and cells were collected, lyophilized and subject to lipids extraction as described before. To remove salts from the medium derived TLE, these samples were resuspended in pure water and subjected to 5 days of dialysis. Subsequently, TLE were lyophilized, resuspended in chloroform:methanol 2:1 (by vol). The radioactivity was evaluated by liquid scintillator. The analysis of the radioactive lipids was performed as described above.

2.7 Statistical analysis

All data are expressed as mean ± SEM. Before any statistical analysis, normality distribution and outliers were evaluated for each dataset by D'Agostino & Pearson test and ROUT test (Q=1%), respectively. Statistical significance for multiple group comparisons was determined by one- or two-way analysis of variance (ANOVA), followed by *post hoc* tests. Unpaired Student's t-tests or Mann–Whitney tests were used for two group comparisons.
All statistical analyses were performed using Prism 8 (Graphpad Software, CA).

Results

3. Characterization of *Mecp2* KO astrocyte morphology

Astrocytes are very dynamic cells whose shape is crucial to exploit their functions properly. They undergo major rearrangement of cytoskeletal proteins, including remodeling of their processes, to control local environment and to contact surrounding cells (*Verkhratsky and Nedergaard, 2018*). With the aim to characterize pathological phenotypes in *Mecp2* KO astrocytes, we started to investigate whether *Mecp2* deficiency could affect astrocyte morphology *in vivo*.

3.1 *In vivo Mecp2* influences the morphology of astrocytes according to the specific brain area and its age

To determine whether the lack of *Mecp2* affects astrocyte morphogenesis in the mouse brain and eventually progresses over time, we measured astrocyte complexity in brain slices. In accordance with accumulating evidence suggesting heterogeneity of astrocytes among different brain regions, we focused our attention on different brain areas, whose functional alterations have been documented in RTT (*Fukuda et al., 2005; Chapleau et al., 2009*; *Jentarra et al., 2010; Gulmez-Karaca et al., 2019*). In particular, we investigated astrocyte morphology in the motor cortex, somatosensory cortex and CA1 area of hippocampus of *Mecp2* KO mice at three different ages. To describe astroglial morphology along with the progression of the disease, the analysis was performed at P20, corresponding to the so-called pre-symptomatic phase, P40 and P70, representing an early and late symptomatic phase, respectively (**Figure 3.1**). Brain slices from KO animals and their WT littermates were immunostained with an antibody against GFAP and morphometric analyses were performed after manual reconstruction of the astrocytic skeleton using the SNT plugin (Fiji). For each experimental group, shape complexity of the reconstructed astrocyte (Sholl analysis), total length and number of its processes were measured.

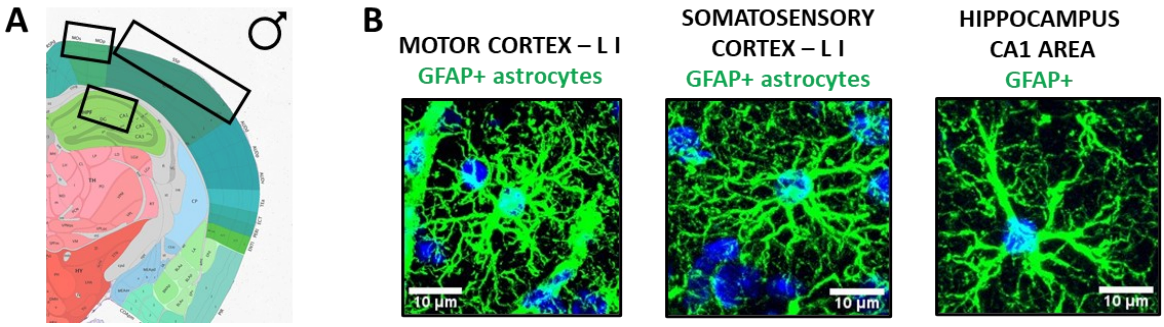

Figure 3.1. A) Coronal section from the Allen Brain Atlas depicting the three analysed areas. **B)** Micrographs are representative images of WT astrocytes immunostained for GFAP (green) in layer I of the motor and somatosensory cortex and the CA1 area of the hippocampus. Scale bar = 10 µm.

3.1.1 Astrocytes in the motor cortex (layer I) of *Mecp2* KO mice show an altered morphology already before the appearance of RTT-like symptoms

Analyses performed on GFAP$^+$ KO astrocytes within layer I of the motor cortex revealed the presence of morphological defects already at P20, when RTT symptoms are not yet manifested. Indeed, they exhibited decreased ramifications at 20, 24 and 28 µm from the soma, together with a decrease in total length and number of processes (**Figure 3.2 A-D**). Morphological impairments continue to be present at later time points. Indeed, astrocyte shape complexity is significantly decreased both at P40 and P70 (P40: at 12,16, 20 µm and P70: at 16 µm from the soma) (**Figure 3.2 E, F, I, J**). Similarly, we reported a decrease in the total length of astrocytic processes as well as in their number (**Figure 3.2 G, H, K, L**).

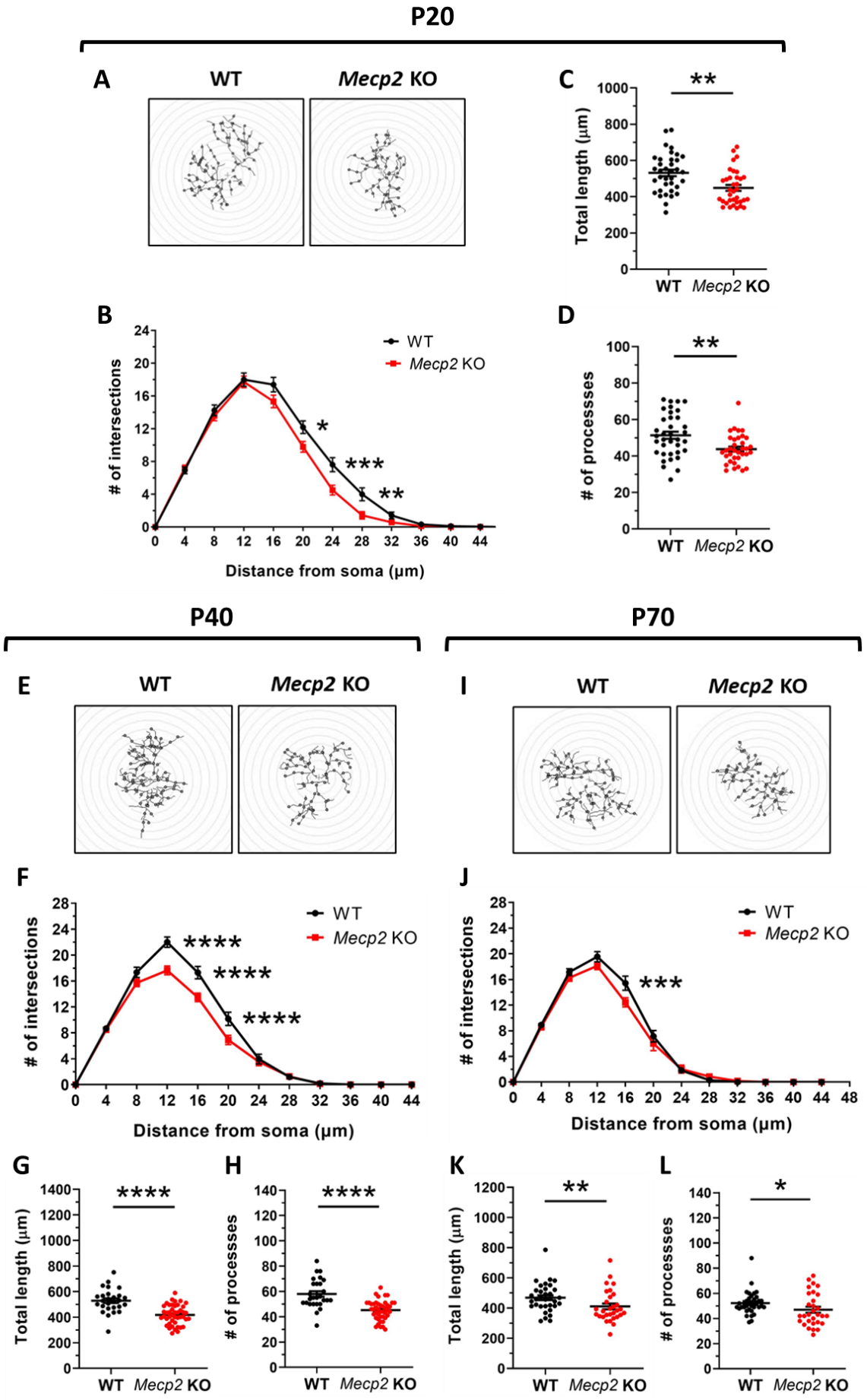
P20
A
WT
Mecp2 KO
C
Total length (µm)
WT
Mecp2 KO
B
# of intersections
Distance from soma (µm)
D
# of processses
P40
P70
E
F
G
H
I
J
K
L

Figure 3.2. *Mecp2* KO astrocytes in the motor cortex (layer I) exhibit an altered morphology at P20, P40 and P70. A, E, I) Representative images of the reconstructed astrocyte arbours by SNT plugin. To measure their complexity, circles spaced by 4 μm and centered on astrocyte nuclei were used. The number of intersections between processes and the concentric circles were counted by the ImageJ plugin "Sholl analysis" (*Abramoff, Megalhaes & Ram, 2004*). **B, F, J)** Quantification of Sholl analysis in WT and *Mecp2* KO astrocytes from mice at P20, P40 and P70. Asterisks indicate statistical significance between the two experimental groups at specific distances from the soma (* $p<0.05$, ** $p<0.01$, *** $p<0.001$, **** $p<0.0001$ by Sidak's *post hoc* test). Two-way ANOVA indicated a significant astrocyte genotype effect (P20 and P40: $p<0.0001$; P70: $p=0.0256$). **C, D, G, H, K, L)** Graphs represent the mean ± SE of the total length (**C, G, K**) and number (**D, H, L**) of astrocytic processes (C: ** $p=0.0010$ by Student's t-test; D: ** $p=0.0046$ by Mann Whitney test; G, H: **** $p<0.0001$ Student's t-test; K: ** $p=0.0067$ by Mann Whitney test; L: * $p=0.0291$ by Mann Whitney test). WT and *Mecp2* KO astrocytes (P20: n=36 WT and n=35 KO; P40: n=27 WT and n=44 KO; P70: n=35 WT and n=30 KO) derived from at least 3 different animals per genotype (P20: n=4 WT and 4 KO mice; P40: n=3 WT and 5 KO mice; P70: n=4 WT and 4 KO mice).

3.1.2 Morphological defects of astrocytes in the somatosensory cortex (layer I) of *Mecp2* KO mice progress along with RTT-like symptoms

Analyses performed on KO $GFAP^+$ astrocytes within layer I of the somatosensory cortex revealed the presence of morphological defects similar to those described in the adjacent motor cortex. Indeed, at P20, although shape complexity of KO astrocytes is comparable to the WT, our analysis reported a significant decrease in total length of processes and in their number (**Figure 3.3 A-D**). Morphological alterations progress severely over time. Indeed, KO astrocytes present a significantly impaired ramification both at P40 and at P70 (P40: at 12, 16, 20, 24 μm and P70: at 16, 20, 24, 28, 32 μm from the soma) (**Figure 3.3 E, F, I, J**). Accordingly, we found a reduction in total length at both ages, together with defects in the number of processes (**Figure 3.3 G, H, K, L**).

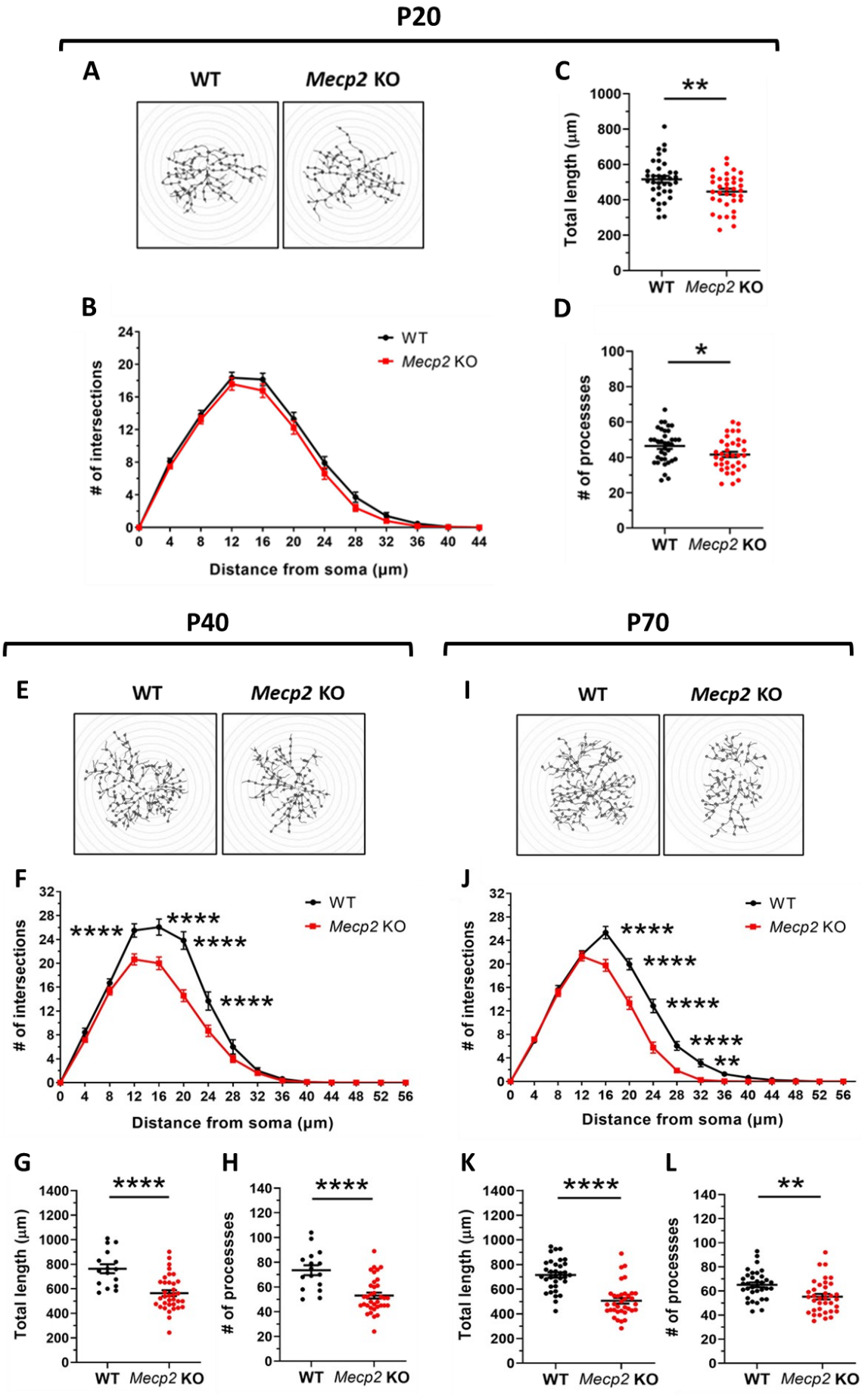
P20
A
WT
Mecp2 KO
C
**
Total length (µm)
1000
800
600
400
200
0
WT
Mecp2 KO
B
WT
Mecp2 KO
# of intersections
24
20
16
12
8
4
0
0 4 8 12 16 20 24 28 32 36 40 44
Distance from soma (µm)
D
*
# of processses
100
80
60
40
20
0
WT
Mecp2 KO
P40
P70
E
WT
Mecp2 KO
I
WT
Mecp2 KO
F
WT
Mecp2 KO
# of intersections
****
****
****
****
0 4 8 12 16 20 24 28 32 36 40 44 48 52 56
Distance from soma (µm)
J
WT
Mecp2 KO
# of intersections
****
****
****
****
**
0 4 8 12 16 20 24 28 32 36 40 44 48 52 56
Distance from soma (µm)
G
****
Total length (µm)
1400
1200
1000
800
600
400
200
0
WT
Mecp2 KO
H
****
# of processses
140
120
100
80
60
40
20
0
WT
Mecp2 KO
K
****
Total length (µm)
1400
1200
1000
800
600
400
200
0
WT
Mecp2 KO
L
**
# of processses
140
120
100
80
60
40
20
0
WT
Mecp2 KO

Figure 3.3. *Mecp2* KO astrocytes in the somatosensory cortex (layer I) manifest alterations at P20 that progress at P40 and P70. A, E, I) Representative images of the reconstructed astrocyte arbours by SNT plugin. **B, F, J)** Quantification of Sholl analysis in WT and *Mecp2* KO astrocytes from P20, P40 and P70 mice. Asterisks indicate statistical significance between the two experimental groups at specific distances from the soma (** p<0.01, **** p<0.0001 by Sidak's *post hoc* test). Two-way ANOVA assessed a significant genotype effect (P20: p<0.0018; P40 and P70: p<0.0001). **C, D, G, H, K, L)** Graphs represent the mean ± SE of the total length (**C, G, K**) and number (**D, H, L**) of astrocytic processes (C: ** p=0.0070 by Student's t-test; D: * p=0.0334 by Student's t-test; G, H: **** p<0.0001 Student's t-test; K: **** p<0.0001 by Mann Whitney test; L: ** p=0.0019 by Student's t-test). WT and *Mecp2* KO astrocytes (P20: n=36 WT and n=36 KO; P40: n=16 WT and n=35 KO; P70: n=34 WT and n=36 KO) derived from at least 3 different animals per genotype (P20: n=4 WT and 4 KO mice; P40: n=3 WT and 5 KO mice; P70: n=4 WT and 4 KO mice).

3.1.3 Hippocampal astrocytes (CA1 area) of *Mecp2* KO mice exhibit an altered morphology only at P70

In the CA1 area of the hippocampus, analyses of KO GFAP$^+$ astrocytes revealed morphological defects only at the latest time point (P70). Indeed, at early time points, the shape complexity of KO astrocytes, the total length of the processes and their number are all comparable to the WT (**Figure 3.4 A-H**). Interestingly, at P70, morphological defects start to appear: process ramification is significantly decreased at 20, 24, and 32 μm from the soma, together with a reduction in total length of astrocytic processes (**Figure 3.4 J-L**). Conversely, no defect in their number is observed (**Figure 3.4 M**).

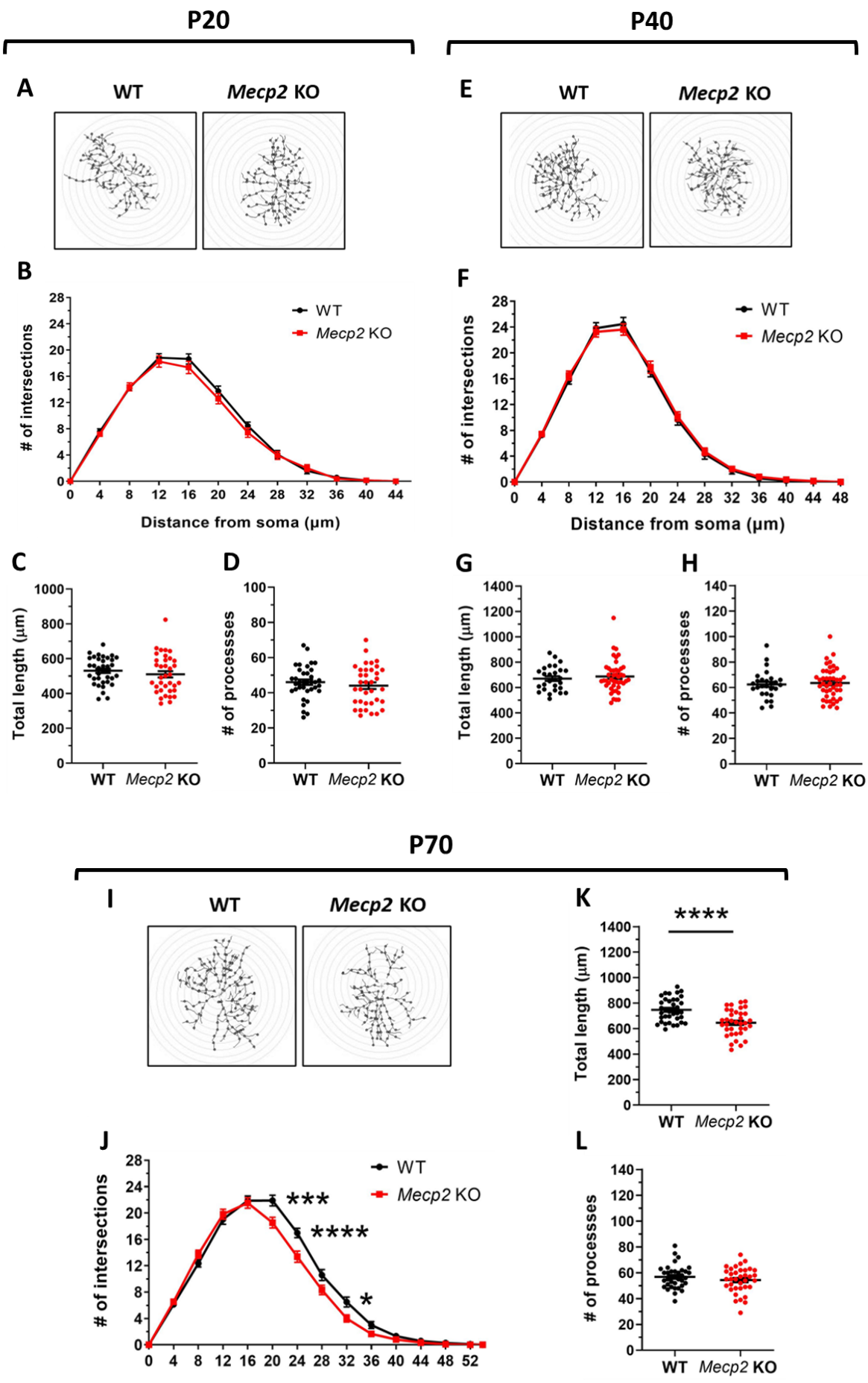
P20
P40
A
WT
Mecp2 KO
E
WT
Mecp2 KO
B
# of intersections
WT
Mecp2 KO
Distance from soma (µm)
F
# of intersections
WT
Mecp2 KO
Distance from soma (µm)
C
Total length (µm)
WT
Mecp2 KO
D
# of processses
WT
Mecp2 KO
G
Total length (µm)
WT
Mecp2 KO
H
# of processses
WT
Mecp2 KO
P70
I
WT
Mecp2 KO
K
****
Total length (µm)
WT
Mecp2 KO
J
# of intersections
WT
Mecp2 KO
***
****
*
L
# of processses
WT
Mecp2 KO

Figure 3.4. *Mecp2* KO astrocytes in the hippocampus (CA1 area) show an altered morphology only at P70. A, E, I) Representative images of the reconstructed astrocyte arbours by SNT plugin. **B, F, J)** Quantification of Sholl analysis in WT and *Mecp2* KO astrocytes from mice at P20, P40 and P70. Asterisks indicate statistical significance between the two experimental groups at specific distances from the soma (* p<0.05, *** p<0.001, **** p<0.0001 by Sidak's *post hoc* test). Two-way ANOVA assessed a significant genotype effect (P20: p=0.1034; P70: p<0.0001). **C, D, G, H, K, L)** Graphs represent the mean ± SE of the total length (**C, G, K**) and number (**D, H, L**) of astrocytic processes (K: **** p<0.0001 by Student's t-test). WT and *Mecp2* KO astrocytes (P20: n=36 WT and n=36 KO astrocytes; P40: n=27 WT and n=45 KO astrocytes; P70: n=36 WT and n=36 KO astrocytes) derived from at least 3 different animals per genotype (P20: n=4 WT and 4 KO mice; P40: n=3 WT and 5 KO mice; P70: n=4 WT and 4 KO mice).

3.1.4 Astroglia cells in the cerebellum of *Mecp2* KO mice do not show altered morphology at the onset of RTT-like symptoms (P40)

In parallel, we found it interesting to investigate the morphology of astrocyte in a less affected area in RTT, as the cerebellum. We focused on P40, characterizing the two main astroglial populations of this brain region: Bergmann glia (BG) and velate astrocytes (VA) (**Figure 3.5**). For velate astrocytes, a subclass of protoplasmic astrocytes, shape complexity and length of processes were analysed as we did for cortex and hippocampus. Results indicated no difference in KO astrocytes by Sholl analysis and total length measurements (**Figure 3.5 B-D**).

Bergmann glia exhibit a completely distinct morphology due to functional differences and developmental derivation. Therefore, taking *Belozor et al., 2019* as a reference, we counted the number of radial processes in 100 µm of the molecular layer and no difference was observed between WT and KO animals (**Figure 3.5 E, F**).

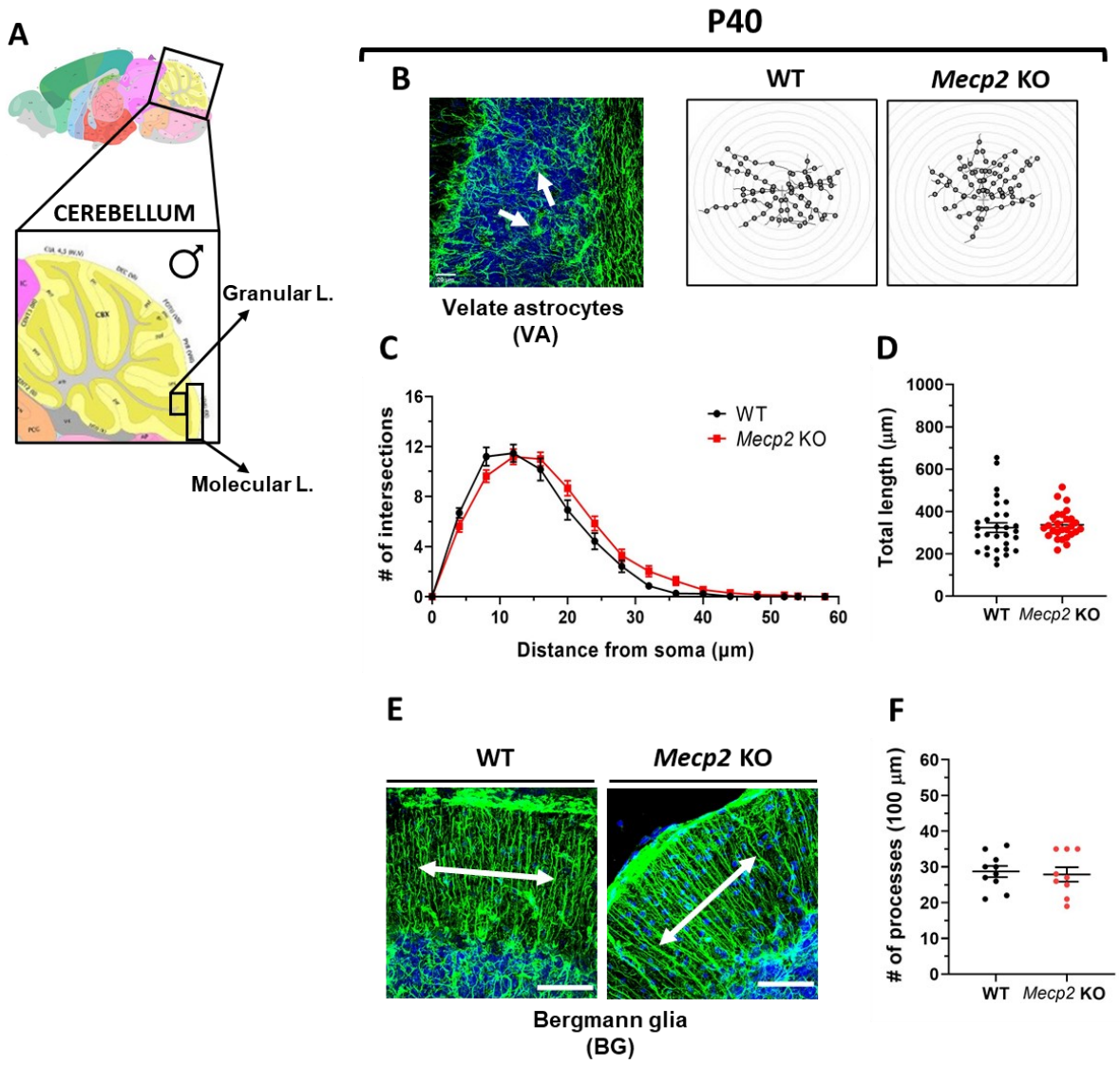

Figure 3.5. Velate astrocytes and Bergmann glia in the cerebellum of early symptomatic *Mecp2* KO mice do not show altered morphology. A) Sagittal section from the Allen Brain Atlas depicting the areas of the cerebellum analysed: the molecular (ML) and granular (GL) layers. **B)** Representative micrograph of WT velate astrocytes (VA) (single head arrows) in the GL immunostained for GFAP (green) and representative images of the reconstructed astrocyte arbours from WT and KO mice by SNT plugin. To measure their complexity, circles spaced by 4 µm and centered on astrocyte nuclei were used. The number of intersections between processes and the concentric circles were counted with the ImageJ plugin "Sholl analysis" (*Abramoff, Megalhaes & Ram, 2004*). **C)** Quantification of Sholl analysis in velate astrocytes from WT and *Mecp2* KO mice at P40. Two-way ANOVA assessed a significant genotype effect (p=0.0412). **D)** The graph represents the mean ± SE of the total length of astrocytic processes. WT and *Mecp2* KO astrocytes (n = 30 WT and n = 27 KO) derived from 3 different animals. **E**) Representative micrographs of WT and KO Bergmann glia (BG) in the ML immunostained for

GFAP (green). Double head arrows represents the 100 µm section analysed for BG processes. Scale bar = 30 µm. **F**) The graph represents the mean ± SE of the number of astrocytic processes in 100 µm section. WT and *Mecp2* KO sections (n=10 WT and n=9 KO) derived from 3 different animals per genotype.

3.1.5 Astrocytes in the somatosensory cortex (L I) of symptomatic heterozygous female mice exhibit morphological defects regardless of Mecp2 expression

To understand whether morphological impairments of KO astrocytes are caused by cell-autonomous or non-cell-autonomous defects, we proceeded analysing the layer I of the somatosensory cortex of heterozygous females at P180, corresponding to a symptomatic phase. The morphological phenotypes of KO astrocytes in the heterozygous brains were compared both to those astrocytes expressing the wild type *Mecp2* allele in the same brains and to WT astrocytes derived from healthy animals. Interestingly, both $Mecp2^{+}$ and $Mecp2^{-}$ astrocytes present in the heterozygous brain present a reduced complexity compared to the WT control (WT (het): at 20, 24, 28, 32 µm; KO (het): at 16, 20, 24, 28, 32 µm from the soma) (**Figure 3.6 B, C**). Intriguingly, WT astrocytes from heterozygous mice show a more affected phenotype than KO cells at 24 µm from the soma. Data were further supported by the analysis of the total length of astrocytic processes, that unveiled a significant decrease in WT astrocytes of heterozygous females respect to WT astrocytes of control animals, while no difference was observed in KO cells (**Figure 3.6 D**). No defect was reported in the number of processes (**Figure 3.6 E**). These data suggest that non-cell-autonomous mechanisms might be involved in the occurrence of astrocyte morphological alterations.

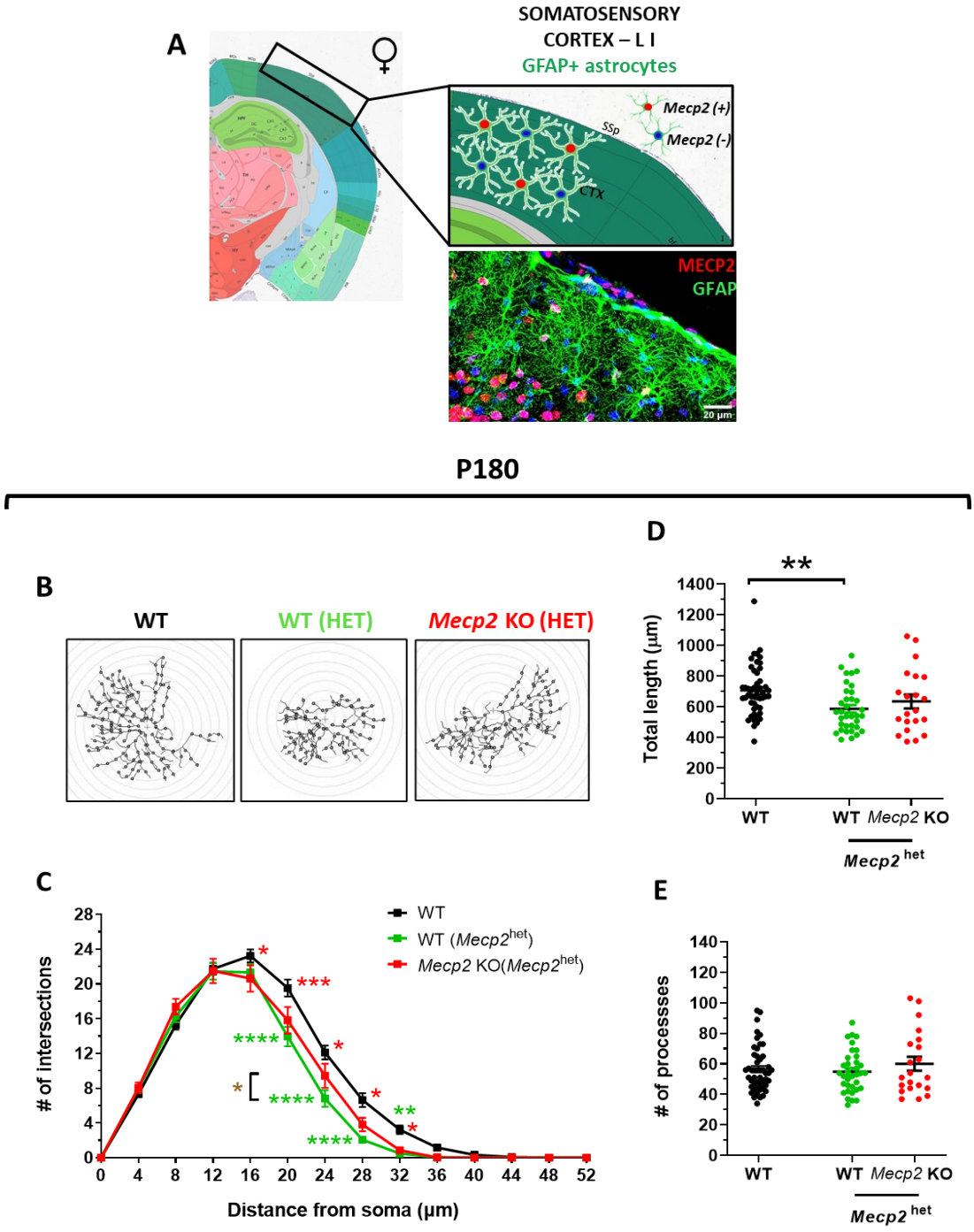

Figure 3.6. WT and *Mecp2* KO astrocytes in the somatosensory cortex (L I) of heterozygous female mice show morphological defects at P180. A) Coronal section from the Allen Brain Atlas depicting the area of the somatosensory cortex analysed. The micrograph is a representative image of a section from a *Mecp2* heterozygous brain immunostained for GFAP (green) and Mecp2 (red) in layer I of the somatosensory cortex. Scale bar = 20 µm. **B)** Representative images of the reconstructed astrocyte arbours by SNT plugin. **C)** Quantification of Sholl analysis of WT and *Mecp2* KO astrocytes from heterozygous mice at P180 compared

to WT littermates. Asterisks indicate statistical significance between the three experimental groups at specific distances from the soma (* p<0.05, ** p<0.01, *** p<0.001, **** p<0.0001 by Tukey's *post hoc* test). Red: WT vs KO (het); green: WT vs WT (het); brown: WT (het) vs KO (het). Two-way ANOVA assessed a significant genotype effect (p < 0.0001). **D, E)** Graphs represent the mean ± SE of total length (**D**) and number (**E**) of astrocytic processes (D: ** p<0.01 by Dunn's *post hoc* test). Astrocytes (n=49 WT, n=35 WT (het) and n=21 KO (het)) derived from 4 different animals per genotype.

3.2 *Mecp2* deficiency affects excitatory synapses depending on the brain area and its age

It has been demonstrated that astrocyte morphogenesis represents a crucial factor for regulating synaptogenesis (*Stogsdill et al., 2017*). Since RTT is defined a synaptopathy (*Faundez et al., 2019*), we decided to characterize excitatory synapses within the same brain areas considered for the morphological analysis of astrocyte, in order to find a correlation between the two phenotypes. Brain slices from KO animals at P20, P40 and P70 and their WT littermates were immunostained for the pre-synaptic marker Synapsin1/2, a vesicle-associated protein which correlates with synaptic maturation and functionality (*Lu et al., 1996; Perlini et al., 2011*) and the excitatory post-synaptic marker PSD95. Analyses were performed after a 3D reconstruction of synaptic puncta using the Arivis Vision4D software. For each experimental group, the density of puncta, their colocalization, an index of functional synapses, and their volume were measured. Immunofluorescence analysis of Synapsin1/2 and PSD95 puncta in the motor cortex of *Mecp2* KO animals indicated an impairment in synaptogenesis of excitatory synapses (**Figure 3.7**). In detail, we found a significant decrease in the volume of pre- and post-synaptic puncta at P20 (- 10.6% and – 10.46% compared to WT) and P40 (- 11.25% and – 17.9% compared to WT), whereas at P70 only a reduction in PSD95 puncta volume is evident (- 10.05% compared to WT) (**Figure 3.7 B, C**). Based on the evidence that spine volume mirrors the maturation state and synaptic strength, our data collectively indicate a prolonged presence of immature spines in KO animals. In parallel, we analysed puncta density, providing details regarding the number of synapses. Indeed, this parameter might be strictly influenced by the degree of maturation of the synapses. We reported a slight increase in the number of pre- and

post-synaptic markers in KO animals at P20 (+28.4% and +18% compared to WT, respectively), together with an increment of their colocalization (+36.6% compared to WT) (**Figure 3.7 D-F**) and a more pronounced effect was observed at P40 (+ 87.8% of Synapsin1/2, + 41.6% of PSD95, + 233% of colocalized puncta compared to WT) (**Figure 3.7 D-F**). Conversely, at later time point (P70), puncta density is unchanged in KO with respect to WT counterparts, unless a slight decrease in the number of PSD95 puncta (- 12.3% compared to WT) (**Figure 3.7 D-F**).

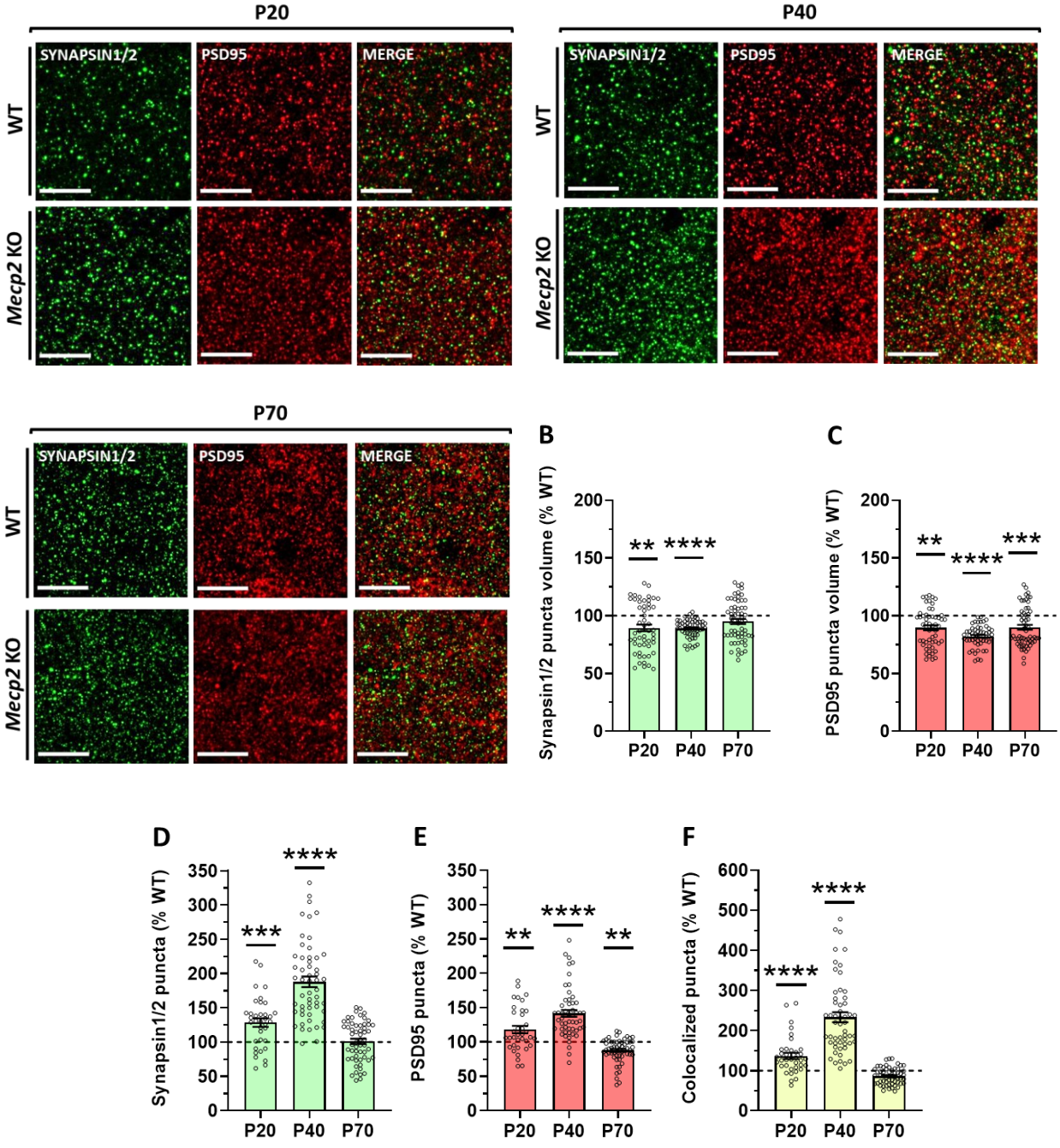

Figure 3.7. Alterations of excitatory synapses in the *Mecp2* KO motor cortex (layer I) are already evident at P20 and progress up to P40. A) Representative images (2D) of brain sections of WT and *Mecp2* KO mice at P20, P40 and P70 immunostained for Synapsin1/2 (green), PSD95 (red) and their colocalization (merge). Scale bar = 10 μm. **B, C)** The graphs represent the mean ± SE of the percentages of the mean volume of Synapsin1/2 puncta (**B**) and PSD95 puncta (**C**) compared to WT animals (100%) (P20: Synapsin1/2: ** p=0.0074; PSD95: ** p=0.0015 by Mann Whitney test. P40: **** p<0.0001 Student's t-test. P70: PSD95: *** p=0.0001 by Mann Whitney test). Measurements (P20: n=54; P40: n=60 for WT and 54 for KO; P70: n=72 for WT and 60 for KO) derived from at least 3 different animals per genotype (P20: n=3 WT and 3 KO mice; P40: n=3 WT and 3 KO mice; P70: n=4 WT and 4 KO mice). **D, E, F)** The graphs represent the mean ± SE of the puncta densities of Synapsin1/2 (**D**), PSD95 (**E**) and colocalized puncta (**F**) in *Mecp2* KO mice at P20, P40 and P70 compared to WT animals (100%) (P20: Synapsin1/2: *** p=0.0005 and PSD95: ** p=0.0023 by Student's t-test; colocalization: **** p<0.0001 by Mann Whitney test. P40: Synapsin1/2: **** p<0.0001 by Student's t-test, PSD95 and colocalized puncta: **** p<0.0001 by Mann Whitney test. P70: PSD95: ** p=0.0060 by Mann Whitney test). Measurements performed for WT and *Mecp2* KO mice (P20: n=46 for WT and 36 for KO; P40: n=48 for WT and 54 for KO; P70: n=69 for WT and 57 for KO) derived from the same animals used to study puncta volume.

Analysis of synaptic phenotypes in layer I of the somatosensory cortex of *Mecp2* KO mice revealed the presence of some defects that partially overlapped with those detected in the motor cortex (**Figure 3.8**). Indeed, we reported a decrement in Synapsin1/2 puncta volume in KO animals at all time points analysed (in order: - 11.76%, - 4.15% and – 13.2% compared to WT), whereas the volume of PSD95 puncta is significantly reduced at P20 and at P70 (- 6.37% and – 8.135% compared to WT) (**Figure 3.8 B, C**). By analysing the synaptic puncta density, we demonstrated only a few alterations in KO animals compared to WT. Indeed, our data indicate an increase in the number of Synapsin1/2 puncta at P20 (+ 35.8% compared to WT) and a small increment of PSD95 puncta at P70 (+ 9% compared to WT) (**Figure 3.8 D, E**). However, no difference was observed in the number of functional synapses at any time point (**Figure 3.8 F**).

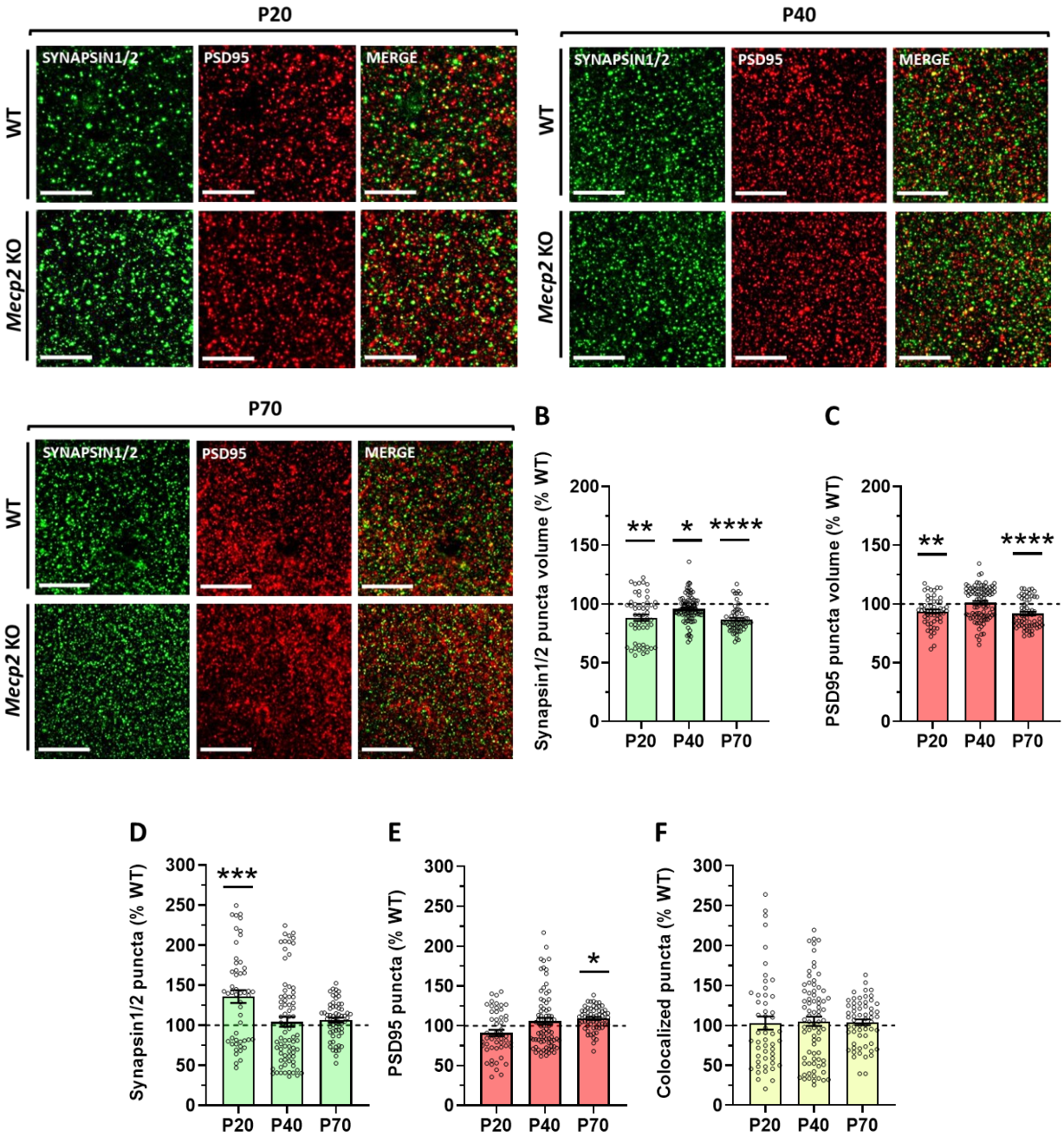

Figure 3.8. Excitatory synapses in the *Mecp2* KO somatosensory cortex (layer I) exhibit alterations in puncta volume and density at specific ages. A) Representative images (2D) of brain sections of WT and *Mecp2* KO mice at P20, P40 and P70 immunostained for Synapsin1/2 (green), PSD95 (red) and their colocalization (merge). Scale bar = 10 µm.. **B, C)** The graphs represent the mean ± SE of the percentages of the mean volume of Synapsin1/2 puncta (**B**) and PSD95 puncta (**C**) compared to WT animals (100%) (Synapsin1/2: P20: ** p=0.0055 by Mann Whitney test; P40: * p=0.0458 by Student's t-test; P70: **** p<0.0001 by Mann Whitney test. PSD95: P20: ** p=0.0093 by Student's t-test; P70 **** p<0.0001 by Mann Whitney test). Measurements (P20: n=54; P40: n=84 for WT and 90 for KO; P70: n=72 for WT

and 60 for KO) derived from at least 3 different animals per genotype (P20: n=3 WT and 3 KO mice; P40: n=5 WT and 5 KO mice; P70: n=4 WT and 4 KO mice). **D, E, F)** The graphs represent the mean ± SE of the percentages of the puncta densities of Synapsin1/2 (**D**), PSD95 (**E**) and colocalized puncta (**F**) in *Mecp2* KO mice at P20, P40 and P70 compared to WT animals (100%) (P20: Synapsin1/2: *** p=0.0003 by Student's t-test. P70: PSD95: * p=0.0138 by Mann Whitney test). Measurements performed for WT and *Mecp2* KO mice (P20: n=47 for WT and 51 for KO; P40: n=71 for WT and 78 for KO; P70: n=72 for WT and 60 for KO) derived from the same animals used to study puncta volume.

Eventually, analyses performed in the CA1 area of the hippocampus revealed the presence of slight modifications (**Figure 3.9**).

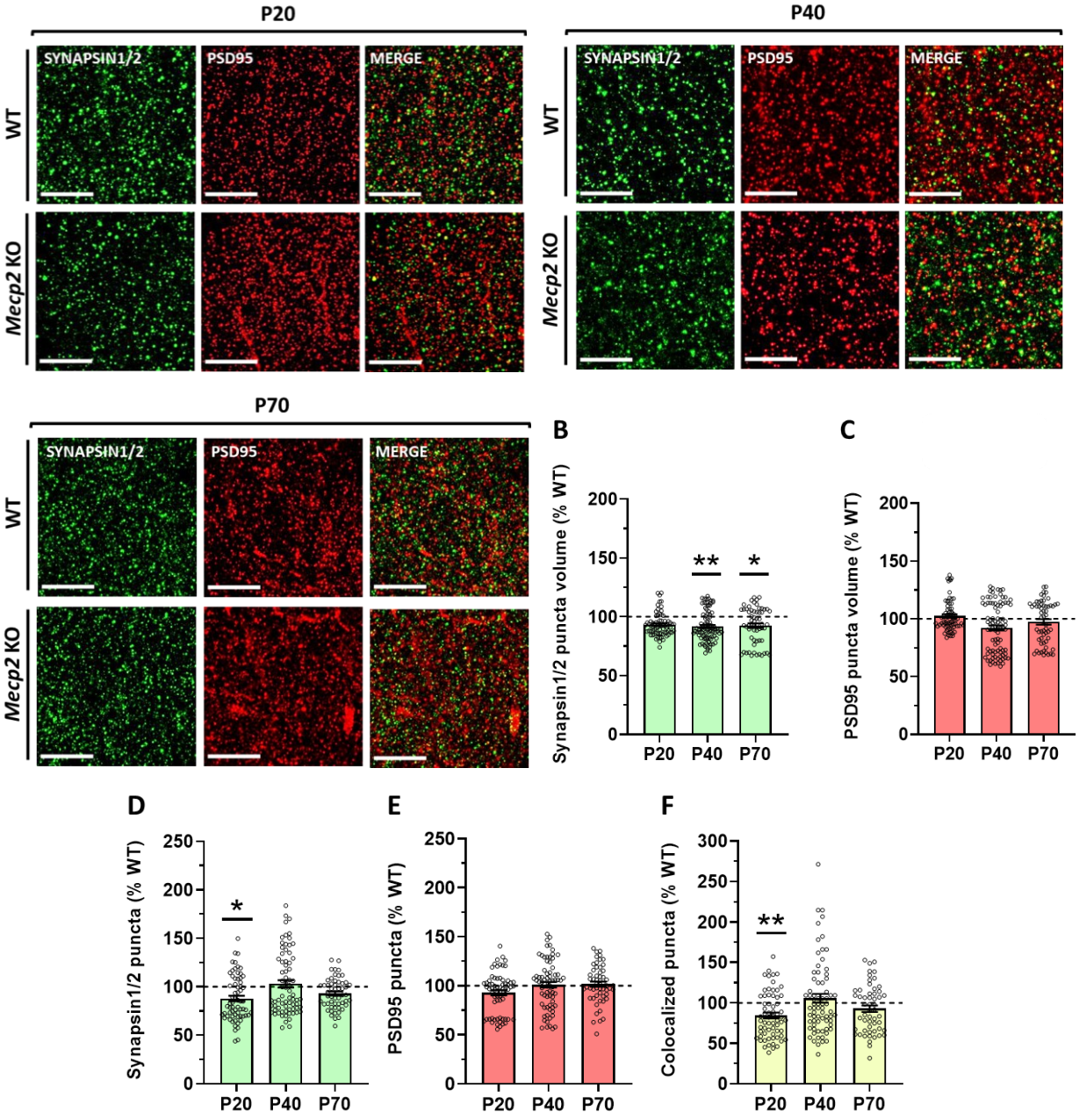

Figure 3.9. Excitatory synapses in the *Mecp2* KO hippocampus (CA1 area) show slight changes and limited to pre-synapses. A) Representative images (2D) of brain sections of WT and *Mecp2* KO mice at P20, P40 and P70 immunostained for Synapsin1/2 (green), PSD95 (red) and their colocalization (merge). Scale bar = 10 μm. **B, C)** The graphs represent the mean ± SE of the percentages of the mean volume of Synapsin1/2 puncta (**B**) and PSD95 puncta (**C**) compared to WT animals (100%) (Synapsin1/2: P40: ** p=0.0012 and P70: * p=0.0162 by Mann Whitney test). Measurements (P20: n=90 for WT and 72 for KO; P40: n=96 for WT and 90 for KO; P70: n=72 for WT and 60 for KO) derived from at least 3 different animals per genotype (P20: n=5 WT and 4 KO mice; P40: n=5 WT and 5 KO mice; P70: n=4 WT and 4 KO mice). **D, E, F)** The graphs represent the mean ± SE of the percentages of the puncta densities of Synapsin1/2 (**D**), PSD95 (**E**) and colocalized puncta (**F**) in *Mecp2* KO mice at P20, P40 and P70 compared to WT animals (100%) (P20: Synapsin1/2 * p=0.0141 and colocalization: ** p=0.0080 by Student's t-test). Measurements performed for WT and *Mecp2* KO mice (P20: n=72 for WT and 66 for KO; P40: n=84 for WT and 72 for KO; P70: n=66 for WT and 54 for KO) derived from the same animals used to study puncta volume.

We reported a selective decrease in the volume of Synapsin1/2 puncta at P40 and P70 in KO animals compared to WT (- 8.36% and – 7.54%) and minor defects in the density of pre-synaptic puncta and excitatory synapses at P20 (- 12.1% and - 15.66% compared to WT, respectively) (**Figure 3.9 B, D, F**).

3.3 *Mecp2* expression in primary astrocyte cultures regulates astrocyte morphology depending on the brain area of origin

Lastly, aware of the limitations of studying astrocyte morphology in cellular cultures, we found interesting to evaluate whether area-related differences due to *Mecp2* loss could be detectable also *in vitro*. Therefore, we labelled cultures of pure astrocytes derived from different cerebral areas with GFAP to delineate cell contours and we calculated the shape index (SI) by the formula: $(\text{Perimeter}^2/\text{Area}) – 4*\pi$ (*Matsutani and Yamamoto, 1998*). Analyses performed on WT and *Mecp2* KO cortical astrocytes revealed no difference in the SI (**Figure 3.10 A, B**). On the contrary, hippocampal and

cerebellar astrocytes lacking *Mecp2* exhibit, respectively, an increased and a decreased SI (**Figure 3.10 C-F**).

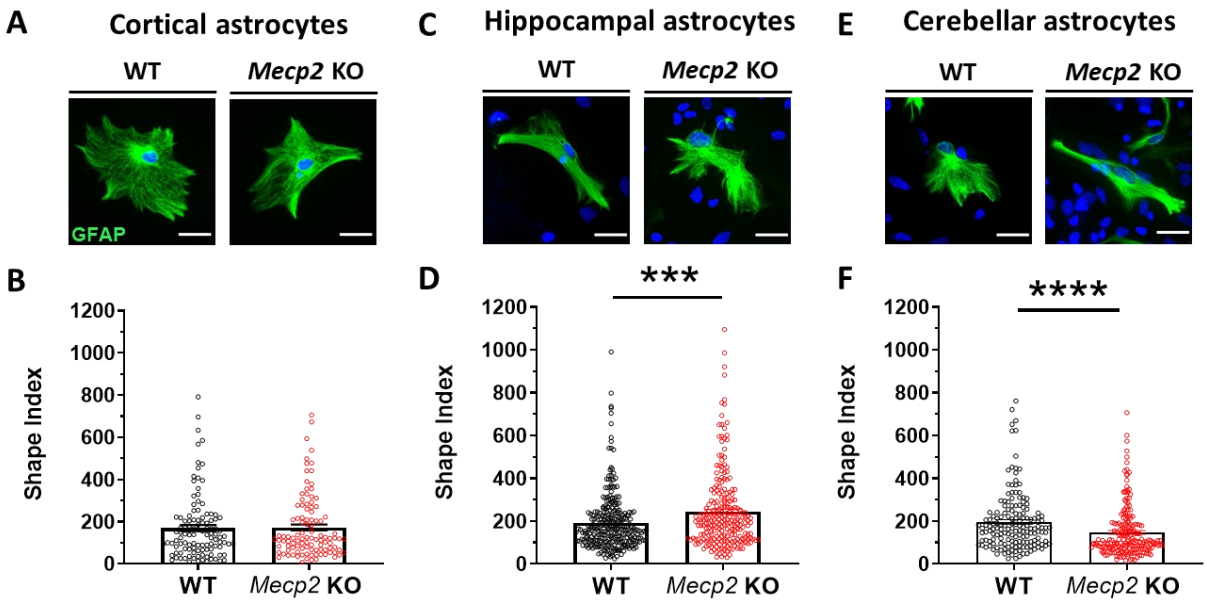

Figure 3.10. Absence of *Mecp2* in astrocyte alters their morphological complexity *in vitro* depending on the brain area of origin. A, C, E) Representative images of WT and *Mecp2* KO astrocytes (DIV14-18) immunostained for GFAP (green) from cortical, hippocampal and cerebellar cultures, respectively. Scale bar = 20 µm. **B, D, F)** The graphs represent the mean ± SE of the Shape Index (SI). **B)** SI of WT (n=111) and KO (n=104) cortical astrocytes derived from 7 different biological samples. **D)** SI of WT (n=284) and KO (n=234) hippocampal astrocytes derived from 7 different biological samples. **F)** SI of WT (n=162) and KO (n=198) cerebellar astrocytes derived from 6 different biological samples. Data from WT and KO astrocytes were compared by Mann Whitney test (D: *** $p<0.001$; F: **** $p<0.0001$).

Although *in vitro* and *in vivo* analyses do not show overlapping results, they both highlight that *Mecp2* expression influences astrocyte morphology depending on the brain area, pointing to heterogeneity as an important aspect to be considered.

4. *Mecp2* expression in astrocytes is fundamental to support neuronal growth and synaptic maturation

Having demonstrated the presence of progressive and brain region-dependent morphological defects of *Mecp2* KO astrocytes, and having postulated a correlation between astrocyte morphology and synaptic phenotype, we next analysed the neuroprotective and synaptogenic potentials of *Mecp2* KO astrocytes. By using *in vitro* primary co-cultures, which permit to investigate astroglia-neuron crosstalk, we analysed neuronal morphology (at DIV7 and DIV14) and synaptogenesis (at DIV14), in order to investigate whether and how *Mecp2* loss in astrocytes contributes to the development of neuronal defects.

4.1 *Mecp2* deficiency in cortical astrocytes affects neuronal morphology of WT neurons along maturation

To investigate which is the role of *Mecp2* in astrocytes to sustain neuronal growth, WT neurons were cultured in contact with WT or *Mecp2* KO astrocytes and their morphology analyzed. KO neurons in culture with either WT or KO astrocytes were also included in the analysis, in order to disclose the contribution of neuronal *versus* astrocytic *Mecp2* for neuronal phenotypes. WT or *Mecp2* KO neurons were seeded at low-density on a feeder layer of WT or KO astrocytes, and neuronal morphology was assessed at DIV7 and DIV14 analysing Microtubule Associated Protein 2 (MAP2) stained cells. Complexity of dendritic arbour (Sholl analysis), total dendritic length, number of dendrites, maximal dendritic length, average dendritic length and percentage of polarized cells were measured (**Figure 4.1, 4.2**).

We revealed that *Mecp2* deficiency in astrocytes does not impair the morphology of WT neurons at early developmental stages. Indeed, at DIV7, we only reported a slight decrease in the number of intersections at 30 μm from the soma in Sholl analysis (**Figure 4.1 B**), whereas total dendritic length, number of dendrites, maximal dendritic length, and percentage of polarized cells were unchanged compared to WT-WT cultures (**Figure 4.1 E-H**). On the other hand, and in accordance with literature (*Ballas et al., 2009*), WT astrocytes increased the total dendritic length of *Mecp2* KO neurons, compared to KO neurons in culture with KO astrocytes (+ 15.1%) (**Figure 4.1 E**).

However, when the other parameters were analysed, no difference emerged (**Figure 4.1 C, F-H**). Interestingly, the comparison between WT-WT and KO-KO co-cultures revealed that the absence of *Mecp2* in both cells causes more prominent defects than the sole neuronal or astrocytic loss, pointing to the importance of *Mecp2* at least in one cell population to prevent neuronal defects. In KO-KO co-cultures, indeed, we observed impairments in dendritic arborization at 80 and 100 µm from the soma together with a decrease in total dendritic length and number of dendrites (- 14.84% and - 16.32% compared to WT neurons, respectively) (**Figure 4.1 D- F**).

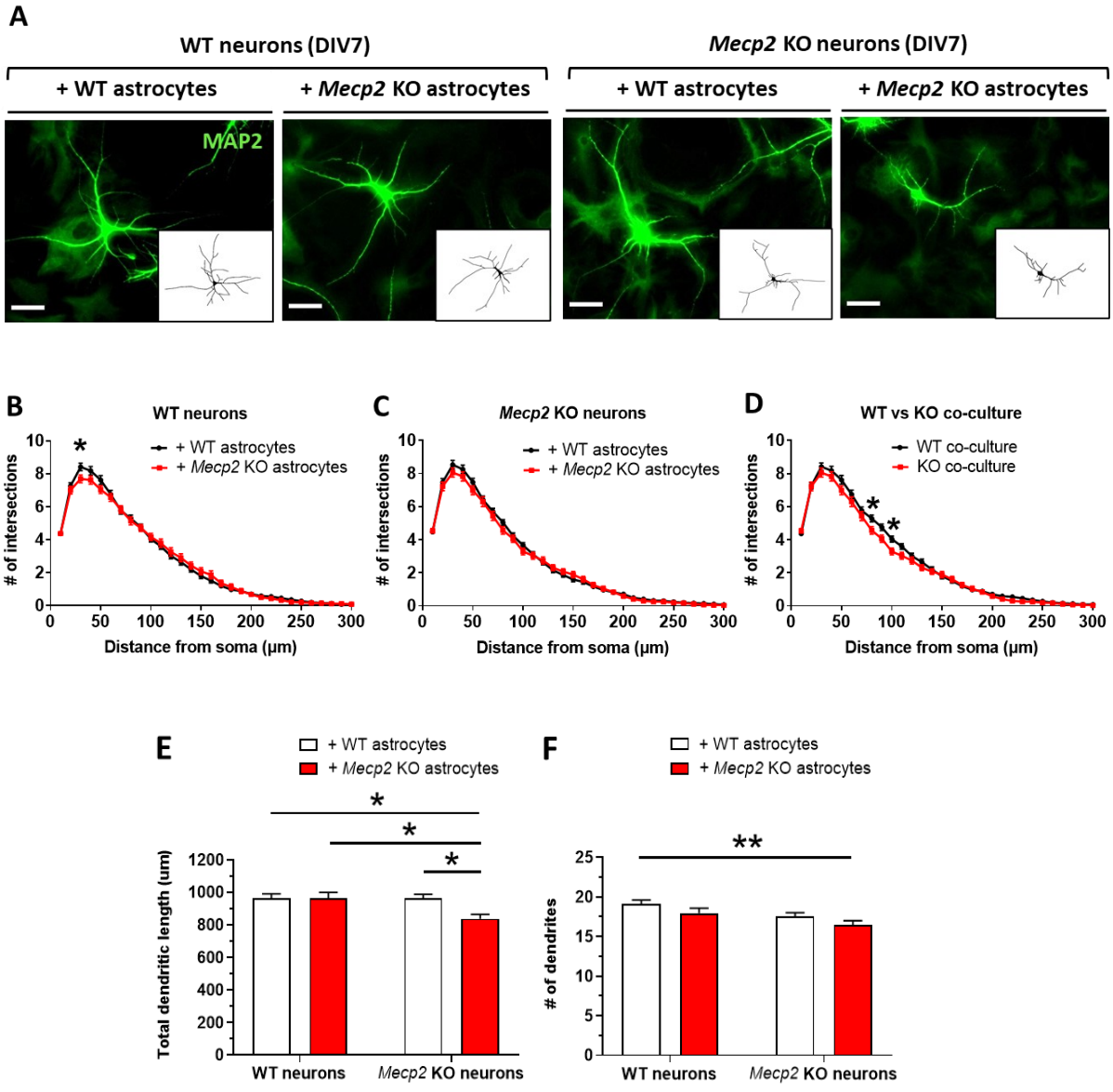

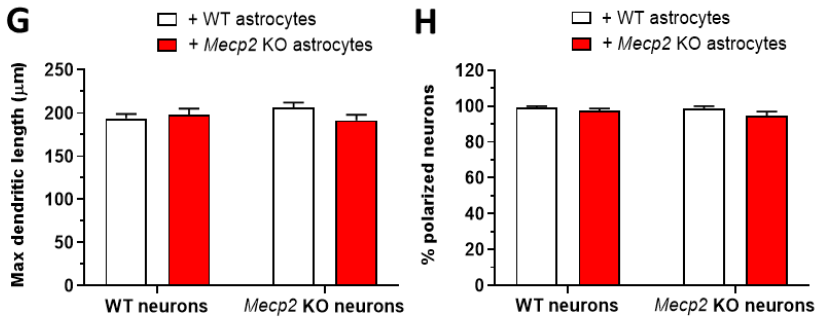

Figure 4.1. *Mecp2* expression in neurons and astrocytes is crucial for neuronal growth at early developmental stages (DIV7). A) Representative images of neurons immunostained for MAP2 (green). Inserts depict the correspondent reconstructed dendritic arbours. Scale bar = 50 µm. **B, C, D)** Quantification of Sholl analysis of: **B** = WT neurons cultured with WT *versus* KO astrocytes, **C**: KO neurons cultured with WT *versus* KO astrocytes, **D**: WT *versus* KO co-cultures. Asterisks indicate statistical significance between the two experimental groups at specific distances from the soma (* $p<0.05$ by Sidak's *post hoc* test). Two-way ANOVA assessed a significant genotype effect (**B***:* $p=0.0233$; **D**: $p<0.0001$). **E-H)** The graphs represent the mean ± SE of total dendritic length (**E**), number of dendrites (**F**), maximal dendritic length (**G**) and percentage of polarized neurons (**H**). * $p<0.05$, F: ** $p<0.01$ by Tukey's *post hoc* test. All the analyses were performed in at least n=3 biological replicates per experimental group for: n=147 neurons for WT-WT co-cultures; n=101 neurons for WT neuron-KO astrocyte co-cultures; n=95 neurons for KO-KO co-cultures; n=138 neurons for KO neuron-WT astrocyte co-cultures. Neurons and astrocytes derived from at least 3 different animals per genotype.

Interestingly, at DIV12-14, WT neurons in co-culture with KO astrocytes developed a peculiar phenotype consisting in aberrant dendritic arborization at 100 µm from the soma, together with a higher number of shortened dendrites (dendrites number:+ 24.20%; average dendritic length: - 13.77%, compared to WT neurons in culture with WT astrocytes) (**Figure 4.2 B, F, H**). Cell-autonomous alterations of KO neurons at DIV12-14, instead, covered the beneficial effects of WT astrocytes, causing impaired neuronal growth and decreased total dendritic length (- 20.16% compared to WT neurons in culture with WT astrocytes) (**Figure 4.2 C, E-H**). As for DIV7, KO neurons cultivated with KO glia presented the worst morphological phenotype. Indeed, they showed a significant decrease in dendritic complexity at 40 and 50 µm from the soma,

together with a decrease in total dendritic length (- 13.48%) and number of dendrites (- 15.8%) (**Figure 4.2 D-F**).

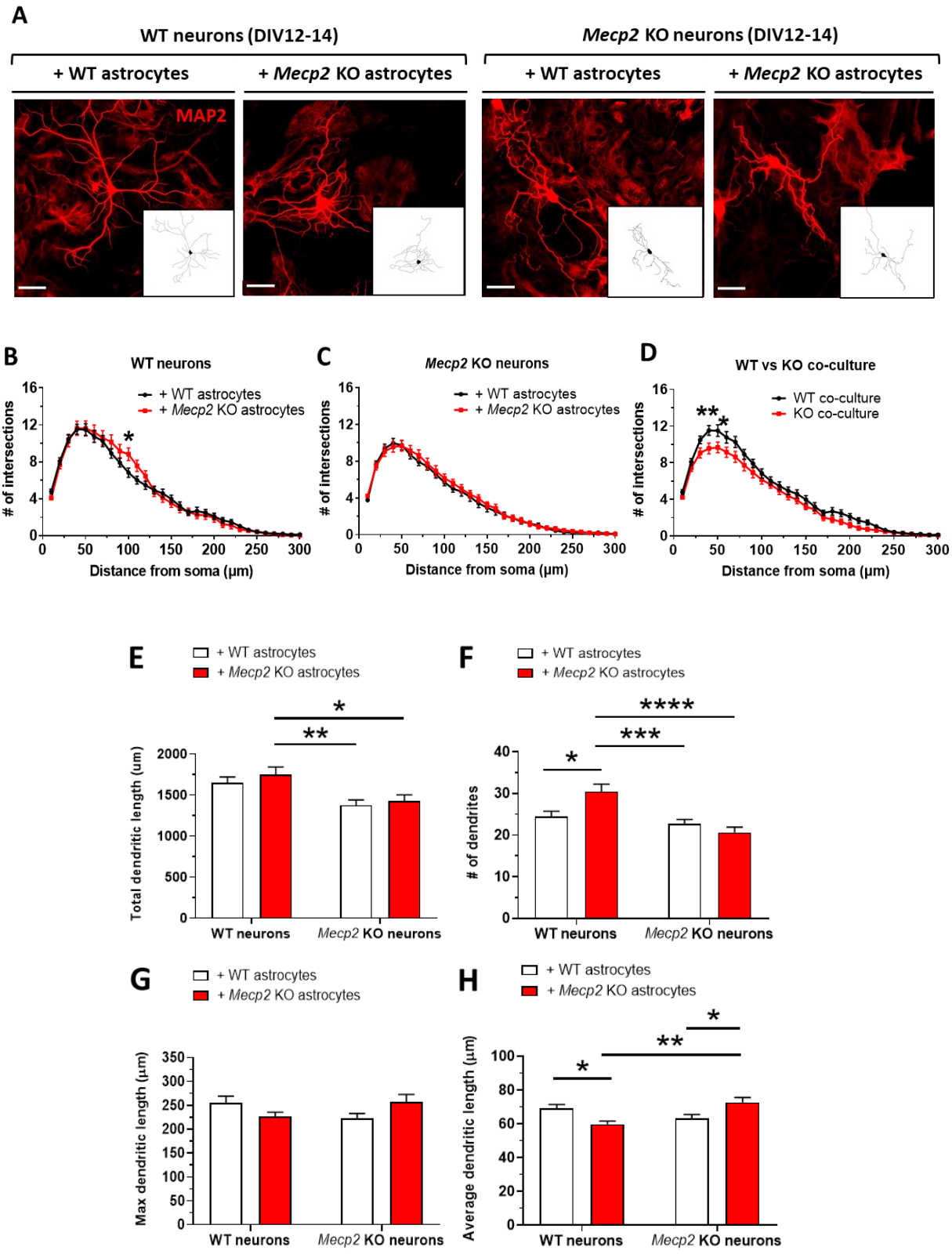

Figure 4.2. *Mecp2* absence in astrocytes causes distinct non-cell autonomous alterations in WT neurons at DI12-DIV14. A) Representative images of neurons immunostained for MAP2 (red). Inserts are the correspondent reconstructed dendritic arbours. Scale bar = 50 µm. **B, C, D)** Sholl analysis of: **B** = WT neurons cultured with WT *versus* KO astrocytes, **C**: KO neurons cultured with WT *versus* KO astrocytes, **D**: WT *versus* KO co-cultures. Asterisks indicate statistical significance between the two experimental groups at specific distances from the soma (* $p<0.05$, ** $p<0.01$ by Sidak's *post hoc* test). Two-way ANOVA assessed a significant genotype effect (**D**: $p<0.0001$). **E-H)** The graphs represent the mean ± SE of total dendritic length (**E**), number of dendrites (**F**), maximal dendritic length (**G**) and average dendritic length (**H**). * $p<0.05$, ** $p<0.01$, *** $p<0.001$, **** $p<0.0001$ by Tukey's *post hoc* test. **B-H**) All the analyses were performed in at least n=5 biological replicates per experimental group for: n=42 neurons for WT-WT co-cultures; n=42 neurons for WT neuron-KO astrocyte co-cultures; n=43 neurons for KO-KO co-cultures; n=50 neurons for KO neuron-WT astrocyte co-cultures. Neurons and astrocytes derived from at least 3 different animals per genotype.

All in all, our data indicate that the presence of *Mecp2* either in neurons or astrocytes is sufficient for proper neuronal development at early developmental stages, whilst the expression in only one cell type cannot support a physiological maturation at later time points. These results suggest that a combination of cell and non-cell autonomous effects participate to the morphological defects featured by *Mecp2* null neurons.

4.2 *Mecp2* deficiency in cortical astrocytes impairs the synaptogenesis of WT neurons

To evaluate whether *Mecp2* deficiency in astrocytes impairs their capacity to correctly support synaptogenesis, by immunofluorescence we investigated density and area of pre-synaptic and post-synaptic puncta, detected by Synapsin1/2 and Shank2 antibody, respectively, in neurons (**Figure 4.3**). The analyses were initially performed in WT and KO neurons cultivated in contact with either WT or KO astrocytes.

Interestingly, we demonstrated that the lack of *Mecp2* in cortical astrocytes dramatically influences the synaptogenesis of WT neurons, which exhibit a significant reduction in number and area of Synapsin1/2 puncta, demonstrating the presence of

fewer and immature spines (puncta density: - 50.83%; puncta area: - 30.3%) (**Figure 4.3 B, C**). In contrast, KO neurons showed a decreased density and area of pre-synaptic puncta, compared to WT-WT cultures, when cultured either with WT or KO astrocytes (puncta density: +WT astrocytes = - 36.76%; + KO astrocytes = - 35.42%; puncta area: +WT astrocytes = - 9.4%; + KO astrocytes = - 10.87%) (**Figure 4.3 B**). These results indicated that *Mecp2* KO cortical astrocytes are detrimental for synaptic maturation of WT neurons. Further, they suggested that cell-autonomous alterations occurring in KO neurons overwhelm the astrocytic contribution. Therefore, to study the effects of *Mecp2* loss in astrocytes, we decided to continue analysing only WT neurons.

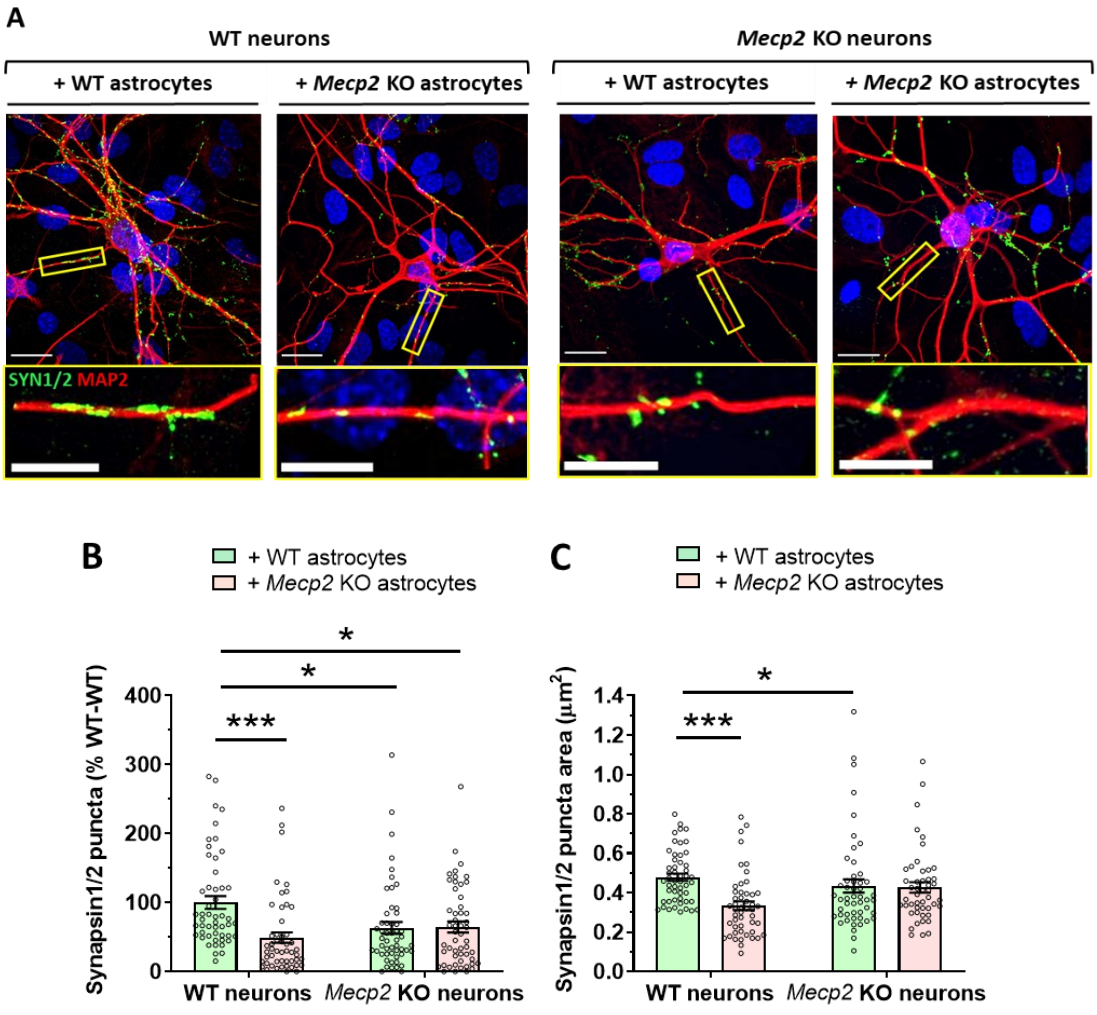

Figure 4.3. *Mecp2* expression in cortical astrocytes is fundamental for synaptogenesis in WT neurons A) Representative images of WT and *Mecp2* KO neurons (DIV12-14) immunostained for MAP2 (red) and Synapsin1/2 (green). Neurons were co-cultured in contact with WT or *Mecp2* KO astrocytes. Scale bar = 20 µm, and 10 µm in the enlarged image. **B, C**) Histograms indicate the mean ± SEM of Synapsin1/2 puncta number and area (green bars =

neurons in co-culture with WT astrocytes; red bars = neurons in co-culture with *Mecp2* KO astrocytes). Values for puncta number are expressed as percentages compared to WT-WT co-cultures (100%). 2-way ANOVA assessed a significant astrocyte genotype effect for both puncta density and area ($p<0.01$). Asterisks indicate statistical significance between the two experimental groups (* $p<0.05$, *** $p<0.001$ by Tukey's *post hoc* test). All the analyses were performed on $n>50$ neurons from 6 biological replicates per experimental group. Neurons and astrocytes derived from at least 3 different animals per genotype.

4.3 Soluble factors secreted by cortical *Mecp2* KO astrocytes exert a detrimental effect on synaptogenesis in WT neurons

Since astrocytes are highly secretory cells within the CNS (*Petrelli and Bezzi, 2015*), we explored whether the negative effects exerted by *Mecp2* KO astrocytes on WT neurons could be ascribable to soluble factors. By using a transwell-based system that prevents cell-to-cell contact but assures paracrine effects, we evaluated synaptogenesis in WT cortical neurons (**Figure 4.4**). To better assess this aspect, we included in the analysis an excitatory post-synaptic marker (Shank2) and measured pre-and post-synaptic puncta colocalization, as an index of functional synapses.

A severe decrease in density of both pre- and post-synaptic markers and in number of functional synapses (Synapsin1/2: - 37.13 %; Shank2: - 30.68 %; colocalization: - 43.48 %) was measured in WT neurons grown under a constant exposure of paracrine signals from *Mecp2* KO astrocytes (**Figure 4.4 D-F**). In contrast to contact co-cultures, we did not report any change of the area of both synaptic markers (**Figure 4.4 B, C**). These observations indicated that soluble factors largely contribute to the detrimental effects that *Mecp2* KO cortical astrocytes exert on synaptogenesis, although a contact component appears to exacerbate synaptic defects. We hypothesized that the observed phenotypes might rely either on the secretion of neurotoxic factors or the deficiency in releasing proper neurotrophic ones, or both.

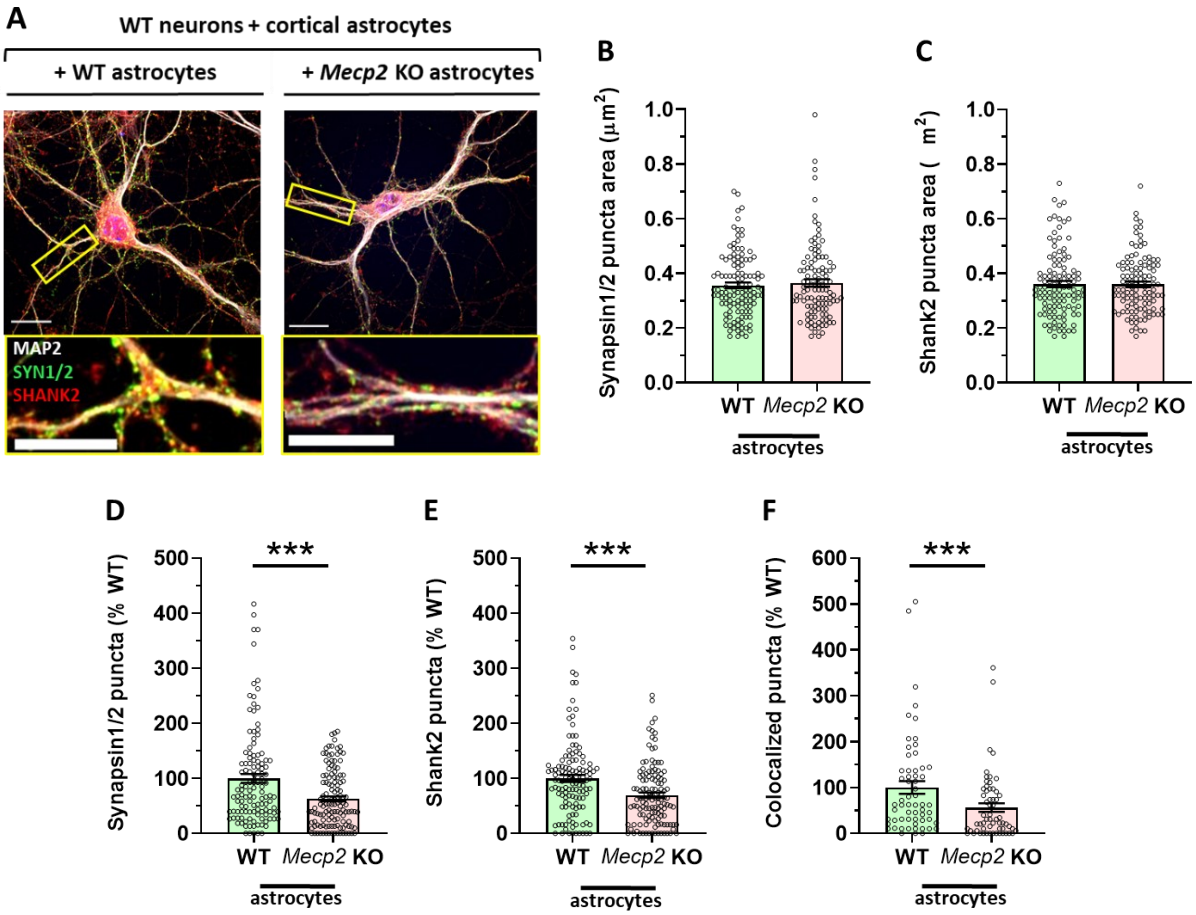

Figure 4.4. Soluble factors secreted by *Mecp2* KO cortical astrocytes affect correct synaptogenesis of WT cortical neurons. A) Representative images of WT neurons (DIV14) immunostained for MAP2 (white), Synapsin1/2 (green) and Shank2 (red). Neurons matured under the exposure of paracrine signals from WT or *Mecp2* KO astrocytes (transwell-based co-culture). Scale bar = 20 µm, and 10 µm in the enlarged image. **B-F**) Histograms indicate the mean ± SEM of Synapsin1/2 (**D**), Shank2 (**E**), colocalized (**F**) puncta number and Synapsin1/2 (**B**) and Shank2 (**C**) puncta area (green bars = WT neurons in co-culture with WT astrocytes; red bars = WT neurons in co-culture with *Mecp2* KO astrocytes). Values for puncta number are expressed as percentages compared to WT-WT co-cultures (set at 100%) (D: *** p=0.0005; E: *** p=0.0001; F: *** p=0.0025 by Mann Whitney test). **B-E**) Analyses were performed on n=124 WT neurons + WT astrocytes from 15 biological replicates, and n=130 WT neurons + *Mecp2* KO astrocytes from n=16 biological replicates. **F**) Analyses were performed on n=60 WT neurons per experimental group from n=7 biological replicates. **B-F**) Neurons and astrocytes derived from at least 3 different animals per genotype.

To corroborate our *in vivo* data suggesting that *Mecp2* deficiency differentially affects astrocytes in function of their cerebral origin, we replicated the transwell-based co-culture set-up using hippocampal and cerebellar astrocytes and we analysed pre- and post-synaptic puncta density and area, together with their colocalization (**Figure 4.5**). Our data confirmed that *Mecp2* deficiency differentially affects astrocytic synaptogenic functions depending on their origin and that cortical astrocytes represent the most affected population. Indeed, similarly to KO cortical astrocytes, hippocampal KO astrocytes altered pre-synaptic puncta density (- 27.18 % of Synapsin1/2 compared to neurons + WT astrocytes), but they also influenced puncta area (- 12.58%) (**Figure 4.5 B, D**). However, no defect was detected either at the post-synaptic level or in functional synapses (**Figure 4.5 C, E, F**). Loss of *Mecp2* in cerebellar KO astrocytes, instead, does not affect the synaptogenesis of WT neurons (**Figure 4.5 H-L**).

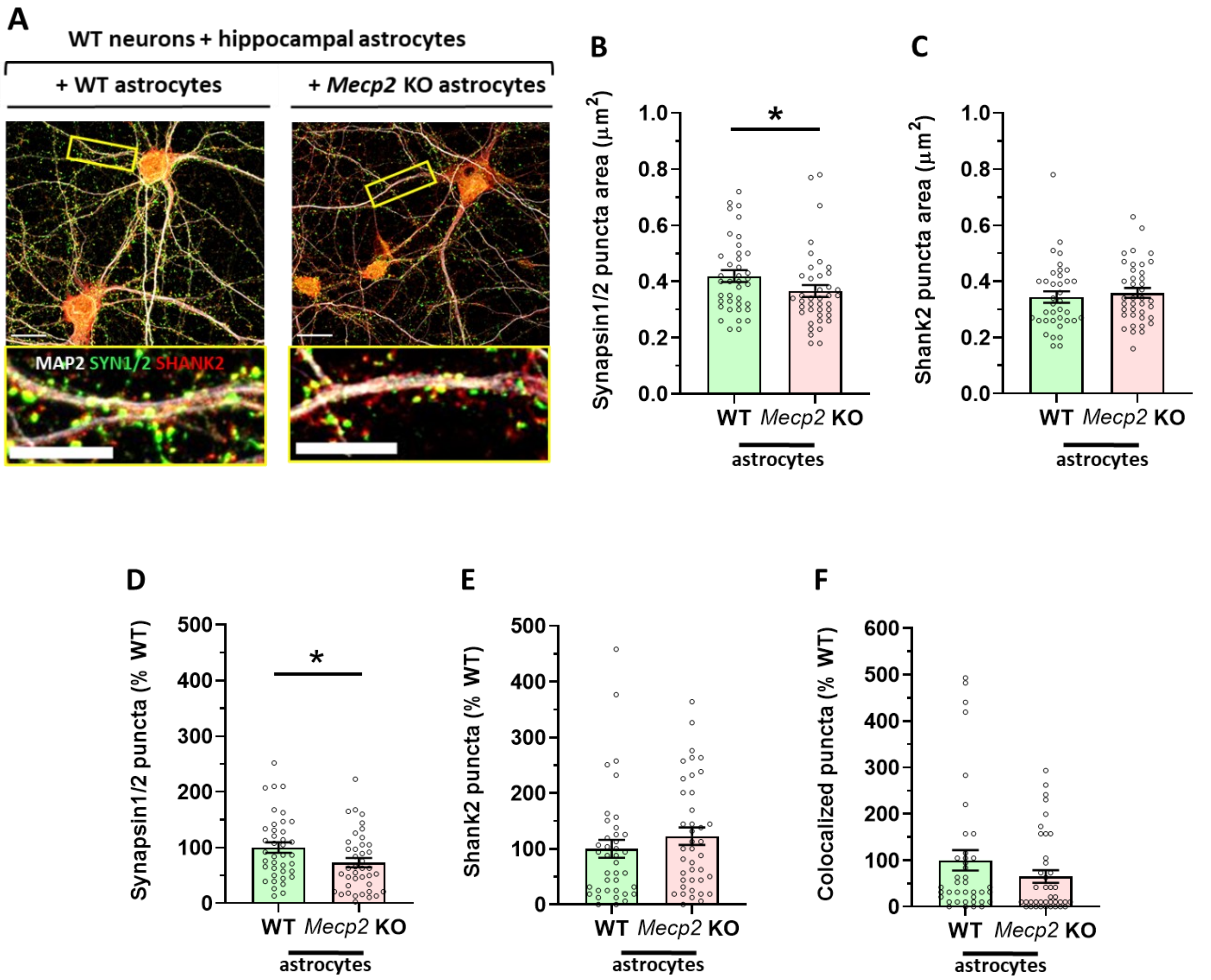

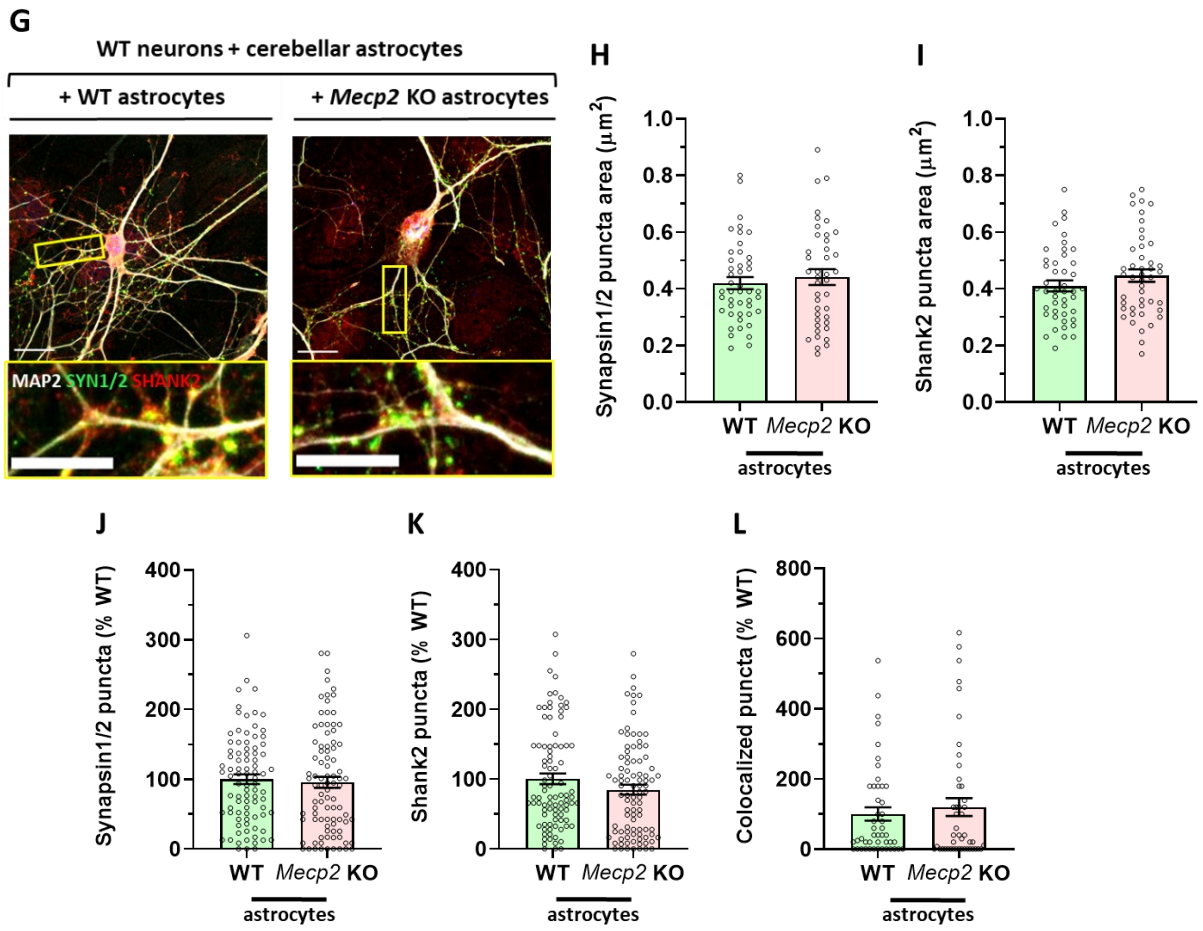

Figure 4.5. *Mecp2* loss slightly affects the synaptogenic potential of hippocampal but not cerebellar astrocytes. A, G) Representative images of WT neurons (DIV14) immunostained for MAP2 (white), Synapsin1/2 (green) and Shank2 (red). Neurons matured under the exposure of paracrine signals from WT or Mecp2 KO hippocampal (**A**) and cerebellar (**G**) astrocytes (transwell-based co-culture). Scale bar = 20 µm, and 10 µm in the enlarged image. **B-F, H-L**) Histograms indicate the mean ± SEM of Synapsin1/2 (**D, J**), Shank2 (**E, K**), colocalized (**F, L**) puncta number and Synapsin1/2 (**B, H**) and Shank2 (**C, I**) puncta area (green bars = WT neurons in co-culture with WT astrocytes; red bars = WT neurons in co-culture with *Mecp2* KO astrocytes). Values for puncta number are expressed as percentages compared to WT-WT co-cultures (100%) (B: * p=0.0456 by Mann Whitney test; D: * p=0.0316 by Student's t-test). **B-F**) Analyses were performed on n=39 WT neurons + WT astrocytes from 4 biological replicates, and n=40 WT neurons + *Mecp2* KO astrocytes from n=4 biological replicates. **J-K**) Analyses were performed on n=87 WT neurons + WT astrocytes from n=9 biological replicates, and n=90 WT neurons + *Mecp2* KO astrocytes from n=10 biological replicates. **H, I, L**) Analyses were performed on n=45 WT neurons + WT astrocytes from n=5 biological replicates,

and n=45 WT neurons + *Mecp2* KO astrocytes from n=6 biological replicates **B-F, H-L**) Neurons and astrocytes derived from at least 3 different animals per genotype.

4.4 Soluble neurotoxic protein(s) are responsible for the synaptic alterations induced by *Mecp2* KO astrocytes on WT neurons

To confirm the involvement of paracrine factors and obtain insights into their nature, WT neurons were treated with Astrocyte Conditioned Medium (ACM) from WT or KO astrocytes. ACM was added to WT neurons at DIV13, when synaptogenesis has already occurred, and by IF we analysed synaptic phenotypes at DIV14. Compared to previous experiments in which neurons matured under a continuous exposure of paracrine signals from astrocytes, which could modify their secretome depending on neuronal demand, in these conditions the effects of ACM on neurons depend on cell-autonomous alterations of astrocytes (as they were cultured alone).

Our results demonstrated that exposure to *Mecp2* KO-ACM induces in neurons a significant reduction in Synapsin1/2 puncta density and area, when compared to neurons exposed to WT-ACM (puncta density: - 23.2% and – 45.5%; puncta area: - 12.2% and – 25.2%, respectively) (**Figure 4.6 A, B, D**). As expected, WT neurons treated with WT-ACM showed a slight, although not significant, increase in the number and area of pre-synaptic puncta (**Figure 4.6 B, D**). Importantly, heat-treatment of KO-ACM completely abolished the negative effects on pre-synapses (Synapsin1/2 puncta density: + 50.24%; puncta area: + 24.6% respect to KO ACM), leading the denatured KO ACM to fully mimic the beneficial effects exerted by the WT ACM. This result proved that one or more neurotoxic proteins released by KO astrocytes are responsible for the detrimental effects on synaptogenesis; moreover, they suggested that neurotrophic effects of the ACM can be supported by non-protein factors equally released by WT and KO astrocytes (**Figure 4.6 B, D**).

Analysis of excitatory post-synapses reported similar results, although less evident. KO ACM caused only a tendency toward a reduction in the density and area of Shank2, compared to WT ACM-exposed neurons, and these defects were not detected when neurons had been exposed to heat-inactivated KO ACM. Indeed, neurons treated with heat-denaturated KO ACM showed a significant increase in the number of puncta with

respect to KO ACM-treated and untreated neurons (+ 65% and + 82.3%, respectively) (**Figure 4.6 C**).

All in all, these data demonstrated that *Mecp2* KO astrocytes secrete toxic proteins that affect synapses in neurons, at least at later stages of synapse maturation.

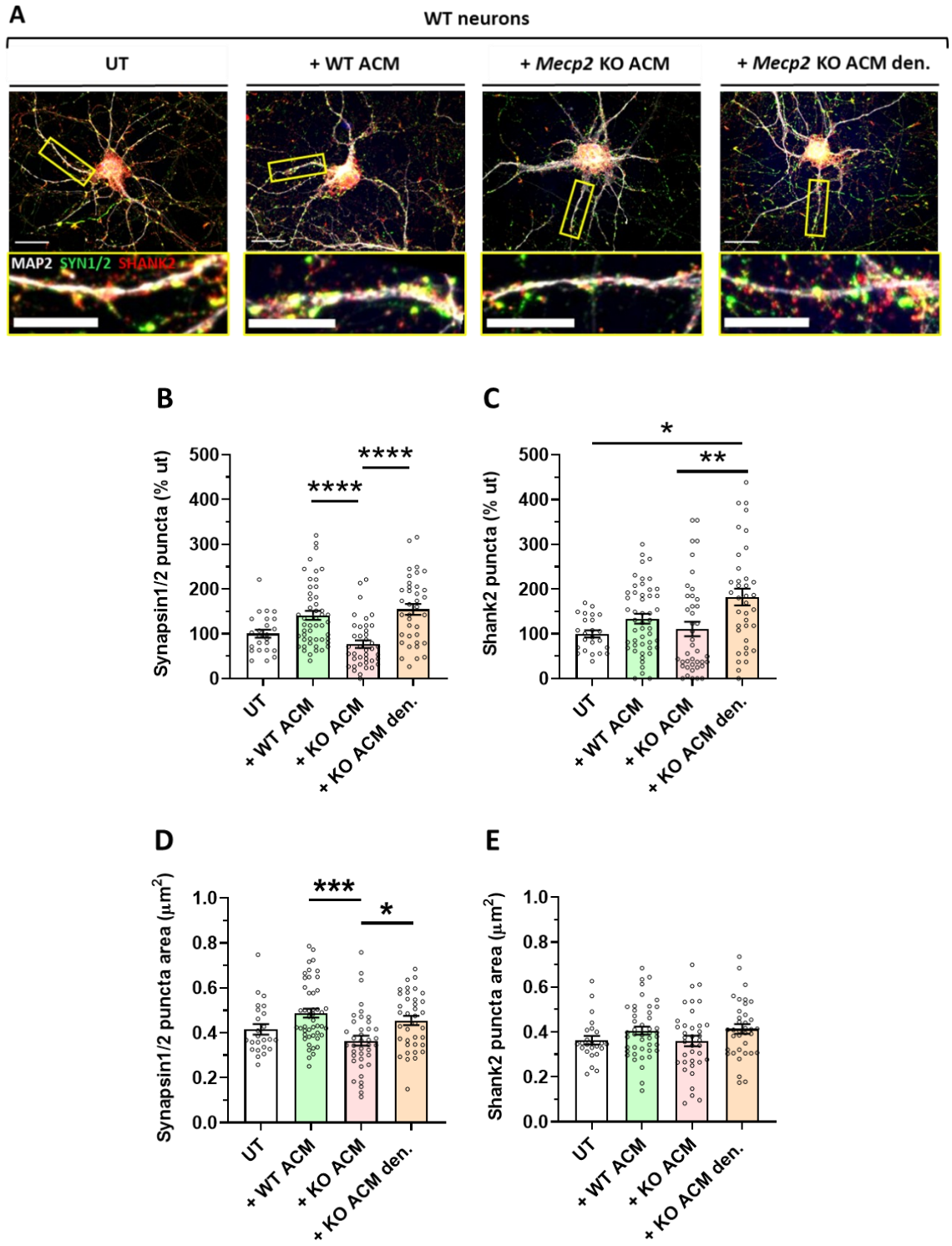

Figure 4.6. Neurotoxic factors within *Mecp2* KO ACM affect synaptogenesis of mature WT neurons. A) Representative images of WT neurons (DIV14) immunostained for MAP2 (white), Synapsin1/2 (green) and Shank2 (red) following 24 hours of treatment. Neurons untreated (UT) or treated with WT ACM (WT ACM), *Mecp2* KO ACM (KO ACM) or heat-denatured *Mecp2* KO ACM (KO ACM den.) (1:1 respect to neuron culture medium). Scale bar = 20 μm, and 10 μm in the enlarged image. **B-D**) Histograms indicate the mean ± SEM of Synapsin1/2 (**B**) and Shank2 (**C**) puncta number and Synapsin1/2 (**D**) and Shank2 (**E**) puncta area (white bar = untreated WT neurons; green bar = WT neurons + WT ACM; red bar = WT neurons + *Mecp2* KO ACM; orange bar = WT neurons + heat-denatured *Mecp2* KO ACM). Values for puncta number are expressed as percentages compared to untreated WT neurons (100%). Asterisks indicate statistical significance between the two experimental groups (* $p<0.05$, ** $p<0.01$, **** $p<0.0001$ by Dunn's *post hoc* test). **B-E**) Analyses were performed on n=24 untreated WT neurons from 2 biological replicates, n=49 WT neurons + WT ACM from n=5 biological replicates, n=40 WT neurons + *Mecp2* KO ACM from n=4 biological replicates, n=37 WT neurons + heat-denatured *Mecp2* KO ACM from n=4 biological replicates. **A-J**) For each independent experiment, WT neurons were a pool derived from 3 different WT animals.

4.5 *Mecp2* KO astrocytes strongly impact the genetic expression of WT neurons: searching for the putative molecular mechanisms underlying synaptic defects

Thousands of proteins of different nature (e.g. neuromodulators, neurotrophins, extracellular matrix proteins, cytokines, glycoproteins, etc.) might participate to the synaptogenic impairments of KO astrocytes. Since the proteomics analysis of the ACM was prevented by the high abundance of BSA, we searched for a different unbiased approach that might reveal the involved molecular mechanisms. We thus used RNA-Seq to analyse at the transcriptional level how WT neurons respond to the paracrine signals released by WT or *Mecp2* KO astrocytes and to identify the downstream deregulated pathways.

To this purpose, we compared the transcriptional profile of 3 different experimental groups: WT neurons co-cultured with WT or *Mecp2* KO astrocytes *versus* WT neurons alone and WT neurons in co-culture with *Mecp2* KO *versus* WT astrocytes. The batch effect was corrected by removing the variable ‘preparation’ in the DESeq2 model, as

confirmed by Principal Component Analysis (PCA) (**Figure 4.7 A)**. By analysing the impact of the 3 different experimental conditions on the distribution of individual sample variances, it emerged that WT neurons in co-culture with astrocytes, regardless of *Mecp2* expression, similarly cluster when compared to neurons cultured alone (**Figure 4.7 B)**. Conversely, when the co-cultures are compared to each other, they do not show an evident clusterization, therefore indicating that the contribution of the co-culture condition overcomes the genotype difference.

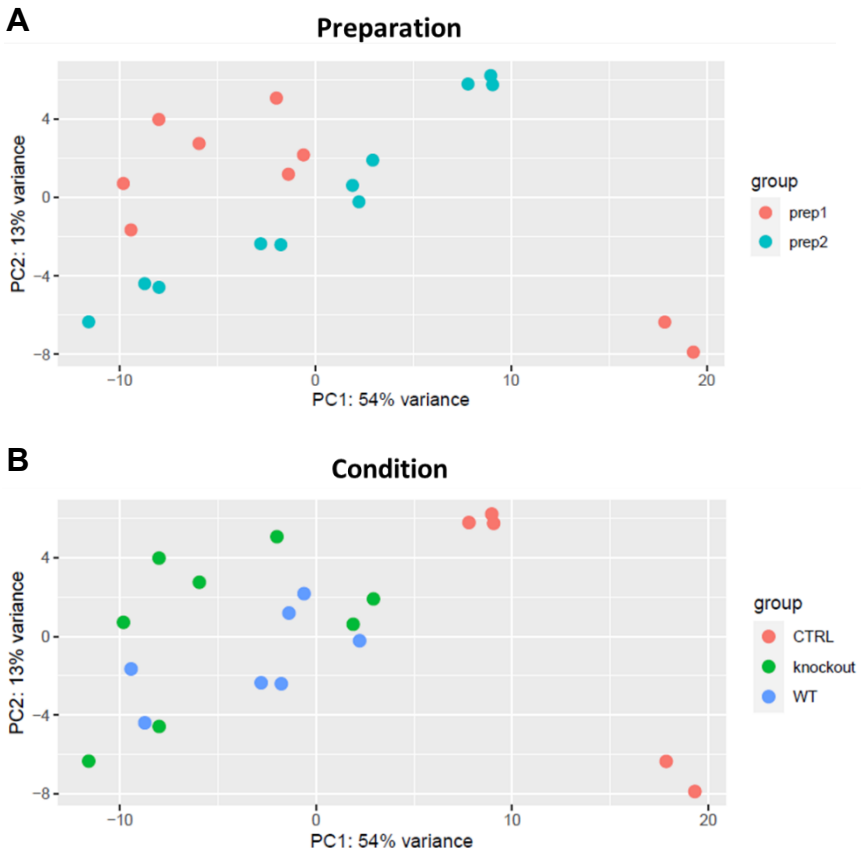

Figure 4.7. PCA plots of individual sample variances according to preparation (A) and experimental condition (B). Individual sample variances between WT neurons alone and WT neurons cultured with WT or *Mecp2* KO astrocytes are displayed as PCA plots. The percentage of total variation represented by each component is reported on the axes. Each dot represents a sample. WT neurons co-cultured with *Mecp2* KO astrocytes: n=8; WT neurons co-cultured with WT astrocytes: n=7. For each preparation (n=2), WT neurons were a pool derived from 3 different animals.

Differential expression analysis provided a list of deregulated genes (DEGs) for each of the 3 comparison groups (**Figure 4.8**).

A

Comparison	p.adj < 0.1	p.adj < 0.1 & LFC > |1|	p.adj < 0.1 & LFC > 1	p.adj < 0.1 & LFC < -1	p.adj < 0.05	p.adj < 0.05 & LFC > |1|	p.adj < 0.05 & LFC > 1	p.adj < 0.05 & LFC < -1
WT vs CTRL	3239	545	437	108	2493	545	437	108
KO vs CTRL	3808	717	573	144	2890	716	572	144
KO vs WT	401	25	24	1	216	19	18	1

B

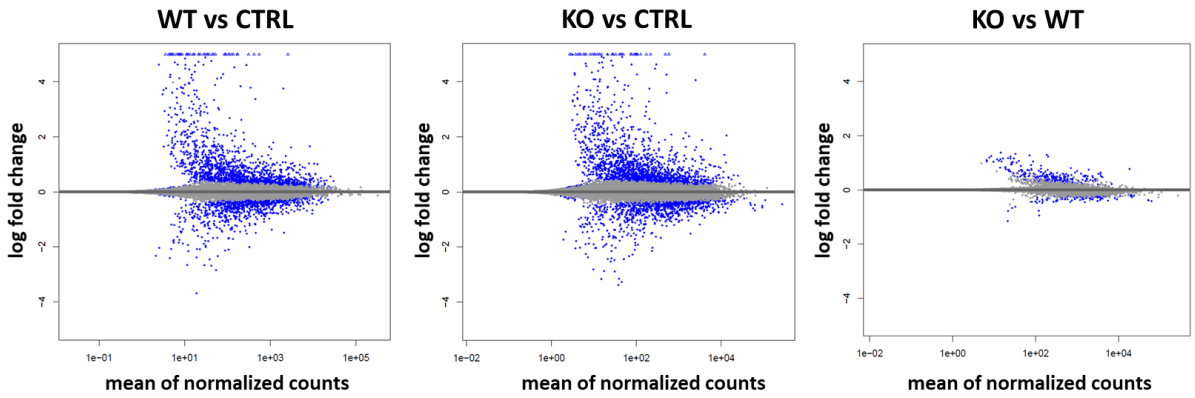

Figure 4.8 Both co-culture conditions and astrocyte genotype influence the transcriptional profile of WT neurons. A) Summary table of the number of the DEGs for each comparison group. They have been divided according to their p-adjusted (blue: p.adj<0.1; yellow: p<0.05) and log2 fold change (LFC) > or < 1. The apeglm method was applied for log2 fold change shrinkage. **B)** MA plot of the LFC of all genes for the 3 different comparison groups. Blue points indicate DEGs with p.adj<0.1 by apeglm shrinkage.

Accordingly with the importance of the astrocyte-neuron crosstalk, co-culture condition greatly impacts the transcriptional profile of neurons. Indeed, the presence of astrocytes in culture changes the expression of thousands of neuronal genes, whilst only few hundreds of DEGs were found in the KO *versus* WT group.

Interestingly, the comparison between neurons cultured with *Mecp2* KO *versus* WT astrocytes revealed that, despite hundreds of DEGs (full list in Appendix I), only few genes are significantly deregulated (log2 fold change > |1|), with almost all of them upregulated (**Figure 4.9**).

They are involved in energetic and metabolic processes (Myh6, ApoC1, Sdsl, Neu4, Srpk3, Abhd14b), pyruvate transport (Slc16a11), immune response (C4a, Lat2), signaling pathways (Lefty2, Slc2a4rg, Gipr, RgS11) and microtubule motor activity (Kif19A).

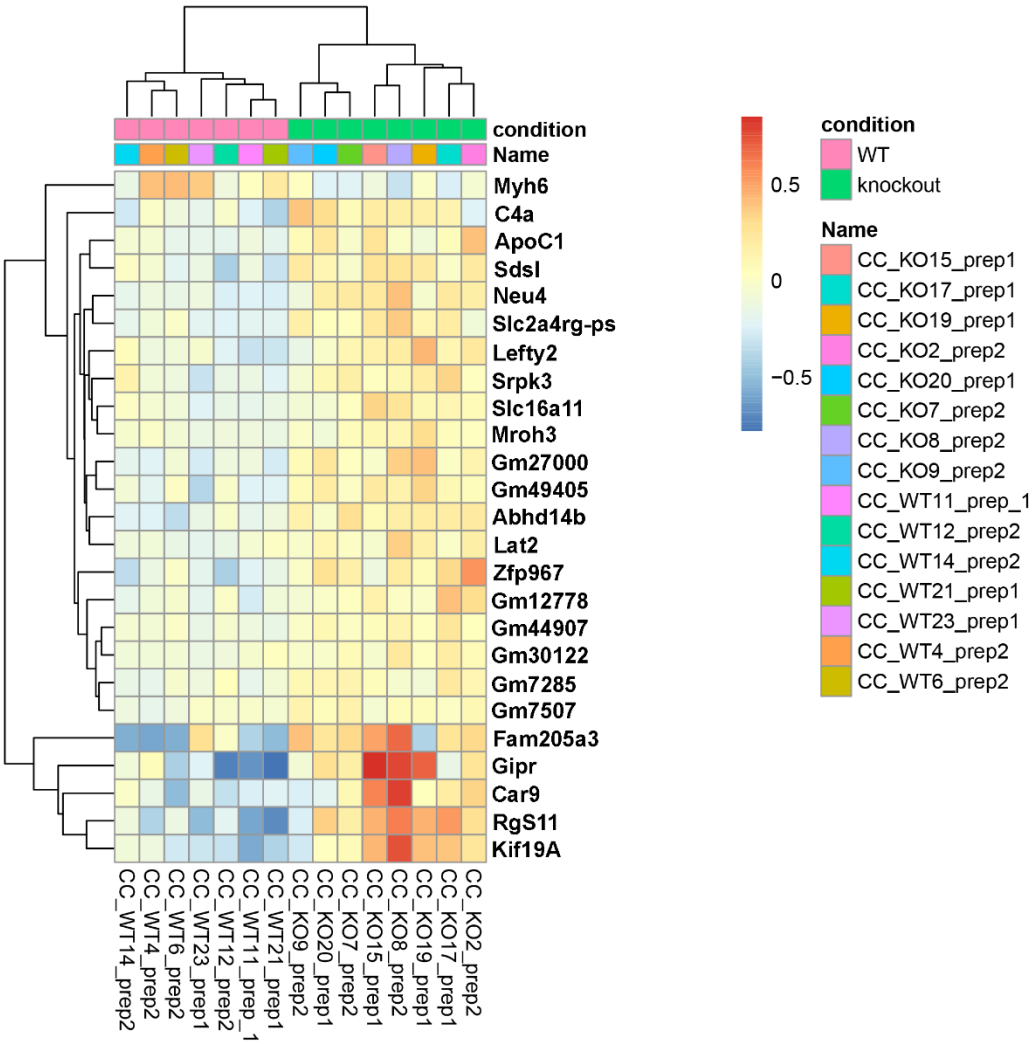

Figure 4.9. Top list of DEGs between neurons co-cultured with *Mecp2* KO *versus* WT astrocytes reveals an overall upregulation. Heatmap of the differentially expressed genes (DEGs) (p.adjust <0.1) with absolute LFC > 1 between neurons co-cultured with *Mecp2* KO *versus* WT astrocytes. For log2 fold change shrinkage the apeglm method was applied. Colour intensity represents the entity of the fold change related to WT neurons co-cultured with *Mecp2* KO *versus* WT astrocytes (red: upregulated genes, blue: downregulated genes).

To determine the biological processes mostly affected, we performed a Gene Ontology (GO) analysis on the DEGs with p.adj <0.1 (**Figure 4.10 A-C**).

As expected, gene enrichment analysis of WT *versus* CTRL and KO *versus* CTRL revealed that the presence of astrocytes is crucial to influence neuronal pathways associated with maturation, such as cell development, cell proliferation, positive regulation of the MAPK cascade, extracellular matrix organization (**Figure 4.10 A,B**). A further confirmation that neuronal responses are triggered by the presence of astrocytes comes from the strong modulation of the gliogenesis pathway. Interestingly, all the above-mentioned processes are similarly influenced by either WT or KO astrocytes, meaning that the co-culture condition is the main cause of these transcriptional changes. In details, a total of 837 biological processes are shared between the two comparison groups. On the contrary, some biological processes are differentially regulated by WT or KO astrocytes with respect to CTRL: 287 and 418, respectively (full list in Appendix II and III). From the WT *versus* CTRL comparison it emerged that there is a significant influence of WT astrocytes on metal ion transport, whilst in KO *versus* CTRL this pathway does not appear in the top 20 list. In addition, by considering all the deregulated processes (p.adjust <0.1), we observed a strong involvement of the transport of ions, neurotransmitters, amino acids or proteins at pre- and post-synaptic levels, that in KO *versus* CTRL are much lower in the rankings or mostly absent. Therefore, in accordance with our data, neurons in the WT-WT co-culture exhibited an increased expression of genes involved in synaptic activity and maturation. On the other hand, *Mecp2* KO astrocytes largely influence neuronal pathways involved in axonogenesis and actin filament organization, indicating a strong impact on neuronal morphology. To our surprise, enrichment analysis also highlighted a higher implication of cell chemotaxis, leukocyte and lymphocyte proliferation, response to Bone Morphogenetic Proteins (BMPs); interestingly, pathways related to positive regulation of reactive oxygen species metabolic process, SMAD protein signal transduction and Toll-like receptor signaling pathway are exclusively present in the KO *versus* CTRL comparison group. These results might suggest altered response to cytokines and pro-inflammatory molecules. Nevertheless, the comparison of KO *versus* WT robustly confirms our previous findings about neuronal alterations caused by *Mecp2* loss in astrocytes regarding morphological and synaptic dysfunctions (**Figure 4.10 C**) (full list in Appendix IV). As a matter of facts, the most enriched pathways are the ones involved in synaptic maturation and assembly, neuronal morphology, axonogenesis, receptor localization to synapses, cell junction assembly and synaptic plasticity. Curiously, also new pathways emerged from that comparison

and include regulation of mRNA metabolic processes and pyrimidine nucleoside triphosphate biosynthetic processes. Future analyses will clarify these aspects.

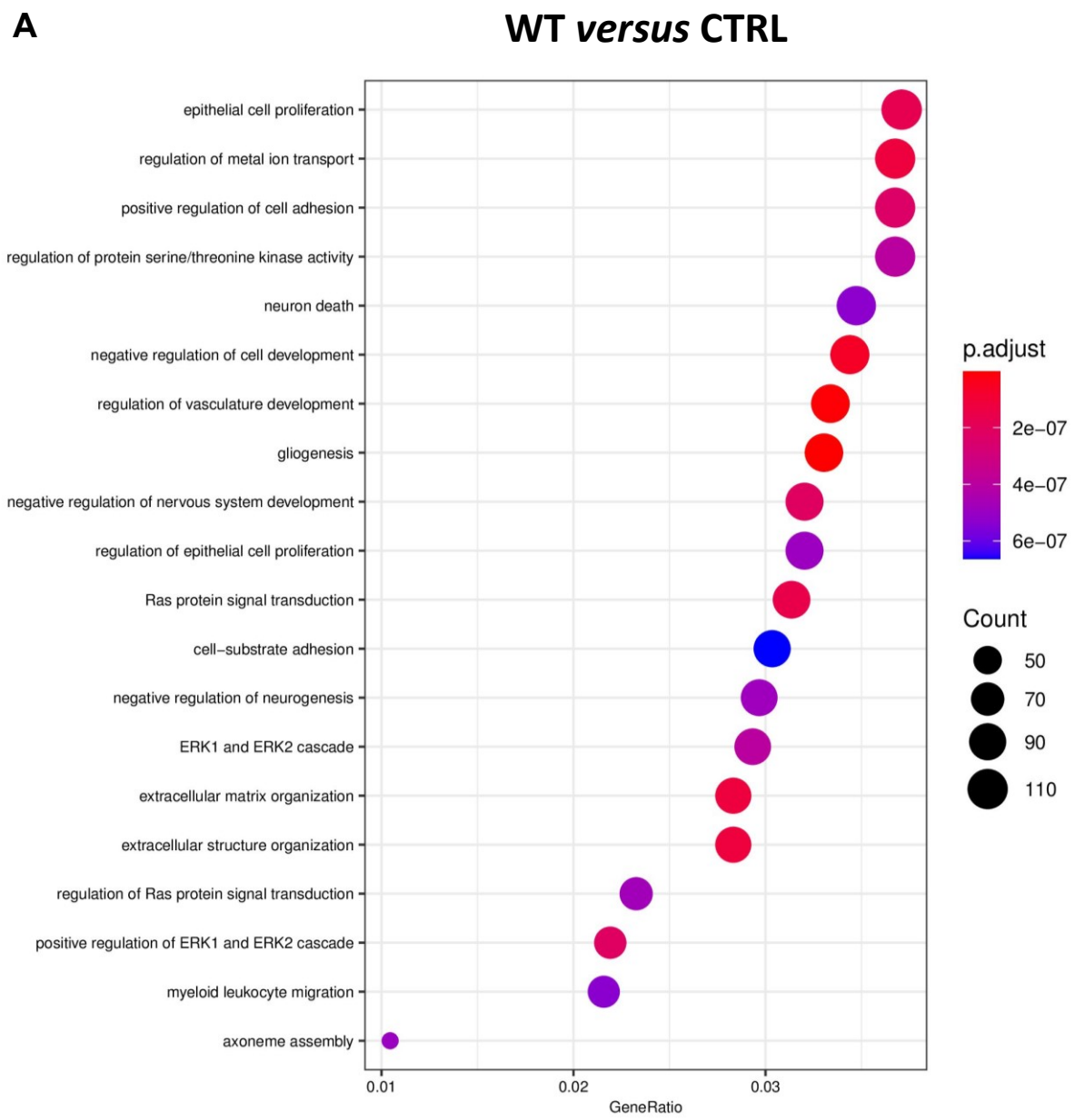

B

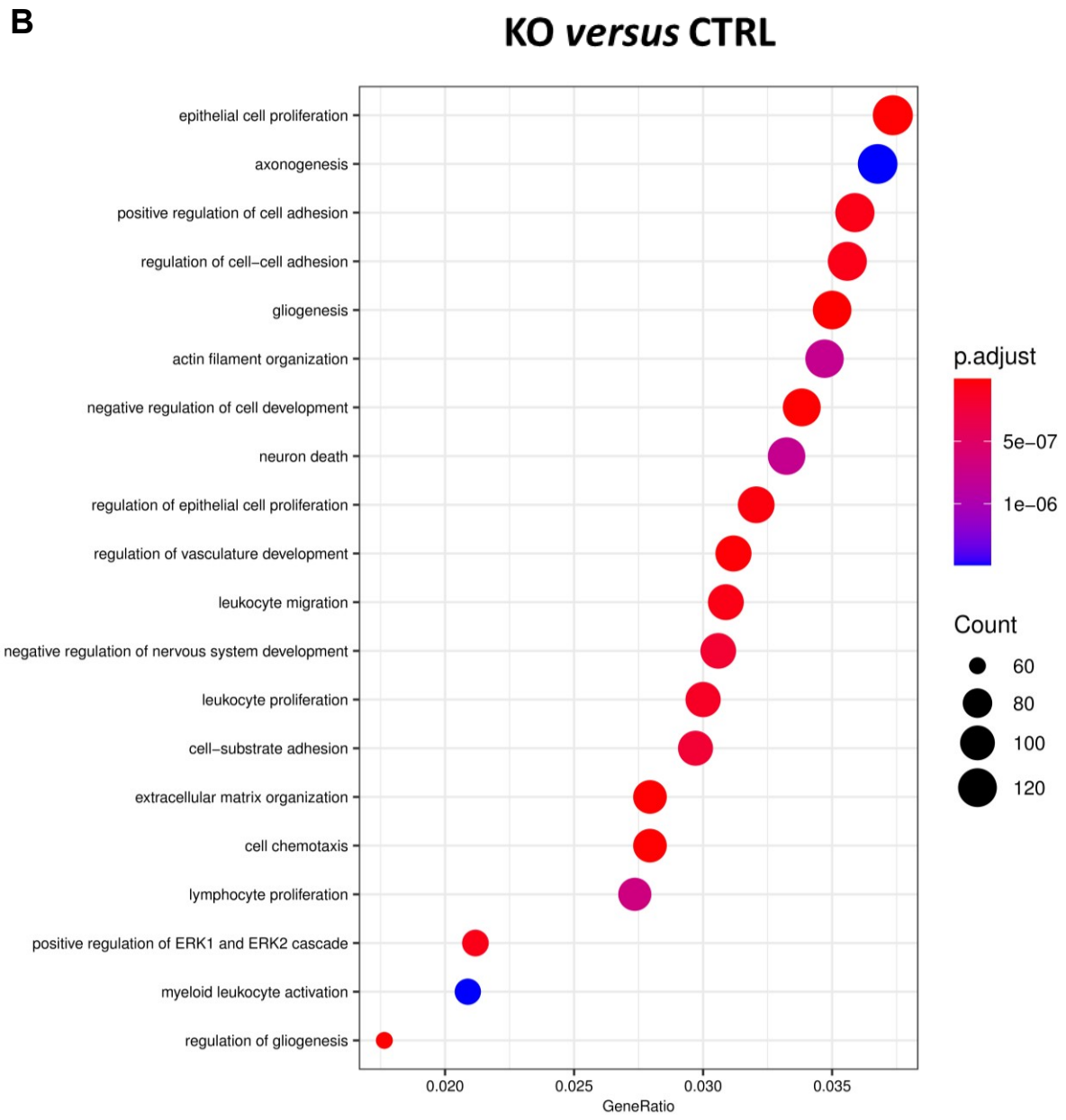
KO versus CTRL
epithelial cell proliferation
axonogenesis
positive regulation of cell adhesion
regulation of cell−cell adhesion
gliogenesis
actin filament organization
negative regulation of cell development
neuron death
regulation of epithelial cell proliferation
regulation of vasculature development
leukocyte migration
negative regulation of nervous system development
leukocyte proliferation
cell−substrate adhesion
extracellular matrix organization
cell chemotaxis
lymphocyte proliferation
positive regulation of ERK1 and ERK2 cascade
myeloid leukocyte activation
regulation of gliogenesis
0.020
0.025
0.030
0.035
GeneRatio
p.adjust
5e−07
1e−06
Count
60
80
100
120

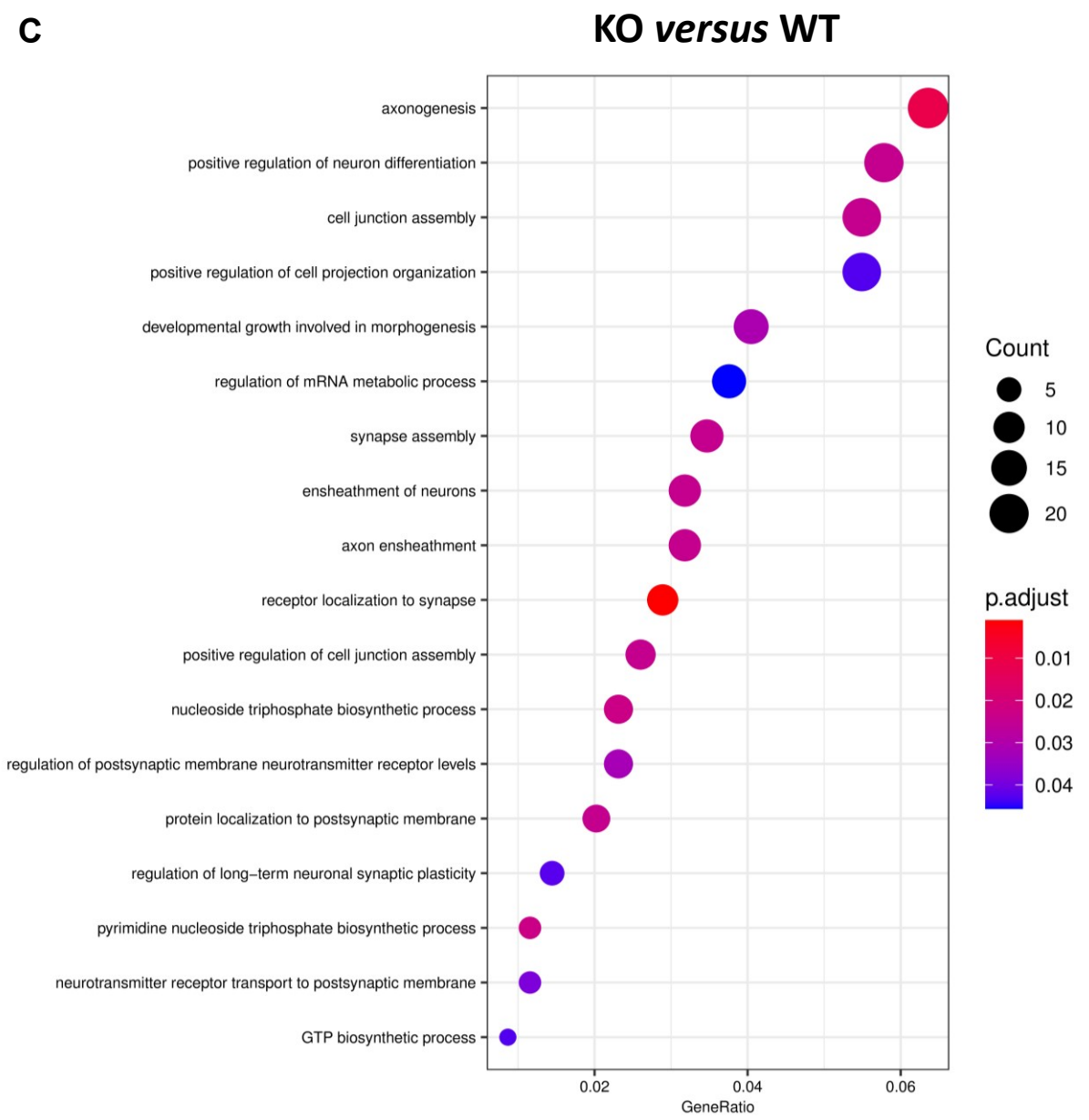

Figure 4.10. Enrichment analysis of GO biological processes confirms the impact of the co-culture on neuronal development and the importance of *Mecp2* expression in astrocytes for synaptic maturation. A, B, C) Gene Ontology (GO) analysis of all comparison groups performed with clusterProfiler (*Yu et al., 2011*). The plots shows the top 20 enriched biological processes from DEGs with q-value <0.2, p.adjust <0.1 and p-value cut-off <0.05. The function *simplify* has been used to remove redundancy of enriched GO terms. Colour intensity indicates the value of the p.adjust related to that biological process (red > p.adj; blue: < p.adj) and the dimension of the dots represents the number of genes counted for that biological process (> size: > counts).

Gene set enrichment analysis (GSEA) performed on genes of the KO *versus* WT comparison group further confirmed the presence of synaptic alterations. In particular, several critical synaptic processes are negatively regulated at both pre- and post-synaptic levels (**Figure 4.11 A-I**). In accordance with our IF data, we observed a decreased regulation of genes associated with protein localization to synapses, dendrite development and regulation of dendritic spine development. Moreover, we also collected indications about functional impairments in the glutamate receptor signaling pathway, regulation of neurotransmitter receptor activity, synaptic transmission and synaptic plasticity. Therefore, these analyses additionally highlighted the importance of *Mecp2* expression in astrocytes to support a correct synaptic maturation and communication.

Searching for the putative molecular mechanisms at the base of synaptic defects, we found of high relevance the identification of the pathway associated with the pyrimidine nucleoside triphosphate biosynthesis, which is significantly deregulated in the GO analysis and whose upregulation in neurons cultured with KO astrocytes was confirmed by GSEA analysis (**Figure 4.11 J**). Indeed, mitochondrial dysfunctions are emerging as a hallmark of several neurological diseases, in particular Alzheimer's disease, where oxidative phosphorylation appears particularly affected with the consequent alteration of reactive oxygens species production and *de novo* synthesis of pyrimidines (*Desler et al, 2018*). Interestingly, GSEA analyses reported a positively regulation of pathways related to mitochondrial translation and oxidative phosphorylation in neurons in co-cultured with KO astrocytes (**Figure 4.11 K, L**), while, as stated above, GO analysis highlighted the involvement of pathways related to a positive regulation of reactive oxygen species. Of note, a significant increase in mitochondrial respiration leads to overproduction of reactive oxygen species (ROS) that, in turn, can damage cellular components via oxidation but can also be a second messenger in various redox-sensitive signaling pathways (*Missiroli et al., 2020*). Importantly, neuronal redox-imbalance and increased ROS generation have already been described in RTT mitochondria (*Can et al., 2019*). On the same line, it is important to acknowledge that inflammatory cytokines or neuroinflammation can cause mitochondrial dysfunctions, altered oxidative phosphorylation and ROS production (*He et al., 2020*). Since our bioinformatic analyses suggested in WT neurons cultured with KO astrocytes the activation of pathways involved with an altered response to cytokines and pro-inflammatory molecules, our future experiments will investigate

whether KO astrocytes might exhibit an aberrant release of cytokines that will then impact on mitochondrial functions.

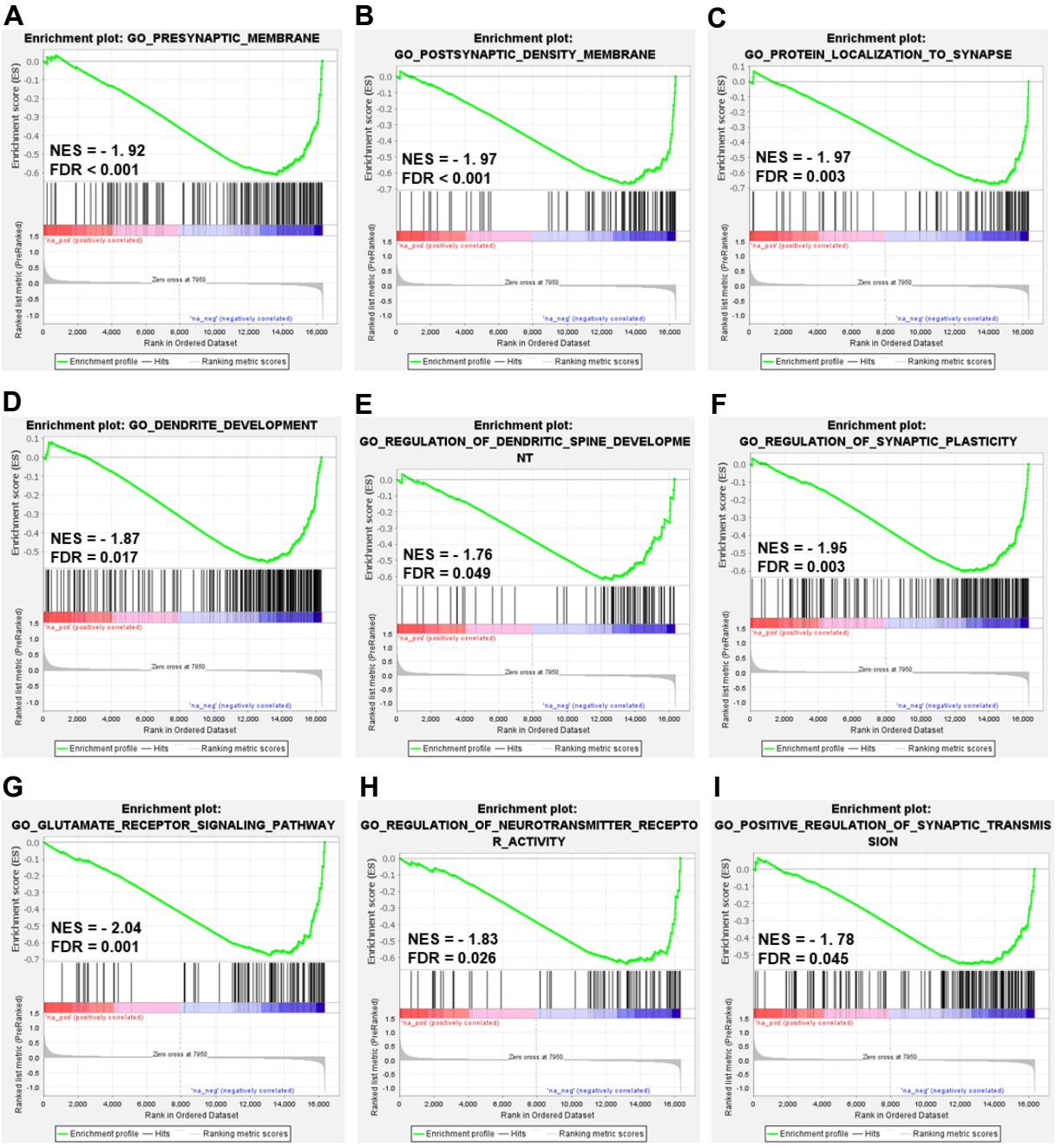

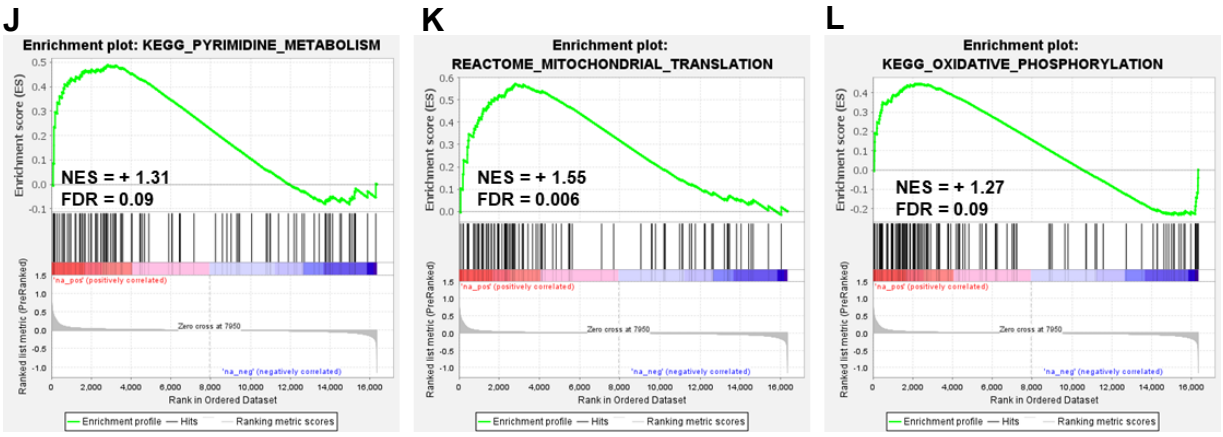

Figure 4.11. Gene set enrichment analysis (GSEA) of the transcriptional profiles of WT neurons confirm that *Mecp2* loss in astrocytes induces a negative regulation of synaptic maturation. The X-axis contains all the genes (KO *versus* WT) in the particular gene set from up-regulated (red) to down-regulated (blue) depending on their LFC. False discovery rates (FDR) and normalized enrichment scores (NES) evaluate whether the gene sets are positively or negatively enriched.

4.6 *Mecp2* loss in astrocytes influences cell sphingolipid pattern of WT neurons

Sphingolipids are essential for the development and maintenance of the functional integrity of the nervous system and play crucial roles in controlling different aspects of synaptic transmission (*Olsen and Faergeman, 2017; Riganti et al., 2018*). Considering the active role of astrocytes in the metabolism/release/exchange of sphingolipids (*Barber and Raben, 2019*), we investigated whether the lack of *Mecp2* affects these processes in collaboration with Dr. M. Aureli's lab. To do this, we used a transwell-based co-culture system and two different experimental conditions (chapter 2.6.1) (**Figure 4.12 A-D**).

In experiment A, we evaluated whether and how *Mecp2* loss in astrocytes influences the global pattern of sphingolipids by adding [1-^{3}H]-sphingosine both to neurons and astrocytes in co-culture(**Figure 4.12 A, B**). Our data indicated that glial *Mecp2* deficiency alters the overall sphingolipid metabolism, although moderately, both in astrocytes and in the adjacent neuronal cells.

In details, comparing WT and KO astrocytes, we observed that in KO astrocytes there is a slight increase of ceramide (Cer), a sphingolipid generally involved in apoptotic processes (*Brocklyn and Williams, 2012*). In accordance with this, we reported a decrease of phosphatidylethanolamine (PE), a glycerophospholipid synthesized by the cells using ^{3}H-ethanolamine which derives from the catabolism of sphingosine-1-phosphate (S1P) typically considered a pro-survival molecule. These data suggests that in KO astrocytes there may be an imbalance in the Cer/S1P rheostat. Moreover, we also observed alterations in the production of simple gangliosides. We reported, indeed, a slight decrease in the content of monosialodihexosylganglioside (GM3) and in sphingomyelin (SM) and a small increment of ganglioside GD3, suggesting possible alterations also in gangliosides metabolism.

Considering the sphingolipid pattern of WT neurons cultured with KO astrocytes, we observed a reduction of complex gangliosides, GD1a and GT1b, if compared with WT neurons co-cultured with WT astrocytes. These gangliosides are generally associated to pre-synaptic membranes and dendritic functions (e.g. neurotransmitters release) (*Sipione et al., 2020*), making the result very interesting and in good accordance with immunofluorescence results. Contrary to astrocytes, we reported an increase of PE in WT neurons co-cultured with KO astrocytes, indicating that sphingolipid impairments might be strictly dependent on the population considered. Unexpectedly, this experiment also revealed that a large quantity of complex gangliosides are released by neurons and shuttled to astrocytes. Indeed, complex polysialylated gangliosides are slightly present in astrocytes cultured alone (confirmed also in experiment B), and they could only be derived from mature neurons.

In experiment B (**Figure 4.12 C, D**), in which only WT/KO astrocytes were fed with [1-^{3}H]-sphingosine and subsequently cultured with WT neurons, we assessed whether and which sphingolipids are released by astrocytes to neurons and how neuronal sphingolipid metabolism changes in response to *Mecp2* loss in astrocytes. While the sphingolipid pattern reported no difference in KO astrocytes, surprisingly, we observed a decrease in PE and an increase in globotriaosylceramide (Gb3Cer) in WT neurons co-cultured with KO astrocytes. These data suggest that KO astrocytes might release lipid vesicles with different compositions and/or that astrocyte-derived sphingolipids are used differently by neurons when co-cultured with KO astrocytes.

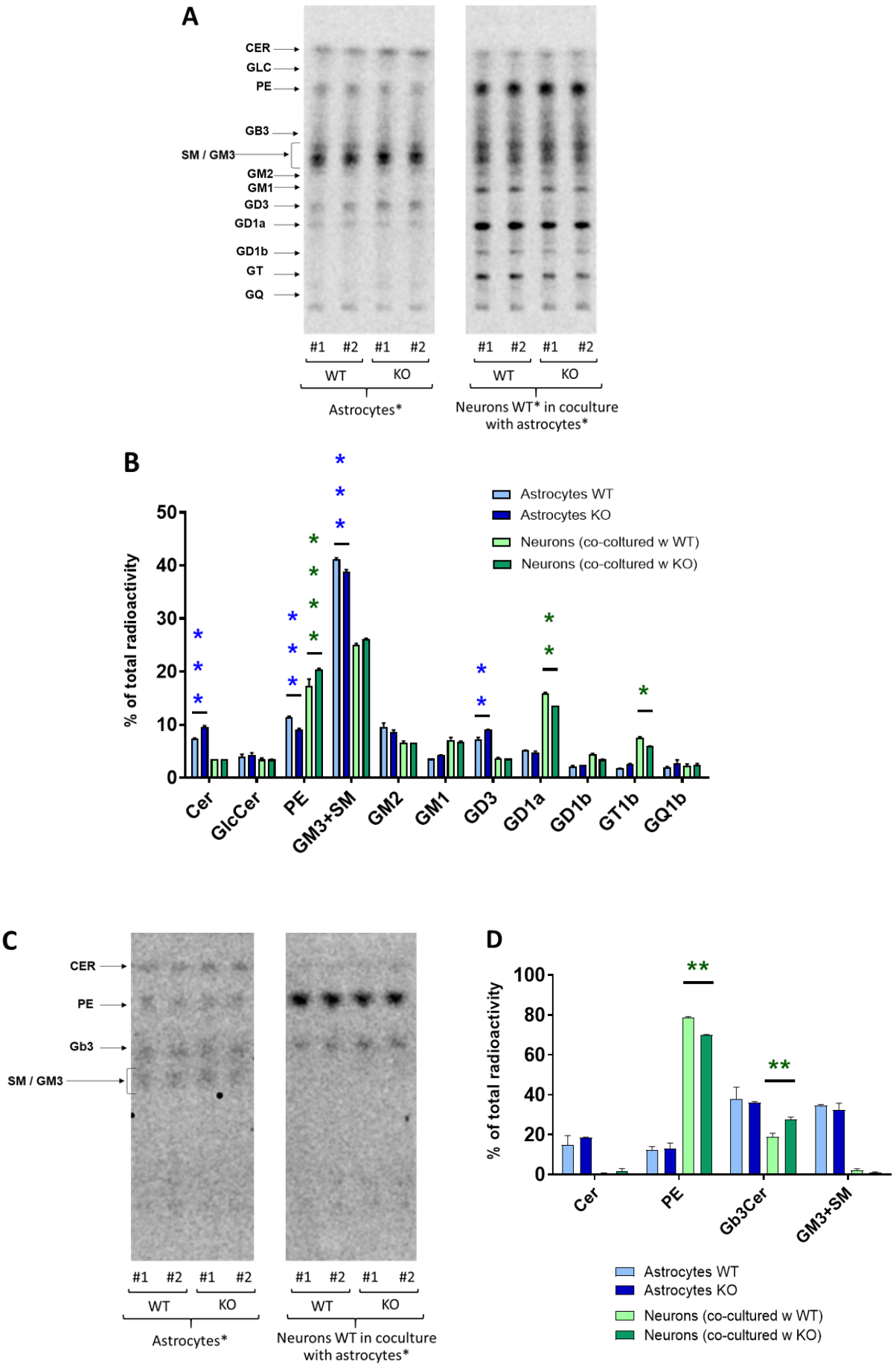
A
CER
GLC
PE
GB3
SM / GM3
GM2
GM1
GD3
GD1a
GD1b
GT
GQ
#1 #2 #1 #2
WT KO
Astrocytes*
#1 #2 #1 #2
WT KO
Neurons WT* in coculture with astrocytes*
B
% of total radioactivity
Astrocytes WT
Astrocytes KO
Neurons (co-coltured w WT)
Neurons (co-coltured w KO)
Cer
GlcCer
PE
GM3+SM
GM2
GM1
GD3
GD1a
GD1b
GT1b
GQ1b
C
CER
PE
Gb3
SM / GM3
#1 #2 #1 #2
WT KO
Astrocytes*
#1 #2 #1 #2
WT KO
Neurons WT in coculture with astrocytes*
D
% of total radioactivity
Cer
PE
Gb3Cer
GM3+SM
Astrocytes WT
Astrocytes KO
Neurons (co-cultured w WT)
Neurons (co-cultured w KO)

Figure 4.12. **WT neurons co-cultured with KO astrocytes exhibit an altered sphingolipid metabolism**. **A, C**) Representative digital autoradiographies of radioactive lipids of astrocytes and neurons under experimental condition A (**A**) and experimental condition B (**C**). **B, D**) Histograms indicate the mean ± SEM of sphingolipid species quantified by digital autoradiography. For each sphingolipid, data are reported as percentage of total sphingolipid incorporated radioactivity. Asterisks refer to statistical significance between WT and KO astrocytes (blue), and between WT neurons in co-culture with WT and KO astrocytes (green) (* $p<0.05$; ** $p<0.01$; *** $p<0.001$; **** $p<0.0001$ by Bonferroni *post hoc* test). Cer: ceramide; GlcCer: glucosylceramide; PE: phosphatidylethanolamine; Gb3: globotriaosylceramide; SM: sphingomyelin; GM1,2,3: monosialic gangliosides type 1,2,3; GD3, GD1a, GD1b, GT1b, GQ1b: different complex gangliosides. Analyses were performed in duplicate. Astrocytes and neurons were pools of 3 different biological replicates.

To test the first hypothesis, we studied the composition of the medium of astrocytes alone (**Figure 4.13**). By analysing the endogenous sphingolipid pattern of astrocytes, no difference was observed between WT and KO, pointing to the importance of neuron-glia crosstalk for the occurrence of such alterations (**Figure 4.13 A, B**). Nevertheless, we reported an increase of SM/GM2/GM1 and a decrease of ganglioside GD3 in the medium of KO astrocytes, revealing the presence of some cell-autonomous changes in the release of lipids (**Figure 4.13 C, D**). However, no change in PE and Gb3Cer content, that could explain the results in neurons, was noted, leading to exclude that a different lipid release in the medium by KO astrocytes might be responsible of the neuronal defects. Therefore, further investigation is needed to clarify these aspects.

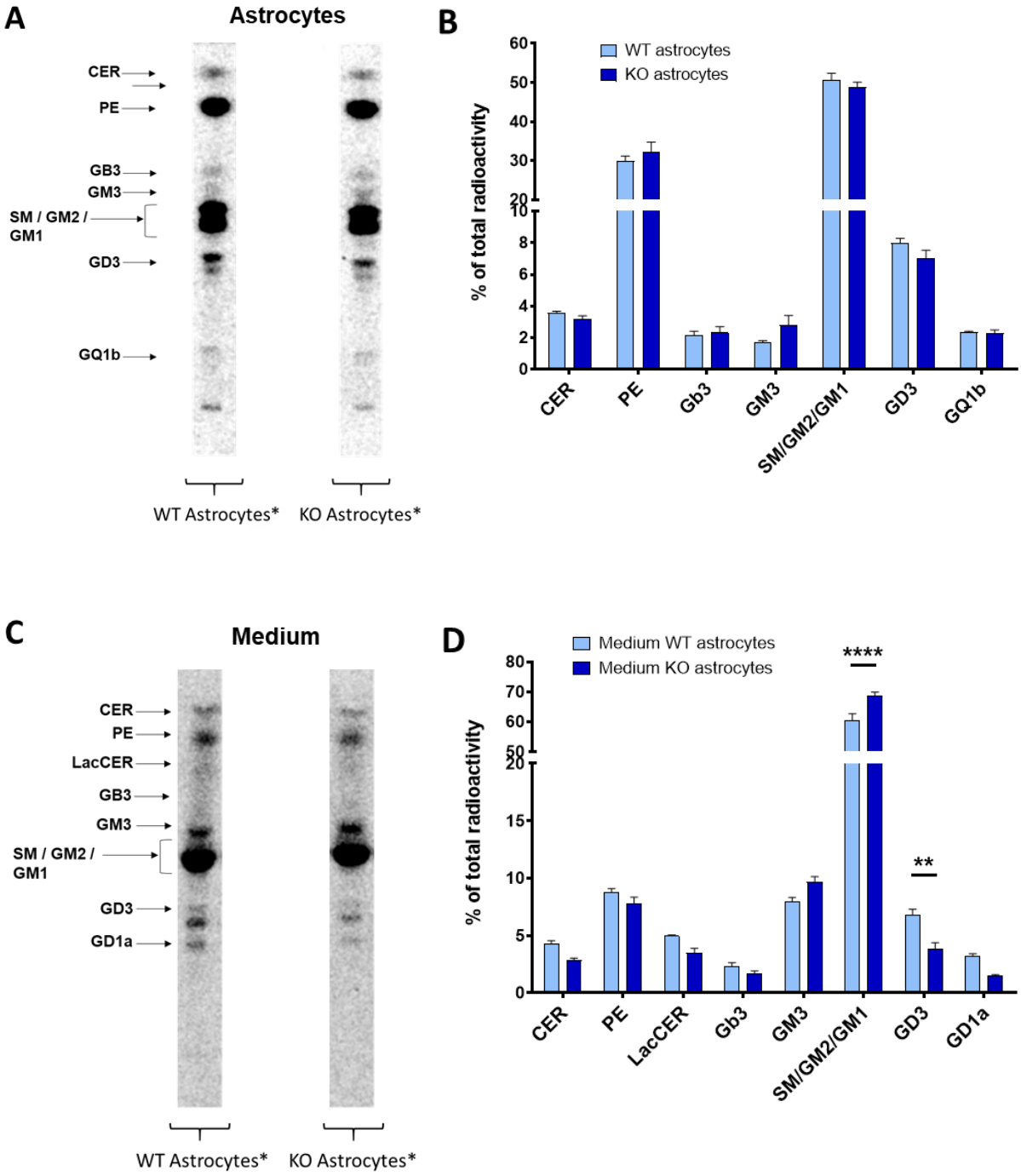

Figure 4.13. The absence of *Mecp2* in astrocytes partially influences their sphingolipids release in the extracellular milieu. A, C) Representative digital autoradiography of radioactive endogenous lipids (**A**) and lipids released by astrocytes in the medium (**C**). **B, D**) Histograms indicate the mean ± SEM of sphingolipid species quantified by digital autoradiography. For each sphingolipid, data are reported as percentage of total sphingolipid incorporated radioactivity. Asterisks refer to statistical significance between WT and null astrocytes (** p<0.01; **** p<0.0001 by Bonferroni *post hoc* test). Cer: ceramide; LacCer:

Lactosylceramides; PE: phosphatidylethanolamine; Gb3: globotriaosylceramide; SM: sphingomyelin; GM1,2,3: monosialic gangliosides type 1,2,3; GD3, GD1a, GQ1b: different complex gangliosides **A-D**) Analyses were performed on pools of 3 different biological replicates.

Discussion

RTT syndrome, a rare and progressive neurodevelopmental disorder, is considered the most common genetic cause of severe intellectual disability in girls (*Chahrour and Zoghbi, 2007*). Almost 40 years of research allowed RTT scientific community to uncover several neurobiological alterations caused by *Mecp2* loss of function in neurons; more recently, the RTT scientific community has initiated to include astrocytes in the studies. However, we still lack a full understanding of relevant downstream deregulated pathways in the different cell types. To date, no cure exists for RTT and available treatments are aimed only at ameliorating secondary symptoms. Hence, the purpose of this thesis was to extend the current knowledge on the pathophysiological mechanisms of RTT, focusing on the impact of *Mecp2* loss on astrocytes, which play an essential role for synaptic transmission and CNS homeostasis.

Although neuronal dysfunctions have been proposed as the major causes of RTT (*Gulmez-Karaca et al., 2019*), the neuro-centric view has been recently challenged by the emergent role of astroglial cells in the pathogenesis of the disease (*Ballas et al., 2009; Lioy et al., 2011*). Astrocytes are essential elements supporting the structure and function of the entire brain and their peculiar shape allows them to contact neurons and surround cells to exploit their roles (*Verkhratsky and Nedergaard, 2018*). Morphological changes strongly affect astrocytic functions and represent a common pathological feature in many neurological disorders (*Zhou et al., 2019*). To date, limited information is available regarding the impact of *Mecp2* loss on the complexity of astroglial shape and our studies aimed at initiating to fill this gap of knowledge.

By analysing the progression of morphological features of *Mecp2* KO $GFAP^+$ astrocytes in brain areas where structural and functional alterations had already been largely documented, we observed that loss of *Mecp2* profoundly affects the morphology of different astrocytic populations; a temporal progression of morphological defects was also reported. Morphological alterations appeared more evident in the motor cortex, then they spread into the somatosensory cortex and lastly appeared in the hippocampus. Interestingly, cortical astrocytes represent the cells mostly affected, and their impairments worsen over time along with the aggravation of the RTT mouse conditions. Defects in astrocyte morphology had previously been detected in the dentate gyrus and corpus callosum of $Mecp2^{308}$ mice and in the CA1 area of the hippocampus following post-natal deletion of *Mecp2 (De Filippis et al., 2011; Nguyen et al., 2012*). Nevertheless, no study has ever investigated the impact

of *Mecp2* loss on astrocyte morphogenesis with respect to the progression of the disease. Further, to the best of our knowledge, our studies provided the first *in vivo* description of *Mecp2* defective astrocytic morphology considering the importance of regionality. Altogether the obtained results suggested not only the relevance of *Mecp2* for cortical astrocytes, but also that *Mecp2* might play a minor role on astrocytes in the hippocampus and, if any, in the cerebellum. Although limited by the experimental conditions, our *in vitro* characterization of the shape complexity of cortical, hippocampal and cerebellar astrocytes confirmed the existence of astrocytic heterogeneity in RTT, thus highlighting the importance of considering it as a probable determinant in the pathophysiology of the disease. Further, *in vivo* data suggested that morphological analyses of astrocytes in *Mecp2* null cortex and hippocampus could be used as biomarkers for disease progression and for testing the efficacy of drugs designed to reverse symptoms or slow their course. Importantly, defects in astroglial morphology is a relevant pathological aspect documented in many neurological diseases, including psychiatric and neurodegenerative disorders (e.g. schizophrenia, Wernicke's encephalopathy, major depressive disorder, toxic encephalopathies with heavy metals, fronto-temporal dementia, amyotrophic lateral sclerosis, Alzheimer's disease) (*Verkhratsky et al., 2019; Verkhratsky et al., 2016; Phatnani and Maniatis, 2015*). Generally, neurodegenerative conditions are associated with astrocyte activation (gliosis), a phenomenon characterized by a multifaced and complex remodelling of shape (hypertrophy), up-regulation of astrocytic markers (GFAP and S100b above all) and secretion of pro-inflammatory molecules (*Verkhratsky et al., 2016)*. On the contrary, astrocytic atrophy leads to hypofunctionality, affecting different aspects of the astroglial homeostatic support, such as synaptic coverage by perisynaptic astrocytic processes (PAPs) and astroglia-dependent neuroprotection. Notably, astroglial atrophy can even precede the morpho-functional changes triggered by the 'reactive state', such as in the earliest phases of Alzheimer's disease. Despite an increase of *Gfap* expression was reported in primary cultures and in RTT brains (*Okabe et al., 2012; Colantuoni et al., 2001*), astrocytes do not show typical hallmarks of reactivity in RTT, although an altered response to inflammatory stimuli was proposed (*Kahanovitch et al., 2019*). We still do not know the molecular bases of the above-mentioned morphological impairments. However, a multi-omics study of the adult $Mecp2^{tm1.1Jae/y}$ KO cortex (P60) reported the alteration of astrocyte-specific genes associated with astrocyte maturation and morphology. Moreover, astrocyte

morphogenesis is the final product of a very fine cytoskeletal reorganization and the result of an interplay among microtubules, intermediate filaments, and actin cytoskeleton (*Schiweck et al., 2018*). Accordingly, several microtubule alterations have been reported in RTT astrocytes, affecting their stability, rate of polymerization and the microtubule-dependent vesicle transport (*Nectoux et al., 2012*; *Delépine et al., 2013; Delépine et al., 2016*). As a matter of facts, activation of brain RhoGTPases, a group of enzymes that induces dynamic changes in microtubule organization, reverts astrocyte atrophy and markedly improves the behavioural phenotype of *Mecp2*$^{308/y}$ mice (*De Filippis et al., 2012*).

Functional astrocytes are critical for proper neuronal maturation since they regulate synaptic formation (*Eroglu and Barres, 2010*). As a result, alterations in astrocyte morphogenesis negatively influence synaptogenesis (*Stogsdill et al., 2017*). RTT is considered a synaptopathy characterized by dendritic spine dysgenesis, impaired spine plasticity, alteration of neuronal excitability and disrupted excitatory/inhibitory balance of circuits (*Landi et al., 2011*; *Xu et al., 2014; Ip et al., 2018*). Therefore, we found it relevant to study excitatory synapses in brain areas affected by astroglial impairments, reporting an immature phenotype of both pre- and post-synaptic excitatory terminals in layer I of motor and somatosensory cortex at all ages analyzed. We have demonstrated that both Synapsin1/2 and PSD95 puncta in KO mice exhibit a smaller volume, which mirrors the presence of weaker and less mature spines (*Dumitriu et al., 2010; Schachtele et al., 2014; Berry and Nedivi, 2017; Bian et al., 2015*). In good accordance with our morphological data, hippocampal synaptic spines are less affected. In line with literature data, by measuring the number of functional synapses, we emphasized the presence of region-specific phenotypes and altered local circuits (*Ip et al., 2018*). Interestingly, we observed a very strong increment of excitatory synapses in layer I of the motor cortex, a defect that manifested both at pre- and early symptomatic stages. This results might be explained hypothesizing that compensatory mechanisms are set in place in the attempt to support neuronal transmission despite of immature spines. Alternatively, we cannot exclude defects in synaptic pruning, a physiological process of extra synapses elimination (*Landi et al., 2011; Schafer et al., 2016*). Notably, all the analyzed areas showed synaptic changes already at P20 supporting previous studies from several laboratories including our suggesting that neurobiological alterations manifest long before the onset of overt RTT symptoms.

We are aware that our *in vivo* studies were performed on a globally null mouse, which prevents from discriminating whether and to what extent synaptic defects are caused by cell or non-cell autonomous mechanisms. Although in the future we will address this issue by exploiting a conditional *Mecp2* mouse model selectively devoid of *Mecp2* in astrocytes, our *in vitro* studies, assessing the astroglia-neuron crosstalk, confirmed the negative role that *Mecp2* null astrocytes exert on synapses. The experimental set-up was planned in order to evaluate if, in accordance with our *in vivo* data, *Mecp2* null astrocytes derived from distinct brain regions could differentially affect excitatory synaptic maturation of cortical WT neurons.

Importantly, our *in vitro* data confirmed that cortical astrocytes are the most affected population as a prolonged exposure of WT neurons to their paracrine signals led to pre- and post-synaptic impairments. Hippocampal and cerebellar astrocytes, instead, induced partial or no effect on excitatory synapse formation, respectively. Altogether, our data provide the first evidence of area-specific alterations of *Mecp2* deficient astrocytes in supporting proper synaptogenesis; further, they clearly highlight the cortex as the most important area for studying astrocytes in RTT.

However, synaptogenesis is regulated not only by secreted molecules but also by a physical interaction with astrocytes (*Hillen et al, 2018*). Considering both these components, our experiments demonstrated the presence of more pronounced defects in WT neurons grown in contact with KO astrocytes, with respect to those produced only by paracrine signals. In accordance with several RNA-Seq data obtained from *Mecp2*-deficient samples, we hypothesise the involvement of cell adhesion molecules in the observed exacerbated phenotype (*Missler et al., 2012; Gandawijaya et al., 2021*). It is relevant to observe however that our *in vitro* experiments clearly indicated that *Mecp2* loss in neurons is by itself very detrimental for synaptogenesis, which is in line with previous evidence (*Baj et al., 2014*). Synapsin1/2 is a pre-synaptic vesicle protein deeply involved in neurotransmitters release and a reduction in the area of puncta can be associated with impairments in maturation and decreased synaptic activity (*Chi et al., 2001; Perlini et al., 2011*). Defects in pre-synaptic terminals in WT neurons in co-culture with KO astrocytes are supported by a reduction in neurons of complex gangliosides (GD1a and GT1b), which are structural components of plasma membranes, highly enriched in synaptic vesicles and associated with pre-synaptic membrane and dendritic functions (e.g. neurotransmitters release) (*Sandhoff et al.,*

2018, Sipione et al., 2020; *Palmano et al., 2015; Sonnino and Prinetti, 2016; Riganti et al., 2018*).

The negative influence exerted by mutant astrocytes on WT neurons is not a novel aspect in RTT. *Ballas* and *Williams* had already demonstrated that mouse and human RTT astrocytes do not support neuronal growth (*Ballas et a., 2009; Williams et al., 2014*); however, the effects on synaptic phenotypes have never been investigated before. Further, with respect to previous data, obtained in co-culture systems avoiding contacts, our contact co-cultures suggested that the presence of *Mecp2* either in neurons or astrocytes is sufficient for proper dendritic development at early developmental stages (DIV7). However, at later stages (DIV14), the methyl-binding protein had to be present in both cell types to correctly support neuronal morphogenesis, stressing the importance of a functional astrocyte-neuron crosstalk for proper maturation. Curiously, the lack of *Mecp2* in astrocytes causes changes in dendritic length and complexity that are different from the once following *Mecp2* loss in neurons. Therefore, we confirmed that a combination of cell and non-cell autonomous effects participate to morphological defects featured by neurons in RTT.

Clearly, and importantly, our data indicated the contribution of thermolabile neurotoxic protein(s), rather than the absence of neurotrophic one(s). However, at this stage, we cannot exclude the involvement of a secreted protein promoting synapse elimination and/or sequestering a neurotrophic factor, as suggested by a recent bioRxiv report (*Caldwell et al., 2020*). Proteomic or multiplex analyses might be considered to quantitatively measure in the culture medium selected proteins; however, we are aware that these factors might be below the threshold of detection.

Since heating completely abolished the negative effects exerted by KO-ACM on neuronal synaptogenesis, we also suggest that astrocytic neurotransmitters are not involved in the observed phenotypes. Furthermore, the presence of the same sphingolipids in the medium of cultured WT and KO astrocytes excluded the involvement of these bioactive lipids. These findings are in line with previous results that ascribed the negative influence of KO astrocyte on both neurons (*Ballas et a., 2009)* and nearby astrocytes (*Maezawa et al., 2009*) to toxic molecules. *Maezawa* and collaborators, indeed, reported that KO astrocytes exhibit an altered phenotype (abnormal growth, defective regulation of BDNF, different release of pro-inflammatory cytokines, altered p38MAPK activity, abnormal neuronal dendritic induction), which progressively spreads in WT astrocytes via a non-cell autonomous mechanism

involving gap junctions (*Maezawa et al., 2009*). Accordingly, our *in vivo* data indicated that WT astrocytes in the somatosensory cortex of heterozygous female mice show a more impaired morphology than the neighbouring KO astrocytes suggesting either an increased susceptibility to specific toxic factors released by *Mecp2* deficient astrocytes, from which KO astrocytes themselves are somehow protected, and/or the involvement of the gap junction mechanism described *in vitro*.

Several different families of gliotransmitters could be involved in the observed synaptic dysfunctions (neuromodulators, neurotrophins, extracellular matrix proteins, cytokines, glycoproteins, etc) (*Petrelli and Bezzi, 2015*). Numerous studies of gene expression have already been performed in RTT (*Jordan et al., 2007*; *Sugino et al., 2014; Ehrhart et al., 2016*; *Bedogni et al., 2016*; *Lin et al., 2016; Osenberg et al., 2018*; *Yasui et al., 2013; Delépine et al., 2015; Pacheco et al., 2017*); however, no one has ever focused the attention exclusively on the astroglia-neuron crosstalk to unveil downstream deregulated pathways affecting neuronal phenotype. We thus used RNA-Seq of WT neurons cultured in the absence or presence of WT/KO astrocytes to identify common and divergent molecular pathways affected by astrocytic secreted factors. The co-culture condition regardless of *Mecp2* expression promotes the expression of several genes involved in neuronal maturation, such as cell development, cell proliferation, extracellular matrix organization, signaling pathways and metabolic processes involved in energy supply. Concerning divergent pathways, we confirmed that *Mecp2* loss in astrocytes strongly affects dendritic spine development, pre- and post-synaptic assembly and synaptic transmission. Of relevance, we also collected very interesting indications about possible mechanisms underlying synaptic deficits. KO astrocytes, in fact, activate neuronal biological processes usually involved in responses to cytokines and other pro-inflammatory molecules; we also observed alterations in mitochondrial functions (oxidative phosphorylation, biosynthesis of pyrimidines, ROS production) that might represent a consequence of the presence of cytotoxic molecules (*Culmsee et al., 2019*). In possible good accordance, we have also described an altered sphingolipid metabolism in neurons and an imbalanced Cer/S1P rheostat of astrocytes in co-cultures, which might be indicative of neuroinflammation (*Deigner et al., 2007;de Wit et al., 2019; Maceyka and Spiegel, 2014*).

Our future studies will focus on identifying the molecular factors involved in the observed phenotypes, initially focusing on the possibility that *Mecp2* deficient astrocytes secrete excessive pro-inflammatory molecules or proteins associated with

synapse elimination. It is well known that neuroinflammation notably affects synaptic organization and function in the developing brain (*Mottahedin et al., 2017*) and therapeutic drugs aimed at treating systemic inflammation have already been investigated in clinical trials for a variety of neurological disorders (*Jiang et al., 2019; Radtke et al., 2017; Hampel et al., 2020*). If the presence of an inflammatory state triggered by astrocytes will be confirmed, new therapeutic targets and strategies could be proposed also for RTT.

Appendix

Appendix I

Gene name	Gene description	log2foldchange	p-value	p-adjust
APOC1	apolipoprotein C-I	1.37875	0.00006	0.01371
CAR9	carbonic anhydrase 9	1.32937	0.00023	0.03088
GIPR	gastric inhibitory polypeptide receptor	1.29683	0.00000	0.00129
KIF19A	kinesin family member 19A	1.27397	0.00000	0.00071
GM44907	predicted gene 44907	1.25427	0.00027	0.03450
GM27000	predicted gene, 27000	1.23335	0.00000	0.00105
RGS11	regulator of G-protein signaling 11	1.23281	0.00000	0.00000
MROH3	maestro heat-like repeat family member 3	1.19620	0.00098	0.06151
GM49405	predicted gene, 49405	1.17613	0.00001	0.00266
NEU4	sialidase 4	1.16284	0.00000	0.00044
LEFTY2	left-right determination factor 2	1.16117	0.00085	0.05700
C4A	complement component 4A (Rodgers blood group)	1.15824	0.00018	0.02797
SRPK3	serine/arginine-rich protein specific kinase 3	1.13546	0.00046	0.04336
LAT2	linker for activation of T cells family, member 2	1.12562	0.00045	0.04336
GM30122	predicted gene, 30122	1.10490	0.00203	0.09133
SLC16A11	solute carrier family 16 (monocarboxylic acid transporters), member 11	1.07371	0.00054	0.04642
ZFP967	zinc finger protein 967	1.06925	0.00001	0.00498
GM12778	predicted gene 12778	1.05132	0.00097	0.06151
FAM205A3	family with sequence similarity 205, member A3	1.04878	0.00037	0.04110
GM7507	predicted gene 7507	1.04853	0.00199	0.09086
GM7285	predicted gene 7285	1.04141	0.00161	0.08155
SDSL	serine dehydratase-like	1.03181	0.00007	0.01600
ABHD14B	abhydrolase domain containing 14b	1.00876	0.00000	0.00044
SLC2A4RG-PS	Slc2a4 regulator, pseudogene	1.00695	0.00001	0.00498
RPSA-PS1	ribosomal protein SA, pseudogene 1	0.94542	0.00028	0.03527
INSC	INSC spindle orientation adaptor protein	0.93980	0.00013	0.02287
GM20605	predicted gene 20605	0.91848	0.00017	0.02594
COL9A3	collagen, type IX, alpha 3	0.89326	0.00000	0.00034
GM49396	predicted gene, 49396	0.88607	0.00000	0.00052
MASP2	mannan-binding lectin serine peptidase 2	0.84288	0.00240	0.09993
GM50432	predicted gene, 50432	0.82135	0.00156	0.07973
GM14036	predicted gene 14036	0.81730	0.00042	0.04298
GM14150	predicted gene 14150	0.80711	0.00002	0.00585
SNHG20	small nucleolar RNA host gene 20	0.78232	0.00000	0.00019
GM11942	predicted gene 11942	0.77569	0.00038	0.04168
MEG3	maternally expressed 3	0.77361	0.00000	0.00079
MIA	melanoma inhibitory activity	0.76313	0.00209	0.09228
SNHG11	small nucleolar RNA host gene 11	0.74787	0.00000	0.00052
UBA7	ubiquitin-like modifier activating enzyme 7	0.74552	0.00219	0.09421
GM10086	predicted pseudogene 10086	0.74519	0.00136	0.07433
LIME1	Lck interacting transmembrane adaptor 1	0.74134	0.00000	0.00000
GM3294	predicted gene 3294	0.73959	0.00002	0.00731
AI480526	expressed sequence AI480526	0.73671	0.00002	0.00639
COL20A1	collagen, type XX, alpha 1	0.73651	0.00009	0.01831

GM8130	predicted gene 8130	0.72667	0.00071	0.05167
GM9797	predicted pseudogene 9797	0.72025	0.00000	0.00140
SSH3	slingshot protein phosphatase 3	0.71021	0.00011	0.02027
CCNL2	cyclin L2	0.70002	0.00000	0.00000
LPIN3	lipin 3	0.69868	0.00024	0.03116
LNCPPARA	long noncoding RNA near Ppara	0.69401	0.00020	0.02878
NMB	neuromedin B	0.67642	0.00112	0.06765
RPS15-PS2	ribosomal protein S15, pseudogene 2	0.67623	0.00139	0.07470
PLXNB3	plexin B3	0.67435	0.00014	0.02293
PPOX	protoporphyrinogen oxidase	0.66166	0.00000	0.00052
MIAT	myocardial infarction associated transcript (non-protein coding)	0.64442	0.00015	0.02401
COL16A1	collagen, type XVI, alpha 1	0.64269	0.00000	0.00058
NKX6-2	NK6 homeobox 2	0.64171	0.00012	0.02178
P3H3	prolyl 3-hydroxylase 3	0.63800	0.00000	0.00071
LRRC45	leucine rich repeat containing 45	0.62905	0.00000	0.00019
ARHGAP4	Rho GTPase activating protein 4	0.62876	0.00028	0.03527
PTGER1	prostaglandin E receptor 1 (subtype EP1)	0.61960	0.00042	0.04298
TMEM125	transmembrane protein 125	0.61498	0.00008	0.01776
S100A6	S100 calcium binding protein A6 (calcyclin)	0.61472	0.00113	0.06767
CCDC159	coiled-coil domain containing 159	0.61212	0.00001	0.00272
GM14325	predicted gene 14325	0.60408	0.00010	0.01917
CCDC84	coiled-coil domain containing 84	0.60347	0.00003	0.00850
RPS27L	ribosomal protein S27-like	0.60271	0.00047	0.04336
RPL26	ribosomal protein L26	0.59878	0.00035	0.04073
RPS19	ribosomal protein S19 [	0.59620	0.00038	0.04168
RASSF10	Ras association (RalGDS/AF-6) domain family (N-terminal) member 10	0.59608	0.00132	0.07391
RTEL1	regulator of telomere elongation helicase 1	0.59249	0.00002	0.00705
FIRRE	functional intergenic repeating RNA element	0.59134	0.00033	0.03974
CFAP100	cilia and flagella associated protein 100	0.58179	0.00129	0.07290
PLPP2	phospholipid phosphatase 2	0.58144	0.00148	0.07824
RPL10A-PS1	ribosomal protein L10A, pseudogene 1	0.57978	0.00019	0.02826
NKX2-2	NK2 homeobox 2	0.57431	0.00039	0.04184
FLNA	filamin, alpha	0.57353	0.00000	0.00034
GM42979	predicted gene 42979	0.57313	0.00017	0.02594
NPHP3	nephronophthisis 3 (adolescent)	0.57303	0.00117	0.06812
RPS18-PS5	ribosomal protein S18, pseudogene 5	0.56480	0.00015	0.02453
MIRG	miRNA containing gene	0.55171	0.00003	0.00850
TMEM256	transmembrane protein 256	0.55106	0.00056	0.04665
MAP4K2	mitogen-activated protein kinase kinase kinase kinase 2	0.55072	0.00007	0.01644
ENPP6	ectonucleotide pyrophosphatase/phosphodiesterase 6	0.54269	0.00143	0.07601
RGL3	ral guanine nucleotide dissociation stimulator-like 3	0.53973	0.00062	0.04840
ID3	inhibitor of DNA binding 3	0.53942	0.00003	0.00770
BC022960	cDNA sequence BC022960	0.53544	0.00059	0.04706
SEC14L5	SEC14-like lipid binding 5	0.53389	0.00055	0.04654
RPL34	ribosomal protein L34	0.52933	0.00058	0.04702
CLDN11	claudin 11	0.52091	0.00026	0.03388

ZFP692	zinc finger protein 692	0.51508	0.00003	0.00850
MOG	myelin oligodendrocyte glycoprotein	0.51375	0.00111	0.06753
B3GNT9	UDP-GlcNAc:betaGal beta-1,3-N-acetylglucosaminyltransferase 9	0.51353	0.00051	0.04514
WSB1	WD repeat and SOCS box-containing 1	0.51239	0.00022	0.03028
WTIP	WT1-interacting protein	0.51210	0.00001	0.00472
RGL2	ral guanine nucleotide dissociation stimulator-like 2	0.51091	0.00012	0.02187
THBS3	thrombospondin 3	0.51089	0.00002	0.00731
TCIRG1	T cell, immune regulator 1, ATPase, H+ transporting, lysosomal V0 protein A3	0.51081	0.00134	0.07433
RSRP1	arginine/serine rich protein 1	0.50973	0.00008	0.01786
VEGFA	vascular endothelial growth factor A	0.50757	0.00072	0.05167
CEROX1	cytoplasmic endogenous regulator of oxidative phosphorylation 1	0.50381	0.00009	0.01831
ZFP983	zinc finger protein 983	0.50374	0.00053	0.04569
DOCK6	dedicator of cytokinesis 6	0.50188	0.00053	0.04569
MIR124A-1HG	Mir124-1 host gene (non-protein coding)	0.50132	0.00013	0.02287
GM10175	predicted gene 10175	0.50050	0.00072	0.05167
ARHGEF1	Rho guanine nucleotide exchange factor (GEF) 1	0.50017	0.00000	0.00071
CNP	2',3'-cyclic nucleotide 3' phosphodiesterase	0.49956	0.00000	0.00126
ZFP57	zinc finger protein 57	0.49671	0.00000	0.00105
PLLP	plasma membrane proteolipid	0.49029	0.00020	0.02922
C78859	expressed sequence C78859	0.48897	0.00001	0.00359
RPL35A	ribosomal protein L35A	0.48809	0.00182	0.08708
MRPL33	mitochondrial ribosomal protein L33	0.48676	0.00019	0.02826
GM50107	predicted gene, 50107	0.48675	0.00180	0.08681
TAZ	tafazzin	0.48598	0.00000	0.00113
ADCK5	aarF domain containing kinase 5	0.48444	0.00037	0.04113
GM15501	predicted pseudogene 15501	0.47370	0.00212	0.09280
PARVB	parvin, beta	0.47343	0.00011	0.02106
SFI1	Sfi1 homolog, spindle assembly associated (yeast)	0.47267	0.00006	0.01468
RPS14	ribosomal protein S14	0.47162	0.00069	0.05167
PNP	purine-nucleoside phosphorylase	0.47056	0.00036	0.04096
RPL22L1	ribosomal protein L22 like 1	0.46900	0.00198	0.09086
ATG16L2	autophagy related 16-like 2 (S. cerevisiae)	0.46455	0.00003	0.00830
HDAC10	histone deacetylase 10	0.45988	0.00003	0.00850
CHUK	conserved helix-loop-helix ubiquitous kinase	0.45686	0.00061	0.04804
RPS18	ribosomal protein S18	0.45448	0.00049	0.04414
ATP5E	ATP synthase, H+ transporting, mitochondrial F1 complex, epsilon subunit	0.44893	0.00199	0.09086
DGAT1	diacylglycerol O-acyltransferase 1	0.44797	0.00003	0.00770
METTL17	methyltransferase like 17	0.44637	0.00001	0.00460
ADAMTS4	a disintegrin-like and metallopeptidase (reprolysin type) with thrombospondin type 1 motif, 4	0.44480	0.00033	0.03940
GALK1	galactokinase 1	0.44426	0.00135	0.07433
TMEM25	transmembrane protein 25	0.44289	0.00026	0.03394
PAMR1	peptidase domain containing associated with muscle regeneration 1	0.43244	0.00152	0.07844
MIIP	migration and invasion inhibitory protein	0.43241	0.00019	0.02826

RPS21	ribosomal protein S21	0.43146	0.00219	0.09421
GM49759	predicted gene, 49759	0.41955	0.00041	0.04259
GM3764	predicted gene 3764	0.41856	0.00000	0.00071
TSPAN15	tetraspanin 15	0.41709	0.00056	0.04665
DENND6B	DENN/MADD domain containing 6B	0.41380	0.00000	0.00055
SDHAF4	succinate dehydrogenase complex assembly factor 4	0.41329	0.00032	0.03897
CLASRP	CLK4-associating serine/arginine rich protein	0.40962	0.00001	0.00234
WDR90	WD repeat domain 90	0.40305	0.00046	0.04336
RPL34-PS1	ribosomal protein L34, pseudogene 1	0.40200	0.00201	0.09086
BCAS1	breast carcinoma amplified sequence 1	0.40047	0.00189	0.08911
S100B	S100 protein, beta polypeptide, neural	0.39767	0.00046	0.04336
FAM162A	family with sequence similarity 162, member A	0.39755	0.00180	0.08681
APBB3	amyloid beta (A4) precursor protein-binding, family B, member 3	0.39753	0.00051	0.04492
ZFP276	zinc finger protein (C2H2 type) 276	0.39723	0.00001	0.00248
FAM193B	family with sequence similarity 193, member B	0.39006	0.00000	0.00000
GAL3ST1	galactose-3-O-sulfotransferase 1	0.38943	0.00050	0.04492
PIGYL	phosphatidylinositol glycan anchor biosynthesis, class Y-like	0.38738	0.00135	0.07433
NME3	NME/NM23 nucleoside diphosphate kinase 3	0.38586	0.00006	0.01479
NME2	NME/NM23 nucleoside diphosphate kinase 2	0.38556	0.00072	0.05167
TRANK1	tetratricopeptide repeat and ankyrin repeat containing 1	0.38488	0.00035	0.04073
MAN2C1	mannosidase, alpha, class 2C, member 1	0.38147	0.00006	0.01414
PLEKHN1	pleckstrin homology domain containing, family N member 1	0.37976	0.00000	0.00118
ACAA1A	acetyl-Coenzyme A acyltransferase 1A	0.37960	0.00037	0.04110
GPT	glutamic pyruvic transaminase, soluble	0.37704	0.00206	0.09167
SMIM20	small integral membrane protein 20	0.37547	0.00130	0.07290
SNAPC4	small nuclear RNA activating complex, polypeptide 4	0.37486	0.00000	0.00086
USP35	ubiquitin specific peptidase 35	0.37474	0.00069	0.05158
DBNDD2	dysbindin (dystrobrevin binding protein 1) domain containing 2	0.37062	0.00029	0.03565
CLCN2	chloride channel, voltage-sensitive 2	0.36994	0.00064	0.04971
RPL10-PS3	ribosomal protein L10, pseudogene 3	0.36767	0.00215	0.09339
SZT2	SZT2 subunit of KICSTOR complex	0.36755	0.00000	0.00127
MAG	myelin-associated glycoprotein	0.36419	0.00211	0.09280
ZNRD2	zinc ribbon domain containing 2	0.36244	0.00085	0.05700
TNIP2	TNFAIP3 interacting protein 2	0.36083	0.00045	0.04336
RAD9B	RAD9 checkpoint clamp component B	0.35705	0.00119	0.06848
ADAMTS20	a disintegrin-like and metallopeptidase (reprolysin type) with thrombospondin type 1 motif, 20	0.35587	0.00220	0.09421
OGT	O-linked N-acetylglucosamine (GlcNAc) transferase (UDP-N-acetylglucosamine:polypeptide-N-acetylglucosaminyl transferase)	0.35526	0.00099	0.06151
HDAC7	histone deacetylase 7	0.35488	0.00121	0.06900
FRMD8	FERM domain containing 8	0.35385	0.00020	0.02872
HOPX	HOP homeobox	0.35322	0.00087	0.05744
TSPAN17	tetraspanin 17	0.35135	0.00053	0.04569
DYNLT1C	dynein light chain Tctex-type 1C	0.34997	0.00002	0.00604
KANK3	KN motif and ankyrin repeat domains 3	0.34994	0.00201	0.09086
ERMARD	ER membrane associated RNA degradation	0.34822	0.00116	0.06812

HEMK1	HemK methyltransferase family member 1	0.34814	0.00170	0.08414
ADAMTS10	a disintegrin-like and metallopeptidase (reprolysin type) with thrombospondin type 1 motif, 10	0.34608	0.00164	0.08257
NENF	neuron derived neurotrophic factor	0.34564	0.00081	0.05604
NEIL1	nei endonuclease VIII-like 1 (E. coli)	0.34495	0.00146	0.07722
CRYM	crystallin, mu	0.34405	0.00078	0.05443
ABCC5	ATP-binding cassette, sub-family C (CFTR/MRP), member 5	0.34256	0.00139	0.07470
HIGD1A	HIG1 domain family, member 1A	0.34238	0.00045	0.04336
SNHG17	small nucleolar RNA host gene 17	0.34167	0.00056	0.04665
ILVBL	ilvB (bacterial acetolactate synthase)-like	0.34097	0.00074	0.05236
NUP85	nucleoporin 85	0.33975	0.00004	0.00984
RNF112	ring finger protein 112	0.33828	0.00115	0.06812
ANKS3	ankyrin repeat and sterile alpha motif domain containing 3	0.33619	0.00014	0.02287
TCEA2	transcription elongation factor A (SII), 2	0.33431	0.00057	0.04684
UTP20	UTP20 small subunit processome component	0.33219	0.00077	0.05437
GPR17	G protein-coupled receptor 17	0.33159	0.00229	0.09696
E4F1	E4F transcription factor 1	0.32967	0.00036	0.04096
CTPS2	cytidine 5'-triphosphate synthase 2	0.32959	0.00095	0.06138
DMPK	dystrophia myotonica-protein kinase	0.32915	0.00199	0.09086
GTF2H4	general transcription factor II H, polypeptide 4	0.32703	0.00078	0.05443
NLE1	notchless homolog 1	0.32495	0.00160	0.08133
PHKA2	phosphorylase kinase alpha 2	0.32303	0.00068	0.05146
TIA1	cytotoxic granule-associated RNA binding protein 1	0.32095	0.00210	0.09228
NSUN5	NOL1/NOP2/Sun domain family, member 5	0.31903	0.00144	0.07646
MRPS14	mitochondrial ribosomal protein S14 [	0.31570	0.00171	0.08437
DALRD3	DALR anticodon binding domain containing 3	0.31359	0.00057	0.04702
CALCA	calcitonin/calcitonin-related polypeptide, alpha	0.31358	0.00173	0.08452
TMEM208	transmembrane protein 208	0.31177	0.00201	0.09086
PTPMT1	protein tyrosine phosphatase, mitochondrial 1	0.31082	0.00156	0.07979
FBXL6	F-box and leucine-rich repeat protein 6	0.30870	0.00014	0.02287
MVB12A	multivesicular body subunit 12A	0.30844	0.00185	0.08762
FAM173A	family with sequence similarity 173, member A	0.30742	0.00114	0.06767
LGI3	leucine-rich repeat LGI family, member 3	0.30668	0.00206	0.09165
TMEM205	transmembrane protein 205	0.30562	0.00201	0.09086
RNPEPL1	arginyl aminopeptidase (aminopeptidase B)-like 1	0.30251	0.00073	0.05167
PXDN	peroxidasin	0.30161	0.00088	0.05755
PFAS	phosphoribosylformylglycinamidine synthase (FGAR amidotransferase)	0.29930	0.00228	0.09640
SCRIB	scribbled planar cell polarity	0.29526	0.00036	0.04096
SAT1	spermidine/spermine N1-acetyl transferase 1	0.29302	0.00181	0.08681
HPS5	HPS5, biogenesis of lysosomal organelles complex 2 subunit 2	0.28731	0.00085	0.05700
TMEM181B-PS	transmembrane protein 181B, pseudogene	0.28728	0.00045	0.04336
PDCD10	programmed cell death 10	0.28576	0.00007	0.01544
TMEM80	transmembrane protein 80	0.28436	0.00067	0.05091
HARS2	histidyl-tRNA synthetase 2	0.27311	0.00029	0.03565
HOOK2	hook microtubule tethering protein 2	0.26891	0.00196	0.09086
DVL1	dishevelled segment polarity protein 1	0.26876	0.00101	0.06236
TRIT1	tRNA isopentenyltransferase 1	0.25898	0.00087	0.05755

ANKZF1	ankyrin repeat and zinc finger domain containing 1	0.25863	0.00183	0.08708
CHKB	choline kinase beta	0.25806	0.00019	0.02826
COQ2	coenzyme Q2 4-hydroxybenzoate polyprenyltransferase [	0.25550	0.00041	0.04278
LYSMD4	LysM, putative peptidoglycan-binding, domain containing 4	0.25460	0.00014	0.02348
PPP1R12C	protein phosphatase 1, regulatory subunit 12C	0.25160	0.00040	0.04259
ZGPAT	zinc finger, CCCH-type with G patch domain [	0.25015	0.00049	0.04414
PRPF40B	pre-mRNA processing factor 40B	0.24556	0.00040	0.04259
SEMA4D	sema domain, immunoglobulin domain (Ig), transmembrane domain (TM) and short cytoplasmic domain, (semaphorin) 4D	0.23793	0.00051	0.04503
ATG16L1	autophagy related 16-like 1 (S. cerevisiae)	0.23745	0.00011	0.02027
DTYMK	deoxythymidylate kinase	0.23429	0.00215	0.09341
JAM3	junction adhesion molecule 3	0.23131	0.00023	0.03116
CARHSP1	calcium regulated heat stable protein 1	0.22225	0.00164	0.08262
ZFYVE27	zinc finger, FYVE domain containing 27	0.22140	0.00231	0.09732
DDX17	DEAD (Asp-Glu-Ala-Asp) box polypeptide 17	0.21581	0.00137	0.07433
ZKSCAN3	zinc finger with KRAB and SCAN domains 3	0.21268	0.00170	0.08410
RFT1	RFT1 homolog	0.20808	0.00213	0.09288
MAT2A	methionine adenosyltransferase II, alpha	0.20805	0.00059	0.04706
PPP1R16B	protein phosphatase 1, regulatory subunit 16B [S	0.19234	0.00135	0.07433
MARCHF8	membrane associated ring-CH-type finger 8	0.18270	0.00010	0.01930
AGRN	agrin	0.17474	0.00150	0.07844
NFX1	nuclear transcription factor, X-box binding 1	0.13717	0.00130	0.07290
GM28037	predicted gene, 28037	-0.00181	0.00000	0.00000
LYVE1	lymphatic vessel endothelial hyaluronan receptor 1	-0.02477	0.00042	0.04298
UBQLN1	ubiquilin 1	-0.13058	0.00068	0.05158
ABI1	abl-interactor 1	-0.13360	0.00198	0.09086
PPP2R5C	protein phosphatase 2, regulatory subunit B', gamma	-0.14265	0.00116	0.06812
HSPH1	heat shock 105kDa/110kDa protein 1 [Source:MGI Symbol;Acc:MGI:105053]	-0.15118	0.00136	0.07433
PATL1	protein associated with topoisomerase II homolog 1 (yeast)	-0.15681	0.00115	0.06812
CLASP1	CLIP associating protein 1	-0.15970	0.00225	0.09592
SC5D	sterol-C5-desaturase	-0.17298	0.00194	0.09081
MAF	avian musculoaponeurotic fibrosarcoma oncogene homolog	-0.17351	0.00179	0.08681
CDH2	cadherin 2	-0.17374	0.00120	0.06865
B4GALT6	UDP-Gal:betaGlcNAc beta 1,4-galactosyltransferase, polypeptide 6	-0.17816	0.00097	0.06151
CPE	carboxypeptidase E [	-0.18088	0.00011	0.02027
NOCT	nocturnin [	-0.18142	0.00110	0.06742
PCYT1B	phosphate cytidylyltransferase 1, choline, beta isoform	-0.18180	0.00088	0.05786
GNAZ	guanine nucleotide binding protein, alpha z subunit	-0.18222	0.00113	0.06767
EIF4E2	eukaryotic translation initiation factor 4E member 2	-0.18246	0.00213	0.09288
STX7	syntaxin 7	-0.18418	0.00047	0.04336
SYT1	synaptotagmin I	-0.18449	0.00049	0.04414
TAOK3	TAO kinase 3	-0.19225	0.00189	0.08911
NPTN	neuroplastin	-0.19336	0.00009	0.01831
SPRED2	sprouty-related EVH1 domain containing 2	-0.19462	0.00208	0.09224
PITPNA	phosphatidylinositol transfer protein, alpha	-0.19818	0.00098	0.06151
ADGRL2	adhesion G protein-coupled receptor L2	-0.19925	0.00169	0.08410
CBLL1	Casitas B-lineage lymphoma-like 1 [	-0.19952	0.00152	0.07844

MMACHC	methylmalonic aciduria cblC type, with homocystinuria	-0.19978	0.00220	0.09421
SHISA9	shisa family member 9 [	-0.20055	0.00100	0.06227
BCL11A	B cell CLL/lymphoma 11A	-0.20282	0.00113	0.06767
RBFOX3	RNA binding protein, fox-1 homolog (C. elegans) 3	-0.20496	0.00227	0.09633
ARXES1	adipocyte-related X-chromosome expressed sequence 1	-0.20506	0.00097	0.06151
EIF4G3	eukaryotic translation initiation factor 4 gamma, 3	-0.20537	0.00040	0.04259
COBL	cordon-bleu WH2 repeat	-0.20639	0.00136	0.07433
CALM2	calmodulin 2	-0.20728	0.00157	0.08003
PABPC1	poly(A) binding protein, cytoplasmic 1	-0.20760	0.00058	0.04702
PTPRA	protein tyrosine phosphatase, receptor type, A	-0.20872	0.00059	0.04706
ATXN7L1	ataxin 7-like 1	-0.20931	0.00235	0.09815
PAXIP1	PAX interacting (with transcription-activation domain) protein 1	-0.21197	0.00049	0.04414
ATP1B1	ATPase, Na+/K+ transporting, beta 1 polypeptide	-0.21222	0.00010	0.01960
GRID1	glutamate receptor, ionotropic, delta 1	-0.21240	0.00072	0.05167
ZHX2	zinc fingers and homeoboxes 2	-0.21364	0.00140	0.07470
GRID2	glutamate receptor, ionotropic, delta 2	-0.21490	0.00155	0.07961
FOXG1	forkhead box G1	-0.21653	0.00152	0.07844
UBAP2L	ubiquitin-associated protein 2-like	-0.21829	0.00032	0.03929
STX6	syntaxin 6	-0.22075	0.00221	0.09443
GPR137B	G protein-coupled receptor 137B	-0.22273	0.00205	0.09141
ELMOD1	ELMO/CED-12 domain containing 1	-0.22386	0.00099	0.06151
MAMLD1	mastermind-like domain containing 1	-0.22503	0.00196	0.09086
YWHAZ	tyrosine 3-monooxygenase/tryptophan 5-monooxygenase activation protein, zeta polypeptide	-0.22544	0.00005	0.01142
HEATR5B	HEAT repeat containing 5B	-0.22610	0.00044	0.04336
ZFP362	zinc finger protein 362	-0.22686	0.00056	0.04665
ATP6V1C1	ATPase, H+ transporting, lysosomal V1 subunit C1	-0.22701	0.00137	0.07433
GATAD1	GATA zinc finger domain containing 1	-0.22817	0.00062	0.04874
ARL8A	ADP-ribosylation factor-like 8A	-0.22842	0.00066	0.05079
SRR	serine racemase	-0.22930	0.00013	0.02237
MLLT11	myeloid/lymphoid or mixed-lineage leukemia; translocated to, 11	-0.22942	0.00105	0.06440
CNOT4	CCR4-NOT transcription complex, subunit 4	-0.23057	0.00234	0.09806
ATP6V1G2	ATPase, H+ transporting, lysosomal V1 subunit G2	-0.23113	0.00071	0.05167
LHX2	LIM homeobox protein 2	-0.23311	0.00021	0.02966
ITSN1	intersectin 1 (SH3 domain protein 1A)	-0.23499	0.00235	0.09815
UBE2D3	ubiquitin-conjugating enzyme E2D 3	-0.23544	0.00071	0.05167
ZBTB45	zinc finger and BTB domain containing 45 [	-0.23591	0.00181	0.08681
WAC	WW domain containing adaptor with coiled-coil	-0.23693	0.00055	0.04665
TOX	thymocyte selection-associated high mobility group box	-0.23761	0.00139	0.07470
GABBR2	gamma-aminobutyric acid (GABA) B receptor, 2	-0.23849	0.00069	0.05167
VSTM2A	V-set and transmembrane domain containing 2A	-0.23891	0.00047	0.04336
RNF180	ring finger protein 180	-0.23892	0.00004	0.01001
RBFOX1	RNA binding protein, fox-1 homolog (C. elegans) 1	-0.23897	0.00047	0.04336
GNAO1	guanine nucleotide binding protein, alpha O	-0.23941	0.00014	0.02287
CXXC4	CXXC finger 4	-0.24195	0.00169	0.08410
UGCG	UDP-glucose ceramide glucosyltransferase	-0.24229	0.00176	0.08587
RAB8A	RAB8A, member RAS oncogene family	-0.24317	0.00166	0.08312

PBX3	pre B cell leukemia homeobox 3	-0.24573	0.00150	0.07844
PMEPA1	prostate transmembrane protein, androgen induced 1	-0.24811	0.00117	0.06812
MEIS2	Meis homeobox 2	-0.25173	0.00099	0.06151
PRRT2	proline-rich transmembrane protein 2	-0.25283	0.00118	0.06812
CADM1	cell adhesion molecule 1	-0.25420	0.00120	0.06858
MTSS1	MTSS I-BAR domain containing 1	-0.25678	0.00046	0.04336
CAMTA1	calmodulin binding transcription activator 1	-0.25750	0.00183	0.08720
SMARCA2	SWI/SNF related, matrix associated, actin dependent regulator of chromatin, subfamily a, member 2	-0.25810	0.00172	0.08437
MBLAC2	metallo-beta-lactamase domain containing 2	-0.25875	0.00098	0.06151
AFF3	AF4/FMR2 family, member 3	-0.25989	0.00201	0.09086
SOWAHA	sosondowah ankyrin repeat domain family member A	-0.26008	0.00055	0.04654
CCDC127	coiled-coil domain containing 127	-0.26234	0.00022	0.03028
ROBO1	roundabout guidance receptor 1	-0.26318	0.00152	0.07844
RAB11A	RAB11A, member RAS oncogene family	-0.26417	0.00030	0.03720
YWHAE	tyrosine 3-monooxygenase/tryptophan 5-monooxygenase activation protein, epsilon polypeptide	-0.26444	0.00001	0.00361
GPR85	G protein-coupled receptor 85	-0.26647	0.00027	0.03450
MAGI2	membrane associated guanylate kinase, WW and PDZ domain containing 2	-0.26927	0.00151	0.07844
CELF5	CUGBP, Elav-like family member 5	-0.27011	0.00117	0.06812
GTDC1	glycosyltransferase-like domain containing 1	-0.27022	0.00038	0.04168
CACNG3	calcium channel, voltage-dependent, gamma subunit 3	-0.27077	0.00086	0.05714
RBM11	RNA binding motif protein 11	-0.27954	0.00220	0.09421
SHTN1	shootin 1	-0.28152	0.00003	0.00850
LINGO2	leucine rich repeat and Ig domain containing 2	-0.28266	0.00059	0.04706
BTBD1	BTB (POZ) domain containing 1	-0.29000	0.00005	0.01191
PCBP3	poly(rC) binding protein 3	-0.29071	0.00137	0.07433
POLR1A	polymerase (RNA) I polypeptide A	-0.29221	0.00035	0.04079
AFAP1	actin filament associated protein 1	-0.29945	0.00082	0.05661
HNMT	histamine N-methyltransferase	-0.30009	0.00071	0.05167
SEPTIN3	septin 3	-0.30050	0.00005	0.01164
GPC4	glypican 4	-0.30292	0.00191	0.08943
GM46620	predicted gene, 46620	-0.30536	0.00035	0.04073
NCOR1	nuclear receptor co-repressor 1	-0.30568	0.00166	0.08312
BRD4	bromodomain containing 4	-0.30847	0.00125	0.07108
SSBP3	single-stranded DNA binding protein 3	-0.30926	0.00027	0.03493
LZIC	leucine zipper and CTNNBIP1 domain containing	-0.31265	0.00085	0.05700
LRRTM3	leucine rich repeat transmembrane neuronal 3	-0.31438	0.00000	0.00103
SEZ6	seizure related gene 6	-0.31732	0.00041	0.04278
RIMKLB	ribosomal modification protein rimK-like family member B	-0.32085	0.00000	0.00127
CDC42EP3	CDC42 effector protein (Rho GTPase binding) 3	-0.32579	0.00014	0.02324
RBM15B	RNA binding motif protein 15B	-0.32861	0.00008	0.01776
INPP1	inositol polyphosphate-1-phosphatase	-0.33347	0.00000	0.00132
MGAT5B	mannoside acetylglucosaminyltransferase 5, isoenzyme B	-0.33378	0.00093	0.06063
GOSR1	golgi SNAP receptor complex member 1	-0.34337	0.00003	0.00857
CAPZA2	capping protein (actin filament) muscle Z-line, alpha 2	-0.34366	0.00110	0.06742
RBM12	RNA binding motif protein 12	-0.34748	0.00084	0.05700
CHIC2	cysteine-rich hydrophobic domain 2	-0.34767	0.00118	0.06825

GPC3	glypican 3	-0.34776	0.00150	0.07844
GNG2	guanine nucleotide binding protein (G protein), gamma 2	-0.34886	0.00000	0.00044
NPY1R	neuropeptide Y receptor Y1	-0.35081	0.00036	0.04096
SP9	trans-acting transcription factor 9	-0.35361	0.00079	0.05494
NETO1	neuropilin (NRP) and tolloid (TLL)-like 1	-0.35453	0.00085	0.05700
SOBP	sine oculis binding protein	-0.35455	0.00004	0.00916
KLF5	Kruppel-like factor 5	-0.36030	0.00042	0.04298
TAF9	TATA-box binding protein associated factor 9	-0.36545	0.00023	0.03113
STT3A	STT3, subunit of the oligosaccharyltransferase complex, homolog A (S. cerevisiae)	-0.37234	0.00009	0.01831
PCDHB8	protocadherin beta 8	-0.37319	0.00055	0.04665
MT-ND5	mitochondrially encoded NADH dehydrogenase 5	-0.37448	0.00232	0.09747
MAPK10	mitogen-activated protein kinase 10	-0.37655	0.00000	0.00126
MKRN2	makorin, ring finger protein, 2	-0.38561	0.00021	0.03001
MT-ND2	mitochondrially encoded NADH dehydrogenase 2	-0.38701	0.00204	0.09133
KDR	kinase insert domain protein receptor	-0.38803	0.00072	0.05167
RAD23B	RAD23 homolog B, nucleotide excision repair protein	-0.39615	0.00000	0.00074
ERI1	exoribonuclease 1	-0.40162	0.00013	0.02237
MYL12B	myosin, light chain 12B, regulatory	-0.41237	0.00044	0.04336
EWSR1	Ewing sarcoma breakpoint region 1	-0.41272	0.00017	0.02594
KIF23	kinesin family member 23	-0.41374	0.00198	0.09086
MT-ND1	mitochondrially encoded NADH dehydrogenase 1	-0.41543	0.00204	0.09133
GM8325	predicted pseudogene 8325	-0.42542	0.00058	0.04702
GM12371	predicted gene 12371	-0.42642	0.00072	0.05167
FMO1	flavin containing monooxygenase 1	-0.42668	0.00079	0.05503
GM8355	predicted pseudogene 8355	-0.43666	0.00045	0.04336
GM5436	predicted pseudogene 5436	-0.43945	0.00023	0.03116
CCDC92	coiled-coil domain containing 92	-0.44366	0.00001	0.00472
SNRPD3	small nuclear ribonucleoprotein D3	-0.45332	0.00021	0.03001
TTC7	tetratricopeptide repeat domain 7	-0.48055	0.00066	0.05058
GLYCAM1	glycosylation dependent cell adhesion molecule 1	-0.48653	0.00095	0.06133
FGF5	fibroblast growth factor 5	-0.62106	0.00111	0.06753
CFAP77	cilia and flagella associated protein 77	-0.66939	0.00085	0.05700
ZIC1	zinc finger protein of the cerebellum 1	-0.76969	0.00089	0.05834
TMEM116	transmembrane protein 116	-0.77681	0.00046	0.04336
IMPA2	inositol (myo)-1(or 4)-monophosphatase 2	-0.94197	0.00003	0.00850
MYH6	myosin, heavy polypeptide 6, cardiac muscle, alpha	-1.15329	0.00046	0.04336

Table 7.1. List of the DEGs (p.adjust <0.1) of KO *versus* WT, ranked by their log2 fold change.

Appendix II

ID	Description	p-value	p.adjust	q-value
GO:0015672	monovalent inorganic cation transport	0.00001	0.00026	0.00019
GO:0051968	positive regulation of synaptic transmission, glutamatergic	0.00001	0.00028	0.00020
GO:0007156	homophilic cell adhesion via plasma membrane adhesion molecules	0.00001	0.00031	0.00022
GO:0098657	import into cell	0.00001	0.00036	0.00026
GO:0016125	sterol metabolic process	0.00004	0.00086	0.00061
GO:0022898	regulation of transmembrane transporter activity	0.00004	0.00096	0.00068
GO:0031643	positive regulation of myelination	0.00004	0.00096	0.00068
GO:0032412	regulation of ion transmembrane transporter activity	0.00004	0.00098	0.00070
GO:0099072	regulation of postsynaptic membrane neurotransmitter receptor levels	0.00004	0.00100	0.00071
GO:1902414	protein localization to cell junction	0.00004	0.00101	0.00072
GO:0071805	potassium ion transmembrane transport	0.00004	0.00104	0.00074
GO:0051966	regulation of synaptic transmission, glutamatergic	0.00005	0.00118	0.00084
GO:0006813	potassium ion transport	0.00005	0.00118	0.00084
GO:0015874	norepinephrine transport	0.00010	0.00197	0.00141
GO:1903825	organic acid transmembrane transport	0.00010	0.00199	0.00142
GO:0099565	chemical synaptic transmission, postsynaptic	0.00011	0.00209	0.00149
GO:0032409	regulation of transporter activity	0.00012	0.00219	0.00156
GO:0006631	fatty acid metabolic process	0.00014	0.00250	0.00179
GO:0046328	regulation of JNK cascade	0.00014	0.00253	0.00181
GO:0008202	steroid metabolic process	0.00014	0.00253	0.00181
GO:0072329	monocarboxylic acid catabolic process	0.00015	0.00262	0.00187
GO:0099633	protein localization to postsynaptic specialization membrane	0.00016	0.00269	0.00192
GO:0099645	neurotransmitter receptor localization to postsynaptic specialization membrane	0.00016	0.00269	0.00192
GO:0009062	fatty acid catabolic process	0.00016	0.00273	0.00195
GO:1903977	positive regulation of glial cell migration	0.00017	0.00287	0.00205
GO:0016054	organic acid catabolic process	0.00018	0.00290	0.00207
GO:0046395	carboxylic acid catabolic process	0.00018	0.00290	0.00207
GO:0030258	lipid modification	0.00019	0.00307	0.00219
GO:1905039	carboxylic acid transmembrane transport	0.00020	0.00326	0.00233
GO:0034440	lipid oxidation	0.00022	0.00349	0.00250
GO:2001234	negative regulation of apoptotic signaling pathway	0.00026	0.00389	0.00278
GO:0002040	sprouting angiogenesis	0.00029	0.00431	0.00308
GO:0052548	regulation of endopeptidase activity	0.00032	0.00466	0.00333
GO:0070593	dendrite self-avoidance	0.00033	0.00469	0.00335
GO:0008306	associative learning	0.00033	0.00471	0.00336
GO:0090181	regulation of cholesterol metabolic process	0.00033	0.00471	0.00336
GO:0097120	receptor localization to synapse	0.00033	0.00472	0.00338
GO:0019395	fatty acid oxidation	0.00039	0.00531	0.00379
GO:0035418	protein localization to synapse	0.00039	0.00531	0.00379
GO:0006635	fatty acid beta-oxidation	0.00040	0.00537	0.00384
GO:0006865	amino acid transport	0.00040	0.00540	0.00386
GO:0007252	I-kappaB phosphorylation	0.00043	0.00559	0.00399
GO:0014061	regulation of norepinephrine secretion	0.00043	0.00559	0.00399
GO:0048243	norepinephrine secretion	0.00043	0.00559	0.00399

GO:0061179	negative regulation of insulin secretion involved in cellular response to glucose stimulus	0.00043	0.00559	0.00399
GO:1990928	response to amino acid starvation	0.00044	0.00571	0.00408
GO:0062237	protein localization to postsynapse	0.00047	0.00608	0.00435
GO:0035767	endothelial cell chemotaxis	0.00049	0.00620	0.00443
GO:0060074	synapse maturation	0.00049	0.00620	0.00443
GO:0002052	positive regulation of neuroblast proliferation	0.00050	0.00631	0.00451
GO:0051881	regulation of mitochondrial membrane potential	0.00050	0.00631	0.00451
GO:0016525	negative regulation of angiogenesis	0.00056	0.00682	0.00488
GO:0048010	vascular endothelial growth factor receptor signaling pathway	0.00057	0.00700	0.00500
GO:0051899	membrane depolarization	0.00060	0.00726	0.00519
GO:1901343	negative regulation of vasculature development	0.00063	0.00747	0.00534
GO:2000648	positive regulation of stem cell proliferation	0.00067	0.00789	0.00564
GO:0010574	regulation of vascular endothelial growth factor production	0.00069	0.00795	0.00569
GO:0043116	negative regulation of vascular permeability	0.00069	0.00795	0.00569
GO:0002064	epithelial cell development	0.00069	0.00801	0.00573
GO:0043271	negative regulation of ion transport	0.00070	0.00801	0.00573
GO:0002028	regulation of sodium ion transport	0.00070	0.00801	0.00573
GO:0072091	regulation of stem cell proliferation	0.00070	0.00801	0.00573
GO:0060079	excitatory postsynaptic potential	0.00071	0.00812	0.00581
GO:0046330	positive regulation of JNK cascade	0.00072	0.00812	0.00581
GO:0009065	glutamine family amino acid catabolic process	0.00073	0.00819	0.00585
GO:0070498	interleukin-1-mediated signaling pathway	0.00073	0.00819	0.00585
GO:1901163	regulation of trophoblast cell migration	0.00073	0.00819	0.00586
GO:0007215	glutamate receptor signaling pathway	0.00083	0.00899	0.00642
GO:0002718	regulation of cytokine production involved in immune response	0.00087	0.00924	0.00660
GO:0051048	negative regulation of secretion	0.00093	0.00975	0.00697
GO:2001028	positive regulation of endothelial cell chemotaxis	0.00096	0.00994	0.00710
GO:2000116	regulation of cysteine-type endopeptidase activity	0.00096	0.00999	0.00714
GO:0031668	cellular response to extracellular stimulus	0.00099	0.01023	0.00731
GO:0006869	lipid transport	0.00101	0.01039	0.00743
GO:0070507	regulation of microtubule cytoskeleton organization	0.00104	0.01066	0.00762
GO:0055064	chloride ion homeostasis	0.00106	0.01074	0.00768
GO:0006633	fatty acid biosynthetic process	0.00106	0.01077	0.00770
GO:0006706	steroid catabolic process	0.00107	0.01077	0.00770
GO:1902683	regulation of receptor localization to synapse	0.00107	0.01077	0.00770
GO:0060402	calcium ion transport into cytosol	0.00118	0.01169	0.00836
GO:0031532	actin cytoskeleton reorganization	0.00122	0.01204	0.00861
GO:0070588	calcium ion transmembrane transport	0.00123	0.01205	0.00862
GO:1903539	protein localization to postsynaptic membrane	0.00128	0.01243	0.00889
GO:0051057	positive regulation of small GTPase mediated signal transduction	0.00128	0.01243	0.00889
GO:0030497	fatty acid elongation	0.00129	0.01243	0.00889
GO:0033127	regulation of histone phosphorylation	0.00129	0.01243	0.00889
GO:0061450	trophoblast cell migration	0.00129	0.01243	0.00889
GO:0051057	positive regulation of small GTPase mediated signal transduction	0.00128	0.01243	0.00889
GO:0030497	fatty acid elongation	0.00129	0.01243	0.00889
GO:0033127	regulation of histone phosphorylation	0.00129	0.01243	0.00889
GO:0061450	trophoblast cell migration	0.00129	0.01243	0.00889

GO:0071711	basement membrane organization	0.00141	0.01340	0.00958
GO:0002367	cytokine production involved in immune response	0.00141	0.01340	0.00958
GO:0043281	regulation of cysteine-type endopeptidase activity involved in apoptotic process	0.00145	0.01367	0.00977
GO:0035272	exocrine system development	0.00148	0.01391	0.00995
GO:0090322	regulation of superoxide metabolic process	0.00149	0.01391	0.00995
GO:1902992	negative regulation of amyloid precursor protein catabolic process	0.00151	0.01407	0.01006
GO:0010575	positive regulation of vascular endothelial growth factor production	0.00152	0.01410	0.01008
GO:0052547	regulation of peptidase activity	0.00152	0.01410	0.01008
GO:0008625	extrinsic apoptotic signaling pathway via death domain receptors	0.00153	0.01415	0.01012
GO:0031102	neuron projection regeneration	0.00156	0.01427	0.01020
GO:2001026	regulation of endothelial cell chemotaxis	0.00157	0.01427	0.01020
GO:0034198	cellular response to amino acid starvation	0.00165	0.01480	0.01058
GO:0001767	establishment of lymphocyte polarity	0.00166	0.01480	0.01058
GO:0001768	establishment of T cell polarity	0.00166	0.01480	0.01058
GO:0030644	cellular chloride ion homeostasis	0.00166	0.01480	0.01058
GO:0033539	fatty acid beta-oxidation using acyl-CoA dehydrogenase	0.00166	0.01480	0.01058
GO:1902624	positive regulation of neutrophil migration	0.00170	0.01514	0.01082
GO:0000819	sister chromatid segregation	0.00172	0.01525	0.01090
GO:0043122	regulation of I-kappaB kinase/NF-kappaB signaling	0.00177	0.01561	0.01116
GO:0051955	regulation of amino acid transport	0.00184	0.01614	0.01154
GO:0140014	mitotic nuclear division	0.00187	0.01631	0.01166
GO:0015800	acidic amino acid transport	0.00189	0.01634	0.01168
GO:1903307	positive regulation of regulated secretory pathway	0.00189	0.01634	0.01168
GO:0090101	negative regulation of transmembrane receptor protein serine/threonine kinase signaling pathway	0.00191	0.01644	0.01176
GO:0043951	negative regulation of cAMP-mediated signaling	0.00192	0.01650	0.01180
GO:1902042	negative regulation of extrinsic apoptotic signaling pathway via death domain receptors	0.00192	0.01650	0.01180
GO:0015804	neutral amino acid transport	0.00193	0.01651	0.01180
GO:1902692	regulation of neuroblast proliferation	0.00193	0.01651	0.01180
GO:0006112	energy reserve metabolic process	0.00199	0.01698	0.01214
GO:0042176	regulation of protein catabolic process	0.00200	0.01702	0.01217
GO:0001780	neutrophil homeostasis	0.00212	0.01787	0.01277
GO:0072337	modified amino acid transport	0.00212	0.01787	0.01277
GO:0051764	actin crosslink formation	0.00214	0.01795	0.01283
GO:0009895	negative regulation of catabolic process	0.00216	0.01809	0.01293
GO:0034332	adherens junction organization	0.00221	0.01843	0.01317
GO:0034109	homotypic cell-cell adhesion	0.00222	0.01846	0.01320
GO:0034331	cell junction maintenance	0.00224	0.01858	0.01329
GO:0046579	positive regulation of Ras protein signal transduction	0.00226	0.01865	0.01333
GO:0048678	response to axon injury	0.00226	0.01865	0.01333
GO:0099601	regulation of neurotransmitter receptor activity	0.00226	0.01865	0.01333
GO:0046676	negative regulation of insulin secretion	0.00227	0.01865	0.01333
GO:0030856	regulation of epithelial cell differentiation	0.00228	0.01867	0.01334
GO:0045956	positive regulation of calcium ion-dependent exocytosis	0.00230	0.01867	0.01334
GO:2001257	regulation of cation channel activity	0.00230	0.01867	0.01334
GO:0009636	response to toxic substance	0.00232	0.01879	0.01343
GO:1903531	negative regulation of secretion by cell	0.00244	0.01953	0.01396

GO:0000070	mitotic sister chromatid segregation	0.00246	0.01965	0.01404
GO:0003254	regulation of membrane depolarization	0.00264	0.02061	0.01473
GO:0017158	regulation of calcium ion-dependent exocytosis	0.00264	0.02061	0.01473
GO:0043954	cellular component maintenance	0.00270	0.02101	0.01502
GO:0061035	regulation of cartilage development	0.00270	0.02101	0.01502
GO:0006814	sodium ion transport	0.00284	0.02185	0.01562
GO:0033004	negative regulation of mast cell activation	0.00293	0.02217	0.01585
GO:0098953	receptor diffusion trapping	0.00293	0.02217	0.01585
GO:0098970	postsynaptic neurotransmitter receptor diffusion trapping	0.00293	0.02217	0.01585
GO:0099628	neurotransmitter receptor diffusion trapping	0.00293	0.02217	0.01585
GO:0038034	signal transduction in absence of ligand	0.00298	0.02247	0.01606
GO:0097192	extrinsic apoptotic signaling pathway in absence of ligand	0.00298	0.02247	0.01606
GO:0060401	cytosolic calcium ion transport	0.00307	0.02313	0.01654
GO:0099590	neurotransmitter receptor internalization	0.00314	0.02351	0.01680
GO:0010657	muscle cell apoptotic process	0.00322	0.02395	0.01712
GO:1902622	regulation of neutrophil migration	0.00329	0.02440	0.01744
GO:0042177	negative regulation of protein catabolic process	0.00333	0.02446	0.01749
GO:0098693	regulation of synaptic vesicle cycle	0.00333	0.02446	0.01749
GO:0016322	neuron remodeling	0.00335	0.02446	0.01749
GO:0098696	regulation of neurotransmitter receptor localization to postsynaptic specialization membrane	0.00335	0.02446	0.01749
GO:1905564	positive regulation of vascular endothelial cell proliferation	0.00335	0.02446	0.01749
GO:2001241	positive regulation of extrinsic apoptotic signaling pathway in absence of ligand	0.00335	0.02446	0.01749
GO:0002673	regulation of acute inflammatory response	0.00337	0.02446	0.01749
GO:0032757	positive regulation of interleukin-8 production	0.00337	0.02446	0.01749
GO:0030002	cellular anion homeostasis	0.00338	0.02446	0.01749
GO:0030320	cellular monovalent inorganic anion homeostasis	0.00338	0.02446	0.01749
GO:0051930	regulation of sensory perception of pain	0.00339	0.02446	0.01749
GO:1901292	nucleoside phosphate catabolic process	0.00339	0.02446	0.01749
GO:0010660	regulation of muscle cell apoptotic process	0.00342	0.02468	0.01764
GO:0043266	regulation of potassium ion transport	0.00345	0.02482	0.01774
GO:0016079	synaptic vesicle exocytosis	0.00360	0.02576	0.01842
GO:0051983	regulation of chromosome segregation	0.00368	0.02617	0.01871
GO:0051953	negative regulation of amine transport	0.00373	0.02643	0.01889
GO:0090314	positive regulation of protein targeting to membrane	0.00389	0.02738	0.01957
GO:0042157	lipoprotein metabolic process	0.00404	0.02822	0.02017
GO:1900449	regulation of glutamate receptor signaling pathway	0.00409	0.02836	0.02027
GO:0071496	cellular response to external stimulus	0.00420	0.02892	0.02067
GO:2000300	regulation of synaptic vesicle exocytosis	0.00420	0.02892	0.02067
GO:0050796	regulation of insulin secretion	0.00424	0.02917	0.02085
GO:0008608	attachment of spindle microtubules to kinetochore	0.00439	0.02997	0.02142
GO:2001237	negative regulation of extrinsic apoptotic signaling pathway	0.00449	0.03048	0.02179
GO:0015698	inorganic anion transport	0.00449	0.03048	0.02179
GO:0032677	regulation of interleukin-8 production	0.00463	0.03128	0.02236
GO:0010469	regulation of signaling receptor activity	0.00472	0.03174	0.02269
GO:0031998	regulation of fatty acid beta-oxidation	0.00481	0.03182	0.02275
GO:0010744	positive regulation of macrophage derived foam cell differentiation	0.00481	0.03182	0.02275
GO:0032604	granulocyte macrophage colony-stimulating factor production	0.00481	0.03182	0.02275

GO:0032645	regulation of granulocyte macrophage colony-stimulating factor production	0.00481	0.03182	0.02275
GO:0042761	very long-chain fatty acid biosynthetic process	0.00481	0.03182	0.02275
GO:0070831	basement membrane assembly	0.00481	0.03182	0.02275
GO:1901201	regulation of extracellular matrix assembly	0.00481	0.03182	0.02275
GO:0098739	import across plasma membrane	0.00490	0.03225	0.02306
GO:0032768	regulation of monooxygenase activity	0.00491	0.03225	0.02306
GO:0033628	regulation of cell adhesion mediated by integrin	0.00491	0.03225	0.02306
GO:2000649	regulation of sodium ion transmembrane transporter activity	0.00498	0.03257	0.02328
GO:0007157	heterophilic cell-cell adhesion via plasma membrane cell adhesion molecules	0.00499	0.03257	0.02328
GO:1902041	regulation of extrinsic apoptotic signaling pathway via death domain receptors	0.00499	0.03257	0.02328
GO:0046488	phosphatidylinositol metabolic process	0.00501	0.03263	0.02332
GO:0051957	positive regulation of amino acid transport	0.00512	0.03326	0.02377
GO:0032637	interleukin-8 production	0.00521	0.03378	0.02415
GO:0006790	sulfur compound metabolic process	0.00527	0.03409	0.02437
GO:0097553	calcium ion transmembrane import into cytosol	0.00527	0.03409	0.02437
GO:0007052	mitotic spindle organization	0.00529	0.03418	0.02444
GO:1904029	regulation of cyclin-dependent protein kinase activity	0.00543	0.03491	0.02496
GO:1903409	reactive oxygen species biosynthetic process	0.00551	0.03520	0.02516
GO:0031338	regulation of vesicle fusion	0.00562	0.03569	0.02551
GO:0055083	monovalent inorganic anion homeostasis	0.00562	0.03569	0.02551
GO:0090090	negative regulation of canonical Wnt signaling pathway	0.00571	0.03612	0.02582
GO:0009266	response to temperature stimulus	0.00579	0.03657	0.02614
GO:0072523	purine-containing compound catabolic process	0.00592	0.03712	0.02654
GO:0007051	spindle organization	0.00606	0.03778	0.02701
GO:0030510	regulation of BMP signaling pathway	0.00626	0.03879	0.02773
GO:0048168	regulation of neuronal synaptic plasticity	0.00639	0.03947	0.02821
GO:0031667	response to nutrient levels	0.00646	0.03986	0.02849
GO:0010950	positive regulation of endopeptidase activity	0.00648	0.03993	0.02855
GO:0008299	isoprenoid biosynthetic process	0.00665	0.04007	0.02864
GO:0072574	hepatocyte proliferation	0.00665	0.04007	0.02864
GO:0072575	epithelial cell proliferation involved in liver morphogenesis	0.00665	0.04007	0.02864
GO:1901889	negative regulation of cell junction assembly	0.00665	0.04007	0.02864
GO:0035493	SNARE complex assembly	0.00666	0.04007	0.02864
GO:0042053	regulation of dopamine metabolic process	0.00666	0.04007	0.02864
GO:0090278	negative regulation of peptide hormone secretion	0.00668	0.04007	0.02864
GO:0099637	neurotransmitter receptor transport	0.00668	0.04007	0.02864
GO:0042542	response to hydrogen peroxide	0.00669	0.04007	0.02864
GO:0055092	sterol homeostasis	0.00670	0.04007	0.02864
GO:0015865	purine nucleotide transport	0.00672	0.04007	0.02864
GO:0015911	long-chain fatty acid import across plasma membrane	0.00672	0.04007	0.02864
GO:0021684	cerebellar granular layer formation	0.00672	0.04007	0.02864
GO:0021707	cerebellar granule cell differentiation	0.00672	0.04007	0.02864
GO:0032000	positive regulation of fatty acid beta-oxidation	0.00672	0.04007	0.02864
GO:0032836	glomerular basement membrane development	0.00672	0.04007	0.02864
GO:0051001	negative regulation of nitric-oxide synthase activity	0.00672	0.04007	0.02864
GO:0060907	positive regulation of macrophage cytokine production	0.00672	0.04007	0.02864
GO:0090129	positive regulation of synapse maturation	0.00672	0.04007	0.02864
GO:1901724	positive regulation of cell proliferation involved in kidney development	0.00672	0.04007	0.02864

GO:1990504	dense core granule exocytosis	0.00672	0.04007	0.02864
GO:2001269	positive regulation of cysteine-type endopeptidase activity involved in apoptotic signaling pathway	0.00672	0.04007	0.02864
GO:0031503	protein-containing complex localization	0.00686	0.04083	0.02919
GO:0043507	positive regulation of JUN kinase activity	0.00705	0.04179	0.02988
GO:0010837	regulation of keratinocyte proliferation	0.00711	0.04203	0.03005
GO:1901379	regulation of potassium ion transmembrane transport	0.00717	0.04232	0.03025
GO:1902883	negative regulation of response to oxidative stress	0.00718	0.04232	0.03025
GO:0010878	cholesterol storage	0.00726	0.04255	0.03042
GO:0033604	negative regulation of catecholamine secretion	0.00726	0.04255	0.03042
GO:1990000	amyloid fibril formation	0.00726	0.04255	0.03042
GO:0043620	regulation of DNA-templated transcription in response to stress	0.00734	0.04276	0.03056
GO:0097484	dendrite extension	0.00740	0.04295	0.03070
GO:0098926	postsynaptic signal transduction	0.00740	0.04295	0.03070
GO:0072171	mesonephric tubule morphogenesis	0.00745	0.04295	0.03070
GO:0002371	dendritic cell cytokine production	0.00745	0.04295	0.03070
GO:0035739	CD4-positive, alpha-beta T cell proliferation	0.00745	0.04295	0.03070
GO:0046642	negative regulation of alpha-beta T cell proliferation	0.00745	0.04295	0.03070
GO:1902001	fatty acid transmembrane transport	0.00745	0.04295	0.03070
GO:1905063	regulation of vascular associated smooth muscle cell differentiation	0.00745	0.04295	0.03070
GO:1901136	carbohydrate derivative catabolic process	0.00749	0.04312	0.03082
GO:0043506	regulation of JUN kinase activity	0.00764	0.04390	0.03138
GO:0006817	phosphate ion transport	0.00779	0.04457	0.03186
GO:0090023	positive regulation of neutrophil chemotaxis	0.00779	0.04457	0.03186
GO:0048144	fibroblast proliferation	0.00782	0.04468	0.03194
GO:2001235	positive regulation of apoptotic signaling pathway	0.00794	0.04528	0.03237
GO:0042158	lipoprotein biosynthetic process	0.00807	0.04585	0.03277
GO:0140029	exocytic process	0.00807	0.04585	0.03277
GO:1902882	regulation of response to oxidative stress	0.00807	0.04585	0.03277
GO:0018958	phenol-containing compound metabolic process	0.00812	0.04602	0.03290
GO:1904063	negative regulation of cation transmembrane transport	0.00820	0.04626	0.03307
GO:0007584	response to nutrient	0.00820	0.04626	0.03307
GO:0010812	negative regulation of cell-substrate adhesion	0.00820	0.04626	0.03307
GO:0030865	cortical cytoskeleton organization	0.00820	0.04626	0.03307
GO:0048011	neurotrophin TRK receptor signaling pathway	0.00850	0.04772	0.03411
GO:1902473	regulation of protein localization to synapse	0.00850	0.04772	0.03411
GO:0140115	export across plasma membrane	0.00853	0.04772	0.03411
GO:0061515	myeloid cell development	0.00878	0.04884	0.03491
GO:0002702	positive regulation of production of molecular mediator of immune response	0.00879	0.04884	0.03491
GO:1903202	negative regulation of oxidative stress-induced cell death	0.00880	0.04884	0.03491
GO:1904036	negative regulation of epithelial cell apoptotic process	0.00880	0.04884	0.03491
GO:0018105	peptidyl-serine phosphorylation	0.00880	0.04884	0.03491
GO:0045933	positive regulation of muscle contraction	0.00880	0.04884	0.03491
GO:0048169	regulation of long-term neuronal synaptic plasticity	0.00888	0.04916	0.03514
GO:0043616	keratinocyte proliferation	0.00897	0.04937	0.03529
GO:0010743	regulation of macrophage derived foam cell differentiation	0.00900	0.04937	0.03529
GO:0034405	response to fluid shear stress	0.00900	0.04937	0.03529
GO:0071276	cellular response to cadmium ion	0.00900	0.04937	0.03529

GO:0043551	regulation of phosphatidylinositol 3-kinase activity	0.00902	0.04942	0.03533
GO:0032006	regulation of TOR signaling	0.00913	0.04996	0.03571

Table 7.2. GO enrichment analysis for biological processes of WT *versus* CTRL ranked by q-value (q-value <0.2, p.adjust <0.1 and p-value cut-off <0.05) not present in KO *versus* CTRL.

Appendix III

ID	Description	p-value	p.adjust	q-value
GO:0009615	response to virus	0.00001	0.00017	0.00012
GO:0051258	protein polymerization	0.00001	0.00019	0.00013
GO:0032272	negative regulation of protein polymerization	0.00001	0.00019	0.00013
GO:0002224	toll-like receptor signaling pathway	0.00001	0.00022	0.00016
GO:0019221	cytokine-mediated signaling pathway	0.00001	0.00027	0.00019
GO:0032271	regulation of protein polymerization	0.00001	0.00034	0.00023
GO:0046324	regulation of glucose import	0.00002	0.00047	0.00033
GO:0001961	positive regulation of cytokine-mediated signaling pathway	0.00002	0.00053	0.00037
GO:0034350	regulation of glial cell apoptotic process	0.00002	0.00053	0.00037
GO:0051099	positive regulation of binding	0.00003	0.00062	0.00043
GO:0051607	defense response to virus	0.00003	0.00064	0.00044
GO:0050772	positive regulation of axonogenesis	0.00003	0.00064	0.00044
GO:0002833	positive regulation of response to biotic stimulus	0.00003	0.00072	0.00050
GO:0030041	actin filament polymerization	0.00005	0.00090	0.00063
GO:0002221	pattern recognition receptor signaling pathway	0.00006	0.00110	0.00076
GO:0034349	glial cell apoptotic process	0.00006	0.00113	0.00078
GO:0003002	regionalization	0.00006	0.00118	0.00082
GO:0001558	regulation of cell growth	0.00007	0.00118	0.00082
GO:0044262	cellular carbohydrate metabolic process	0.00007	0.00121	0.00084
GO:0060537	muscle tissue development	0.00007	0.00122	0.00085
GO:0032606	type I interferon production	0.00008	0.00140	0.00098
GO:0014706	striated muscle tissue development	0.00009	0.00158	0.00110
GO:0010827	regulation of glucose transmembrane transport	0.00013	0.00205	0.00143
GO:0030832	regulation of actin filament length	0.00014	0.00221	0.00154
GO:0042771	intrinsic apoptotic signaling pathway in response to DNA damage by p53 class mediator	0.00015	0.00228	0.00159
GO:0048638	regulation of developmental growth	0.00017	0.00251	0.00174
GO:0043113	receptor clustering	0.00017	0.00255	0.00177
GO:0043367	CD4-positive, alpha-beta T cell differentiation	0.00017	0.00256	0.00178
GO:0032091	negative regulation of protein binding	0.00020	0.00288	0.00200
GO:0051090	regulation of DNA-binding transcription factor activity	0.00021	0.00305	0.00212
GO:0001959	regulation of cytokine-mediated signaling pathway	0.00021	0.00305	0.00212
GO:0038061	NIK/NF-kappaB signaling	0.00021	0.00305	0.00212
GO:0046321	positive regulation of fatty acid oxidation	0.00021	0.00305	0.00212
GO:0051639	actin filament network formation	0.00023	0.00321	0.00223

GO:0030837	negative regulation of actin filament polymerization	0.00023	0.00325	0.00226
GO:0032479	regulation of type I interferon production	0.00023	0.00326	0.00227
GO:0002285	lymphocyte activation involved in immune response	0.00024	0.00334	0.00232
GO:0009152	purine ribonucleotide biosynthetic process	0.00025	0.00344	0.00239
GO:0009142	nucleoside triphosphate biosynthetic process	0.00025	0.00345	0.00240
GO:0072332	intrinsic apoptotic signaling pathway by p53 class mediator	0.00025	0.00345	0.00240
GO:0071398	cellular response to fatty acid	0.00026	0.00347	0.00242
GO:0030833	regulation of actin filament polymerization	0.00026	0.00353	0.00245
GO:0042129	regulation of T cell proliferation	0.00026	0.00357	0.00248
GO:0002292	T cell differentiation involved in immune response	0.00027	0.00366	0.00255
GO:0008154	actin polymerization or depolymerization	0.00027	0.00367	0.00255
GO:0016358	dendrite development	0.00028	0.00367	0.00255
GO:0001774	microglial cell activation	0.00028	0.00370	0.00257
GO:0002269	leukocyte activation involved in inflammatory response	0.00028	0.00370	0.00257
GO:0006081	cellular aldehyde metabolic process	0.00033	0.00429	0.00298
GO:0048545	response to steroid hormone	0.00035	0.00446	0.00310
GO:0008064	regulation of actin polymerization or depolymerization	0.00035	0.00447	0.00311
GO:0002286	T cell activation involved in immune response	0.00043	0.00512	0.00356
GO:0046632	alpha-beta T cell differentiation	0.00043	0.00512	0.00356
GO:0090100	positive regulation of transmembrane receptor protein serine/threonine kinase signaling pathway	0.00043	0.00512	0.00356
GO:1903076	regulation of protein localization to plasma membrane	0.00043	0.00512	0.00356
GO:0007218	neuropeptide signaling pathway	0.00044	0.00517	0.00360
GO:0045088	regulation of innate immune response	0.00045	0.00530	0.00369
GO:0034638	phosphatidylcholine catabolic process	0.00046	0.00536	0.00372
GO:0006826	iron ion transport	0.00047	0.00551	0.00383
GO:0030038	contractile actin filament bundle assembly	0.00048	0.00555	0.00386
GO:0043149	stress fiber assembly	0.00048	0.00555	0.00386
GO:0051147	regulation of muscle cell differentiation	0.00050	0.00568	0.00395
GO:0046326	positive regulation of glucose import	0.00051	0.00576	0.00401
GO:0001906	cell killing	0.00051	0.00578	0.00402
GO:0002696	positive regulation of leukocyte activation	0.00052	0.00591	0.00411
GO:0048640	negative regulation of developmental growth	0.00057	0.00636	0.00442
GO:1900745	positive regulation of p38MAPK cascade	0.00058	0.00636	0.00442
GO:0010828	positive regulation of glucose transmembrane transport	0.00064	0.00701	0.00487
GO:0061387	regulation of extent of cell growth	0.00065	0.00702	0.00488
GO:0051100	negative regulation of binding	0.00065	0.00703	0.00489
GO:2000379	positive regulation of reactive oxygen species metabolic process	0.00068	0.00722	0.00502
GO:0062014	negative regulation of small molecule metabolic process	0.00068	0.00724	0.00504
GO:2000514	regulation of CD4-positive, alpha-beta T cell activation	0.00068	0.00724	0.00504
GO:0048562	embryonic organ morphogenesis	0.00069	0.00732	0.00509
GO:0007163	establishment or maintenance of cell polarity	0.00070	0.00744	0.00517
GO:0043299	leukocyte degranulation	0.00072	0.00754	0.00524
GO:0051153	regulation of striated muscle cell differentiation	0.00073	0.00764	0.00532
GO:0009394	2'-deoxyribonucleotide metabolic process	0.00075	0.00775	0.00539
GO:0019692	deoxyribose phosphate metabolic process	0.00075	0.00775	0.00539
GO:0010565	regulation of cellular ketone metabolic process	0.00079	0.00812	0.00565
GO:0048663	neuron fate commitment	0.00080	0.00817	0.00568

GO:0072676	lymphocyte migration	0.00081	0.00825	0.00574
GO:0021795	cerebral cortex cell migration	0.00083	0.00844	0.00587
GO:0048247	lymphocyte chemotaxis	0.00083	0.00844	0.00587
GO:0072350	tricarboxylic acid metabolic process	0.00085	0.00850	0.00591
GO:0150117	positive regulation of cell-substrate junction organization	0.00085	0.00850	0.00591
GO:0034121	regulation of toll-like receptor signaling pathway	0.00085	0.00852	0.00593
GO:1901222	regulation of NIK/NF-kappaB signaling	0.00085	0.00852	0.00593
GO:0002532	production of molecular mediator involved in inflammatory response	0.00088	0.00868	0.00604
GO:0050798	activated T cell proliferation	0.00088	0.00868	0.00604
GO:0006084	acetyl-CoA metabolic process	0.00090	0.00884	0.00615
GO:0042119	neutrophil activation	0.00090	0.00884	0.00615
GO:0009144	purine nucleoside triphosphate metabolic process	0.00095	0.00918	0.00639
GO:2001169	regulation of ATP biosynthetic process	0.00096	0.00920	0.00639
GO:0110020	regulation of actomyosin structure organization	0.00101	0.00961	0.00668
GO:0014897	striated muscle hypertrophy	0.00101	0.00961	0.00668
GO:0046847	filopodium assembly	0.00106	0.01000	0.00695
GO:0008643	carbohydrate transport	0.00107	0.01007	0.00700
GO:0048738	cardiac muscle tissue development	0.00108	0.01007	0.00700
GO:0010884	positive regulation of lipid storage	0.00111	0.01035	0.00720
GO:0009896	positive regulation of catabolic process	0.00112	0.01041	0.00724
GO:0150116	regulation of cell-substrate junction organization	0.00116	0.01066	0.00741
GO:0002793	positive regulation of peptide secretion	0.00119	0.01091	0.00759
GO:0032607	interferon-alpha production	0.00121	0.01100	0.00765
GO:0021954	central nervous system neuron development	0.00121	0.01100	0.00765
GO:0030516	regulation of axon extension	0.00123	0.01110	0.00772
GO:0014002	astrocyte development	0.00126	0.01136	0.00790
GO:0002287	alpha-beta T cell activation involved in immune response	0.00131	0.01175	0.00817
GO:0044264	cellular polysaccharide metabolic process	0.00134	0.01192	0.00829
GO:0002523	leukocyte migration involved in inflammatory response	0.00145	0.01272	0.00884
GO:0032727	positive regulation of interferon-alpha production	0.00145	0.01272	0.00884
GO:0006825	copper ion transport	0.00146	0.01272	0.00884
GO:0070486	leukocyte aggregation	0.00146	0.01272	0.00884
GO:0010611	regulation of cardiac muscle hypertrophy	0.00145	0.01272	0.00884
GO:0031331	positive regulation of cellular catabolic process	0.00152	0.01323	0.00920
GO:0002011	morphogenesis of an epithelial sheet	0.00157	0.01357	0.00943
GO:0060563	neuroepithelial cell differentiation	0.00159	0.01360	0.00945
GO:0001818	negative regulation of cytokine production	0.00159	0.01360	0.00945
GO:0062013	positive regulation of small molecule metabolic process	0.00159	0.01360	0.00945
GO:0050771	negative regulation of axonogenesis	0.00161	0.01370	0.00952
GO:0061099	negative regulation of protein tyrosine kinase activity	0.00161	0.01370	0.00952
GO:1904994	regulation of leukocyte adhesion to vascular endothelial cell	0.00161	0.01370	0.00952
GO:0032963	collagen metabolic process	0.00162	0.01371	0.00953
GO:0005976	polysaccharide metabolic process	0.00166	0.01404	0.00976
GO:0051549	positive regulation of keratinocyte migration	0.00169	0.01411	0.00981
GO:0060340	positive regulation of type I interferon-mediated signaling pathway	0.00169	0.01411	0.00981
GO:0072110	glomerular mesangial cell proliferation	0.00169	0.01411	0.00981
GO:1902285	semaphorin-plexin signaling pathway involved in neuron projection guidance	0.00169	0.01411	0.00981

GO:0045686	negative regulation of glial cell differentiation	0.00171	0.01418	0.00986
GO:0050868	negative regulation of T cell activation	0.00173	0.01433	0.00997
GO:0007422	peripheral nervous system development	0.00177	0.01445	0.01005
GO:0042102	positive regulation of T cell proliferation	0.00177	0.01445	0.01005
GO:0009265	2'-deoxyribonucleotide biosynthetic process	0.00179	0.01445	0.01005
GO:0032351	negative regulation of hormone metabolic process	0.00179	0.01445	0.01005
GO:0046385	deoxyribose phosphate biosynthetic process	0.00179	0.01445	0.01005
GO:0048143	astrocyte activation	0.00188	0.01497	0.01041
GO:0060252	positive regulation of glial cell proliferation	0.00188	0.01497	0.01041
GO:0046718	viral entry into host cell	0.00191	0.01520	0.01057
GO:0007219	Notch signaling pathway	0.00196	0.01559	0.01084
GO:0030048	actin filament-based movement	0.00199	0.01574	0.01095
GO:0045834	positive regulation of lipid metabolic process	0.00202	0.01591	0.01106
GO:0001909	leukocyte mediated cytotoxicity	0.00203	0.01598	0.01111
GO:0045786	negative regulation of cell cycle	0.00205	0.01605	0.01116
GO:0000041	transition metal ion transport	0.00213	0.01658	0.01153
GO:0021544	subpallium development	0.00214	0.01659	0.01154
GO:1900543	negative regulation of purine nucleotide metabolic process	0.00214	0.01659	0.01154
GO:0008593	regulation of Notch signaling pathway	0.00215	0.01666	0.01158
GO:0045089	positive regulation of innate immune response	0.00219	0.01687	0.01173
GO:0060337	type I interferon signaling pathway	0.00222	0.01707	0.01187
GO:0071357	cellular response to type I interferon	0.00222	0.01707	0.01187
GO:1901987	regulation of cell cycle phase transition	0.00223	0.01711	0.01190
GO:0032647	regulation of interferon-alpha production	0.00228	0.01737	0.01208
GO:0022411	cellular component disassembly	0.00228	0.01737	0.01208
GO:1901224	positive regulation of NIK/NF-kappaB signaling	0.00229	0.01737	0.01208
GO:0034142	toll-like receptor 4 signaling pathway	0.00230	0.01738	0.01208
GO:0045746	negative regulation of Notch signaling pathway	0.00230	0.01738	0.01208
GO:1900119	positive regulation of execution phase of apoptosis	0.00238	0.01786	0.01242
GO:0003300	cardiac muscle hypertrophy	0.00242	0.01806	0.01256
GO:0071772	response to BMP	0.00249	0.01853	0.01288
GO:0071773	cellular response to BMP stimulus	0.00249	0.01853	0.01288
GO:0010883	regulation of lipid storage	0.00253	0.01868	0.01299
GO:0001952	regulation of cell-matrix adhesion	0.00257	0.01884	0.01310
GO:0014020	primary neural tube formation	0.00257	0.01884	0.01310
GO:0071383	cellular response to steroid hormone stimulus	0.00258	0.01889	0.01314
GO:0050777	negative regulation of immune response	0.00260	0.01896	0.01319
GO:1903038	negative regulation of leukocyte cell-cell adhesion	0.00264	0.01916	0.01332
GO:0010717	regulation of epithelial to mesenchymal transition	0.00265	0.01919	0.01334
GO:0002293	alpha-beta T cell differentiation involved in immune response	0.00265	0.01919	0.01334
GO:0009145	purine nucleoside triphosphate biosynthetic process	0.00265	0.01919	0.01334
GO:0034340	response to type I interferon	0.00272	0.01960	0.01363
GO:0043502	regulation of muscle adaptation	0.00273	0.01965	0.01366
GO:0007517	muscle organ development	0.00274	0.01966	0.01367
GO:0032693	negative regulation of interleukin-10 production	0.00283	0.02013	0.01400
GO:0045063	T-helper 1 cell differentiation	0.00283	0.02013	0.01400
GO:2000726	negative regulation of cardiac muscle cell differentiation	0.00283	0.02013	0.01400
GO:0038179	neurotrophin signaling pathway	0.00289	0.02046	0.01423

GO:0045124	regulation of bone resorption	0.00291	0.02046	0.01423
GO:1902930	regulation of alcohol biosynthetic process	0.00291	0.02046	0.01423
GO:0051054	positive regulation of DNA metabolic process	0.00292	0.02046	0.01423
GO:0019511	peptidyl-proline hydroxylation	0.00293	0.02046	0.01423
GO:0042559	pteridine-containing compound biosynthetic process	0.00293	0.02046	0.01423
GO:0044764	multi-organism cellular process	0.00293	0.02046	0.01423
GO:0071281	cellular response to iron ion	0.00293	0.02046	0.01423
GO:1902563	regulation of neutrophil activation	0.00293	0.02046	0.01423
GO:1903078	positive regulation of protein localization to plasma membrane	0.00295	0.02056	0.01430
GO:0002456	T cell mediated immunity	0.00299	0.02085	0.01450
GO:0030574	collagen catabolic process	0.00304	0.02105	0.01464
GO:2000781	positive regulation of double-strand break repair	0.00304	0.02105	0.01464
GO:0032878	regulation of establishment or maintenance of cell polarity	0.00307	0.02113	0.01469
GO:0045980	negative regulation of nucleotide metabolic process	0.00307	0.02113	0.01469
GO:0051894	positive regulation of focal adhesion assembly	0.00307	0.02113	0.01469
GO:0072528	pyrimidine-containing compound biosynthetic process	0.00307	0.02113	0.01469
GO:0090330	regulation of platelet aggregation	0.00307	0.02113	0.01469
GO:1902993	positive regulation of amyloid precursor protein catabolic process	0.00307	0.02113	0.01469
GO:0021884	forebrain neuron development	0.00314	0.02149	0.01494
GO:0034260	negative regulation of GTPase activity	0.00314	0.02149	0.01494
GO:0006220	pyrimidine nucleotide metabolic process	0.00316	0.02157	0.01500
GO:0061050	regulation of cell growth involved in cardiac muscle cell development	0.00316	0.02157	0.01500
GO:2000272	negative regulation of signaling receptor activity	0.00316	0.02157	0.01500
GO:0061050	regulation of cell growth involved in cardiac muscle cell development	0.00316	0.02157	0.01500
GO:0044772	mitotic cell cycle phase transition	0.00329	0.02228	0.01549
GO:1905477	positive regulation of protein localization to membrane	0.00331	0.02242	0.01559
GO:0042100	B cell proliferation	0.00335	0.02268	0.01577
GO:0071219	cellular response to molecule of bacterial origin	0.00337	0.02273	0.01580
GO:0009219	pyrimidine deoxyribonucleotide metabolic process	0.00341	0.02274	0.01581
GO:0018401	peptidyl-proline hydroxylation to 4-hydroxy-L-proline	0.00341	0.02274	0.01581
GO:0038180	nerve growth factor signaling pathway	0.00341	0.02274	0.01581
GO:0043500	muscle adaptation	0.00340	0.02274	0.01581
GO:0002449	lymphocyte mediated immunity	0.00352	0.02338	0.01626
GO:0048863	stem cell differentiation	0.00358	0.02376	0.01652
GO:0051496	positive regulation of stress fiber assembly	0.00361	0.02380	0.01655
GO:2000351	regulation of endothelial cell apoptotic process	0.00361	0.02380	0.01655
GO:0016051	carbohydrate biosynthetic process	0.00362	0.02382	0.01656
GO:2000573	positive regulation of DNA biosynthetic process	0.00365	0.02400	0.01669
GO:0006085	acetyl-CoA biosynthetic process	0.00369	0.02411	0.01676
GO:0021542	dentate gyrus development	0.00369	0.02411	0.01676
GO:0046184	aldehyde biosynthetic process	0.00369	0.02411	0.01676
GO:2001185	regulation of CD8-positive, alpha-beta T cell activation	0.00369	0.02411	0.01676
GO:0031032	actomyosin structure organization	0.00382	0.02481	0.01725
GO:0046635	positive regulation of alpha-beta T cell activation	0.00386	0.02501	0.01739
GO:0030851	granulocyte differentiation	0.00397	0.02550	0.01773
GO:0043303	mast cell degranulation	0.00397	0.02550	0.01773
GO:0045744	negative regulation of G protein-coupled receptor signaling pathway	0.00399	0.02550	0.01773
GO:0051893	regulation of focal adhesion assembly	0.00399	0.02550	0.01773

GO:0090109	regulation of cell-substrate junction assembly	0.00399	0.02550	0.01773
GO:0030509	BMP signaling pathway	0.00406	0.02585	0.01797
GO:0150115	cell-substrate junction organization	0.00409	0.02596	0.01805
GO:0006221	pyrimidine nucleotide biosynthetic process	0.00412	0.02596	0.01805
GO:0008356	asymmetric cell division	0.00412	0.02596	0.01805
GO:0010039	response to iron ion	0.00412	0.02596	0.01805
GO:2000353	positive regulation of endothelial cell apoptotic process	0.00412	0.02596	0.01805
GO:0009262	deoxyribonucleotide metabolic process	0.00429	0.02668	0.01855
GO:0048714	positive regulation of oligodendrocyte differentiation	0.00429	0.02668	0.01855
GO:0120178	steroid hormone biosynthetic process	0.00429	0.02668	0.01855
GO:1902751	positive regulation of cell cycle G2/M phase transition	0.00429	0.02668	0.01855
GO:0032303	regulation of icosanoid secretion	0.00430	0.02668	0.01855
GO:0002260	lymphocyte homeostasis	0.00432	0.02675	0.01860
GO:0007622	rhythmic behavior	0.00433	0.02678	0.01862
GO:0042093	T-helper cell differentiation	0.00433	0.02678	0.01862
GO:0045600	positive regulation of fat cell differentiation	0.00462	0.02807	0.01952
GO:0150076	neuroinflammatory response	0.00462	0.02807	0.01952
GO:0051251	positive regulation of lymphocyte activation	0.00471	0.02846	0.01979
GO:0061049	cell growth involved in cardiac muscle cell development	0.00473	0.02846	0.01979
GO:0046890	regulation of lipid biosynthetic process	0.00474	0.02846	0.01979
GO:0001845	phagolysosome assembly	0.00475	0.02846	0.01979
GO:0021781	glial cell fate commitment	0.00475	0.02846	0.01979
GO:0051547	regulation of keratinocyte migration	0.00475	0.02846	0.01979
GO:0051988	regulation of attachment of spindle microtubules to kinetochore	0.00475	0.02846	0.01979
GO:0060700	regulation of ribonuclease activity	0.00475	0.02846	0.01979
GO:1902165	regulation of intrinsic apoptotic signaling pathway in response to DNA damage by p53 class mediator	0.00475	0.02846	0.01979
GO:0003298	physiological muscle hypertrophy	0.00473	0.02846	0.01979
GO:0003301	physiological cardiac muscle hypertrophy	0.00473	0.02846	0.01979
GO:0061049	cell growth involved in cardiac muscle cell development	0.00473	0.02846	0.01979
GO:0032615	interleukin-12 production	0.00485	0.02888	0.02008
GO:2001238	positive regulation of extrinsic apoptotic signaling pathway	0.00485	0.02888	0.02008
GO:0051145	smooth muscle cell differentiation	0.00488	0.02901	0.02017
GO:0002279	mast cell activation involved in immune response	0.00492	0.02918	0.02029
GO:0002448	mast cell mediated immunity	0.00492	0.02918	0.02029
GO:0001841	neural tube formation	0.00496	0.02938	0.02043
GO:0002761	regulation of myeloid leukocyte differentiation	0.00496	0.02938	0.02043
GO:0021915	neural tube development	0.00500	0.02954	0.02054
GO:1904019	epithelial cell apoptotic process	0.00501	0.02956	0.02056
GO:0009205	purine ribonucleoside triphosphate metabolic process	0.00509	0.02995	0.02083
GO:1901880	negative regulation of protein depolymerization	0.00509	0.02995	0.02083
GO:0042180	cellular ketone metabolic process	0.00509	0.02995	0.02083
GO:0097028	dendritic cell differentiation	0.00511	0.02997	0.02084
GO:0120032	regulation of plasma membrane bounded cell projection assembly	0.00512	0.03003	0.02088
GO:0002294	CD4-positive, alpha-beta T cell differentiation involved in immune response	0.00520	0.03039	0.02113
GO:0009206	purine ribonucleoside triphosphate biosynthetic process	0.00520	0.03039	0.02113
GO:0042982	amyloid precursor protein metabolic process	0.00520	0.03039	0.02113
GO:1900542	regulation of purine nucleotide metabolic process	0.00526	0.03072	0.02136

GO:0019058	viral life cycle	0.00528	0.03081	0.02142
GO:0042490	mechanoreceptor differentiation	0.00540	0.03135	0.02180
GO:0043242	negative regulation of protein-containing complex disassembly	0.00540	0.03135	0.02180
GO:0030517	negative regulation of axon extension	0.00542	0.03135	0.02180
GO:0002861	regulation of inflammatory response to antigenic stimulus	0.00545	0.03135	0.02180
GO:0048710	regulation of astrocyte differentiation	0.00545	0.03135	0.02180
GO:1902003	regulation of amyloid-beta formation	0.00545	0.03135	0.02180
GO:0014741	negative regulation of muscle hypertrophy	0.00545	0.03135	0.02180
GO:1904377	positive regulation of protein localization to cell periphery	0.00550	0.03146	0.02188
GO:0009200	deoxyribonucleoside triphosphate metabolic process	0.00551	0.03146	0.02188
GO:0010566	regulation of ketone biosynthetic process	0.00551	0.03146	0.02188
GO:0014051	gamma-aminobutyric acid secretion	0.00551	0.03146	0.02188
GO:0048712	negative regulation of astrocyte differentiation	0.00551	0.03146	0.02188
GO:0051546	keratinocyte migration	0.00551	0.03146	0.02188
GO:0048675	axon extension	0.00553	0.03154	0.02193
GO:1903578	regulation of ATP metabolic process	0.00559	0.03185	0.02215
GO:0000132	establishment of mitotic spindle orientation	0.00572	0.03233	0.02248
GO:0055075	potassium ion homeostasis	0.00572	0.03233	0.02248
GO:0045932	negative regulation of muscle contraction	0.00572	0.03233	0.02248
GO:0051604	protein maturation	0.00575	0.03250	0.02260
GO:0060080	inhibitory postsynaptic potential	0.00584	0.03267	0.02272
GO:0021871	forebrain regionalization	0.00588	0.03267	0.02272
GO:0044342	type B pancreatic cell proliferation	0.00588	0.03267	0.02272
GO:1905809	negative regulation of synapse organization	0.00588	0.03267	0.02272
GO:0001878	response to yeast	0.00592	0.03267	0.02272
GO:0003356	regulation of cilium beat frequency	0.00592	0.03267	0.02272
GO:0009437	carnitine metabolic process	0.00592	0.03267	0.02272
GO:0030388	fructose 1,6-bisphosphate metabolic process	0.00592	0.03267	0.02272
GO:0042135	neurotransmitter catabolic process	0.00592	0.03267	0.02272
GO:0048241	epinephrine transport	0.00592	0.03267	0.02272
GO:0072124	regulation of glomerular mesangial cell proliferation	0.00592	0.03267	0.02272
GO:1900272	negative regulation of long-term synaptic potentiation	0.00592	0.03267	0.02272
GO:1902287	semaphorin-plexin signaling pathway involved in axon guidance	0.00592	0.03267	0.02272
GO:0051148	negative regulation of muscle cell differentiation	0.00584	0.03267	0.02272
GO:0009395	phospholipid catabolic process	0.00603	0.03314	0.02304
GO:0051651	maintenance of location in cell	0.00613	0.03366	0.02340
GO:0006140	regulation of nucleotide metabolic process	0.00614	0.03366	0.02340
GO:0046637	regulation of alpha-beta T cell differentiation	0.00621	0.03398	0.02363
GO:0060491	regulation of cell projection assembly	0.00623	0.03406	0.02368
GO:0046887	positive regulation of hormone secretion	0.00635	0.03461	0.02407
GO:0007623	circadian rhythm	0.00652	0.03532	0.02456
GO:0032655	regulation of interleukin-12 production	0.00656	0.03546	0.02466
GO:0072577	endothelial cell apoptotic process	0.00656	0.03546	0.02466
GO:0030098	lymphocyte differentiation	0.00665	0.03593	0.02499
GO:0046638	positive regulation of alpha-beta T cell differentiation	0.00670	0.03608	0.02509
GO:0070527	platelet aggregation	0.00670	0.03608	0.02509
GO:2000725	regulation of cardiac muscle cell differentiation	0.00670	0.03608	0.02509
GO:0051146	striated muscle cell differentiation	0.00676	0.03629	0.02523

GO:0006469	negative regulation of protein kinase activity	0.00692	0.03712	0.02581
GO:0046513	ceramide biosynthetic process	0.00700	0.03745	0.02604
GO:0050994	regulation of lipid catabolic process	0.00700	0.03745	0.02604
GO:0021846	cell proliferation in forebrain	0.00702	0.03745	0.02604
GO:0035886	vascular associated smooth muscle cell differentiation	0.00702	0.03745	0.02604
GO:0070306	lens fiber cell differentiation	0.00702	0.03745	0.02604
GO:2000191	regulation of fatty acid transport	0.00702	0.03745	0.02604
GO:0001738	morphogenesis of a polarized epithelium	0.00713	0.03792	0.02637
GO:0046467	membrane lipid biosynthetic process	0.00730	0.03864	0.02687
GO:2001171	positive regulation of ATP biosynthetic process	0.00730	0.03864	0.02687
GO:2001212	regulation of vasculogenesis	0.00730	0.03864	0.02687
GO:0043300	regulation of leukocyte degranulation	0.00734	0.03882	0.02699
GO:0001843	neural tube closure	0.00738	0.03892	0.02707
GO:0044319	wound healing, spreading of cells	0.00750	0.03929	0.02732
GO:0046475	glycerophospholipid catabolic process	0.00750	0.03929	0.02732
GO:0090505	epiboly involved in wound healing	0.00750	0.03929	0.02732
GO:2000515	negative regulation of CD4-positive, alpha-beta T cell activation	0.00750	0.03929	0.02732
GO:0044843	cell cycle G1/S phase transition	0.00757	0.03965	0.02757
GO:0045787	positive regulation of cell cycle	0.00766	0.04005	0.02785
GO:0002090	regulation of receptor internalization	0.00768	0.04011	0.02789
GO:0045780	positive regulation of bone resorption	0.00787	0.04092	0.02845
GO:0046852	positive regulation of bone remodeling	0.00787	0.04092	0.02845
GO:1902668	negative regulation of axon guidance	0.00787	0.04092	0.02845
GO:0048016	inositol phosphate-mediated signaling	0.00789	0.04093	0.02846
GO:0071887	leukocyte apoptotic process	0.00791	0.04096	0.02848
GO:0070228	regulation of lymphocyte apoptotic process	0.00792	0.04096	0.02848
GO:0080182	histone H3-K4 trimethylation	0.00793	0.04096	0.02848
GO:1900746	regulation of vascular endothelial growth factor signaling pathway	0.00793	0.04096	0.02848
GO:0045986	negative regulation of smooth muscle contraction	0.00793	0.04096	0.02848
GO:0016331	morphogenesis of embryonic epithelium	0.00797	0.04106	0.02855
GO:0050714	positive regulation of protein secretion	0.00804	0.04132	0.02874
GO:0031954	positive regulation of protein autophosphorylation	0.00806	0.04134	0.02875
GO:0010663	positive regulation of striated muscle cell apoptotic process	0.00806	0.04134	0.02875
GO:0043154	negative regulation of cysteine-type endopeptidase activity involved in apoptotic process	0.00811	0.04151	0.02887
GO:1902991	regulation of amyloid precursor protein catabolic process	0.00816	0.04167	0.02898
GO:0043370	regulation of CD4-positive, alpha-beta T cell differentiation	0.00821	0.04183	0.02908
GO:0048255	mRNA stabilization	0.00821	0.04183	0.02908
GO:0031341	regulation of cell killing	0.00823	0.04193	0.02915
GO:0048008	platelet-derived growth factor receptor signaling pathway	0.00834	0.04233	0.02944
GO:0006641	triglyceride metabolic process	0.00840	0.04254	0.02958
GO:0071222	cellular response to lipopolysaccharide	0.00865	0.04374	0.03042
GO:0000768	syncytium formation by plasma membrane fusion	0.00871	0.04395	0.03056
GO:0009201	ribonucleoside triphosphate biosynthetic process	0.00871	0.04395	0.03056
GO:0140253	cell-cell fusion	0.00871	0.04395	0.03056
GO:0099173	postsynapse organization	0.00880	0.04438	0.03086
GO:0070542	response to fatty acid	0.00888	0.04465	0.03105
GO:0051294	establishment of spindle orientation	0.00893	0.04474	0.03111

GO:0008361	regulation of cell size	0.00904	0.04518	0.03142
GO:1902667	regulation of axon guidance	0.00915	0.04564	0.03174
GO:0050663	cytokine secretion	0.00922	0.04592	0.03193
GO:0009199	ribonucleoside triphosphate metabolic process	0.00939	0.04663	0.03242
GO:0044106	cellular amine metabolic process	0.00939	0.04663	0.03242
GO:0070231	T cell apoptotic process	0.00943	0.04675	0.03251
GO:0009263	deoxyribonucleotide biosynthetic process	0.00954	0.04690	0.03261
GO:0014052	regulation of gamma-aminobutyric acid secretion	0.00954	0.04690	0.03261
GO:0038094	Fc-gamma receptor signaling pathway	0.00954	0.04690	0.03261
GO:0002709	regulation of T cell mediated immunity	0.00956	0.04690	0.03261
GO:1904035	regulation of epithelial cell apoptotic process	0.00956	0.04690	0.03261
GO:0061052	negative regulation of cell growth involved in cardiac muscle cell development	0.00954	0.04690	0.03261
GO:0060395	SMAD protein signal transduction	0.00959	0.04694	0.03264
GO:0032673	regulation of interleukin-4 production	0.00968	0.04701	0.03269
GO:0032958	inositol phosphate biosynthetic process	0.00968	0.04701	0.03269
GO:0048841	regulation of axon extension involved in axon guidance	0.00968	0.04701	0.03269
GO:0071354	cellular response to interleukin-6	0.00968	0.04701	0.03269
GO:1903579	negative regulation of ATP metabolic process	0.00968	0.04701	0.03269
GO:0009755	hormone-mediated signaling pathway	0.00976	0.04738	0.03294
GO:0048813	dendrite morphogenesis	0.00990	0.04799	0.03337
GO:0050773	regulation of dendrite development	0.00993	0.04808	0.03343
GO:0051489	regulation of filopodium assembly	0.00997	0.04822	0.03353
GO:0045165	cell fate commitment	0.01008	0.04868	0.03385
GO:0010737	protein kinase A signaling	0.01016	0.04889	0.03399
GO:0021955	central nervous system neuron axonogenesis	0.01016	0.04889	0.03399
GO:0051154	negative regulation of striated muscle cell differentiation	0.01016	0.04889	0.03399
GO:0051592	response to calcium ion	0.01023	0.04901	0.03408
GO:0001838	embryonic epithelial tube formation	0.01026	0.04908	0.03413
GO:0018126	protein hydroxylation	0.01035	0.04934	0.03431
GO:0021952	central nervous system projection neuron axonogenesis	0.01035	0.04934	0.03431
GO:0042133	neurotransmitter metabolic process	0.01035	0.04934	0.03431

Table 7.3. GO enrichment analysis for biological processes of KO *versus* CTRL ranked by q-value (q-value <0.2, p.adjust <0.1 and p-value cut-off <0.05) not present in WT *versus* CTRL.

Appendix IV

ID	Description	p-value	p.adjust	q-value
GO:0097120	receptor localization to synapse	0.00000	0.00107	0.00099
GO:1902414	protein localization to cell junction	0.00000	0.00192	0.00178
GO:0035418	protein localization to synapse	0.00001	0.00886	0.00820
GO:0007409	axonogenesis	0.00001	0.01133	0.01049
GO:0009142	nucleoside triphosphate biosynthetic process	0.00004	0.02294	0.02124

GO:0009148	pyrimidine nucleoside triphosphate biosynthetic process	0.00004	0.02294	0.02124
GO:1903539	protein localization to postsynaptic membrane	0.00006	0.02443	0.02262
GO:0007416	synapse assembly	0.00006	0.02443	0.02262
GO:0034329	cell junction assembly	0.00007	0.02443	0.02262
GO:0062237	protein localization to postsynapse	0.00010	0.02443	0.02262
GO:0009147	pyrimidine nucleoside triphosphate metabolic process	0.00010	0.02443	0.02262
GO:0045666	positive regulation of neuron differentiation	0.00010	0.02443	0.02262
GO:0007272	ensheathment of neurons	0.00010	0.02443	0.02262
GO:0008366	axon ensheathment	0.00010	0.02443	0.02262
GO:1901890	positive regulation of cell junction assembly	0.00011	0.02443	0.02262
GO:0009201	ribonucleoside triphosphate biosynthetic process	0.00012	0.02443	0.02262
GO:0010976	positive regulation of neuron projection development	0.00014	0.02744	0.02541
GO:0050770	regulation of axonogenesis	0.00015	0.02744	0.02541
GO:0060560	developmental growth involved in morphogenesis	0.00018	0.03107	0.02877
GO:0099072	regulation of postsynaptic membrane neurotransmitter receptor levels	0.00019	0.03217	0.02980
GO:0050772	positive regulation of axonogenesis	0.00025	0.03879	0.03593
GO:0098969	neurotransmitter receptor transport to postsynaptic membrane	0.00026	0.03879	0.03593
GO:0048169	regulation of long-term neuronal synaptic plasticity	0.00029	0.04249	0.03935
GO:0098877	neurotransmitter receptor transport to plasma membrane	0.00031	0.04286	0.03969
GO:0009141	nucleoside triphosphate metabolic process	0.00035	0.04286	0.03969
GO:0031346	positive regulation of cell projection organization	0.00036	0.04286	0.03969
GO:0006221	pyrimidine nucleotide biosynthetic process	0.00038	0.04286	0.03969
GO:1903540	establishment of protein localization to postsynaptic membrane	0.00038	0.04286	0.03969
GO:0042552	myelination	0.00039	0.04286	0.03969
GO:0009199	ribonucleoside triphosphate metabolic process	0.00040	0.04286	0.03969
GO:1990138	neuron projection extension	0.00044	0.04286	0.03969
GO:0048675	axon extension	0.00044	0.04286	0.03969
GO:0006183	GTP biosynthetic process	0.00045	0.04286	0.03969
GO:0009209	pyrimidine ribonucleoside triphosphate biosynthetic process	0.00045	0.04286	0.03969
GO:0098887	neurotransmitter receptor transport, endosome to postsynaptic membrane	0.00045	0.04286	0.03969
GO:1903311	regulation of mRNA metabolic process	0.00049	0.04565	0.04228

Table 7.4. GO enrichment analysis for biological processes of KO *versus* WT (q-value <0.2, p.adjust <0.1 and p-value cut-off <0.05), ranked by q-value.

Bibliography

- ‘MECP2 Variant List’. Accessed 28 March 2020. http://mecp2.chw.edu.au/mecp2/mecp2_upgrade_proband_list_copy.php.
- A P Mullin et al., ‘Neurodevelopmental Disorders: Mechanisms and Boundary Definitions from Genomes, Interactomes and Proteomes’, Translational Psychiatry 3, no. 12 (December 2013): e329, https://doi.org/10.1038/tp.2013.108.
- Abdala, Ana P. L., Mathias Dutschmann, John M. Bissonnette, and Julian F. R. Paton. ‘Correction of Respiratory Disorders in a Mouse Model of Rett Syndrome’. Proceedings of the National Academy of Sciences of the United States of America 107, no. 42 (19 October 2010): 18208–13. https://doi.org/10.1073/pnas.1012104107.
- Abdala, Ana P., Daniel T. Lioy, Saurabh K. Garg, Sharon J. Knopp, Julian F. R. Paton, and John M. Bissonnette. ‘Effect of Sarizotan, a 5-HT1a and D2-like Receptor Agonist, on Respiration in Three Mouse Models of Rett Syndrome’. American Journal of Respiratory Cell and Molecular Biology 50, no. 6 (June 2014): 1031–39. https://doi.org/10.1165/rcmb.2013-0372OC.
- Abrajano, Joseph J., Irfan A. Qureshi, Solen Gokhan, Deyou Zheng, Aviv Bergman, and Mark F. Mehler. ‘Differential Deployment of REST and CoREST Promotes Glial Subtype Specification and Oligodendrocyte Lineage Maturation’. PloS One 4, no. 11 (3 November 2009): e7665. https://doi.org/10.1371/journal.pone.0007665.
- Abramoff MD, Magalhaes PJ, Ram SJ.. ‘Image Processing with ImageJ’. Biophotonics. 2004
- Adachi, Megumi, Anita E. Autry, Herb E. Covington, and Lisa M. Monteggia. ‘MeCP2-Mediated Transcription Repression in the Basolateral Amygdala May Underlie Heightened Anxiety in a Mouse Model of Rett Syndrome’. The Journal of Neuroscience: The Official Journal of the Society for Neuroscience 29, no. 13 (1 April 2009): 4218–27. https://doi.org/10.1523/JNEUROSCI.4225-08.2009.
- Adkins, Nicholas L., and Philippe T. Georgel. ‘MeCP2: Structure and Function’. Biochemistry and Cell Biology = Biochimie Et Biologie Cellulaire 89, no. 1 (February 2011): 1–11. https://doi.org/10.1139/O10-112.
- Agulhon, Cendra, Min-Yu Sun, Thomas Murphy, Timothy Myers, Kelli Lauderdale, and Todd A. Fiacco. ‘Calcium Signaling and Gliotransmission in Normal vs. Reactive Astrocytes’. Frontiers in Pharmacology 3 (2012): 139. https://doi.org/10.3389/fphar.2012.00139.
- Akbarian, Schahram, Yan Jiang, and Genevieve Laforet. ‘The Molecular Pathology of Rett Syndrome’. NeuroMolecular Medicine 8, no. 4 (1 December 2006): 485–94. https://doi.org/10.1385/NMM:8:4:485.
- Albrecht, David, Francisco José López-Murcia, Anna P. Pérez-González, Gregor Lichtner, Carles Solsona, and Artur Llobet. ‘SPARC Prevents Maturation of Cholinergic Presynaptic Terminals’. Molecular and Cellular Neuroscience 49, no. 3 (1 March 2012): 364–74. https://doi.org/10.1016/j.mcn.2012.01.005.
- Allen, Nicola J. ‘Synaptic Plasticity: Astrocytes Wrap It Up’. Current Biology: CB 24, no. 15 (4 August 2014): R697-699. https://doi.org/10.1016/j.cub.2014.06.030.
- Allen, Nicola J., and Ben A. Barres. ‘Glia — More than Just Brain Glue’. Nature 457, no. 7230 (February 2009): 675–77. https://doi.org/10.1038/457675a.
- Allen, Nicola J., Mariko L. Bennett, Lynette C. Foo, Gordon X. Wang, Chandrani Chakraborty, Stephen J. Smith, and Ben A. Barres. ‘Astrocyte Glypicans 4 and 6 Promote Formation of Excitatory Synapses via GluA1 AMPA Receptors’. Nature 486, no. 7403 (27 May 2012): 410–14. https://doi.org/10.1038/nature11059.
- Amir, R. E., I. B. Van den Veyver, M. Wan, C. Q. Tran, U. Francke, and H. Y. Zoghbi. ‘Rett Syndrome Is Caused by Mutations in X-Linked MECP2, Encoding Methyl-CpG-Binding Protein 2’. Nature Genetics 23, no. 2 (October 1999): 185–88. https://doi.org/10.1038/13810.

- Ango, Fabrice, Caizhi Wu, Johannes J. Van der Want, Priscilla Wu, Melitta Schachner, and Z. Josh Huang. 'Bergmann Glia and the Recognition Molecule CHL1 Organize GABAergic Axons and Direct Innervation of Purkinje Cell Dendrites'. PLOS Biology 6, no. 4 (29 April 2008): e103. https://doi.org/10.1371/journal.pbio.0060103.
- Angulo, María Cecilia, Andreï S. Kozlov, Serge Charpak, and Etienne Audinat. 'Glutamate Released from Glial Cells Synchronizes Neuronal Activity in the Hippocampus'. Journal of Neuroscience 24, no. 31 (4 August 2004): 6920–27. https://doi.org/10.1523/JNEUROSCI.0473-04.2004.
- Anthony, Todd E., Corinna Klein, Gord Fishell, and Nathaniel Heintz. 'Radial Glia Serve as Neuronal Progenitors in All Regions of the Central Nervous System'. Neuron 41, no. 6 (25 March 2004): 881–90. https://doi.org/10.1016/s0896-6273(04)00140-0.
- Araque, A., V. Parpura, R. P. Sanzgiri, and P. G. Haydon. 'Glutamate-Dependent Astrocyte Modulation of Synaptic Transmission between Cultured Hippocampal Neurons'. The European Journal of Neuroscience 10, no. 6 (June 1998): 2129–42. https://doi.org/10.1046/j.1460-9568.1998.00221.x.
- Araque, Alfonso, Giorgio Carmignoto, Philip G. Haydon, Stéphane H. R. Oliet, Richard Robitaille, and Andrea Volterra. 'Gliotransmitters Travel in Time and Space'. Neuron 81, no. 4 (19 February 2014): 728–39. https://doi.org/10.1016/j.neuron.2014.02.007.
- Armstrong, Dawna Duncan. 'Neuropathology of Rett Syndrome'. Journal of Child Neurology 20, no. 9 (September 2005): 747–53. https://doi.org/10.1177/08830738050200090901.
- Bae, James J., Yun-Yan Xiang, Alonso Martinez-Canabal, Paul W. Frankland, Burton B. Yang, and Wei-Yang Lu. 'Increased Transforming Growth Factor-B1 Modulates Glutamate Receptor Expression in the Hippocampus'. International Journal of Physiology, Pathophysiology and Pharmacology 3, no. 1 (2011): 9–20.
- Baj, Gabriele, Angela Patrizio, Alberto Montalbano, Marina Sciancalepore, and Enrico Tongiorgi. 'Developmental and Maintenance Defects in Rett Syndrome Neurons Identified by a New Mouse Staging System in Vitro'. Frontiers in Cellular Neuroscience 8 (2014). https://doi.org/10.3389/fncel.2014.00018.
- Bak, Lasse K., Anne B. Walls, Arne Schousboe, and Helle S. Waagepetersen. 'Astrocytic Glycogen Metabolism in the Healthy and Diseased Brain'. The Journal of Biological Chemistry 293, no. 19 (11 May 2018): 7108–16. https://doi.org/10.1074/jbc.R117.803239.
- Bak, Lasse K., Arne Schousboe, Ursula Sonnewald, and Helle S. Waagepetersen. 'Glucose Is Necessary to Maintain Neurotransmitter Homeostasis during Synaptic Activity in Cultured Glutamatergic Neurons'. Journal of Cerebral Blood Flow and Metabolism: Official Journal of the International Society of Cerebral Blood Flow and Metabolism 26, no. 10 (October 2006): 1285–97. https://doi.org/10.1038/sj.jcbfm.9600281.
- Baker, Steven Andrew, Lin Chen, Angela Dawn Wilkins, Peng Yu, Olivier Lichtarge, and Huda Yahya Zoghbi. 'An AT-Hook Domain in MeCP2 Determines the Clinical Course of Rett Syndrome and Related Disorders'. Cell 152, no. 5 (28 February 2013): 984–96. https://doi.org/10.1016/j.cell.2013.01.038.
- Ballas, Nurit, Daniel T. Lioy, Christopher Grunseich, and Gail Mandel. 'Non-Cell Autonomous Influence of MeCP2-Deficient Glia on Neuronal Dendritic Morphology'. Nature Neuroscience 12, no. 3 (March 2009): 311–17. https://doi.org/10.1038/nn.2275.
- Bandeira, Fabiana, R (Oberheim et al., 2009). oberto Lent, and Suzana Herculano-Houzel. 'Changing Numbers of Neuronal and Non-Neuronal Cells Underlie Postnatal Brain Growth in the Rat'. Proceedings of the National Academy of Sciences 106, no. 33 (18 August 2009): 14108–13. https://doi.org/10.1073/pnas.0804650106.

- Banerjee, Abhishek, Rajeev V. Rikhye, Vincent Breton-Provencher, Xin Tang, Chenchen Li, Keji Li, Caroline A. Runyan, Zhanyan Fu, Rudolf Jaenisch, and Mriganka Sur. 'Jointly Reduced Inhibition and Excitation Underlies Circuit-Wide Changes in Cortical Processing in Rett Syndrome'. Proceedings of the National Academy of Sciences of the United States of America 113, no. 46 (15 2016): E7287–96. https://doi.org/10.1073/pnas.1615330113.
- Barber, Casey N., and Daniel M. Raben. 'Lipid Metabolism Crosstalk in the Brain: Glia and Neurons'. Frontiers in Cellular Neuroscience 13 (2019). https://doi.org/10.3389/fncel.2019.00212.
- Barker, Alison J., Selina M. Koch, Jamian Reed, Ben A. Barres, and Erik M. Ullian. 'Developmental Control of Synaptic Receptivity'. The Journal of Neuroscience: The Official Journal of the Society for Neuroscience 28, no. 33 (13 August 2008): 8150–60. https://doi.org/10.1523/JNEUROSCI.1744-08.2008.
- Barros, L. Felipe, and Joachim W. Deitmer. 'Glucose and Lactate Supply to the Synapse'. Brain Research Reviews, Synaptic Processes - the role of glial cells, 63, no. 1 (1 May 2010): 149–59. https://doi.org/10.1016/j.brainresrev.2009.10.002.
- Bartos, Marlene, Imre Vida, and Peter Jonas. 'Synaptic Mechanisms of Synchronized Gamma Oscillations in Inhibitory Interneuron Networks'. Nature Reviews Neuroscience 8, no. 1 (January 2007): 45–56. https://doi.org/10.1038/nrn2044.
- Bashaw, Greg J., and Rüdiger Klein. 'Signaling from Axon Guidance Receptors'. Cold Spring Harbor Perspectives in Biology 2, no. 5 (May 2010): a001941. https://doi.org/10.1101/cshperspect.a001941.
- Bassani, Silvia, Jonathan Zapata, Laura Gerosa, Edoardo Moretto, Luca Murru, and Maria Passafaro. 'The Neurobiology of X-Linked Intellectual Disability'. The Neuroscientist: A Review Journal Bringing Neurobiology, Neurology and Psychiatry 19, no. 5 (October 2013): 541–52. https://doi.org/10.1177/1073858413493972.
- Batiuk, Mykhailo Y., Araks Martirosyan, Jérôme Wahis, Filip de Vin, Catherine Marneffe, Carola Kusserow, Jordan Koeppen, et al. 'Identification of Region-Specific Astrocyte Subtypes at Single Cell Resolution'. Nature Communications 11, no. 1 (5 March 2020): 1220. https://doi.org/10.1038/s41467-019-14198-8.
- Bauman, M. L., T. L. Kemper, and D. M. Arin. 'Pervasive Neuroanatomic Abnormalities of the Brain in Three Cases of Rett's Syndrome'. Neurology 45, no. 8 (August 1995): 1581–86. https://doi.org/10.1212/wnl.45.8.1581.
- Bayraktar, Omer Ali, Luis C. Fuentealba, Arturo Alvarez-Buylla, and David H. Rowitch. 'Astrocyte Development and Heterogeneity'. Cold Spring Harbor Perspectives in Biology 7, no. 1 (1 January 2015): a020362. https://doi.org/10.1101/cshperspect.a020362.
- Bayraktar, Omer Ali, Theresa Bartels, Staffan Holmqvist, Vitalii Kleshchevnikov, Araks Martirosyan, Damon Polioudakis, Lucile Ben Haim, et al. 'Astrocyte Layers in the Mammalian Cerebral Cortex Revealed by a Single-Cell in Situ Transcriptomic Map'. Nature Neuroscience 23, no. 4 (April 2020): 500–509. https://doi.org/10.1038/s41593-020-0602-1.
- Bazargani, Narges, and David Attwell. 'Astrocyte Calcium Signaling: The Third Wave'. Nature Neuroscience 19, no. 2 (February 2016): 182–89. https://doi.org/10.1038/nn.4201.
- Beattie, Eric C., David Stellwagen, Wade Morishita, Jacqueline C. Bresnahan, Byeong Keun Ha, Mark Von Zastrow, Michael S. Beattie, and Robert C. Malenka. 'Control of Synaptic Strength by Glial TNFalpha'. Science (New York, N.Y.) 295, no. 5563 (22 March 2002): 2282–85. https://doi.org/10.1126/science.1067859.
- Bebensee, Dörthe F., Karolina Can, and Michael Müller. 'Increased Mitochondrial Mass and Cytosolic Redox Imbalance in Hippocampal Astrocytes of a Mouse Model of Rett Syndrome: Subcellular Changes Revealed by Ratiometric Imaging of JC-1 and RoGFP1 Fluorescence'.

Oxidative Medicine and Cellular Longevity 2017 (2017): 3064016. https://doi.org/10.1155/2017/3064016.

- Bedogni, Francesco, Clementina Cobolli Gigli, Davide Pozzi, Riccardo Lorenzo Rossi, Linda Scaramuzza, Grazisa Rossetti, Massimiliano Pagani, Charlotte Kilstrup-Nielsen, Michela Matteoli, and Nicoletta Landsberger. 'Defects During Mecp2 Null Embryonic Cortex Development Precede the Onset of Overt Neurological Symptoms'. Cerebral Cortex (New York, N.Y.: 1991) 26, no. 6 (2016): 2517–29. https://doi.org/10.1093/cercor/bhv078.
- Bedogni, Francesco, Riccardo L. Rossi, Francesco Galli, Clementina Cobolli Gigli, Anna Gandaglia, Charlotte Kilstrup-Nielsen, and Nicoletta Landsberger. 'Rett Syndrome and the Urge of Novel Approaches to Study MeCP2 Functions and Mechanisms of Action'. Neuroscience & Biobehavioral Reviews, Common mechanisms in intellectual disabilities: a challenge for translational outlooks, 46 (1 October 2014): 187–201. https://doi.org/10.1016/j.neubiorev.2014.01.011.
- Belichenko, Nadia P., Pavel V. Belichenko, Hong Hua Li, William C. Mobley, and Uta Francke. 'Comparative Study of Brain Morphology in Mecp2 Mutant Mouse Models of Rett Syndrome'. The Journal of Comparative Neurology 508, no. 1 (1 May 2008): 184–95. https://doi.org/10.1002/cne.21673.
- Belichenko, P. V., A. Oldfors, B. Hagberg, and A. Dahlström. 'Rett Syndrome: 3-D Confocal Microscopy of Cortical Pyramidal Dendrites and Afferents'. Neuroreport 5, no. 12 (21 July 1994): 1509–13.
- Belichenko, Pavel V., Elena E. Wright, Nadia P. Belichenko, Eliezer Masliah, Hong Hua Li, William C. Mobley, and Uta Francke. 'Widespread Changes in Dendritic and Axonal Morphology in Mecp2-Mutant Mouse Models of Rett Syndrome: Evidence for Disruption of Neuronal Networks'. Journal of Comparative Neurology 514, no. 3 (2009): 240–58. https://doi.org/10.1002/cne.22009.
- Bellesi, Michele, Luisa de Vivo, Giulio Tononi, and Chiara Cirelli. 'Effects of Sleep and Wake on Astrocytes: Clues from Molecular and Ultrastructural Studies'. BMC Biology 13, no. 1 (25 August 2015): 66. https://doi.org/10.1186/s12915-015-0176-7.
- Bellini, Elisa, Giulio Pavesi, Isabella Barbiero, Anna Bergo, Chetan Chandola, Mohammad S. Nawaz, Laura Rusconi, et al. 'MeCP2 Post-Translational Modifications: A Mechanism to Control Its Involvement in Synaptic Plasticity and Homeostasis?' Frontiers in Cellular Neuroscience 8 (13 August 2014). https://doi.org/10.3389/fncel.2014.00236.
- Belozor, Olga S., Dariya A. Yakovleva, Ilya V. Potapenko, Andrey N. Shuvaev, Marina V. Smolnikova, Alex Vasilev, Elena A. Pozhilenkova, and Anton N. Shuvaev. 'Extracellular S100β Disrupts Bergman Glia Morphology and Synaptic Transmission in Cerebellar Purkinje Cells'. Brain Sciences 9, no. 4 (12 April 2019). https://doi.org/10.3390/brainsci9040080.
- Beltrao, Pedro, Véronique Albanèse, Lillian R. Kenner, Danielle L. Swaney, Alma Burlingame, Judit Villén, Wendell A. Lim, James S. Fraser, Judith Frydman, and Nevan J. Krogan. 'Systematic Functional Prioritization of Protein Post-Translational Modifications'. Cell 150, no. 2 (20 July 2012): 413–25. https://doi.org/10.1016/j.cell.2012.05.036.
- Ben Haim, Lucile, and David H. Rowitch. 'Functional Diversity of Astrocytes in Neural Circuit Regulation'. Nature Reviews. Neuroscience 18, no. 1 (2017): 31–41. https://doi.org/10.1038/nrn.2016.159.
- Benner, Eric J., Dominic Luciano, Rebecca Jo, Khadar Abdi, Patricia Paez-Gonzalez, Huaxin Sheng, David S. Warner, Chunlei Liu, Cagla Eroglu, and Chay T. Kuo. 'Protective Astrogenesis from the SVZ Niche after Injury Is Controlled by Notch Modulator Thbs4'. Nature 497, no. 7449 (16 May 2013): 369–73. https://doi.org/10.1038/nature12069.
- Bergami, Matteo, Spartaco Santi, Elena Formaggio, Cinzia Cagnoli, Claudia Verderio, Robert Blum, Benedikt Berninger, Michela Matteoli, and Marco Canossa. 'Uptake and Recycling of Pro-

BDNF for Transmitter-Induced Secretion by Cortical Astrocytes'. The Journal of Cell Biology 183, no. 2 (20 October 2008): 213–21. https://doi.org/10.1083/jcb.200806137.

- Bergo, Anna, Marta Strollo, Marta Gai, Isabella Barbiero, Gilda Stefanelli, Sarah Sertic, Clementina Cobolli Gigli, Ferdinando Di Cunto, Charlotte Kilstrup-Nielsen, and Nicoletta Landsberger. 'Methyl-CpG Binding Protein 2 (MeCP2) Localizes at the Centrosome and Is Required for Proper Mitotic Spindle Organization'. The Journal of Biological Chemistry 290, no. 6 (6 February 2015): 3223–37. https://doi.org/10.1074/jbc.M114.608125.
- Bernardinelli, Yann, Dominique Muller, and Irina Nikonenko. 'Astrocyte-Synapse Structural Plasticity'. Review Article. Neural Plasticity. Hindawi, 8 January 2014. https://doi.org/10.1155/2014/232105.
- Berry, Kalen P., and Elly Nedivi. 'Spine Dynamics: Are They All the Same?' Neuron 96, no. 1 (27 September 2017): 43–55. https://doi.org/10.1016/j.neuron.2017.08.008.
- Bezzi, P., G. Carmignoto, L. Pasti, S. Vesce, D. Rossi, B.L. Rizzini, T. Pozzant, and A. Volterra. 'Prostaglandins Stimulate Calcium-Dependent Glutamate Release in Astrocytes'. Nature 391, no. 6664 (1998): 281–85. https://doi.org/10.1038/34651.
- Bezzi, Paola, Vidar Gundersen, José Luis Galbete, Gerald Seifert, Christian Steinhäuser, Ethel Pilati, and Andrea Volterra. 'Astrocytes Contain a Vesicular Compartment That Is Competent for Regulated Exocytosis of Glutamate'. Nature Neuroscience 7, no. 6 (June 2004): 613–20. https://doi.org/10.1038/nn1246.
- Bialas, Allison R., and Beth Stevens. 'TGF-β Signaling Regulates Neuronal C1q Expression and Developmental Synaptic Refinement'. Nature Neuroscience 16, no. 12 (December 2013): 1773–82. https://doi.org/10.1038/nn.3560.
- Bian, Wen-Jie, Wan-Ying Miao, Shun-Ji He, Zilong Qiu, and Xiang Yu. 'Coordinated Spine Pruning and Maturation Mediated by Inter-Spine Competition for Cadherin/Catenin Complexes'. Cell 162, no. 4 (13 August 2015): 808–22. https://doi.org/10.1016/j.cell.2015.07.018.
- Blanco-Suárez, Elena, Alison L. M. Caldwell, and Nicola J. Allen. 'Role of Astrocyte–Synapse Interactions in CNS Disorders'. The Journal of Physiology 595, no. 6 (2017): 1903–16. https://doi.org/10.1113/JP270988.
- Blondel, Olivier, Carlos Collin, William J. McCarran, Shiaoping Zhu, Rachel Zamostiano, Illana Gozes, Douglas E. Brenneman, and Ronald D. G. McKay. 'A Glia-Derived Signal Regulating Neuronal Differentiation'. Journal of Neuroscience 20, no. 21 (1 November 2000): 8012–20. https://doi.org/10.1523/JNEUROSCI.20-21-08012.2000.
- Boddum, Kim, Thomas P. Jensen, Vincent Magloire, Uffe Kristiansen, Dmitri A. Rusakov, Ivan Pavlov, and Matthew C. Walker. 'Astrocytic GABA Transporter Activity Modulates Excitatory Neurotransmission'. Nature Communications 7 (25 2016): 13572. https://doi.org/10.1038/ncomms13572.
- Bonansco, Christian, Alejandro Couve, Gertrudis Perea, Carla Á Ferradas, Manuel Roncagliolo, and Marco Fuenzalida. 'Glutamate Released Spontaneously from Astrocytes Sets the Threshold for Synaptic Plasticity'. The European Journal of Neuroscience 33, no. 8 (April 2011): 1483–92. https://doi.org/10.1111/j.1460-9568.2011.07631.x.
- Brahmachari, Saurav, Yiu K. Fung, and Kalipada Pahan. 'Induction of Glial Fibrillary Acidic Protein Expression in Astrocytes by Nitric Oxide'. The Journal of Neuroscience 26, no. 18 (3 May 2006): 4930–39. https://doi.org/10.1523/JNEUROSCI.5480-05.2006.
- Bröer, Stefan, and Neville Brookes. 'Transfer of Glutamine between Astrocytes and Neurons'. Journal of Neurochemistry 77, no. 3 (2001): 705–19. https://doi.org/10.1046/j.1471-4159.2001.00322.x.
- Brown, Kyla, Jim Selfridge, Sabine Lagger, John Connelly, Dina De Sousa, Alastair Kerr, Shaun Webb, et al. 'The Molecular Basis of Variable Phenotypic Severity among Common Missense

Mutations Causing Rett Syndrome'. Human Molecular Genetics 25, no. 3 (1 February 2016): 558–70. https://doi.org/10.1093/hmg/ddv496.

- Buchovecky, Christie M., Stephen D. Turley, Hannah M. Brown, Stephanie M. Kyle, Jeffrey G. McDonald, Benny Liu, Andrew A. Pieper, et al. 'A Suppressor Screen in Mecp2 Mutant Mice Implicates Cholesterol Metabolism in Rett Syndrome'. Nature Genetics 45, no. 9 (September 2013): 1013–20. https://doi.org/10.1038/ng.2714.
- Buffo, Annalisa, and Ferdinando Rossi. 'Origin, Lineage and Function of Cerebellar Glia'. Progress in Neurobiology 109 (1 October 2013): 42–63. https://doi.org/10.1016/j.pneurobio.2013.08.001.
- Buosi, Andrea Schmidt, Isadora Matias, Ana Paula Bergamo Araujo, Carolina Batista, and Flávia Carvalho Alcantara Gomes. 'Heterogeneity in Synaptogenic Profile of Astrocytes from Different Brain Regions'. Molecular Neurobiology 55, no. 1 (1 January 2018): 751–62. https://doi.org/10.1007/s12035-016-0343-z.
- Bushong, Eric A., Maryann E. Martone, Ying Z. Jones, and Mark H. Ellisman. 'Protoplasmic Astrocytes in CA1 Stratum Radiatum Occupy Separate Anatomical Domains'. The Journal of Neuroscience: The Official Journal of the Society for Neuroscience 22, no. 1 (1 January 2002): 183–92.
- Butt, A. M., K. Colquhoun, M. Tutton, and M. Berry. 'Three-Dimensional Morphology of Astrocytes and Oligodendrocytes in the Intact Mouse Optic Nerve'. Journal of Neurocytology 23, no. 8 (1 August 1994): 469–85. https://doi.org/10.1007/BF01184071.
- Cahoy, John D., Ben Emery, Amit Kaushal, Lynette C. Foo, Jennifer L. Zamanian, Karen S. Christopherson, Yi Xing, et al. 'A Transcriptome Database for Astrocytes, Neurons, and Oligodendrocytes: A New Resource for Understanding Brain Development and Function'. Journal of Neuroscience 28, no. 1 (2 January 2008): 264–78. https://doi.org/10.1523/JNEUROSCI.4178-07.2008.
- Caldwell, Alison L. M., Jolene K. Diedrich, Maxim N. Shokhirev, and Nicola J. Allen. 'Aberrant Astrocyte Protein Secretion Contributes to Altered Neuronal Development in Diverse Disorders'. BioRxiv, 17 February 2020, 2020.02.17.939991. https://doi.org/10.1101/2020.02.17.939991.
- Calfa, Gaston, Wei Li, John M. Rutherford, and Lucas Pozzo-Miller. 'Excitation/Inhibition Imbalance and Impaired Synaptic Inhibition in Hippocampal Area CA3 of Mecp2 Knockout Mice'. Hippocampus 25, no. 2 (February 2015): 159–68. https://doi.org/10.1002/hipo.22360.
- Calì, Corrado, Arnaud Tauffenberger, and Pierre Magistretti. 'The Strategic Location of Glycogen and Lactate: From Body Energy Reserve to Brain Plasticity'. Frontiers in Cellular Neuroscience 13 (2019). https://doi.org/10.3389/fncel.2019.00082.
- Campbell, Kenneth. 'Dorsal-Ventral Patterning in the Mammalian Telencephalon'. Current Opinion in Neurobiology 13, no. 1 (February 2003): 50–56. https://doi.org/10.1016/s0959-4388(03)00009-6.
- Can, Karolina, Christiane Menzfeld, Lena Rinne, Peter Rehling, Sebastian Kügler, Gocha Golubiani, Jan Dudek, and Michael Müller. 'Neuronal Redox-Imbalance in Rett Syndrome Affects Mitochondria as Well as Cytosol, and Is Accompanied by Intensified Mitochondrial O2 Consumption and ROS Release'. Frontiers in Physiology 10 (30 April 2019). https://doi.org/10.3389/fphys.2019.00479.
- Carter, J.C., D.C. Lanham, D. Pham, G. Bibat, S. Naidu, and W.E. Kaufmann. 'Selective Cerebral Volume Reduction in Rett Syndrome: A Multiple Approach MRI Study'. AJNR. American Journal of Neuroradiology 29, no. 3 (March 2008): 436–41. https://doi.org/10.3174/ajnr.A0857.
- Cebolla, Beatriz, and Mario Vallejo. 'Nuclear Factor-I Regulates Glial Fibrillary Acidic Protein Gene Expression in Astrocytes Differentiated from Cortical Precursor Cells'. Journal of Neurochemistry 97, no. 4 (2006): 1057–70. https://doi.org/10.1111/j.1471-4159.2006.03804.x.

- Cerrato, Valentina, Elena Parmigiani, María Figueres-Oñate, Marion Betizeau, Jessica Aprato, Ishira Nanavaty, Paola Berchialla, et al. 'Multiple Origins and Modularity in the Spatiotemporal Emergence of Cerebellar Astrocyte Heterogeneity'. PLoS Biology 16, no. 9 (27 September 2018). https://doi.org/10.1371/journal.pbio.2005513.
- Chahrour, Maria, and Huda Y. Zoghbi. 'The Story of Rett Syndrome: From Clinic to Neurobiology'. Neuron 56, no. 3 (8 November 2007): 422–37. https://doi.org/10.1016/j.neuron.2007.10.001.
- Chahrour, Maria, Sung Yun Jung, Chad Shaw, Xiaobo Zhou, Stephen T. C. Wong, Jun Qin, and Huda Y. Zoghbi. 'MeCP2, a Key Contributor to Neurological Disease, Activates and Represses Transcription'. Science (New York, N.Y.) 320, no. 5880 (30 May 2008): 1224–29. https://doi.org/10.1126/science.1153252.
- Chandler, S. P., D. Guschin, N. Landsberger, and A. P. Wolffe. 'The Methyl-CpG Binding Transcriptional Repressor MeCP2 Stably Associates with Nucleosomal DNA'. Biochemistry 38, no. 22 (1 June 1999): 7008–18. https://doi.org/10.1021/bi990224y.
- Chang, Qiang, Gargi Khare, Vardhan Dani, Sacha Nelson, and Rudolf Jaenisch. 'The Disease Progression of Mecp2 Mutant Mice Is Affected by the Level of BDNF Expression'. Neuron 49, no. 3 (2 February 2006): 341–48. https://doi.org/10.1016/j.neuron.2005.12.027.
- Chan-Palay, Victoria, and Sanford L. Palay. 'The Form of Velate Astrocytes in the Cerebellar Cortex of Monkey and Rat: High Voltage Electron Microscopy of Rapid Golgi Preparations'. Zeitschrift Für Anatomie Und Entwicklungsgeschichte 138, no. 1 (1 January 1972): 1–19. https://doi.org/10.1007/BF00519921.
- Chao, Hsiao-Tuan, Hongmei Chen, Rodney C. Samaco, Mingshan Xue, Maria Chahrour, Jong Yoo, Jeffrey L. Neul, et al. 'Dysfunction in GABA Signalling Mediates Autism-like Stereotypies and Rett Syndrome Phenotypes'. Nature 468, no. 7321 (11 November 2010): 263–69. https://doi.org/10.1038/nature09582.
- Chao, Hsiao-Tuan, Huda Y. Zoghbi, and Christian Rosenmund. 'MeCP2 Controls Excitatory Synaptic Strength by Regulating Glutamatergic Synapse Number'. Neuron 56, no. 1 (4 October 2007): 58–65. https://doi.org/10.1016/j.neuron.2007.08.018.
- Chapleau, Christopher A., Gaston D. Calfa, Meredith C. Lane, Asher J. Albertson, Jennifer L. Larimore, Shinichi Kudo, Dawna L. Armstrong, Alan K. Percy, and Lucas Pozzo-Miller. 'Dendritic Spine Pathologies in Hippocampal Pyramidal Neurons from Rett Syndrome Brain and after Expression of Rett-Associated MECP2 Mutations'. Neurobiology of Disease, Biomarkers of Neuropsychiatric Disease, 35, no. 2 (1 August 2009): 219–33. https://doi.org/10.1016/j.nbd.2009.05.001.
- Chen, R. Z., S. Akbarian, M. Tudor, and R. Jaenisch. 'Deficiency of Methyl-CpG Binding Protein-2 in CNS Neurons Results in a Rett-like Phenotype in Mice'. Nature Genetics 27, no. 3 (March 2001): 327–31. https://doi.org/10.1038/85906.
- Cheng, Ju, Min Huang, Ying Zhu, Yong-Juan Xin, Yun-Ke Zhao, Jian Huang, Jian-Xiu Yu, Wen-Hao Zhou, and Zilong Qiu. 'SUMOylation of MeCP2 Is Essential for Transcriptional Repression and Hippocampal Synapse Development'. Journal of Neurochemistry 128, no. 6 (March 2014): 798–806. https://doi.org/10.1111/jnc.12523.
- Cheng, Tian-Lin, and Zilong Qiu. 'MeCP2: Multifaceted Roles in Gene Regulation and Neural Development'. Neuroscience Bulletin 30, no. 4 (August 2014): 601–9. https://doi.org/10.1007/s12264-014-1452-6.
- Cheng, Tian-Lin, Jingqi Chen, Huida Wan, Bin Tang, Weidong Tian, Lujian Liao, and Zilong Qiu. 'Regulation of MRNA Splicing by MeCP2 via Epigenetic Modifications in the Brain'. Scientific Reports 7 (17 February 2017). https://doi.org/10.1038/srep42790.
- Cheng, Tian-Lin, Zhizhi Wang, Qiuming Liao, Ying Zhu, Wen-Hao Zhou, Wenqing Xu, and Zilong Qiu. 'MeCP2 Suppresses Nuclear MicroRNA Processing and Dendritic Growth by Regulating the

DGCR8/Drosha Complex'. Developmental Cell 28, no. 5 (10 March 2014): 547–60. https://doi.org/10.1016/j.devcel.2014.01.032.

- Cheval, Hélène, Jacky Guy, Cara Merusi, Dina De Sousa, Jim Selfridge, and Adrian Bird. 'Postnatal Inactivation Reveals Enhanced Requirement for MeCP2 at Distinct Age Windows'. Human Molecular Genetics 21, no. 17 (1 September 2012): 3806–14. https://doi.org/10.1093/hmg/dds208.
- Chi, P., P. Greengard, and T. A. Ryan. 'Synapsin Dispersion and Reclustering during Synaptic Activity'. Nature Neuroscience 4, no. 12 (December 2001): 1187–93. https://doi.org/10.1038/nn756.
- Christodoulou, John, and Linda S. Weaving. 'MECP2 and beyond: Phenotype-Genotype Correlations in Rett Syndrome'. Journal of Child Neurology 18, no. 10 (October 2003): 669–74. https://doi.org/10.1177/08830738030180100901.
- Christopherson, Karen S., Erik M. Ullian, Caleb C. A. Stokes, Christine E. Mullowney, Johannes W. Hell, Azin Agah, Jack Lawler, Deane F. Mosher, Paul Bornstein, and Ben A. Barres. 'Thrombospondins Are Astrocyte-Secreted Proteins That Promote CNS Synaptogenesis'. Cell 120, no. 3 (11 February 2005): 421–33. https://doi.org/10.1016/j.cell.2004.12.020.
- Chung, Won-Suk, Nicola J. Allen, and Cagla Eroglu. 'Astrocytes Control Synapse Formation, Function, and Elimination'. Cold Spring Harbor Perspectives in Biology 7, no. 9 (6 February 2015): a020370. https://doi.org/10.1101/cshperspect.a020370.
- Ciani, Lorenza, Kieran A. Boyle, Ellen Dickins, Macarena Sahores, Derek Anane, Douglas M. Lopes, Alasdair J. Gibb, and Patricia C. Salinas. 'Wnt7a Signaling Promotes Dendritic Spine Growth and Synaptic Strength through Ca2+/Calmodulin-Dependent Protein Kinase II'. Proceedings of the National Academy of Sciences of the United States of America 108, no. 26 (28 June 2011): 10732–37. https://doi.org/10.1073/pnas.1018132108.
- Claveria-Gimeno, Rafael, Pilar M. Lanuza, Ignacio Morales-Chueca, Olga C. Jorge-Torres, Sonia Vega, Olga Abian, Manel Esteller, and Adrian Velazquez-Campoy. 'The Intervening Domain from MeCP2 Enhances the DNA Affinity of the Methyl Binding Domain and Provides an Independent DNA Interaction Site'. Scientific Reports 7, no. 1 (March 2017): 41635. https://doi.org/10.1038/srep41635.
- Cobolli Gigli, Clementina, Linda Scaramuzza, Anna Gandaglia, Elisa Bellini, Marina Gabaglio, Daniela Parolaro, Charlotte Kilstrup-Nielsen, Nicoletta Landsberger, and Francesco Bedogni. 'MeCP2 Related Studies Benefit from the Use of CD1 as Genetic Background'. PloS One 11, no. 4 (2016): e0153473. https://doi.org/10.1371/journal.pone.0153473.
- Colantuoni, C., O. H. Jeon, K. Hyder, A. Chenchik, A. H. Khimani, V. Narayanan, E. P. Hoffman, W. E. Kaufmann, S. Naidu, and J. Pevsner. 'Gene Expression Profiling in Postmortem Rett Syndrome Brain: Differential Gene Expression and Patient Classification'. Neurobiology of Disease 8, no. 5 (October 2001): 847–65. https://doi.org/10.1006/nbdi.2001.0428.
- Connor, J. R., and E. M. Berkowitz. 'A Demonstration of Glial Filament Distribution in Astrocytes Isolated from Rat Cerebral Cortex'. Neuroscience 16, no. 1 (1 September 1985): 33–44. https://doi.org/10.1016/0306-4522(85)90044-2.
- Conti, Elena, and Elisa Izaurralde. 'Nonsense-Mediated MRNA Decay: Molecular Insights and Mechanistic Variations across Species'. Current Opinion in Cell Biology 17, no. 3 (June 2005): 316–25. https://doi.org/10.1016/j.ceb.2005.04.005.
- Cooper, A J, and F Plum. 'Biochemistry and Physiology of Brain Ammonia.' Physiological Reviews 67, no. 2 (1 April 1987): 440–519. https://doi.org/10.1152/physrev.1987.67.2.440.
- Correa-Gillieron, E. M., and L. A. Cavalcante. 'Synaptogenesis in Retino-Receptive Layers of the Superior Colliculus of the Opossum Didelphis Marsupialis'. Brain, Behavior and Evolution 54, no. 2 (August 1999): 71–84. https://doi.org/10.1159/000006614.

- Cortelazzo, Alessio, Claudio De Felice, Bianca De Filippis, Laura Ricceri, Giovanni Laviola, Silvia Leoncini, Cinzia Signorini, et al. 'Persistent Unresolved Inflammation in the Mecp2-308 Female Mutated Mouse Model of Rett Syndrome'. Mediators of Inflammation 2017 (2017). https://doi.org/10.1155/2017/9467819.
- Covelo, Ana, and Alfonso Araque. 'Neuronal Activity Determines Distinct Gliotransmitter Release from a Single Astrocyte'. ELife 7 (30 2018). https://doi.org/10.7554/eLife.32237.
- Cresto, Noémie, Laure-Elise Pillet, Pierre Billuart, and Nathalie Rouach. 'Do Astrocytes Play a Role in Intellectual Disabilities?' Trends in Neurosciences 42, no. 8 (August 2019): 518–27. https://doi.org/10.1016/j.tins.2019.05.011.
- Cuevas, Magdalena E., Mónica A. Carrasco, Yuly Fuentes, Patricio Castro, Francisco Nualart, Jorge Roa, and Luis G. Aguayo. 'The Presence of Glia Stimulates the Appearance of Glycinergic Synaptic Transmission in Spinal Cord Neurons'. Molecular and Cellular Neurosciences 28, no. 4 (April 2005): 770–78. https://doi.org/10.1016/j.mcn.2005.01.001.
- Cukier, Holly N., Alma M. Perez, Ann L. Collins, Zhaolan Zhou, Huda Y. Zoghbi, and Juan Botas. 'Genetic Modifiers of MeCP2 Function in Drosophila'. PLoS Genetics 4, no. 9 (5 September 2008). https://doi.org/10.1371/journal.pgen.1000179.
- Culmsee, Carsten, Susanne Michels, Stefanie Scheu, Volker Arolt, Udo Dannlowski, and Judith Alferink. 'Mitochondria, Microglia, and the Immune System—How Are They Linked in Affective Disorders?' Frontiers in Psychiatry 9 (2019). https://doi.org/10.3389/fpsyt.2018.00739.
- D'Ercole, A. J., P. Ye, A. S. Calikoglu, and G. Gutierrez-Ospina. 'The Role of the Insulin-like Growth Factors in the Central Nervous System'. Molecular Neurobiology 13, no. 3 (December 1996): 227–55. https://doi.org/10.1007/BF02740625.
- Dani, Vardhan S., Qiang Chang, Arianna Maffei, Gina G. Turrigiano, Rudolf Jaenisch, and Sacha B. Nelson. 'Reduced Cortical Activity Due to a Shift in the Balance between Excitation and Inhibition in a Mouse Model of Rett Syndrome'. Proceedings of the National Academy of Sciences of the United States of America 102, no. 35 (30 August 2005): 12560–65. https://doi.org/10.1073/pnas.0506071102.
- Darios, Frédéric, Catherine Wasser, Anastasia Shakirzyanova, Artur Giniatullin, Kerry Goodman, Jose L. Munoz-Bravo, Jesica Raingo, et al. 'Sphingosine Facilitates SNARE Complex Assembly and Activates Synaptic Vesicle Exocytosis'. Neuron 62, no. 5 (11 June 2009): 683–94. https://doi.org/10.1016/j.neuron.2009.04.024.
- Dave, Arpita, Foram Shukla, Hemendra Wala, and Prakash Pillai. 'Mitochondrial Electron Transport Chain Complex Dysfunction in MeCP2 Knock-Down Astrocytes: Protective Effects of Quercetin Hydrate'. Journal of Molecular Neuroscience: MN 67, no. 1 (January 2019): 16–27. https://doi.org/10.1007/s12031-018-1197-9.
- De Filippis, Bianca, Alessia Fabbri, Daiana Simone, Rossella Canese, Laura Ricceri, Fiorella Malchiodi-Albedi, Giovanni Laviola, and Carla Fiorentini. 'Modulation of RhoGTPases Improves the Behavioral Phenotype and Reverses Astrocytic Deficits in a Mouse Model of Rett Syndrome'. Neuropsychopharmacology 37, no. 5 (April 2012): 1152–63. https://doi.org/10.1038/npp.2011.301.
- Deacon, Robert M. J., Larry Glass, Mike Snape, Michael J. Hurley, Francisco J. Altimiras, Rodolfo R. Biekofsky, and Patricia Cogram. 'NNZ-2566, a Novel Analog of (1–3) IGF-1, as a Potential Therapeutic Agent for Fragile X Syndrome'. NeuroMolecular Medicine 17, no. 1 (1 March 2015): 71–82. https://doi.org/10.1007/s12017-015-8341-2.
- Deemyad, Tara, Joel Lüthi, and Nelson Spruston. 'Astrocytes Integrate and Drive Action Potential Firing in Inhibitory Subnetworks'. Nature Communications 9, no. 1 (18 2018): 4336. https://doi.org/10.1038/s41467-018-06338-3.

- Deigner, H. P., E. Gulbins, and R. A. Claus. ‘Sphingolipid Metabolism in Systemic Inflammation’. Intensive Care Medicine 2007 (2007): 249–66. https://doi.org/10.1007/978-3-540-49433-1_23.
- Deijk, Anne-Lieke F. van, Nutabi Camargo, Jaap Timmerman, Tim Heistek, Jos F. Brouwers, Floriana Mogavero, Huibert D. Mansvelder, August B. Smit, and Mark H.G. Verheijen. ‘Astrocyte Lipid Metabolism Is Critical for Synapse Development and Function in Vivo: Van Deijk et Al.’ Glia 65, no. 4 (April 2017): 670–82. https://doi.org/10.1002/glia.23120.
- Delépine, Chloé, Hamid Meziane, Juliette Nectoux, Matthieu Opitz, Amos B. Smith, Carlo Ballatore, Yoann Saillour, et al. ‘Altered Microtubule Dynamics and Vesicular Transport in Mouse and Human MeCP2-Deficient Astrocytes’. Human Molecular Genetics 25, no. 1 (1 January 2016): 146–57. https://doi.org/10.1093/hmg/ddv464.
- Delépine, Chloé, Juliette Nectoux, Franck Letourneur, Véronique Baud, Jamel Chelly, Pierre Billuart, and Thierry Bienvenu. ‘Astrocyte Transcriptome from the Mecp2(308)-Truncated Mouse Model of Rett Syndrome’. Neuromolecular Medicine 17, no. 4 (December 2015): 353–63. https://doi.org/10.1007/s12017-015-8363-9.
- Delépine, Chloé, Juliette Nectoux, Nadia Bahi-Buisson, Jamel Chelly, and Thierry Bienvenu. ‘MeCP2 Deficiency Is Associated with Impaired Microtubule Stability’. FEBS Letters 587, no. 2 (16 January 2013): 245–53. https://doi.org/10.1016/j.febslet.2012.11.033.
- Deneen, Benjamin, Ritchie Ho, Agnes Lukaszewicz, Christian J. Hochstim, Richard M. Gronostajski, and David J. Anderson. ‘The Transcription Factor NFIA Controls the Onset of Gliogenesis in the Developing Spinal Cord’. Neuron 52, no. 6 (21 December 2006): 953–68. https://doi.org/10.1016/j.neuron.2006.11.019.
- Dent, Erik W., Stephanie L. Gupton, and Frank B. Gertler. ‘The Growth Cone Cytoskeleton in Axon Outgrowth and Guidance’. Cold Spring Harbor Perspectives in Biology 3, no. 3 (1 March 2011). https://doi.org/10.1101/cshperspect.a001800.
- Deogracias, Rubén, Morteza Yazdani, Martijn P. J. Dekkers, Jacky Guy, Mihai Constantin S. Ionescu, Kaspar E. Vogt, and Yves-Alain Barde. ‘Fingolimod, a Sphingosine-1 Phosphate Receptor Modulator, Increases BDNF Levels and Improves Symptoms of a Mouse Model of Rett Syndrome’. Proceedings of the National Academy of Sciences of the United States of America 109, no. 35 (28 August 2012): 14230–35. https://doi.org/10.1073/pnas.1206093109.
- Derouet, Damien, François Rousseau, Fabienne Alfonsi, Josy Froger, Jacques Hermann, Fabien Barbier, David Perret, et al. ‘Neuropoietin, a New IL-6-Related Cytokine Signaling through the Ciliary Neurotrophic Factor Receptor’. Proceedings of the National Academy of Sciences of the United States of America 101, no. 14 (6 April 2004): 4827–32. https://doi.org/10.1073/pnas.0306178101.
- Derouiche, A, E Anlauf, G Aumann, B Mühlstädt, and M Lavialle. ‘Anatomical Aspects of Glia–Synapse Interaction: The Perisynaptic Glial Sheath Consists of a Specialized Astrocyte Compartment’. Journal of Physiology-Paris 96, no. 3 (1 May 2002): 177–82. https://doi.org/10.1016/S0928-4257(02)00004-9.
- Derouiche, A. ‘The Perisynaptic Astrocyte Process as a Glial Compartment-Immunolabeling for Glutamine Synthetase and Other Glial Markers’. In Advances in Molecular and Cell Biology, 31:147–63. Non-Neuronal Cells of the Nervous System: Function and Dysfunction. Elsevier, 2003. https://doi.org/10.1016/S1569-2558(03)31006-9.
- Derouiche, Amin, Julia Haseleu, and Horst-Werner Korf. ‘Fine Astrocyte Processes Contain Very Small Mitochondria: Glial Oxidative Capability May Fuel Transmitter Metabolism’. Neurochemical Research 40, no. 12 (1 December 2015): 2402–13. https://doi.org/10.1007/s11064-015-1563-8.
- Descalzi, Giannina, Virginia Gao, Michael Q. Steinman, Akinobu Suzuki, and Cristina M. Alberini. ‘Lactate from Astrocytes Fuels Learning-Induced MRNA Translation in Excitatory and Inhibitory Neurons’. Communications Biology 2, no. 1 (2 July 2019): 1–11. https://doi.org/10.1038/s42003-019-0495-2.

- Desler, Claus, Meryl S. Lillenes, Tone Tønjum, and Lene Juel Rasmussen. 'The Role of Mitochondrial Dysfunction in the Progression of Alzheimer's Disease'. Current Medicinal Chemistry 25, no. 40 (December 2018): 5578–87. https://doi.org/10.2174/0929867324666170616110111.
- Díaz-Vera, Jésica, Yézer G. Morales, Juan R. Hernández-Fernaud, Marcial Camacho, Mónica S. Montesinos, Federico Calegari, Wieland B. Huttner, Ricardo Borges, and José D. Machado. 'Chromogranin B Gene Ablation Reduces the Catecholamine Cargo and Decelerates Exocytosis in Chromaffin Secretory Vesicles'. The Journal of Neuroscience: The Official Journal of the Society for Neuroscience 30, no. 3 (20 January 2010): 950–57. https://doi.org/10.1523/JNEUROSCI.2894-09.2010.
- Dierssen, M., and G. J. A. Ramakers. 'Dendritic Pathology in Mental Retardation: From Molecular Genetics to Neurobiology'. Genes, Brain, and Behavior 5 Suppl 2 (2006): 48–60. https://doi.org/10.1111/j.1601-183X.2006.00224.x.
- Diniz, Luan Pereira, Juliana Carvalho Almeida, Vanessa Tortelli, Charles Vargas Lopes, Pedro Setti-Perdigão, Joice Stipursky, Suzana Assad Kahn, et al. 'Astrocyte-Induced Synaptogenesis Is Mediated by Transforming Growth Factor β Signaling through Modulation of D-Serine Levels in Cerebral Cortex Neurons'. The Journal of Biological Chemistry 287, no. 49 (30 November 2012): 41432–45. https://doi.org/10.1074/jbc.M112.380824.
- Diniz, Luan Pereira, Vanessa Tortelli, Matheus Nunes Garcia, Ana Paula Bérgamo Araújo, Helen M. Melo, Gisele S. Seixas da Silva, Fernanda G. De Felice, et al. 'Astrocyte Transforming Growth Factor Beta 1 Promotes Inhibitory Synapse Formation via CaM Kinase II Signaling'. Glia 62, no. 12 (December 2014): 1917–31. https://doi.org/10.1002/glia.22713.
- Donato, R., B. R. Cannon, G. Sorci, F. Riuzzi, K. Hsu, D. J. Weber, and C. L. Geczy. 'Functions of S100 Proteins'. Current Molecular Medicine 13, no. 1 (January 2013): 24–57.
- Dong, Qiping, Jason Kim, Linh Nguyen, Qian Bu, and Qiang Chang. 'An Astrocytic Influence on Impaired Tonic Inhibition in Hippocampal CA1 Pyramidal Neurons in a Mouse Model of Rett Syndrome'. Journal of Neuroscience, 2 July 2020. https://doi.org/10.1523/JNEUROSCI.3042-19.2020.
- Dong, Qiping, Qing Liu, Ronghui Li, Anxin Wang, Qian Bu, Kuan Hong Wang, and Qiang Chang. 'Mechanism and Consequence of Abnormal Calcium Homeostasis in Rett Syndrome Astrocytes'. ELife 7 (29 March 2018). https://doi.org/10.7554/eLife.33417.
- Downs, Jenny, Kingsley Wong, Madhur Ravikumara, Carolyn Ellaway, Elizabeth J. Elliott, John Christodoulou, Peter Jacoby, and Helen Leonard. 'Experience of Gastrostomy Using a Quality Care Framework: The Example of Rett Syndrome'. Medicine 93, no. 28 (December 2014): e328. https://doi.org/10.1097/MD.0000000000000328.
- Dumitriu, Dani, Jiandong Hao, Yuko Hara, Jeffrey Kaufmann, William G. M. Janssen, Wendy Lou, Peter R. Rapp, and John H. Morrison. 'Selective Changes in Thin Spine Density and Morphology in Monkey Prefrontal Cortex Correlate with Aging-Related Cognitive Impairment'. Journal of Neuroscience 30, no. 22 (2 June 2010): 7507–15. https://doi.org/10.1523/JNEUROSCI.6410-09.2010.
- Durand, Severine, Annarita Patrizi, Kathleen B. Quast, Lea Hachigian, Roman Pavlyuk, Alka Saxena, Piero Carninci, Takao K. Hensch, and Michela Fagiolini. 'NMDA Receptor Regulation Prevents Regression of Visual Cortical Function in the Absence of Mecp2'. Neuron 76, no. 6 (20 December 2012): 1078–90. https://doi.org/10.1016/j.neuron.2012.12.004.
- Durkee, Caitlin A., and Alfonso Araque. 'Diversity and Specificity of Astrocyte–Neuron Communication'. Neuroscience 396 (1 January 2019): 73–78. https://doi.org/10.1016/j.neuroscience.2018.11.010.
- Ebert, Daniel H., Harrison W. Gabel, Nathaniel D. Robinson, Nathaniel R. Kastan, Linda S. Hu, Sonia Cohen, Adrija J. Navarro, et al. 'Activity-Dependent Phosphorylation of MeCP2 Threonine

308 Regulates Interaction with NCoR'. Nature 499, no. 7458 (18 July 2013): 341–45. https://doi.org/10.1038/nature12348.

- Ehinger, Yann, Valerie Matagne, Laurent Villard, and Jean-Christophe Roux. 'Rett Syndrome from Bench to Bedside: Recent Advances'. F1000Research 7 (26 March 2018). https://doi.org/10.12688/f1000research.14056.1.
- Ehrhart, Friederike, Susan L. M. Coort, Elisa Cirillo, Eric Smeets, Chris T. Evelo, and Leopold Curfs. 'New Insights in Rett Syndrome Using Pathway Analysis for Transcriptomics Data'. Wiener Medizinische Wochenschrift (1946) 166, no. 11–12 (September 2016): 346–52. https://doi.org/10.1007/s10354-016-0488-4.
- Elias, Laura A. B., Doris D. Wang, and Arnold R. Kriegstein. 'Gap Junction Adhesion Is Necessary for Radial Migration in the Neocortex'. Nature 448, no. 7156 (23 August 2007): 901–7. https://doi.org/10.1038/nature06063.
- Elmariah, Sarina B., Eun Joo Oh, Ethan G. Hughes, and Rita J. Balice-Gordon. 'Astrocytes Regulate Inhibitory Synapse Formation via Trk-Mediated Modulation of Postsynaptic GABAA Receptors'. The Journal of Neuroscience: The Official Journal of the Society for Neuroscience 25, no. 14 (6 April 2005): 3638–50. https://doi.org/10.1523/JNEUROSCI.3980-04.2005.
- Emsley, Jason G., and Jeffrey D. Macklis. 'Astroglial Heterogeneity Closely Reflects the Neuronal-Defined Anatomy of the Adult Murine CNS'. Neuron Glia Biology 2, no. 3 (August 2006): 175–86. https://doi.org/10.1017/S1740925X06000202.
- Eng, L. F., J. J. Vanderhaeghen, A. Bignami, and B. Gerstl. 'An Acidic Protein Isolated from Fibrous Astrocytes'. Brain Research 28, no. 2 (7 May 1971): 351–54. https://doi.org/10.1016/0006-8993(71)90668-8.
- Eom, Tae-Yeon, Amelia Stanco, Jill Weimer, Kristen Stabingas, Elizabeth Sibrack, Vladimir Gukassyan, JrGang Cheng, and E. S. Anton. 'Direct Visualization of Microtubules Using a Genetic Tool to Analyse Radial Progenitor-Astrocyte Continuum in Brain'. Nature Communications 2, no. 1 (23 August 2011): 446. https://doi.org/10.1038/ncomms1460.
- Ericsson, Aaron C., Marcus J. Crim, and Craig L. Franklin. 'A Brief History of Animal Modeling'. Missouri Medicine 110, no. 3 (June 2013): 201–5.
- Erlandson, Anna, and Bengt Hagberg. 'MECP2 Abnormality Phenotypes: Clinicopathologic Area with Broad Variability'. Journal of Child Neurology 20, no. 9 (September 2005): 727–32. https://doi.org/10.1177/08830738050200090501.
- Eroglu, Cagla, and Ben A. Barres. 'Regulation of Synaptic Connectivity by Glia'. Nature 468, no. 7321 (11 November 2010): 223–31. https://doi.org/10.1038/nature09612.
- Eroglu, Cagla. 'The Role of Astrocyte-Secreted Matricellular Proteins in Central Nervous System Development and Function'. Journal of Cell Communication and Signaling 3, no. 3–4 (December 2009): 167–76. https://doi.org/10.1007/s12079-009-0078-y.
- Escartin, Carole, Elena Galea, András Lakatos, James P. O'Callaghan, Gabor C. Petzold, Alberto Serrano-Pozo, Christian Steinhäuser, et al. 'Reactive Astrocyte Nomenclature, Definitions, and Future Directions'. Nature Neuroscience, 15 February 2021, 1–14. https://doi.org/10.1038/s41593-020-00783-4.
- Eulenburg, Volker, Marina Retiounskaia, Theofilos Papadopoulos, Jesús Gomeza, and Heinrich Betz. 'Glial Glycine Transporter 1 Function Is Essential for Early Postnatal Survival but Dispensable in Adult Mice'. Glia 58, no. 9 (July 2010): 1066–73. https://doi.org/10.1002/glia.20987.
- Fagiolini, Michela, Annarita Patrizi, Jocelyn LeBlanc, Lee-Way Jin, Izumi Maezawa, Sarah Sinnett, Steven J. Gray, et al. 'Intellectual and Developmental Disabilities Research Centers: A Multidisciplinary Approach to Understand the Pathogenesis of Methyl-CpG Binding Protein 2-

Related Disorders'. Neuroscience, 29 April 2020. https://doi.org/10.1016/j.neuroscience.2020.04.037.

- Fantuzzo, J. A., V. R. Mirabella, A. H. Hamod, R. P. Hart, J. D. Zahn, and Z. P. Pang. 'Intellicount: High-Throughput Quantification of Fluorescent Synaptic Protein Puncta by Machine Learning'. ENeuro 4, no. 6 (6 December 2017). https://doi.org/10.1523/ENEURO.0219-17.2017.
- Farhy-Tselnicker, Isabella, Adriana C. M. van Casteren, Aletheia Lee, Veronica T. Chang, A. Radu Aricescu, and Nicola J. Allen. 'Astrocyte-Secreted Glypican 4 Regulates Release of Neuronal Pentraxin 1 from Axons to Induce Functional Synapse Formation'. Neuron 96, no. 2 (11 October 2017): 428-445.e13. https://doi.org/10.1016/j.neuron.2017.09.053.
- Farhy-Tselnicker, Isabella, and Nicola J. Allen. 'Astrocytes, Neurons, Synapses: A Tripartite View on Cortical Circuit Development'. Neural Development 13, no. 1 (01 2018): 7. https://doi.org/10.1186/s13064-018-0104-y.
- Farmer, W. Todd, Therése Abrahamsson, Sabrina Chierzi, Christopher Lui, Cristian Zaelzer, Emma V. Jones, Blandine Ponroy Bally, et al. 'Neurons Diversify Astrocytes in the Adult Brain through Sonic Hedgehog Signaling'. Science (New York, N.Y.) 351, no. 6275 (19 February 2016): 849–54. https://doi.org/10.1126/science.aab3103.
- Faundez, Victor, Meghan Wynne, Amanda Crocker, and Daniel Tarquinio. 'Molecular Systems Biology of Neurodevelopmental Disorders, Rett Syndrome as an Archetype'. Frontiers in Integrative Neuroscience 13 (2019). https://doi.org/10.3389/fnint.2019.00030.
- Ferreira, Ana C., Vitor Pinto, Sandro D. Mesquita, Ashley Novais, Joao C. Sousa, Margarida Correia-Neves, Nuno Sousa, Joana A. Palha, and Fernanda Marques. 'Lipocalin-2 Is Involved in Emotional Behaviors and Cognitive Function'. Frontiers in Cellular Neuroscience 7 (2013). https://doi.org/10.3389/fncel.2013.00122.
- Filosa, Alessandro, Sónia Paixão, Silke D. Honsek, Maria A. Carmona, Lore Becker, Berend Feddersen, Louise Gaitanos, et al. 'Neuron-Glia Communication via EphA4/Ephrin-A3 Modulates LTP through Glial Glutamate Transport'. Nature Neuroscience 12, no. 10 (October 2009): 1285–92. https://doi.org/10.1038/nn.2394.
- Flames, Nuria, Ramón Pla, Diego M. Gelman, John L. R. Rubenstein, Luis Puelles, and Oscar Marín. 'Delineation of Multiple Subpallial Progenitor Domains by the Combinatorial Expression of Transcriptional Codes'. The Journal of Neuroscience: The Official Journal of the Society for Neuroscience 27, no. 36 (5 September 2007): 9682–95. https://doi.org/10.1523/JNEUROSCI.2750-07.2007.
- Fleming, Jonathan T., Wenjuan He, Chuanming Hao, Tatiana Ketova, Fong C. Pan, Christopher C. V. Wright, Ying Litingtung, and Chin Chiang. 'The Purkinje Neuron Acts as a Central Regulator of Spatially and Functionally Distinct Cerebellar Precursors'. Developmental Cell 27, no. 3 (11 November 2013): 278–92. https://doi.org/10.1016/j.devcel.2013.10.008.
- Foo, Lynette C., Nicola J. Allen, Eric A. Bushong, P. Britten Ventura, Won-Suk Chung, Lu Zhou, John D. Cahoy, et al. 'Development of a Novel Method for the Purification and Culture of Rodent Astrocytes'. Neuron 71, no. 5 (8 September 2011): 799–811. https://doi.org/10.1016/j.neuron.2011.07.022.
- Fossat, Pascal, Fabrice R. Turpin, Silvia Sacchi, Jérôme Dulong, Ting Shi, Jean-Michel Rivet, Jonathan V. Sweedler, et al. 'Glial D-Serine Gates NMDA Receptors at Excitatory Synapses in Prefrontal Cortex'. Cerebral Cortex (New York, N.Y.: 1991) 22, no. 3 (March 2012): 595–606. https://doi.org/10.1093/cercor/bhr130.
- Frasca, Angelisa, Eleonora Spiombi, Michela Palmieri, Elena Albizzati, Maria Maddalena Valente, Anna Bergo, Barbara Leva, et al. 'MECP2 Mutations Affect Ciliogenesis: A Novel Perspective for Rett Syndrome and Related Disorders'. EMBO Molecular Medicine n/a, no. n/a (8 May 2020): e10270. https://doi.org/10.15252/emmm.201910270.

- Freeman, Marc R. ‘Specification and Morphogenesis of Astrocytes’. Science (New York, N.Y.) 330, no. 6005 (5 November 2010): 774–78. https://doi.org/10.1126/science.1190928.
- Frei, Jeannine A., Irwin Andermatt, Matthias Gesemann, and Esther T. Stoeckli. ‘The SynCAM Synaptic Cell Adhesion Molecules Are Involved in Sensory Axon Pathfinding by Regulating Axon-Axon Contacts’. Journal of Cell Science 127, no. Pt 24 (15 December 2014): 5288–5302. https://doi.org/10.1242/jcs.157032.
- Fukuda, Tetsuya, Masayuki Itoh, Tomio Ichikawa, Kazuo Washiyama, and Yu-ichi Goto. ‘Delayed Maturation of Neuronal Architecture and Synaptogenesis in Cerebral Cortex of Mecp2-Deficient Mice’. Journal of Neuropathology and Experimental Neurology 64, no. 6 (June 2005): 537–44. https://doi.org/10.1093/jnen/64.6.537.
- Fyffe, Sharyl L., Jeff L. Neul, Rodney C. Samaco, Hsiao-Tuan Chao, Shay Ben-Shachar, Paolo Moretti, Bryan E. McGill, et al. ‘Deletion of Mecp2 in Sim1-Expressing Neurons Reveals a Critical Role for MeCP2 in Feeding Behavior, Aggression, and the Response to Stress’. Neuron 59, no. 6 (25 September 2008): 947–58. https://doi.org/10.1016/j.neuron.2008.07.030.
- Gabel, Harrison W., Benyam Z. Kinde, Hume Stroud, Caitlin S. Gilbert, David A. Harmin, Nathaniel R. Kastan, Martin Hemberg, Daniel H. Ebert, and Michael E. Greenberg. ‘Disruption of DNA Methylation-Dependent Long Gene Repression in Rett Syndrome’. Nature 522, no. 7554 (4 June 2015): 89–93. https://doi.org/10.1038/nature14319.
- Gadalla, Kamal K. E., Thishnapha Vudhironarit, Ralph D. Hector, Sarah Sinnett, Noha G. Bahey, Mark E. S. Bailey, Steven J. Gray, and Stuart R. Cobb. ‘Development of a Novel AAV Gene Therapy Cassette with Improved Safety Features and Efficacy in a Mouse Model of Rett Syndrome’. Molecular Therapy - Methods & Clinical Development 5 (16 June 2017): 180–90. https://doi.org/10.1016/j.omtm.2017.04.007.
- Gandaglia, Anna, Elena Brivio, Sara Carli, Michela Palmieri, Francesco Bedogni, Gilda Stefanelli, Anna Bergo, et al. ‘A Novel Mecp2Y120D Knock-in Model Displays Similar Behavioral Traits But Distinct Molecular Features Compared to the Mecp2-Null Mouse Implying Precision Medicine for the Treatment of Rett Syndrome’. Molecular Neurobiology 56, no. 7 (July 2019): 4838–54. https://doi.org/10.1007/s12035-018-1412-2.
- Gandawijaya, Josan, Rosemary A. Bamford, J. Peter H. Burbach, and Asami Oguro-Ando. ‘Cell Adhesion Molecules Involved in Neurodevelopmental Pathways Implicated in 3p-Deletion Syndrome and Autism Spectrum Disorder’. Frontiers in Cellular Neuroscience 14 (2021). https://doi.org/10.3389/fncel.2020.611379.
- García-Marín, Virginia, Pablo García-López, and Miguel Freire. ‘Cajal’s Contributions to Glia Research’. Trends in Neurosciences 30, no. 9 (1 September 2007): 479–87. https://doi.org/10.1016/j.tins.2007.06.008.
- Garg, Saurabh K., Daniel T. Lioy, Hélène Cheval, James C. McGann, John M. Bissonnette, Matthew J. Murtha, Kevin D. Foust, Brian K. Kaspar, Adrian Bird, and Gail Mandel. ‘Systemic Delivery of MeCP2 Rescues Behavioral and Cellular Deficits in Female Mouse Models of Rett Syndrome’. The Journal of Neuroscience 33, no. 34 (21 August 2013): 13612–20. https://doi.org/10.1523/JNEUROSCI.1854-13.2013.
- Garg, Saurabh K., Daniel T. Lioy, Sharon J. Knopp, and John M. Bissonnette. ‘Conditional Depletion of Methyl-CpG-Binding Protein 2 in Astrocytes Depresses the Hypercapnic Ventilatory Response in Mice’. Journal of Applied Physiology (Bethesda, Md.: 1985) 119, no. 6 (15 September 2015): 670–76. https://doi.org/10.1152/japplphysiol.00411.2015.
- Gatto, Cheryl L., and Kendal Broadie. ‘Genetic Controls Balancing Excitatory and Inhibitory Synaptogenesis in Neurodevelopmental Disorder Models’. Frontiers in Synaptic Neuroscience 2 (7 June 2010). https://doi.org/10.3389/fnsyn.2010.00004.

- Ge, Woo-Ping, Atsushi Miyawaki, Fred H. Gage, Yuh Nung Jan, and Lily Yeh Jan. 'Local Generation of Glia Is a Major Astrocyte Source in Postnatal Cortex'. Nature 484, no. 7394 (28 March 2012): 376–80. https://doi.org/10.1038/nature10959.
- Gemelli, Terry, Olivier Berton, Erika D. Nelson, Linda I. Perrotti, Rudolf Jaenisch, and Lisa M. Monteggia. 'Postnatal Loss of Methyl-CpG Binding Protein 2 in the Forebrain Is Sufficient to Mediate Behavioral Aspects of Rett Syndrome in Mice'. Biological Psychiatry 59, no. 5 (1 March 2006): 468–76. https://doi.org/10.1016/j.biopsych.2005.07.025.
- Genoud, Christel, Charles Quairiaux, Pascal Steiner, Harald Hirling, Egbert Welker, and Graham W. Knott. 'Plasticity of Astrocytic Coverage and Glutamate Transporter Expression in Adult Mouse Cortex'. PLOS Biology 4, no. 11 (17 October 2006): e343. https://doi.org/10.1371/journal.pbio.0040343.
- Georgel, Philippe T., Rachel A. Horowitz-Scherer, Nick Adkins, Christopher L. Woodcock, Paul A. Wade, and Jeffrey C. Hansen. 'Chromatin Compaction by Human MeCP2 ASSEMBLY OF NOVEL SECONDARY CHROMATIN STRUCTURES IN THE ABSENCE OF DNA METHYLATION'. Journal of Biological Chemistry 278, no. 34 (22 August 2003): 32181–88. https://doi.org/10.1074/jbc.M305308200.
- Ghézali, Grégory, Charles-Félix Calvo, Laure-Elise Pillet, Flora Llense, Pascal Ezan, Ulrike Pannasch, Alexis-Pierre Bemelmans, Sandrine Etienne Manneville, and Nathalie Rouach. 'Connexin 30 Controls Astroglial Polarization during Postnatal Brain Development'. Development (Cambridge, England) 145, no. 4 (23 2018). https://doi.org/10.1242/dev.155275.
- Gold, Wendy A, Rahul Krishnarajy, Carolyn Ellaway, and John Christodoulou. 'Rett Syndrome: A Genetic Update and Clinical Review Focusing on Comorbidities'. ACS Chemical Neuroscience 9, no. 2 (21 February 2018): 167–76. https://doi.org/10.1021/acschemneuro.7b00346.
- Golgi C. Sulla sostanza connettiva del cervello (nevroglia). *Rendiconti del R Instituto Lombardo di Scienze e Lettere* 3: 275–277, 1870.
- Gómez-Casati, Maria E., Joshua C. Murtie, Carlos Rio, Konstantina Stankovic, M. Charles Liberman, and Gabriel Corfas. 'Nonneuronal Cells Regulate Synapse Formation in the Vestibular Sensory Epithelium via ErbB-Dependent BDNF Expression'. Proceedings of the National Academy of Sciences of the United States of America 107, no. 39 (28 September 2010): 17005–10. https://doi.org/10.1073/pnas.1008938107.
- Gonzales, Michael L., Sarrita Adams, Keith W. Dunaway, and Janine M. LaSalle. 'Phosphorylation of Distinct Sites in MeCP2 Modifies Cofactor Associations and the Dynamics of Transcriptional Regulation'. Molecular and Cellular Biology 32, no. 14 (July 2012): 2894–2903. https://doi.org/10.1128/MCB.06728-11.
- Goritz, Christian, Daniela H. Mauch, and Frank W. Pfrieger. 'Multiple Mechanisms Mediate Cholesterol-Induced Synaptogenesis in a CNS Neuron'. Molecular and Cellular Neurosciences 29, no. 2 (June 2005): 190–201. https://doi.org/10.1016/j.mcn.2005.02.006.
- Gourine, Alexander V., Vitaliy Kasymov, Nephtali Marina, Feige Tang, Melina F. Figueiredo, Samantha Lane, Anja G. Teschemacher, K. Michael Spyer, Karl Deisseroth, and Sergey Kasparov. 'Astrocytes Control Breathing through PH-Dependent Release of ATP'. Science (New York, N.Y.) 329, no. 5991 (30 July 2010): 571–75. https://doi.org/10.1126/science.1190721.
- Grosche, Jens, Helmut Kettenmann, and Andreas Reichenbach. 'Bergmann glial cells form distinct morphological structures to interact with cerebellar neurons'. Journal of Neuroscience Research 68, no. 2 (2002): 138–49. https://doi.org/10.1002/jnr.10197.
- Grosche, Jens, Vitali Matyash, Thomas Möller, Alexej Verkhratsky, Andreas Reichenbach, and Helmut Kettenmann. 'Microdomains for Neuron–Glia Interaction: Parallel Fiber Signaling to Bergmann Glial Cells'. Nature Neuroscience 2, no. 2 (February 1999): 139–43. https://doi.org/10.1038/5692.

- Grosser, Emanuel, Ursula Hirt, Oliwia A. Janc, Christiane Menzfeld, Marc Fischer, Belinda Kempkes, Steffen Vogelgesang, et al. 'Oxidative Burden and Mitochondrial Dysfunction in a Mouse Model of Rett Syndrome'. Neurobiology of Disease 48, no. 1 (October 2012): 102–14. https://doi.org/10.1016/j.nbd.2012.06.007.
- Guemez-Gamboa, Alicia, Nicole G. Coufal, and Joseph G. Gleeson. 'Primary Cilia in the Developing and Mature Brain'. Neuron 82, no. 3 (7 May 2014): 511–21. https://doi.org/10.1016/j.neuron.2014.04.024.
- Gulmez Karaca, Kubra, David V.C. Brito, and Ana M.M. Oliveira. 'MeCP2: A Critical Regulator of Chromatin in Neurodevelopment and Adult Brain Function'. International Journal of Molecular Sciences 20, no. 18 (16 September 2019). https://doi.org/10.3390/ijms20184577.
- Guy, J., B. Hendrich, M. Holmes, J. E. Martin, and A. Bird. 'A Mouse Mecp2-Null Mutation Causes Neurological Symptoms That Mimic Rett Syndrome'. Nature Genetics 27, no. 3 (March 2001): 322–26. https://doi.org/10.1038/85899.
- Guy, Jacky, Hélène Cheval, Jim Selfridge, and Adrian Bird. 'The Role of MeCP2 in the Brain'. Annual Review of Cell and Developmental Biology 27, no. 1 (10 October 2011): 631–52. https://doi.org/10.1146/annurev-cellbio-092910-154121.
- Guy, Jacky, Jian Gan, Jim Selfridge, Stuart Cobb, and Adrian Bird. 'Reversal of Neurological Defects in a Mouse Model of Rett Syndrome'. Science (New York, N.Y.) 315, no. 5815 (23 February 2007): 1143–47. https://doi.org/10.1126/science.1138389.
- Hagberg, B., J. Aicardi, K. Dias, and O. Ramos. 'A Progressive Syndrome of Autism, Dementia, Ataxia, and Loss of Purposeful Hand Use in Girls: Rett's Syndrome: Report of 35 Cases'. Annals of Neurology 14, no. 4 (October 1983): 471–79. https://doi.org/10.1002/ana.410140412.
- Halassa, Michael M., Tommaso Fellin, Hajime Takano, Jing-Hui Dong, and Philip G. Haydon. 'Synaptic Islands Defined by the Territory of a Single Astrocyte'. Journal of Neuroscience 27, no. 24 (13 June 2007): 6473–77. https://doi.org/10.1523/JNEUROSCI.1419-07.2007.
- Hama, Hiroshi, Chikako Hara, Kazuhiko Yamaguchi, and Atsushi Miyawaki. 'PKC Signaling Mediates Global Enhancement of Excitatory Synaptogenesis in Neurons Triggered by Local Contact with Astrocytes'. Neuron 41, no. 3 (5 February 2004): 405–15. https://doi.org/10.1016/s0896-6273(04)00007-8.
- Hampel, Harald, Filippo Caraci, A. Claudio Cuello, Giuseppe Caruso, Robert Nisticò, Massimo Corbo, Filippo Baldacci, et al. 'A Path Toward Precision Medicine for Neuroinflammatory Mechanisms in Alzheimer's Disease'. Frontiers in Immunology 11 (31 March 2020). https://doi.org/10.3389/fimmu.2020.00456.
- Hanefeld, F. 'The Clinical Pattern of the Rett Syndrome'. Brain & Development 7, no. 3 (1985): 320–25. https://doi.org/10.1016/s0387-7604(85)80037-1.
- Hansson, Elisabeth. 'Transport of Monoamine and Amino Acid Neurotransmitters by Primary Astroglial Cultures'. Neurochemical Research 10, no. 5 (1 May 1985): 667–75. https://doi.org/10.1007/BF00964405.
- Harikrishnan, K. N., Maggie Z. Chow, Emma K. Baker, Sharmistha Pal, Sahar Bassal, Daniella Brasacchio, Li Wang, et al. 'Brahma Links the SWI/SNF Chromatin-Remodeling Complex with MeCP2-Dependent Transcriptional Silencing'. Nature Genetics 37, no. 3 (March 2005): 254–64. https://doi.org/10.1038/ng1516.
- Haydon, Philip G., and Giorgio Carmignoto. 'Astrocyte Control of Synaptic Transmission and Neurovascular Coupling'. Physiological Reviews 86, no. 3 (July 2006): 1009–31. https://doi.org/10.1152/physrev.00049.2005.
- He, Jingyi, Guofu Zhu, Guoqing Wang, and Feng Zhang. 'Oxidative Stress and Neuroinflammation Potentiate Each Other to Promote Progression of Dopamine

Neurodegeneration'. Review Article. Oxidative Medicine and Cellular Longevity. Hindawi, 3 July 2020. https://doi.org/10.1155/2020/6137521.

- Heller, Janosch P., and Dmitri A. Rusakov. 'Morphological Plasticity of Astroglia: Understanding Synaptic Microenvironment'. Glia 63, no. 12 (2015): 2133–51. https://doi.org/10.1002/glia.22821.
- Hendrich, Brian, and Susan Tweedie. 'The Methyl-CpG Binding Domain and the Evolving Role of DNA Methylation in Animals'. Trends in Genetics: TIG 19, no. 5 (May 2003): 269–77. https://doi.org/10.1016/S0168-9525(03)00080-5.
- Henneberger, Christian, Thomas Papouin, Stéphane H. R. Oliet, and Dmitri A. Rusakov. 'Long-Term Potentiation Depends on Release of D-Serine from Astrocytes'. Nature 463, no. 7278 (14 January 2010): 232–36. https://doi.org/10.1038/nature08673.
- Hertz, L., Y. Chen, M. E. Gibbs, P. Zang, and L. Peng. 'Astrocytic Adrenoceptors: A Major Drug Target in Neurological and Psychiatric Disorders?' Current Drug Targets. CNS and Neurological Disorders 3, no. 3 (June 2004): 239–67. https://doi.org/10.2174/1568007043337535.
- Hertz, Leif, Ralf Dringen, Arne Schousboe, and Stephen R. Robinson. 'Astrocytes: Glutamate Producers for Neurons'. Journal of Neuroscience Research 57, no. 4 (1999): 417–28. https://doi.org/10.1002/(SICI)1097-4547(19990815)57:4<417::AID-JNR1>3.0.CO;2-N.
- Hertz, Leif. 'The Glutamate-Glutamine (GABA) Cycle: Importance of Late Postnatal Development and Potential Reciprocal Interactions between Biosynthesis and Degradation'. Frontiers in Endocrinology 4 (2013): 59. https://doi.org/10.3389/fendo.2013.00059.
- Hillen, Anne E. J., J. Peter H. Burbach, and Elly M. Hol. 'Cell Adhesion and Matricellular Support by Astrocytes of the Tripartite Synapse'. Progress in Neurobiology 165–167 (August 2018): 66–86. https://doi.org/10.1016/j.pneurobio.2018.02.002.
- Hinderer, Christian, Nathan Katz, Elizabeth L. Buza, Cecilia Dyer, Tamara Goode, Peter Bell, Laura K. Richman, and James M. Wilson. 'Severe Toxicity in Nonhuman Primates and Piglets Following High-Dose Intravenous Administration of an Adeno-Associated Virus Vector Expressing Human SMN'. Human Gene Therapy 29, no. 3 (29 January 2018): 285–98. https://doi.org/10.1089/hum.2018.015.
- Hines, Dustin J., and Philip G. Haydon. 'Astrocytic Adenosine: From Synapses to Psychiatric Disorders'. Philosophical Transactions of the Royal Society B: Biological Sciences 369, no. 1654 (19 October 2014). https://doi.org/10.1098/rstb.2013.0594.
- Hirabayashi, Yusuke, Nao Suzki, Masafumi Tsuboi, Takaho A. Endo, Tetsuro Toyoda, Jun Shinga, Haruhiko Koseki, Miguel Vidal, and Yukiko Gotoh. 'Polycomb Limits the Neurogenic Competence of Neural Precursor Cells to Promote Astrogenic Fate Transition'. Neuron 63, no. 5 (10 September 2009): 600–613. https://doi.org/10.1016/j.neuron.2009.08.021.
- Hirrlinger, Johannes, Swen Hülsmann, and Frank Kirchhoff. 'Astroglial Processes Show Spontaneous Motility at Active Synaptic Terminals in Situ'. European Journal of Neuroscience 20, no. 8 (2004): 2235–39. https://doi.org/10.1111/j.1460-9568.2004.03689.x.
- Hite, Kristopher C., Valerie H. Adams, and Jeffrey C. Hansen. 'Recent Advances in MeCP2 Structure and Function'. Biochemistry and Cell Biology = Biochimie et Biologie Cellulaire 87, no. 1 (February 2009): 219–27. https://doi.org/10.1139/o08-115.
- Hoogland, Tycho M., and Bernd Kuhn. 'Recent Developments in the Understanding of Astrocyte Function in the Cerebellum In Vivo'. The Cerebellum 9, no. 3 (1 September 2010): 264–71. https://doi.org/10.1007/s12311-009-0139-z.
- Howarth, Clare. 'The Contribution of Astrocytes to the Regulation of Cerebral Blood Flow'. Frontiers in Neuroscience 8 (2014). https://doi.org/10.3389/fnins.2014.00103.
- Howell, C. James, Michael P. Sceniak, Min Lang, Wenceslas Krakowiecki, Fatimah E. Abouelsoud, Saloni U. Lad, Heping Yu, and David M. Katz. 'Activation of the Medial Prefrontal

Cortex Reverses Cognitive and Respiratory Symptoms in a Mouse Model of Rett Syndrome'. ENeuro 4, no. 6 (December 2017). https://doi.org/10.1523/ENEURO.0277-17.2017.

- Hu, Xin, Yimin Yuan, Dan Wang, and Zhida Su. 'Heterogeneous Astrocytes: Active Players in CNS'. Brain Research Bulletin 125 (2016): 1–18. https://doi.org/10.1016/j.brainresbull.2016.03.017.
- Huang, Y., S. J. Myers, and R. Dingledine. 'Transcriptional Repression by REST: Recruitment of Sin3A and Histone Deacetylase to Neuronal Genes'. Nature Neuroscience 2, no. 10 (October 1999): 867–72. https://doi.org/10.1038/13165.
- Hughes, Ethan G., Sarina B. Elmariah, and Rita J. Balice-Gordon. 'Astrocyte Secreted Proteins Selectively Increase Hippocampal GABAergic Axon Length, Branching, and Synaptogenesis'. Molecular and Cellular Neuroscience 43, no. 1 (1 January 2010): 136–45. https://doi.org/10.1016/j.mcn.2009.10.004.
- Inan, Melis, and Michael C. Crair. 'Development of Cortical Maps: Perspectives From the Barrel Cortex': The Neuroscientist, 29 June 2016. https://doi.org/10.1177/1073858406296257.
- Ip, Jacque P. K., Nikolaos Mellios, and Mriganka Sur. 'Rett Syndrome: Insights into Genetic, Molecular and Circuit Mechanisms'. Nature Reviews. Neuroscience 19, no. 6 (2018): 368–82. https://doi.org/10.1038/s41583-018-0006-3.
- Irmady, Krithi, Sabrina Zechel, and Klaus Unsicker. 'Fibroblast Growth Factor 2 Regulates Astrocyte Differentiation in a Region-Specific Manner in the Hindbrain'. Glia 59, no. 5 (May 2011): 708–19. https://doi.org/10.1002/glia.21141.
- Jakimiec, Martyna, Justyna Paprocka, and Robert Śmigiel. 'CDKL5 Deficiency Disorder-A Complex Epileptic Encephalopathy'. Brain Sciences 10, no. 2 (17 February 2020). https://doi.org/10.3390/brainsci10020107.
- Jentarra, Garilyn M., Shannon L. Olfers, Stephen G. Rice, Nishit Srivastava, Gregg E. Homanics, Mary Blue, SakkuBai Naidu, and Vinodh Narayanan. 'Abnormalities of Cell Packing Density and Dendritic Complexity in the MeCP2 A140V Mouse Model of Rett Syndrome/X-Linked Mental Retardation'. BMC Neuroscience 11, no. 1 (17 February 2010): 19. https://doi.org/10.1186/1471-2202-11-19.
- Jiang, Nona M., Maureen Cowan, Shannon N. Moonah, and William A. Petri. 'The Impact of Systemic Inflammation on Neurodevelopment'. Trends in Molecular Medicine 24, no. 9 (September 2018): 794–804. https://doi.org/10.1016/j.molmed.2018.06.008.
- Jin, Jing, Xinhua Bao, Hansen Wang, Hong Pan, Yuzhi Zhang, and Xiru Wu. 'RNAi-Induced down-Regulation of Mecp2 Expression in the Rat Brain'. International Journal of Developmental Neuroscience: The Official Journal of the International Society for Developmental Neuroscience 26, no. 5 (August 2008): 457–65. https://doi.org/10.1016/j.ijdevneu.2008.02.009.
- Jin, Xu-Rui, Xing-Shu Chen, and Lan Xiao. 'MeCP2 Deficiency in Neuroglia: New Progress in the Pathogenesis of Rett Syndrome'. Frontiers in Molecular Neuroscience 10 (2017): 316. https://doi.org/10.3389/fnmol.2017.00316.
- Jo, Seonmi, Oleg Yarishkin, Yu Jin Hwang, Ye Eun Chun, Mijeong Park, Dong Ho Woo, Jin Young Bae, et al. 'GABA from Reactive Astrocytes Impairs Memory in Mouse Models of Alzheimer's Disease'. Nature Medicine 20, no. 8 (August 2014): 886–96. https://doi.org/10.1038/nm.3639.
- Jobe, Emily M., Andrea L. McQuate, and Xinyu Zhao. 'Crosstalk among Epigenetic Pathways Regulates Neurogenesis'. Frontiers in Neuroscience 6 (2012). https://doi.org/10.3389/fnins.2012.00059.
- Johnson, Brian S., Ying-Tao Zhao, Maria Fasolino, Janine M. Lamonica, Yoon Jung Kim, George Georgakilas, Kathleen H. Wood, et al. 'Biotin Tagging of MeCP2 in Mice Reveals Contextual Insights into the Rett Syndrome Transcriptome'. Nature Medicine 23, no. 10 (October 2017): 1203–14. https://doi.org/10.1038/nm.4406.

- Johnston, I. G., T. Paladino, J. W. Gurd, and I. R. Brown. ‘Molecular Cloning of SC1: A Putative Brain Extracellular Matrix Glycoprotein Showing Partial Similarity to Osteonectin/BM40/SPARC’. Neuron 4, no. 1 (January 1990): 165–76. https://doi.org/10.1016/0896-6273(90)90452-l.
- Jones, Emma V., and David S. Bouvier. ‘Astrocyte-Secreted Matricellular Proteins in CNS Remodelling during Development and Disease’. Neural Plasticity 2014 (2014): 321209. https://doi.org/10.1155/2014/321209.
- Jones, Emma V., Yann Bernardinelli, Yiu Chung Tse, Sabrina Chierzi, Tak Pan Wong, and Keith K. Murai. ‘Astrocytes Control Glutamate Receptor Levels at Developing Synapses through SPARC-Beta-Integrin Interactions’. The Journal of Neuroscience: The Official Journal of the Society for Neuroscience 31, no. 11 (16 March 2011): 4154–65. https://doi.org/10.1523/JNEUROSCI.4757-10.2011.
- Jordan, ChaRandle, Hong Hua Li, Helen C. Kwan, and Uta Francke. ‘Cerebellar Gene Expression Profiles of Mouse Models for Rett Syndrome Reveal Novel MeCP2 Targets’. BMC Medical Genetics 8 (20 June 2007): 36. https://doi.org/10.1186/1471-2350-8-36.
- Jourdain, Pascal, Linda H. Bergersen, Khaleel Bhaukaurally, Paola Bezzi, Mirko Santello, Maria Domercq, Carlos Matute, Fiorella Tonello, Vidar Gundersen, and Andrea Volterra. ‘Glutamate Exocytosis from Astrocytes Controls Synaptic Strength’. Nature Neuroscience 10, no. 3 (March 2007): 331–39. https://doi.org/10.1038/nn1849.
- Jugloff, Denis G. M., Richard Logan, and James H. Eubanks. ‘Breeding and Maintenance of an Mecp2-Deficient Mouse Model of Rett Syndrome’. Journal of Neuroscience Methods 154, no. 1–2 (30 June 2006): 89–95. https://doi.org/10.1016/j.jneumeth.2005.12.002.
- Kahanovitch, Uri, Kelsey C. Patterson, Raymundo Hernandez, and Michelle L. Olsen. ‘Glial Dysfunction in MeCP2 Deficiency Models: Implications for Rett Syndrome’. International Journal of Molecular Sciences 20, no. 15 (5 August 2019). https://doi.org/10.3390/ijms20153813.
- Kahanovitch, Uri, Vishnu A. Cuddapah, Natasha L. Pacheco, Leanne M. Holt, Daniel K. Mulkey, Alan K. Percy, and Michelle L. Olsen. ‘MeCP2 Deficiency Leads to Loss of Glial Kir4.1’. ENeuro 5, no. 1 (February 2018). https://doi.org/10.1523/ENEURO.0194-17.2018.
- Kang, Peng, Hyun Kyoung Lee, Stacey M. Glasgow, Meggie Finley, Tataka Donti, Zachary B. Gaber, Brett H. Graham, et al. ‘Sox9 and NFIA Coordinate a Transcriptional Regulatory Cascade during the Initiation of Gliogenesis’. Neuron 74, no. 1 (12 April 2012): 79–94. https://doi.org/10.1016/j.neuron.2012.01.024.
- Kanski, Regina, Miriam E. van Strien, Paula van Tijn, and Elly M. Hol. ‘A Star Is Born: New Insights into the Mechanism of Astrogenesis’. Cellular and Molecular Life Sciences: CMLS 71, no. 3 (February 2014): 433–47. https://doi.org/10.1007/s00018-013-1435-9.
- Karhunen, T., C. Tilgmann, I. Ulmanen, and P. Panula. ‘Neuronal and Non-Neuronal Catechol-O-Methyltransferase in Primary Cultures of Rat Brain Cells’. International Journal of Developmental Neuroscience: The Official Journal of the International Society for Developmental Neuroscience 13, no. 8 (December 1995): 825–34. https://doi.org/10.1016/0736-5748(95)00070-4.
- Kasparov, Sergey. ‘Are Astrocytes the Pressure-Reservoirs of Lactate in the Brain?’ Cell Metabolism 23, no. 1 (12 January 2016): 1–2. https://doi.org/10.1016/j.cmet.2015.11.001.
- Katz, David M., Joanne E. Berger-Sweeney, James H. Eubanks, Monica J. Justice, Jeffrey L. Neul, Lucas Pozzo-Miller, Mary E. Blue, et al. ‘Preclinical Research in Rett Syndrome: Setting the Foundation for Translational Success’. Disease Models & Mechanisms 5, no. 6 (November 2012): 733–45. https://doi.org/10.1242/dmm.011007.
- Kerr, Kimberly S., Yuly Fuentes-Medel, Cassandra Brewer, Romina Barria, James Ashley, Katharine C. Abruzzi, Amy Sheehan, Ozge E. Tasdemir-Yilmaz, Marc R. Freeman, and Vivian Budnik. ‘Glial Wingless/Wnt Regulates Glutamate Receptor Clustering and Synaptic Physiology

at the Drosophila Neuromuscular Junction'. The Journal of Neuroscience: The Official Journal of the Society for Neuroscience 34, no. 8 (19 February 2014): 2910–20. https://doi.org/10.1523/JNEUROSCI.3714-13.2014.

- Kim, Kun-Yong, Eriona Hysolli, and In-Hyun Park. 'Neuronal Maturation Defect in Induced Pluripotent Stem Cells from Patients with Rett Syndrome'. Proceedings of the National Academy of Sciences of the United States of America 108, no. 34 (23 August 2011): 14169–74. https://doi.org/10.1073/pnas.1018979108.
- Kimelberg, Harold K. 'The Problem of Astrocyte Identity'. Neurochemistry International, Glial Biology: Functional Interactions Among Glia and Neurons, 45, no. 2 (1 July 2004): 191–202. https://doi.org/10.1016/j.neuint.2003.08.015.
- Kinde, Benyam, Harrison W. Gabel, Caitlin S. Gilbert, Eric C. Griffith, and Michael E. Greenberg. 'Reading the Unique DNA Methylation Landscape of the Brain: Non-CpG Methylation, Hydroxymethylation, and MeCP2'. Proceedings of the National Academy of Sciences 112, no. 22 (2 June 2015): 6800–6806. https://doi.org/10.1073/pnas.1411269112.
- Kintner, Douglas B., Jing Luo, Josiah Gerdts, Andy J. Ballard, Gary E. Shull, and Dandan Sun. 'Role of Na+-K+-Cl− Cotransport and Na+/Ca2+ Exchange in Mitochondrial Dysfunction in Astrocytes Following in Vitro Ischemia'. American Journal of Physiology-Cell Physiology 292, no. 3 (1 March 2007): C1113–22. https://doi.org/10.1152/ajpcell.00412.2006.
- Kita, Yoshiaki, Koichi Kawakami, Yoshiko Takahashi, and Fujio Murakami. 'Development of Cerebellar Neurons and Glias Revealed by in Utero Electroporation: Golgi-Like Labeling of Cerebellar Neurons and Glias'. PLOS ONE 8, no. 7 (23 July 2013): e70091. https://doi.org/10.1371/journal.pone.0070091.
- Klengel, Torsten, and Elisabeth B. Binder. 'FKBP5 Allele-Specific Epigenetic Modification in Gene by Environment Interaction'. Neuropsychopharmacology: Official Publication of the American College of Neuropsychopharmacology 40, no. 1 (January 2015): 244–46. https://doi.org/10.1038/npp.2014.208.
- Kohyama, Jun, Tsukasa Sanosaka, Akinori Tokunaga, Eriko Takatsuka, Keita Tsujimura, Hideyuki Okano, and Kinichi Nakashima. 'BMP-Induced REST Regulates the Establishment and Maintenance of Astrocytic Identity'. The Journal of Cell Biology 189, no. 1 (5 April 2010): 159–70. https://doi.org/10.1083/jcb.200908048.
- Koulakoff, Annette, Pascal Ezan, and Christian Giaume. 'Neurons Control the Expression of Connexin 30 and Connexin 43 in Mouse Cortical Astrocytes'. Glia 56, no. 12 (2008): 1299–1311. https://doi.org/10.1002/glia.20698.
- Krencik, Robert, Jason P. Weick, Yan Liu, Zhi-Jian Zhang, and Su-Chun Zhang. 'Specification of Transplantable Astroglial Subtypes from Human Pluripotent Stem Cells'. Nature Biotechnology 29, no. 6 (22 May 2011): 528–34. https://doi.org/10.1038/nbt.1877.
- Krishnaraj, Rahul, Florencia Haase, Bronte Coorey, Edward J. Luca, Ingar Wong, Alexandra Boyling, Carolyn Ellaway, John Christodoulou, and Wendy A. Gold. 'Genome-Wide Transcriptomic and Proteomic Studies of Rett Syndrome Mouse Models Identify Common Signaling Pathways and Cellular Functions as Potential Therapeutic Targets'. Human Mutation 40, no. 12 (2019): 2184–96. https://doi.org/10.1002/humu.23887.
- Krishnaraj, Rahul, Gladys Ho, and John Christodoulou. 'RettBASE: Rett Syndrome Database Update'. Human Mutation 38, no. 8 (2017): 922–31. https://doi.org/10.1002/humu.23263.
- Kron, Miriam, C. James Howell, Ian T. Adams, Michael Ransbottom, Diana Christian, Michael Ogier, and David M. Katz. 'Brain Activity Mapping in Mecp2 Mutant Mice Reveals Functional Deficits in Forebrain Circuits, Including Key Nodes in the Default Mode Network, That Are Reversed with Ketamine Treatment'. The Journal of Neuroscience: The Official Journal of the Society for Neuroscience 32, no. 40 (3 October 2012): 13860–72. https://doi.org/10.1523/JNEUROSCI.2159-12.2012.

- Kruusvee, Valdeko, Matthew J. Lyst, Ceitidh Taylor, Žygimantė Tarnauskaitė, Adrian P. Bird, and Atlanta G. Cook. 'Structure of the MeCP2–TBLR1 Complex Reveals a Molecular Basis for Rett Syndrome and Related Disorders'. Proceedings of the National Academy of Sciences of the United States of America 114, no. 16 (18 April 2017): E3243–50. https://doi.org/10.1073/pnas.1700731114.
- Kucukdereli, Hakan, Nicola J. Allen, Anthony T. Lee, Ava Feng, M. Ilcim Ozlu, Laura M. Conatser, Chandrani Chakraborty, et al. 'Control of Excitatory CNS Synaptogenesis by Astrocyte-Secreted Proteins Hevin and SPARC'. Proceedings of the National Academy of Sciences 108, no. 32 (9 August 2011): 12983–84.
- Kullmann, Dimitri M. 'Interneuron Networks in the Hippocampus'. Current Opinion in Neurobiology 21, no. 5 (October 2011): 709–16. https://doi.org/10.1016/j.conb.2011.05.006.
- Kyle, Stephanie M., Neeti Vashi, and Monica J. Justice. 'Rett Syndrome: A Neurological Disorder with Metabolic Components'. Open Biology 8, no. 2 (2018). https://doi.org/10.1098/rsob.170216.
- Landén, M., B. Grenfeldt, P. Davidsson, M. Stridsberg, B. Regland, C. G. Gottfries, and K. Blennow. 'Reduction of Chromogranin A and B but Not C in the Cerebrospinal Fluid in Subjects with Schizophrenia'. European Neuropsychopharmacology: The Journal of the European College of Neuropsychopharmacology 9, no. 4 (June 1999): 311–15. https://doi.org/10.1016/s0924-977x(98)00042-x.
- Landi, Silvia, Elena Putignano, Elena Maria Boggio, Maurizio Giustetto, Tommaso Pizzorusso, and Gian Michele Ratto. 'The Short-Time Structural Plasticity of Dendritic Spines Is Altered in a Model of Rett Syndrome'. Scientific Reports 1, no. 1 (25 July 2011): 45. https://doi.org/10.1038/srep00045.
- Lanjakornsiripan, Darin, Baek-Jun Pior, Daichi Kawaguchi, Shohei Furutachi, Tomoaki Tahara, Yu Katsuyama, Yutaka Suzuki, Yugo Fukazawa, and Yukiko Gotoh. 'Layer-Specific Morphological and Molecular Differences in Neocortical Astrocytes and Their Dependence on Neuronal Layers'. Nature Communications 9, no. 1 (24 April 2018): 1623. https://doi.org/10.1038/s41467-018-03940-3.
- Lavialle, Monique, Georg Aumann, Enrico Anlauf, Felicitas Pröls, Monique Arpin, and Amin Derouiche. 'Structural Plasticity of Perisynaptic Astrocyte Processes Involves Ezrin and Metabotropic Glutamate Receptors'. Proceedings of the National Academy of Sciences 108, no. 31 (2 August 2011): 12915–19. https://doi.org/10.1073/pnas.1100957108.
- Le, Thi Thanh Huong, Ngoc Tung Tran, Thi Mai Lan Dao, Dinh Dung Nguyen, Huy Duong Do, Thi Lien Ha, Ralf Kühn, Thanh Liem Nguyen, Klaus Rajewsky, and Van Trung Chu. 'Efficient and Precise CRISPR/Cas9-Mediated MECP2 Modifications in Human-Induced Pluripotent Stem Cells'. Frontiers in Genetics 10 (2 July 2019). https://doi.org/10.3389/fgene.2019.00625.
- Lee, Joon-Hyuk, Ji-young Kim, Seulgi Noh, Hyoeun Lee, Se Young Lee, Ji Young Mun, Hyungju Park, and Won-Suk Chung. 'Astrocytes Phagocytose Adult Hippocampal Synapses for Circuit Homeostasis'. Nature, 23 December 2020, 1–6. https://doi.org/10.1038/s41586-020-03060-3.
- Lee, Soojung, Bo-Eun Yoon, Ken Berglund, Soo-Jin Oh, Hyungju Park, Hee-Sup Shin, George J. Augustine, and C. Justin Lee. 'Channel-Mediated Tonic GABA Release from Glia'. Science (New York, N.Y.) 330, no. 6005 (5 November 2010): 790–96. https://doi.org/10.1126/science.1184334.
- Lelieveld, Stefan H., Margot R. F. Reijnders, Rolph Pfundt, Helger G. Yntema, Erik-Jan Kamsteeg, Petra de Vries, Bert B. A. de Vries, et al. 'Meta-Analysis of 2,104 Trios Provides Support for 10 New Genes for Intellectual Disability'. Nature Neuroscience 19, no. 9 (September 2016): 1194–96. https://doi.org/10.1038/nn.4352.
- Lenhossék M.*, Der feinere Bau des Nervensystems im Lichte neuester Forschung (2nd ed.). Berlin: Fischer's Medicinische Buchhandlung H. Kornfield, 1895.*

- Leonard, Helen, Stuart Cobb, and Jenny Downs. 'Clinical and Biological Progress over 50 Years in Rett Syndrome'. Nature Reviews. Neurology 13, no. 1 (January 2017): 37–51. https://doi.org/10.1038/nrneurol.2016.186.
- Liddelow, Shane A., and Ben A. Barres. 'Reactive Astrocytes: Production, Function, and Therapeutic Potential'. Immunity 46, no. 6 (20 June 2017): 957–67. https://doi.org/10.1016/j.immuni.2017.06.006.
- Lin, Peijie, Laura Nicholls, Hassan Assareh, Zhiming Fang, Timothy G. Amos, Richard J. Edwards, Amelia A. Assareh, and Irina Voineagu. 'Transcriptome Analysis of Human Brain Tissue Identifies Reduced Expression of Complement Complex C1Q Genes in Rett Syndrome'. BMC Genomics 17, no. 1 (6 June 2016): 427. https://doi.org/10.1186/s12864-016-2746-7.
- Lindeberg, Jonas, Dmitry Usoskin, Henrik Bengtsson, Anna Gustafsson, Annika Kylberg, Stine Söderström, and Ted Ebendal. 'Transgenic Expression of Cre Recombinase from the Tyrosine Hydroxylase Locus'. Genesis (New York, N.Y.: 2000) 40, no. 2 (October 2004): 67–73. https://doi.org/10.1002/gene.20065.
- Lioy, Daniel T., Saurabh K. Garg, Caitlin E. Monaghan, Jacob Raber, Kevin D. Foust, Brian K. Kaspar, Petra G. Hirrlinger, et al. 'A Role for Glia in the Progression of Rett's Syndrome'. Nature 475, no. 7357 (29 June 2011): 497–500. https://doi.org/10.1038/nature10214.
- Liu, Rong-Zong, Raja Mita, Michael Beaulieu, Zhihua Gao, and Roseline Godbout. 'Fatty Acid Binding Proteins in Brain Development and Disease'. International Journal of Developmental Biology 54, no. 8–9 (14 May 2010): 1229–39. https://doi.org/10.1387/ijdb.092976rl.
- Lively, Starlee, and Ian R. Brown. 'Analysis of the Extracellular Matrix Protein SC1 during Reactive Gliosis in the Rat Lithium-Pilocarpine Seizure Model'. Brain Research 1163 (13 August 2007): 1–9. https://doi.org/10.1016/j.brainres.2007.05.052.
- Liyanage, Vichithra R. B., and Mojgan Rastegar. 'Rett Syndrome and MeCP2'. Neuromolecular Medicine 16, no. 2 (June 2014): 231–64. https://doi.org/10.1007/s12017-014-8295-9.
- Lombardi, Laura Marie, Steven Andrew Baker, and Huda Yahya Zoghbi. 'MECP2 Disorders: From the Clinic to Mice and Back'. The Journal of Clinical Investigation 125, no. 8 (3 August 2015): 2914–23. https://doi.org/10.1172/JCI78167.
- Long, Steven W., Jenny Y. Y. Ooi, Peter M. Yau, and Peter L. Jones. 'A Brain-Derived MeCP2 Complex Supports a Role for MeCP2 in RNA Processing'. Bioscience Reports 31, no. 5 (1 October 2011): 333–43. https://doi.org/10.1042/BSR20100124.
- Lopes, Fátima, Mafalda Barbosa, Adam Ameur, Gabriela Soares, Joaquim de Sá, Ana Isabel Dias, Guiomar Oliveira, et al. 'Identification of Novel Genetic Causes of Rett Syndrome-like Phenotypes'. Journal of Medical Genetics 53, no. 3 (1 March 2016): 190–99. https://doi.org/10.1136/jmedgenet-2015-103568.
- López-Murcia, Francisco J., Beatrice Terni, and Artur Llobet. 'SPARC Triggers a Cell-Autonomous Program of Synapse Elimination'. Proceedings of the National Academy of Sciences of the United States of America 112, no. 43 (27 October 2015): 13366–71. https://doi.org/10.1073/pnas.1512202112.
- Lovatt, Ditte, Qiwu Xu, Wei Liu, Takahiro Takano, Nathan A. Smith, Jurgen Schnermann, Kim Tieu, and Maiken Nedergaard. 'Neuronal Adenosine Release, and Not Astrocytic ATP Release, Mediates Feedback Inhibition of Excitatory Activity'. Proceedings of the National Academy of Sciences 109, no. 16 (17 April 2012): 6265–70. https://doi.org/10.1073/pnas.1120997109.
- Lovatt, Ditte, Ursula Sonnewald, Helle S. Waagepetersen, Arne Schousboe, Wei He, Jane H.-C. Lin, Xiaoning Han, et al. 'The Transcriptome and Metabolic Gene Signature of Protoplasmic Astrocytes in the Adult Murine Cortex'. Journal of Neuroscience 27, no. 45 (7 November 2007): 12255–66. https://doi.org/10.1523/JNEUROSCI.3404-07.2007.

- Lu, B., A. J. Czernik, S. Popov, T. Wang, M. -M. Poo, and P. Greengard. 'Expression of Synapsin i Correlates with Maturation of the Neuromuscular Synapse'. Neuroscience 74, no. 4 (1 October 1996): 1087–97. https://doi.org/10.1016/0306-4522(96)00187-X.
- Luikenhuis, Sandra, Emanuela Giacometti, Caroline F. Beard, and Rudolf Jaenisch. 'Expression of MeCP2 in Postmitotic Neurons Rescues Rett Syndrome in Mice'. Proceedings of the National Academy of Sciences of the United States of America 101, no. 16 (20 April 2004): 6033–38. https://doi.org/10.1073/pnas.0401626101.
- Lundgaard, I., M. J. Osório, B. T. Kress, S. Sanggaard, and M. Nedergaard. 'White Matter Astrocytes in Health and Disease'. Neuroscience, Secrets of the CNS White Matter, 276 (12 September 2014): 161–73. https://doi.org/10.1016/j.neuroscience.2013.10.050.
- Lundstrom, Kenneth. 'Viral Vectors in Gene Therapy'. Diseases 6, no. 2 (21 May 2018). https://doi.org/10.3390/diseases6020042.
- Lyst, Matthew J, Robert Ekiert, Daniel H Ebert, Cara Merusi, Jakub Nowak, Jim Selfridge, Jacky Guy, et al. 'Rett Syndrome Mutations Abolish the Interaction of MeCP2 with the NCoR/SMRT Co-Repressor'. Nature Neuroscience 16, no. 7 (July 2013). https://doi.org/10.1038/nn.3434.
- MacDonald, Jennifer M., Margaret G. Beach, Ermelinda Porpiglia, Amy E. Sheehan, Ryan J. Watts, and Marc R. Freeman. 'The Drosophila Cell Corpse Engulfment Receptor Draper Mediates Glial Clearance of Severed Axons'. Neuron 50, no. 6 (15 June 2006): 869–81. https://doi.org/10.1016/j.neuron.2006.04.028.
- Maceyka, Michael, and Sarah Spiegel. 'Sphingolipid Metabolites in Inflammatory Disease'. Nature 510, no. 7503 (June 2014): 58–67. https://doi.org/10.1038/nature13475.
- Maezawa, Izumi, Susan Swanberg, Danielle Harvey, Janine M. LaSalle, and Lee-Way Jin. 'Rett Syndrome Astrocytes Are Abnormal and Spread MeCP2 Deficiency through Gap Junctions'. Journal of Neuroscience 29, no. 16 (22 April 2009): 5051–61. https://doi.org/10.1523/JNEUROSCI.0324-09.2009.
- Maffei, Silvia, Claudio De Felice, Pierpaolo Cannarile, Silvia Leoncini, Cinzia Signorini, Alessandra Pecorelli, Barbara Montomoli, et al. 'Effects of ω-3 PUFAs Supplementation on Myocardial Function and Oxidative Stress Markers in Typical Rett Syndrome'. Mediators of Inflammation 2014 (2014): 983178. https://doi.org/10.1155/2014/983178.
- Marazziti, Daniela, Chiara Di Pietro, Elisabetta Golini, Silvia Mandillo, Gina La Sala, Rafaele Matteoni, and Glauco P. Tocchini-Valentini. 'Precocious Cerebellum Development and Improved Motor Functions in Mice Lacking the Astrocyte Cilium-, Patched 1-Associated Gpr37l1 Receptor'. Proceedings of the National Academy of Sciences of the United States of America 110, no. 41 (8 October 2013): 16486–91. https://doi.org/10.1073/pnas.1314819110.
- Marcaggi, Païkan, and David Attwell. 'Role of Glial Amino Acid Transporters in Synaptic Transmission and Brain Energetics'. Glia 47, no. 3 (2004): 217–25. https://doi.org/10.1002/glia.20027.
- Marcaggi, Païkan, Marion Jeanne, and Jonathan A. Coles. 'Neuron–Glial Trafficking of NH4+ and K+: Separate Routes of Uptake into Glial Cells of Bee Retina'. European Journal of Neuroscience 19, no. 4 (2004): 966–76. https://doi.org/10.1111/j.0953-816X.2004.03165.x.
- Marksteiner, J., T. Lechner, W. A. Kaufmann, P. Gurka, C. Humpel, C. Nowakowski, H. Maier, and K. A. Jellinger. 'Distribution of Chromogranin B-like Immunoreactivity in the Human Hippocampus and Its Changes in Alzheimer's Disease'. Acta Neuropathologica 100, no. 2 (1 July 2000): 205–12. https://doi.org/10.1007/s004010000239.
- Marschik, Peter B., Walter E. Kaufmann, Jeff Sigafoos, Thomas Wolin, Dajie Zhang, Katrin D. Bartl-Pokorny, Giorgio Pini, et al. 'Changing the Perspective on Early Development of Rett Syndrome'. Research in Developmental Disabilities 34, no. 4 (April 2013): 1236–39. https://doi.org/10.1016/j.ridd.2013.01.014.

- Martín, R., R. Bajo-Grañeras, R. Moratalla, G. Perea, and A. Araque. ‘Circuit-Specific Signaling in Astrocyte-Neuron Networks in Basal Ganglia Pathways’. Science (New York, N.Y.) 349, no. 6249 (14 August 2015): 730–34. https://doi.org/10.1126/science.aaa7945.
- Martineau, Magalie, Ting Shi, Julien Puyal, Ann M. Knolhoff, Jérôme Dulong, Bruno Gasnier, Jürgen Klingauf, Jonathan V. Sweedler, Reinhard Jahn, and Jean-Pierre Mothet. ‘Storage and Uptake of D-Serine into Astrocytic Synaptic-Like Vesicles Specify Gliotransmission’. The Journal of Neuroscience 33, no. 8 (20 February 2013): 3413–23. https://doi.org/10.1523/JNEUROSCI.3497-12.2013.
- Martineau, Magalie, Vladimir Parpura, and Jean-Pierre Mothet. ‘Cell-Type Specific Mechanisms of D-Serine Uptake and Release in the Brain’. Frontiers in Synaptic Neuroscience 6 (2014). https://doi.org/10.3389/fnsyn.2014.00012.
- Martínez de Paz, Alexia, Leila Khajavi, Hélène Martin, Rafael Claveria-Gimeno, Susanne Tom Dieck, Manjinder S. Cheema, Jose V. Sanchez-Mut, et al. ‘MeCP2-E1 Isoform Is a Dynamically Expressed, Weakly DNA-Bound Protein with Different Protein and DNA Interactions Compared to MeCP2-E2’. Epigenetics & Chromatin 12, no. 1 (10 October 2019): 63. https://doi.org/10.1186/s13072-019-0298-1.
- Matarazzo, Valéry, and Gabriele V. Ronnett. ‘Temporal and Regional Differences in the Olfactory Proteome as a Consequence of MeCP2 Deficiency’. Proceedings of the National Academy of Sciences 101, no. 20 (18 May 2004): 7763–68. https://doi.org/10.1073/pnas.0307083101.
- Matos, Marco, Anthony Bosson, Ilse Riebe, Clare Reynell, Joanne Vallée, Isabel Laplante, Aude Panatier, Richard Robitaille, and Jean-Claude Lacaille. ‘Astrocytes Detect and Upregulate Transmission at Inhibitory Synapses of Somatostatin Interneurons onto Pyramidal Cells’. Nature Communications 9, no. 1 (12 October 2018): 4254. https://doi.org/10.1038/s41467-018-06731-y.
- Matsutani, Shinji, and Noboru Yamamoto. ‘Neuronal Regulation of Astrocyte Morphology in Vitro Is Mediated by GABAergic Signaling’. Glia 20, no. 1 (1997): 1–9. https://doi.org/10.1002/(SICI)1098-1136(199705)20:1<1::AID-GLIA1>3.0.CO;2-E.
- Mauch, D. H., K. Nägler, S. Schumacher, C. Göritz, E. C. Müller, A. Otto, and F. W. Pfrieger. ‘CNS Synaptogenesis Promoted by Glia-Derived Cholesterol’. Science (New York, N.Y.) 294, no. 5545 (9 November 2001): 1354–57. https://doi.org/10.1126/science.294.5545.1354.
- Mazaré, Noémie, Marc Oudart, Julien Moulard, Giselle Cheung, Romain Tortuyaux, Philippe Mailly, David Mazaud, et al. ‘Local Translation in Perisynaptic Astrocytic Processes Is Specific and Regulated by Fear Conditioning’. BioRxiv, 23 January 2020, 2020.01.21.913970. https://doi.org/10.1101/2020.01.21.913970.
- McCarthy, K. D., and J. de Vellis. ‘Preparation of Separate Astroglial and Oligodendroglial Cell Cultures from Rat Cerebral Tissue’. The Journal of Cell Biology 85, no. 3 (June 1980): 890–902. https://doi.org/10.1083/jcb.85.3.890.
- McGraw, Christopher M., Rodney C. Samaco, and Huda Y. Zoghbi. ‘Adult Neural Function Requires MeCP2’. Science (New York, N.Y.) 333, no. 6039 (8 July 2011): 186. https://doi.org/10.1126/science.1206593.
- Mederos, Sara, Candela González-Arias, and Gertrudis Perea. ‘Astrocyte-Neuron Networks: A Multilane Highway of Signaling for Homeostatic Brain Function’. Frontiers in Synaptic Neuroscience 10 (2018): 45. https://doi.org/10.3389/fnsyn.2018.00045.
- Medrihan, L., E. Tantalaki, G. Aramuni, V. Sargsyan, I. Dudanova, M. Missler, and W. Zhang. ‘Early Defects of GABAergic Synapses in the Brain Stem of a MeCP2 Mouse Model of Rett Syndrome’. Journal of Neurophysiology 99, no. 1 (January 2008): 112–21. https://doi.org/10.1152/jn.00826.2007.
- Meijering, E., M. Jacob, J.-C. F. Sarria, P. Steiner, H. Hirling, and M. Unser. ‘Design and Validation of a Tool for Neurite Tracing and Analysis in Fluorescence Microscopy Images’.

Cytometry. Part A: The Journal of the International Society for Analytical Cytology 58, no. 2 (April 2004): 167–76. https://doi.org/10.1002/cyto.a.20022.

- Mellén, Marian, Pinar Ayata, Scott Dewell, Skirmantas Kriaucionis, and Nathaniel Heintz. 'MeCP2 Binds to 5hmC Enriched within Active Genes and Accessible Chromatin in the Nervous System'. Cell 151, no. 7 (21 December 2012): 1417–30. https://doi.org/10.1016/j.cell.2012.11.022.
- Meng, Xiangling, Wei Wang, Hui Lu, Ling-Jie He, Wu Chen, Eugene S. Chao, Marta L. Fiorotto, et al. 'Manipulations of MeCP2 in Glutamatergic Neurons Highlight Their Contributions to Rett and Other Neurological Disorders'. ELife 5 (21 2016). https://doi.org/10.7554/eLife.14199.
- Min, Rogier, and Thomas Nevian. 'Astrocyte Signaling Controls Spike Timing-Dependent Depression at Neocortical Synapses'. Nature Neuroscience 15, no. 5 (25 March 2012): 746–53. https://doi.org/10.1038/nn.3075.
- Miranda, Magdalena, Juan Facundo Morici, María Belén Zanoni, and Pedro Bekinschtein. 'Brain-Derived Neurotrophic Factor: A Key Molecule for Memory in the Healthy and the Pathological Brain'. Frontiers in Cellular Neuroscience 13 (2019). https://doi.org/10.3389/fncel.2019.00363.
- Missiroli, Sonia, Ilaria Genovese, Mariasole Perrone, Bianca Vezzani, Veronica A. M. Vitto, and Carlotta Giorgi. 'The Role of Mitochondria in Inflammation: From Cancer to Neurodegenerative Disorders'. Journal of Clinical Medicine 9, no. 3 (9 March 2020). https://doi.org/10.3390/jcm9030740.
- Missler, Markus, Thomas C. Südhof, and Thomas Biederer. 'Synaptic Cell Adhesion'. Cold Spring Harbor Perspectives in Biology 4, no. 4 (1 April 2012): a005694. https://doi.org/10.1101/cshperspect.a005694.
- Miyata, Takaki, Daichi Kawaguchi, Ayano Kawaguchi, and Yukiko Gotoh. 'Mechanisms That Regulate the Number of Neurons during Mouse Neocortical Development'. Current Opinion in Neurobiology 20, no. 1 (February 2010): 22–28. https://doi.org/10.1016/j.conb.2010.01.001.
- Mochel, Fanny, Pascale DeLonlay, Guy Touati, Henri Brunengraber, Renee P. Kinman, Daniel Rabier, Charles R. Roe, and Jean-Marie Saudubray. 'Pyruvate Carboxylase Deficiency: Clinical and Biochemical Response to Anaplerotic Diet Therapy'. Molecular Genetics and Metabolism 84, no. 4 (1 April 2005): 305–12. https://doi.org/10.1016/j.ymgme.2004.09.007.
- Moeton, Martina, Oscar M. J. A. Stassen, Jacqueline A. Sluijs, Vincent W. N. van der Meer, Liselot J. Kluivers, Hedde van Hoorn, Thomas Schmidt, Eric A. J. Reits, Miriam E. van Strien, and Elly M. Hol. 'GFAP Isoforms Control Intermediate Filament Network Dynamics, Cell Morphology, and Focal Adhesions'. Cellular and Molecular Life Sciences 73, no. 21 (2016): 4101–20. https://doi.org/10.1007/s00018-016-2239-5.
- Molofsky, Anna V., Kevin W. Kelley, Hui-Hsin Tsai, Stephanie A. Redmond, Sandra M. Chang, Lohith Madireddy, Jonah R. Chan, Sergio E. Baranzini, Erik M. Ullian, and David H. Rowitch. 'Astrocyte-Encoded Positional Cues Maintain Sensorimotor Circuit Integrity'. Nature 509, no. 7499 (8 May 2014): 189–94. https://doi.org/10.1038/nature13161.
- Molofsky, Anna V., Robert Krencik, Robert Krenick, Erik M. Ullian, Erik Ullian, Hui-hsin Tsai, Benjamin Deneen, William D. Richardson, Ben A. Barres, and David H. Rowitch. 'Astrocytes and Disease: A Neurodevelopmental Perspective'. Genes & Development 26, no. 9 (1 May 2012): 891–907. https://doi.org/10.1101/gad.188326.112.
- Molofsky, Anna Victoria, and Benjamin Deneen. 'Astrocyte Development: A Guide for the Perplexed'. Glia 63, no. 8 (2015): 1320–29. https://doi.org/10.1002/glia.22836.
- Moretti, Paolo, Jonathan M. Levenson, Fortunato Battaglia, Richard Atkinson, Ryan Teague, Barbara Antalffy, Dawna Armstrong, Ottavio Arancio, J. David Sweatt, and Huda Y. Zoghbi. 'Learning and Memory and Synaptic Plasticity Are Impaired in a Mouse Model of Rett Syndrome'. Journal of Neuroscience 26, no. 1 (4 January 2006): 319–27. https://doi.org/10.1523/JNEUROSCI.2623-05.2006.

- Moroto, M., A. Nishimura, M. Morimoto, K. Isoda, T. Morita, M. Yoshida, S. Morioka, et al. 'Altered Somatosensory Barrel Cortex Refinement in the Developing Brain of Mecp2-Null Mice'. Brain Research 1537 (6 November 2013): 319–26. https://doi.org/10.1016/j.brainres.2013.09.017.
- Mothet, Jean-Pierre, Loredano Pollegioni, Gilles Ouanounou, Magalie Martineau, Philippe Fossier, and Gérard Baux. 'Glutamate Receptor Activation Triggers a Calcium-Dependent and SNARE Protein-Dependent Release of the Gliotransmitter D-Serine'. Proceedings of the National Academy of Sciences of the United States of America 102, no. 15 (12 April 2005): 5606–11. https://doi.org/10.1073/pnas.0408483102.
- Mottahedin, Amin, Maryam Ardalan, Tetyana Chumak, Ilse Riebe, Joakim Ek, and Carina Mallard. 'Effect of Neuroinflammation on Synaptic Organization and Function in the Developing Brain: Implications for Neurodevelopmental and Neurodegenerative Disorders'. Frontiers in Cellular Neuroscience 11 (2017). https://doi.org/10.3389/fncel.2017.00190.
- Mulligan, Sean J., and Brian A. MacVicar. 'Calcium Transients in Astrocyte Endfeet Cause Cerebrovascular Constrictions'. Nature 431, no. 7005 (9 September 2004): 195–99. https://doi.org/10.1038/nature02827.
- Nagao, Motoshi, Toru Ogata, Yasuhiro Sawada, and Yukiko Gotoh. 'Zbtb20 Promotes Astrocytogenesis during Neocortical Development'. Nature Communications 7 (22 March 2016). https://doi.org/10.1038/ncomms11102.
- Naka, Hayato, Shiho Nakamura, Takuya Shimazaki, and Hideyuki Okano. 'Requirement for COUP-TFI and II in the Temporal Specification of Neural Stem Cells in CNS Development'. Nature Neuroscience 11, no. 9 (September 2008): 1014–23. https://doi.org/10.1038/nn.2168.
- Namihira, Masakazu, Jun Kohyama, Katsunori Semi, Tsukasa Sanosaka, Benjamin Deneen, Tetsuya Taga, and Kinichi Nakashima. 'Committed Neuronal Precursors Confer Astrocytic Potential on Residual Neural Precursor Cells'. Developmental Cell 16, no. 2 (17 February 2009): 245–55. https://doi.org/10.1016/j.devcel.2008.12.014.
- Nan, X., F. J. Campoy, and A. Bird. 'MeCP2 Is a Transcriptional Repressor with Abundant Binding Sites in Genomic Chromatin'. Cell 88, no. 4 (21 February 1997): 471–81. https://doi.org/10.1016/s0092-8674(00)81887-5.
- Nan, Xinsheng, Huck-Hui Ng, Colin A. Johnson, Carol D. Laherty, Bryan M. Turner, Robert N. Eisenman, and Adrian Bird. 'Transcriptional Repression by the Methyl-CpG-Binding Protein MeCP2 Involves a Histone Deacetylase Complex'. Nature 393, no. 6683 (May 1998): 386–89. https://doi.org/10.1038/30764.
- Nan, Xinsheng, Jianghui Hou, Alan Maclean, Jamal Nasir, Maria Jose Lafuente, Xinhua Shu, Skirmantas Kriaucionis, and Adrian Bird. 'Interaction between Chromatin Proteins MECP2 and ATRX Is Disrupted by Mutations That Cause Inherited Mental Retardation'. Proceedings of the National Academy of Sciences 104, no. 8 (20 February 2007): 2709–14. https://doi.org/10.1073/pnas.0608056104.
- Nectoux, Juliette, Cedrick Florian, Chloe Delepine, Nadia Bahi-Buisson, Malik Khelfaoui, Sophie Reibel, Jamel Chelly, and Thierry Bienvenu. 'Altered Microtubule Dynamics in Mecp2-Deficient Astrocytes'. Journal of Neuroscience Research 90, no. 5 (May 2012): 990–98. https://doi.org/10.1002/jnr.23001.
- Nelson, Sacha B., and Vera Valakh. 'Excitatory/Inhibitory Balance and Circuit Homeostasis in Autism Spectrum Disorders'. Neuron 87, no. 4 (19 August 2015): 684–98. https://doi.org/10.1016/j.neuron.2015.07.033.
- Neul, J. L., Kaufmann, W. E., Glaze, D. G., Christodoulou, J., Clarke, A. J., Bahi-Buisson, N., Leonard, H., Bailey, M. E., Schanen, N. C., Zappella, M., Renieri, A., Huppke, P., Percy, A. K., & RettSearch Consortium (2010). Rett syndrome: revised diagnostic criteria and nomenclature. Annals of neurology, 68(6), 944–950. https://doi.org/10.1002/ana.22124

- Nguyen, Minh Vu Chuong, Fang Du, Christy A. Felice, Xiwei Shan, Aparna Nigam, Gail Mandel, John K. Robinson, and Nurit Ballas. 'MeCP2 Is Critical for Maintaining Mature Neuronal Networks and Global Brain Anatomy during Late Stages of Postnatal Brain Development and in the Mature Adult Brain'. The Journal of Neuroscience: The Official Journal of the Society for Neuroscience 32, no. 29 (18 July 2012): 10021–34. https://doi.org/10.1523/JNEUROSCI.1316-12.2012.
- Nielsen, J. B., P. B. Toft, E. Reske-Nielsen, K. E. Jensen, P. Christiansen, C. Thomsen, O. Henriksen, and H. C. Lou. 'Cerebral Magnetic Resonance Spectroscopy in Rett Syndrome. Failure to Detect Mitochondrial Disorder'. Brain & Development 15, no. 2 (April 1993): 107–12. https://doi.org/10.1016/0387-7604(93)90046-b.
- Nixdorf-Bergweiler, Barbara E., Dorothea Albrecht, and Uwe Heinemann. 'Developmental Changes in the Number, Size, and Orientation of GFAP-Positive Cells in the CA1 Region of Rat Hippocampus'. Glia 12, no. 3 (1994): 180–95. https://doi.org/10.1002/glia.440120304.
- Nolte, C., M. Matyash, T. Pivneva, C. G. Schipke, C. Ohlemeyer, U. K. Hanisch, F. Kirchhoff, and H. Kettenmann. 'GFAP Promoter-Controlled EGFP-Expressing Transgenic Mice: A Tool to Visualize Astrocytes and Astrogliosis in Living Brain Tissue'. Glia 33, no. 1 (January 2001): 72–86.
- Norenberg, Michael D., and Antonio Martinez-Hernandez. 'Fine Structural Localization of Glutamine Synthetase in Astrocytes of Rat Brain'. Brain Research 161, no. 2 (2 February 1979): 303–10. https://doi.org/10.1016/0006-8993(79)90071-4.
- Nott, Alexi, Jemmie Cheng, Fan Gao, Yuan-Ta Lin, Elizabeta Gjoneska, Tak Ko, Paras Minhas, et al. 'Histone Deacetylase 3 Associates with MeCP2 to Regulate FOXO and Social Behavior'. Nature Neuroscience 19, no. 11 (November 2016): 1497–1505. https://doi.org/10.1038/nn.4347.
- O'Donnell, Michael, Rebecca K. Chance, and Greg J. Bashaw. 'Axon Growth and Guidance: Receptor Regulation and Signal Transduction'. Annual Review of Neuroscience 32, no. 1 (1 June 2009): 383–412. https://doi.org/10.1146/annurev.neuro.051508.135614.
- Oberheim Bush, Nancy Ann, and Maiken Nedergaard. 'Do Evolutionary Changes in Astrocytes Contribute to the Computational Power of the Hominid Brain?' Neurochemical Research 42, no. 9 (September 2017): 2577–87. https://doi.org/10.1007/s11064-017-2363-0.
- Oberheim, Nancy Ann, Takahiro Takano, Xiaoning Han, Wei He, Jane H. C. Lin, Fushun Wang, Qiwu Xu, et al. 'Uniquely Hominid Features of Adult Human Astrocytes'. The Journal of Neuroscience: The Official Journal of the Society for Neuroscience 29, no. 10 (11 March 2009): 3276–87. https://doi.org/10.1523/JNEUROSCI.4707-08.2009.
- Oberheim, Nancy Ann, Xiaohai Wang, Steven Goldman, and Maiken Nedergaard. 'Astrocytic Complexity Distinguishes the Human Brain'. Trends in Neurosciences 29, no. 10 (October 2006): 547–53. https://doi.org/10.1016/j.tins.2006.08.004.
- Ogata, K, and T Kosaka. 'Structural and Quantitative Analysis of Astrocytes in the Mouse Hippocampus'. Neuroscience 113, no. 1 (2 August 2002): 221–33. https://doi.org/10.1016/S0306-4522(02)00041-6.
- Okabe, Yasunori, Tomoyuki Takahashi, Chiaki Mitsumasu, Ken-ichiro Kosai, Eiichiro Tanaka, and Toyojiro Matsuishi. 'Alterations of Gene Expression and Glutamate Clearance in Astrocytes Derived from an MeCP2-Null Mouse Model of Rett Syndrome'. PloS One 7, no. 4 (2012): e35354. https://doi.org/10.1371/journal.pone.0035354.
- Okamura, Masashi, Hiromi Kudo, Ken-ichi Wakabayashi, Toshiya Tanaka, Aya Nonaka, Aoi Uchida, Shuichi Tsutsumi, et al. 'COUP-TFII Acts Downstream of Wnt/β-Catenin Signal to Silence PPARγ Gene Expression and Repress Adipogenesis'. Proceedings of the National Academy of Sciences of the United States of America 106, no. 14 (7 April 2009): 5819–24. https://doi.org/10.1073/pnas.0901676106.

- Olsen, Anne S. B., and Nils J. Færgeman. ‘Sphingolipids: Membrane Microdomains in Brain Development, Function and Neurological Diseases’. Open Biology 7, no. 5 (31 May 2017). https://doi.org/10.1098/rsob.170069.
- Olsen, Michelle L., Baljit S. Khakh, Serguei N. Skatchkov, Min Zhou, C. Justin Lee, and Nathalie Rouach. ‘New Insights on Astrocyte Ion Channels: Critical for Homeostasis and Neuron-Glia Signaling’. Journal of Neuroscience 35, no. 41 (14 October 2015): 13827–35. https://doi.org/10.1523/JNEUROSCI.2603-15.2015.
- Olude, Matthew A., Oluwaseun A. Mustapha, Oluwatunde A. Aderounmu, James O. Olopade, and Amadi O. Ihunwo. ‘Astrocyte Morphology, Heterogeneity, and Density in the Developing African Giant Rat (Cricetomys Gambianus)’. Frontiers in Neuroanatomy 9 (2015). https://doi.org/10.3389/fnana.2015.00067.
- Osenberg, Sivan, Ariel Karten, Jialin Sun, Jin Li, Shaun Charkowick, Christy A. Felice, Mary Kritzer, Minh Vu Chuong Nguyen, Peng Yu, and Nurit Ballas. ‘Activity-Dependent Aberrations in Gene Expression and Alternative Splicing in a Mouse Model of Rett Syndrome’. Proceedings of the National Academy of Sciences 115, no. 23 (5 June 2018): E5363–72. https://doi.org/10.1073/pnas.1722546115.
- Owada, Yuji. ‘Fatty Acid Binding Protein: Localization and Functional Significance in the Brain’. The Tohoku Journal of Experimental Medicine 214, no. 3 (2008): 213–20. https://doi.org/10.1620/tjem.214.213.
- Pacheco, Natasha L., Michael R. Heaven, Leanne M. Holt, David K. Crossman, Kristin J. Boggio, Scott A. Shaffer, Daniel L. Flint, and Michelle L. Olsen. ‘RNA Sequencing and Proteomics Approaches Reveal Novel Deficits in the Cortex of Mecp2-Deficient Mice, a Model for Rett Syndrome’. Molecular Autism 8 (24 October 2017). https://doi.org/10.1186/s13229-017-0174-4.
- Pala, Rajasekharreddy, Nedaa Alomari, and Surya M. Nauli. ‘Primary Cilium-Dependent Signaling Mechanisms’. International Journal of Molecular Sciences 18, no. 11 (28 October 2017). https://doi.org/10.3390/ijms18112272.
- Palmano, Kate, Angela Rowan, Rozey Guillermo, Jian Guan, and Paul Mc Jarrow. ‘The Role of Gangliosides in Neurodevelopment’. Nutrients 7, no. 5 (22 May 2015): 3891–3913. https://doi.org/10.3390/nu7053891.
- Pan, Han-Chi, Yun-Chia Chou, and Synthia H. Sun. ‘P2X7 R-Mediated Ca(2+) -Independent d-Serine Release via Pannexin-1 of the P2X7 R-Pannexin-1 Complex in Astrocytes’. Glia 63, no. 5 (May 2015): 877–93. https://doi.org/10.1002/glia.22790.
- Panatier, Aude, Joanne Vallée, Michael Haber, Keith K. Murai, Jean-Claude Lacaille, and Richard Robitaille. ‘Astrocytes Are Endogenous Regulators of Basal Transmission at Central Synapses’. Cell 146, no. 5 (2 September 2011): 785–98. https://doi.org/10.1016/j.cell.2011.07.022.
- Pardridge, William M. ‘Blood-Brain Barrier Delivery’. Drug Discovery Today 12, no. 1–2 (January 2007): 54–61. https://doi.org/10.1016/j.drudis.2006.10.013.
- Park, Sang Min, Hee Jin Jang, and Jeong Ho Lee. ‘Roles of Primary Cilia in the Developing Brain’. Frontiers in Cellular Neuroscience 13 (2019): 218. https://doi.org/10.3389/fncel.2019.00218.
- Parpura, V., T. A. Basarsky, F. Liu, K. Jeftinija, S. Jeftinija, and P. G. Haydon. ‘Glutamate-Mediated Astrocyte-Neuron Signalling’. Nature 369, no. 6483 (30 June 1994): 744–47. https://doi.org/10.1038/369744a0.
- Pascual, Olivier, Kristen B. Casper, Cathryn Kubera, Jing Zhang, Raquel Revilla-Sanchez, Jai-Yoon Sul, Hajime Takano, Stephen J. Moss, Ken McCarthy, and Philip G. Haydon. ‘Astrocytic Purinergic Signaling Coordinates Synaptic Networks’. Science (New York, N.Y.) 310, no. 5745 (7 October 2005): 113–16. https://doi.org/10.1126/science.1116916.
- Patrizi, Annarita, Nathalie Picard, Alex Joseph Simon, Georgia Gunner, Eleonora Centofante, Nick Arthur Andrews, and Michela Fagiolini. ‘Chronic Administration of the N-Methyl-D-Aspartate

Receptor Antagonist Ketamine Improves Rett Syndrome Phenotype'. Biological Psychiatry 79, no. 9 (1 May 2016): 755–64. https://doi.org/10.1016/j.biopsych.2015.08.018.

- Percy, Alan K. 'Progress in Rett Syndrome: From Discovery to Clinical Trials'. Wiener Medizinische Wochenschrift (1946) 166, no. 11–12 (September 2016): 325–32. https://doi.org/10.1007/s10354-016-0491-9.
- Perea, Gertrudis, and Alfonso Araque. 'Astrocytes Potentiate Transmitter Release at Single Hippocampal Synapses'. Science (New York, N.Y.) 317, no. 5841 (24 August 2007): 1083–86. https://doi.org/10.1126/science.1144640.
- Perea, Gertrudis, Marta Navarrete, and Alfonso Araque. 'Tripartite Synapses: Astrocytes Process and Control Synaptic Information'. Trends in Neurosciences 32, no. 8 (August 2009): 421–31. https://doi.org/10.1016/j.tins.2009.05.001.
- Perea, Gertrudis, Ricardo Gómez, Sara Mederos, Ana Covelo, Jesús J Ballesteros, Laura Schlosser, Alicia Hernández-Vivanco, et al. 'Activity-Dependent Switch of GABAergic Inhibition into Glutamatergic Excitation in Astrocyte-Neuron Networks'. Edited by Marlene Bartos. ELife 5 (24 December 2016): e20362. https://doi.org/10.7554/eLife.20362.
- Perego, C., C. Vanoni, M. Bossi, S. Massari, H. Basudev, R. Longhi, and G. Pietrini. 'The GLT-1 and GLAST Glutamate Transporters Are Expressed on Morphologically Distinct Astrocytes and Regulated by Neuronal Activity in Primary Hippocampal Cocultures'. Journal of Neurochemistry 75, no. 3 (September 2000): 1076–84. https://doi.org/10.1046/j.1471-4159.2000.0751076.x.
- Perlini, Laura E., Francesca Botti, Eugenio F. Fornasiero, Maila Giannandrea, Dario Bonanomi, Mario Amendola, Luigi Naldini, Fabio Benfenati, and Flavia Valtorta. 'Effects of Phosphorylation and Neuronal Activity on the Control of Synapse Formation by Synapsin I'. Journal of Cell Science 124, no. Pt 21 (1 November 2011): 3643–53. https://doi.org/10.1242/jcs.086223.
- Peters A, Palay SL, Webster HF. *The Fine Structure of the Nervous System: Neurons and Their Supporting Cells by Alan Peters,* 1991
- Petrelli, Francesco, and Paola Bezzi. 'Novel Insights into Gliotransmitters'. Current Opinion in Pharmacology 26 (February 2016): 138–45. https://doi.org/10.1016/j.coph.2015.11.010.
- Phatnani, Hemali, and Tom Maniatis. 'Astrocytes in Neurodegenerative Disease'. Cold Spring Harbor Perspectives in Biology 7, no. 6 (June 2015). https://doi.org/10.1101/cshperspect.a020628.
- Picker, Jonathan D., Rebecca Yang, Laura Ricceri, and Joanne Berger-Sweeney. 'An Altered Neonatal Behavioral Phenotype in Mecp2 Mutant Mice'. Neuroreport 17, no. 5 (3 April 2006): 541–44. https://doi.org/10.1097/01.wnr.0000208995.38695.2f.
- Pietri, Thomas, Angel-Carlos Roman, Nicolas Guyon, Sebastián A. Romano, Philip Washbourne, Cecilia B. Moens, Gonzalo G. de Polavieja, and Germán Sumbre. 'The First Mecp2-Null Zebrafish Model Shows Altered Motor Behaviors'. Frontiers in Neural Circuits 7 (16 July 2013). https://doi.org/10.3389/fncir.2013.00118.
- Pines, Gilia, Niels C. Danbolt, Magnar Bjørås, Yumin Zhang, Annie Bendahan, Lars Eide, Hermann Koepsell, Jon Storm-Mathisen, Erling Seeberg, and Baruch I. Kanner. 'Cloning and Expression of a Rat Brain L-Glutamate Transporter'. Nature 360, no. 6403 (December 1992): 464–67. https://doi.org/10.1038/360464a0.
- Pins, Benoit de, Carmen Cifuentes-Díaz, Amel Thamila Farah, Laura López-Molina, Enrica Montalban, Anna Sancho-Balsells, Ana López, et al. 'Conditional BDNF Delivery from Astrocytes Rescues Memory Deficits, Spine Density, and Synaptic Properties in the 5xFAD Mouse Model of Alzheimer Disease'. Journal of Neuroscience 39, no. 13 (27 March 2019): 2441–58. https://doi.org/10.1523/JNEUROSCI.2121-18.2019.

- Piotr Przanowski et al., ‘Pharmacological Reactivation of Inactive X-Linked Mecp2 in Cerebral Cortical Neurons of Living Mice’, Proceedings of the National Academy of Sciences 115, no. 31 (31 July 2018): 7991–96, https://doi.org/10.1073/pnas.1803792115.
- Pitzianti, Maria Bernarda, Angelo Santamaria Palombo, Susanna Esposito, and Augusto Pasini. ‘Rett Syndrome in Males: The Different Clinical Course in Two Brothers with the Same Microduplication MECP2 Xq28’. International Journal of Environmental Research and Public Health 16, no. 17 (January 2019): 3075. https://doi.org/10.3390/ijerph16173075.
- Pöyhönen, Suvi, Safak Er, Andrii Domanskyi, and Mikko Airavaara. ‘Effects of Neurotrophic Factors in Glial Cells in the Central Nervous System: Expression and Properties in Neurodegeneration and Injury’. Frontiers in Physiology 10 (26 April 2019). https://doi.org/10.3389/fphys.2019.00486.
- Prada, Ilaria, Julie Marchaland, Paola Podini, Lorenzo Magrassi, Rosalba D’Alessandro, Paola Bezzi, and Jacopo Meldolesi. ‘REST/NRSF Governs the Expression of Dense-Core Vesicle Gliosecretion in Astrocytes’. The Journal of Cell Biology 193, no. 3 (2 May 2011): 537–49. https://doi.org/10.1083/jcb.201010126.
- Pratt, D. W., J. V. Warner, and M. G. Williams. ‘Genotyping FOXG1 Mutations in Patients with Clinical Evidence of the FOXG1 Syndrome’. Molecular Syndromology 3, no. 6 (January 2013): 284–87. https://doi.org/10.1159/000345845.
- Pringle, Nigel P., Wei-Ping Yu, Marisa Howell, Jennifer S. Colvin, David M. Ornitz, and William D. Richardson. ‘Fgfr3 Expression by Astrocytes and Their Precursors: Evidence That Astrocytes and Oligodendrocytes Originate in Distinct Neuroepithelial Domains’. Development 130, no. 1 (1 January 2003): 93–102. https://doi.org/10.1242/dev.00184.
- Puelles, Luis, and John L. R. Rubenstein. ‘Forebrain Gene Expression Domains and the Evolving Prosomeric Model’. Trends in Neurosciences 26, no. 9 (September 2003): 469–76. https://doi.org/10.1016/S0166-2236(03)00234-0.
- Pyka, Martin, Christian Wetzel, Ainhara Aguado, Maren Geissler, Hanns Hatt, and Andreas Faissner. ‘Chondroitin Sulfate Proteoglycans Regulate Astrocyte-Dependent Synaptogenesis and Modulate Synaptic Activity in Primary Embryonic Hippocampal Neurons’. The European Journal of Neuroscience 33, no. 12 (June 2011): 2187–2202. https://doi.org/10.1111/j.1460-9568.2011.07690.x.
- Radtke, Franziska A., Gareth Chapman, Jeremy Hall, and Yasir A. Syed. ‘Modulating Neuroinflammation to Treat Neuropsychiatric Disorders’. Review Article. BioMed Research International. Hindawi, 18 October 2017. https://doi.org/10.1155/2017/5071786.
- Rakela, Benjamin, Paul Brehm, and Gail Mandel. ‘Astrocytic Modulation of Excitatory Synaptic Signaling in a Mouse Model of Rett Syndrome’. ELife 7 (9 January 2018). https://doi.org/10.7554/eLife.31629.
- Raman, Ayush T., Amy E. Pohodich, Ying-Wooi Wan, Hari Krishna Yalamanchili, William E. Lowry, Huda Y. Zoghbi, and Zhandong Liu. ‘Apparent Bias toward Long Gene Misregulation in MeCP2 Syndromes Disappears after Controlling for Baseline Variations’. Nature Communications 9, no. 1 (13 August 2018): 1–13. https://doi.org/10.1038/s41467-018-05627-1.
- Reddy, Linga V., Samir Koirala, Yoshie Sugiura, Albert A. Herrera, and Chien-Ping Ko. ‘Glial Cells Maintain Synaptic Structure and Function and Promote Development of the Neuromuscular Junction In Vivo’. Neuron 40, no. 3 (30 October 2003): 563–80. https://doi.org/10.1016/S0896-6273(03)00682-2.
- Reichenbach, Andreas, Amin Derouiche, and Frank Kirchhoff. ‘Morphology and Dynamics of Perisynaptic Glia’. Brain Research Reviews, Synaptic Processes - the role of glial cells, 63, no. 1 (1 May 2010): 11–25. https://doi.org/10.1016/j.brainresrev.2010.02.003.

- Rett, A. '[On a unusual brain atrophy syndrome in hyperammonemia in childhood]'. Wiener Medizinische Wochenschrift (1946) 116, no. 37 (10 September 1966): 723–26.
- Ricciardi, Sara, Elena M. Boggio, Stefano Grosso, Giuseppina Lonetti, Greta Forlani, Gilda Stefanelli, Eleonora Calcagno, et al. 'Reduced AKT/MTOR Signaling and Protein Synthesis Dysregulation in a Rett Syndrome Animal Model'. Human Molecular Genetics 20, no. 6 (15 March 2011): 1182–96. https://doi.org/10.1093/hmg/ddq563.
- Riederer, P., C. Konradi, V. Schay, E. Kienzl, G. Birkmayer, W. Danielczyk, E. Sofic, and M. B. Youdim. 'Localization of MAO-A and MAO-B in Human Brain: A Step in Understanding the Therapeutic Action of L-Deprenyl'. Advances in Neurology 45 (1987): 111–18.
- Riganti, Loredana, Flavia Antonucci, Martina Gabrielli, Ilaria Prada, Paola Giussani, Paola Viani, Flavia Valtorta, Elisabetta Menna, Michela Matteoli, and Claudia Verderio. 'Sphingosine-1-Phosphate (S1P) Impacts Presynaptic Functions by Regulating Synapsin I Localization in the Presynaptic Compartment'. The Journal of Neuroscience: The Official Journal of the Society for Neuroscience 36, no. 16 (20 April 2016): 4624–34. https://doi.org/10.1523/JNEUROSCI.3588-15.2016.
- Risher, W. Christopher, and Cagla Eroglu. 'Thrombospondins as Key Regulators of Synaptogenesis in the Central Nervous System'. Matrix Biology : Journal of the International Society for Matrix Biology 31, no. 3 (April 2012): 170–77. https://doi.org/10.1016/j.matbio.2012.01.004.
- Rodrigues, Deivid C., Dae-Sung Kim, Guang Yang, Kirill Zaslavsky, Kevin C. H. Ha, Rebecca S. F. Mok, P. Joel Ross, et al. 'MECP2 Is Post-Transcriptionally Regulated during Human Neurodevelopment by Combinatorial Action of RNA-Binding Proteins and MiRNAs'. Cell Reports 17, no. 3 (11 2016): 720–34. https://doi.org/10.1016/j.celrep.2016.09.049.
- Roe, Charles R., Lawrence Sweetman, Diane S. Roe, France David, and Henri Brunengraber. 'Treatment of Cardiomyopathy and Rhabdomyolysis in Long-Chain Fat Oxidation Disorders Using an Anaplerotic Odd-Chain Triglyceride'. The Journal of Clinical Investigation 110, no. 2 (15 July 2002): 259–69. https://doi.org/10.1172/JCI15311.
- Ross, Paul D., Jacky Guy, Jim Selfridge, Bushra Kamal, Noha Bahey, K. Elizabeth Tanner, Thomas H. Gillingwater, et al. 'Exclusive Expression of MeCP2 in the Nervous System Distinguishes between Brain and Peripheral Rett Syndrome-like Phenotypes'. Human Molecular Genetics 25, no. 20 (15 October 2016): 4389–4404. https://doi.org/10.1093/hmg/ddw269.
- Rouach, Nathalie, Annette Koulakoff, Veronica Abudara, Klaus Willecke, and Christian Giaume. 'Astroglial Metabolic Networks Sustain Hippocampal Synaptic Transmission'. Science (New York, N.Y.) 322, no. 5907 (5 December 2008): 1551–55. https://doi.org/10.1126/science.1164022.
- Roux, Jean-Christophe, Emmanuelle Dura, Anne Moncla, Josette Mancini, and Laurent Villard. 'Treatment with Desipramine Improves Breathing and Survival in a Mouse Model for Rett Syndrome'. The European Journal of Neuroscience 25, no. 7 (April 2007): 1915–22. https://doi.org/10.1111/j.1460-9568.2007.05466.x.
- Samaco, Rodney C., Caleigh Mandel-Brehm, Hsiao-Tuan Chao, Christopher S. Ward, Sharyl L. Fyffe-Maricich, Jun Ren, Keith Hyland, et al. 'Loss of MeCP2 in Aminergic Neurons Causes Cell-Autonomous Defects in Neurotransmitter Synthesis and Specific Behavioral Abnormalities'. Proceedings of the National Academy of Sciences of the United States of America 106, no. 51 (22 December 2009): 21966–71. https://doi.org/10.1073/pnas.0912257106.
- Sandhoff, Roger, and Konrad Sandhoff. 'Emerging Concepts of Ganglioside Metabolism'. FEBS Letters 592, no. 23 (2018): 3835–64. https://doi.org/10.1002/1873-3468.13114.
- Sato, Koichi, Enkhzol Malchinkhuu, Yuta Horiuchi, Chihiro Mogi, Hideaki Tomura, Masahiko Tosaka, Yuhei Yoshimoto, Atsushi Kuwabara, and Fumikazu Okajima. 'Critical Role of ABCA1 Transporter in Sphingosine 1-Phosphate Release from Astrocytes'. Journal of Neurochemistry 103, no. 6 (December 2007): 2610–19. https://doi.org/10.1111/j.1471-4159.2007.04958.x.

- Saura, J, R Kettler, M Da Prada, J G Richards, and F Hoffmann-La Roche Ltd. 'Quantitative Enzyme Radioautography with 3H-Ro 41-I 049 and 3H-Ro 19-6327 in Vitro: Localization and Abundance of MAO-A and MAO-B in Rat CNS, Peripheral Organs, and Human Brain', n.d., 23.
- Savtchouk, Iaroslav, and Andrea Volterra. 'Gliotransmission: Beyond Black-and-White'. The Journal of Neuroscience: The Official Journal of the Society for Neuroscience 38, no. 1 (03 2018): 14–25. https://doi.org/10.1523/JNEUROSCI.0017-17.2017.
- Schachtele, Scott J., Joe Losh, Michael E. Dailey, and Steven H. Green. 'Spine Formation and Maturation in the Developing Rat Auditory Cortex'. The Journal of Comparative Neurology 519, no. 16 (1 November 2011): 3327–45. https://doi.org/10.1002/cne.22728.
- Schaevitz, L. R., N. B. Gómez, D. P. Zhen, and J. E. Berger-Sweeney. 'MeCP2 R168X Male and Female Mutant Mice Exhibit Rett-like Behavioral Deficits'. Genes, Brain and Behavior 12, no. 7 (2013): 732–40. https://doi.org/10.1111/gbb.12070.
- Schafer, Dorothy P., Emily K. Lehrman, Amanda G. Kautzman, Ryuta Koyama, Alan R. Mardinly, Ryo Yamasaki, Richard M. Ransohoff, Michael E. Greenberg, Ben A. Barres, and Beth Stevens. 'Microglia Sculpt Postnatal Neural Circuits in an Activity and Complement-Dependent Manner'. Neuron 74, no. 4 (24 May 2012): 691–705. https://doi.org/10.1016/j.neuron.2012.03.026.
- Schiweck, Juliane, Britta J. Eickholt, and Kai Murk. 'Important Shapeshifter: Mechanisms Allowing Astrocytes to Respond to the Changing Nervous System During Development, Injury and Disease'. Frontiers in Cellular Neuroscience 12 (21 August 2018). https://doi.org/10.3389/fncel.2018.00261.
- Schönewolf-Greulich, Bitten, Anne-Marie Bisgaard, Morten Dunø, Cathrine Jespersgaard, Mette Rokkjaer, Lars K. Hansen, Eirini Tsoutsou, et al. 'Mosaic MECP2 Variants in Males with Classical Rett Syndrome Features, Including Stereotypical Hand Movements'. Clinical Genetics 95, no. 3 (2019): 403–8. https://doi.org/10.1111/cge.13473.
- Schousboe, Arne, Susanna Scafidi, Lasse K. Bak, Helle S. Waagepetersen, and Mary C. McKenna. 'Glutamate Metabolism in the Brain Focusing on Astrocytes'. In Glutamate and ATP at the Interface of Metabolism and Signaling in the Brain, edited by Vladimir Parpura, Arne Schousboe, and Alexei Verkhratsky, 13–30. Advances in Neurobiology. Cham: Springer International Publishing, 2014. https://doi.org/10.1007/978-3-319-08894-5_2.
- Segatto, Marco, Laura Trapani, Ilenia Di Tunno, Claudia Sticozzi, Giuseppe Valacchi, Joussef Hayek, and Valentina Pallottini. 'Cholesterol Metabolism Is Altered in Rett Syndrome: A Study on Plasma and Primary Cultured Fibroblasts Derived from Patients'. PLOS ONE 9, no. 8 (12 August 2014): e104834. https://doi.org/10.1371/journal.pone.0104834.
- Shahbazian, Mona D., Barbara Antalffy, Dawna L. Armstrong, and Huda Y. Zoghbi. 'Insight into Rett Syndrome: MeCP2 Levels Display Tissue- and Cell-Specific Differences and Correlate with Neuronal Maturation'. Human Molecular Genetics 11, no. 2 (15 January 2002): 115–24. https://doi.org/10.1093/hmg/11.2.115.
- Shahbazian, Mona D., Juan I. Young, Lisa A. Yuva-Paylor, Corinne M. Spencer, Barbara A. Antalffy, Jeffrey L. Noebels, Dawna L. Armstrong, Richard Paylor, and Huda Y. Zoghbi. 'Mice with Truncated MeCP2 Recapitulate Many Rett Syndrome Features and Display Hyperacetylation of Histone H3'. Neuron 35, no. 2 (18 July 2002): 243–54. https://doi.org/10.1016/S0896-6273(02)00768-7.
- Sharma, Kedarlal, Juhi Singh, Emma E. Frost, and Prakash P. Pillai. 'MeCP2 in Central Nervous System Glial Cells: Current Updates'. Acta Neurobiologiae Experimentalis 78, no. 1 (2018): 30–40.
- Shibata, Takashi, Keiko Yamada, Masahiko Watanabe, Kazuhiro Ikenaka, Keiji Wada, Kohichi Tanaka, and Yoshiro Inoue. 'Glutamate Transporter GLAST Is Expressed in the Radial Glia–Astrocyte Lineage of Developing Mouse Spinal Cord'. Journal of Neuroscience 17, no. 23 (1 December 1997): 9212–19. https://doi.org/10.1523/JNEUROSCI.17-23-09212.1997.

- Siddiqui, Tabrez J., and Ann Marie Craig. ‘Synaptic Organizing Complexes’. Current Opinion in Neurobiology 21, no. 1 (February 2011): 132–43. https://doi.org/10.1016/j.conb.2010.08.016.
- Signorini, Cinzia, Claudio De Felice, Silvia Leoncini, Thierry Durand, Jean-Marie Galano, Alessio Cortelazzo, Gloria Zollo, et al. ‘Altered Erythrocyte Membrane Fatty Acid Profile in Typical Rett Syndrome: Effects of Omega-3 Polyunsaturated Fatty Acid Supplementation’. Prostaglandins, Leukotrienes, and Essential Fatty Acids 91, no. 5 (November 2014): 183–93. https://doi.org/10.1016/j.plefa.2014.08.002.
- Simard, Marie, Gregory Arcuino, Takahiro Takano, Qing Song Liu, and Maiken Nedergaard. ‘Signaling at the Gliovascular Interface’. The Journal of Neuroscience: The Official Journal of the Society for Neuroscience 23, no. 27 (8 October 2003): 9254–62.
- Simhal, Anish K., Yi Zuo, Marc M. Perez, Daniel V. Madison, Guillermo Sapiro, and Kristina D. Micheva. ‘Multifaceted Changes in Synaptic Composition and Astrocytic Involvement in a Mouse Model of Fragile X Syndrome’. Scientific Reports 9, no. 1 (25 September 2019): 13855. https://doi.org/10.1038/s41598-019-50240-x.
- Singh, Jasmine, Alka Saxena, John Christodoulou, and David Ravine. ‘MECP2 Genomic Structure and Function: Insights from ENCODE’. Nucleic Acids Research 36, no. 19 (November 2008): 6035–47. https://doi.org/10.1093/nar/gkn591.
- Singh, Sandeep K., Jeff A. Stogsdill, Nisha S. Pulimood, Hayley Dingsdale, Yong Ho Kim, Louis-Jan Pilaz, Il Hwan Kim, et al. ‘Astrocytes Assemble Thalamocortical Synapses by Bridging NRX1α and NL1 via Hevin’. Cell 164, no. 1–2 (14 January 2016): 183–96. https://doi.org/10.1016/j.cell.2015.11.034.
- Sinnett, Sarah E., Ralph D. Hector, Kamal K. E. Gadalla, Clifford Heindel, Daphne Chen, Violeta Zaric, Mark E. S. Bailey, Stuart R. Cobb, and Steven J. Gray. ‘Improved MECP2 Gene Therapy Extends the Survival of MeCP2-Null Mice without Apparent Toxicity after Intracisternal Delivery’. Molecular Therapy - Methods & Clinical Development 5 (16 June 2017): 106–15. https://doi.org/10.1016/j.omtm.2017.04.006.
- Sipione, Simonetta, John Monyror, Danny Galleguillos, Noam Steinberg, and Vaibhavi Kadam. ‘Gangliosides in the Brain: Physiology, Pathophysiology and Therapeutic Applications’. Frontiers in Neuroscience 14 (2020). https://doi.org/10.3389/fnins.2020.572965.
- Skene, Peter J., Robert S. Illingworth, Shaun Webb, Alastair R. W. Kerr, Keith D. James, Daniel J. Turner, Rob Andrews, and Adrian P. Bird. ‘Neuronal MeCP2 Is Expressed at near Histone-Octamer Levels and Globally Alters the Chromatin State’. Molecular Cell 37, no. 4 (26 February 2010): 457–68. https://doi.org/10.1016/j.molcel.2010.01.030.
- Smith, Elizabeth S., Dani R. Smith, Charlotte Eyring, Maria Braileanu, Karen S. Smith-Connor, Yew Ei Tan, Amanda Y. Fowler, et al. ‘Altered Trajectories of Neurodevelopment and Behavior in Mouse Models of Rett Syndrome’. Neurobiology of Learning and Memory 165 (2019): 106962. https://doi.org/10.1016/j.nlm.2018.11.007.
- Smitha Sripathy et al., ‘Screen for Reactivation of MeCP2 on the Inactive X Chromosome Identifies the BMP/TGF-β Superfamily as a Regulator of XIST Expression’, Proceedings of the National Academy of Sciences of the United States of America 114, no. 7 (14 2017): 1619–24, https://doi.org/10.1073/pnas.1621356114.
- Smrt, Richard D., Julialea Eaves-Egenes, Basam Z. Barkho, Nicholas J. Santistevan, Chunmei Zhao, James B. Aimone, Fred H. Gage, and Xinyu Zhao. ‘Mecp2 Deficiency Leads to Delayed Maturation and Altered Gene Expression in Hippocampal Neurons’. Neurobiology of Disease 27, no. 1 (July 2007): 77–89. https://doi.org/10.1016/j.nbd.2007.04.005.
- Sonnino, Sandro, and Alessandro Prinetti. ‘The Role of Sphingolipids in Neuronal Plasticity of the Brain’. Journal of Neurochemistry 137, no. 4 (1 May 2016): 485–88. https://doi.org/10.1111/jnc.13589.

- Stahlberg, Markus A., Sebastian Kügler, and Camin Dean. ‘Visualizing BDNF Cell-to-Cell Transfer Reveals Astrocytes Are the Primary Recipient of Neuronal BDNF’. BioRxiv, 30 January 2018, 255935. https://doi.org/10.1101/255935.
- Stearns, N. A., L. R. Schaevitz, H. Bowling, N. Nag, U. V. Berger, and J. Berger-Sweeney. ‘Behavioral and Anatomical Abnormalities in Mecp2 Mutant Mice: A Model for Rett Syndrome’. Neuroscience 146, no. 3 (25 May 2007): 907–21. https://doi.org/10.1016/j.neuroscience.2007.02.009.
- Stefanelli, Gilda, Anna Gandaglia, Mario Costa, Manjinder S. Cheema, Daniele Di Marino, Isabella Barbiero, Charlotte Kilstrup-Nielsen, Juan Ausió, and Nicoletta Landsberger. ‘Brain Phosphorylation of MeCP2 at Serine 164 Is Developmentally Regulated and Globally Alters Its Chromatin Association’. Scientific Reports 6 (21 2016): 28295. https://doi.org/10.1038/srep28295.
- Steiner, Johann, Hans-Gert Bernstein, Hendrik Bielau, Annika Berndt, Ralf Brisch, Christian Mawrin, Gerburg Keilhoff, and Bernhard Bogerts. ‘Evidence for a Wide Extra-Astrocytic Distribution of S100B in Human Brain’. BMC Neuroscience 8 (2 January 2007): 2. https://doi.org/10.1186/1471-2202-8-2.
- Stellwagen, David, and Robert C. Malenka. ‘Synaptic Scaling Mediated by Glial TNF-Alpha’. Nature 440, no. 7087 (20 April 2006): 1054–59. https://doi.org/10.1038/nature04671.
- Stellwagen, David, Eric C. Beattie, Jae Y. Seo, and Robert C. Malenka. ‘Differential Regulation of AMPA Receptor and GABA Receptor Trafficking by Tumor Necrosis Factor-Alpha’. The Journal of Neuroscience: The Official Journal of the Society for Neuroscience 25, no. 12 (23 March 2005): 3219–28. https://doi.org/10.1523/JNEUROSCI.4486-04.2005.
- Storck, T., S. Schulte, K. Hofmann, and W. Stoffel. ‘Structure, Expression, and Functional Analysis of a Na(+)-Dependent Glutamate/Aspartate Transporter from Rat Brain’. Proceedings of the National Academy of Sciences 89, no. 22 (15 November 1992): 10955–59. https://doi.org/10.1073/pnas.89.22.10955.
- Stroud, Hume, Susan C. Su, Sinisa Hrvatin, Alexander W. Greben, William Renthal, Lisa D. Boxer, M. Aurel Nagy, et al. ‘Early-Life Gene Expression in Neurons Modulates Lasting Epigenetic States’. Cell 171, no. 5 (16 November 2017): 1151-1164.e16. https://doi.org/10.1016/j.cell.2017.09.047.
- Studer, F. E., D. E. Fedele, A. Marowsky, C. Schwerdel, K. Wernli, K. Vogt, J. M. Fritschy, and D. Boison. ‘Shift of Adenosine Kinase Expression from Neurons to Astrocytes during Postnatal Development Suggests Dual Functionality of the Enzyme’. Neuroscience 142, no. 1 (29 September 2006): 125–37. https://doi.org/10.1016/j.neuroscience.2006.06.016.
- Sugino, Ken, Chris M. Hempel, Benjamin W. Okaty, Hannah A. Arnson, Saori Kato, Vardhan S. Dani, and Sacha B. Nelson. ‘Cell-Type-Specific Repression by Methyl-CpG-Binding Protein 2 Is Biased toward Long Genes’. The Journal of Neuroscience: The Official Journal of the Society for Neuroscience 34, no. 38 (17 September 2014): 12877–83. https://doi.org/10.1523/JNEUROSCI.2674-14.2014.
- Sultan, Sébastien, Liyi Li, Jonathan Moss, Francesco Petrelli, Frédéric Cassé, Elias Gebara, Jan Lopatar, et al. ‘Synaptic Integration of Adult-Born Hippocampal Neurons Is Locally Controlled by Astrocytes’. Neuron 88, no. 5 (2 December 2015): 957–72. https://doi.org/10.1016/j.neuron.2015.10.037.
- Sultana, S., S. W. Sernett, R. M. Bellin, R. M. Robson, and O. Skalli. ‘Intermediate Filament Protein Synemin Is Transiently Expressed in a Subset of Astrocytes during Development’. Glia 30, no. 2 (April 2000): 143–53. https://doi.org/10.1002/(sici)1098-1136(200004)30:2<143::aid-glia4>3.0.co;2-z.
- Sun, Yi E., and Hao Wu. ‘The Ups and Downs of BDNF in Rett Syndrome’. Neuron 49, no. 3 (2 February 2006): 321–23. https://doi.org/10.1016/j.neuron.2006.01.014.

- Suzuki, Akinobu, Sarah A. Stern, Ozlem Bozdagi, George W. Huntley, Ruth H. Walker, Pierre J. Magistretti, and Cristina M. Alberini. 'Astrocyte-Neuron Lactate Transport Is Required for Long-Term Memory Formation'. Cell 144, no. 5 (4 March 2011): 810–23. https://doi.org/10.1016/j.cell.2011.02.018.
- Suzuki, Ryusuke, Jun Watanabe, Satoru Arata, Hisayuki Funahashi, Sakae Kikuyama, and Seiji Shioda. 'A Transgenic Mouse Model for the Detailed Morphological Study of Astrocytes'. Neuroscience Research 47, no. 4 (December 2003): 451–54. https://doi.org/10.1016/j.neures.2003.08.008.
- Szulwach, Keith E., Xuekun Li, Richard D. Smrt, Yujing Li, Yuping Luo, Li Lin, Nicholas J. Santistevan, Wendi Li, Xinyu Zhao, and Peng Jin. 'Cross Talk between MicroRNA and Epigenetic Regulation in Adult Neurogenesis'. Journal of Cell Biology 189, no. 1 (5 April 2010): 127–41. https://doi.org/10.1083/jcb.200908151.
- Takano, Tetsuya, John T. Wallace, Katherine T. Baldwin, Alicia M. Purkey, Akiyoshi Uezu, Jamie L. Courtland, Erik J. Soderblom, et al. 'Chemico-Genetic Discovery of Astrocytic Control of Inhibition in Vivo'. Nature 588, no. 7837 (December 2020): 296–302. https://doi.org/10.1038/s41586-020-2926-0.
- Takouda, Jun, Sayako KATADA, and Kinichi NAKASHIMA. 'Emerging Mechanisms Underlying Astrogenesis in the Developing Mammalian Brain'. Proceedings of the Japan Academy. Series B, Physical and Biological Sciences 93, no. 6 (9 June 2017): 386–98. https://doi.org/10.2183/pjab.93.024.
- Taneja, Praveen, Michael Ogier, Gabriel Brooks-Harris, Danielle A. Schmid, David M. Katz, and Sacha B. Nelson. 'Pathophysiology of Locus Ceruleus Neurons in a Mouse Model of Rett Syndrome'. The Journal of Neuroscience: The Official Journal of the Society for Neuroscience 29, no. 39 (30 September 2009): 12187–95. https://doi.org/10.1523/JNEUROSCI.3156-09.2009.
- Tang, F., S. Lane, A. Korsak, J. F. R. Paton, A. V. Gourine, S. Kasparov, and A. G. Teschemacher. 'Lactate-Mediated Glia-Neuronal Signalling in the Mammalian Brain'. Nature Communications 5 (2014): 3284. https://doi.org/10.1038/ncomms4284.
- Tavares, Gabriela, Manuella Martins, Joana Sofia Correia, Vanessa Morais Sardinha, Sónia Guerra-Gomes, Sofia Pereira das Neves, Fernanda Marques, Nuno Sousa, and João Filipe Oliveira. 'Employing an Open-Source Tool to Assess Astrocyte Tridimensional Structure'. Brain Structure & Function 222, no. 4 (May 2017): 1989–99. https://doi.org/10.1007/s00429-016-1316-8.
- Tchieu, Jason, Elizabeth L. Calder, Sudha R. Guttikonda, Eveline M. Gutzwiller, Kelly A. Aromolaran, Julius A. Steinbeck, Peter A. Goldstein, and Lorenz Studer. 'NFIA Is a Gliogenic Switch Enabling Rapid Derivation of Functional Human Astrocytes from Pluripotent Stem Cells'. Nature Biotechnology 37, no. 3 (2019): 267–75. https://doi.org/10.1038/s41587-019-0035-0.
- Tecalco-Cruz, Angeles C., Diana G. Ríos-López, Genaro Vázquez-Victorio, Reyna E. Rosales-Alvarez, and Marina Macías-Silva. 'Transcriptional Cofactors Ski and SnoN Are Major Regulators of the TGF-β/Smad Signaling Pathway in Health and Disease'. Signal Transduction and Targeted Therapy 3, no. 1 (8 June 2018): 1–15. https://doi.org/10.1038/s41392-018-0015-8.
- Theis, Martin, Goran Söhl, Jürgen Eiberger, and Klaus Willecke. 'Emerging Complexities in Identity and Function of Glial Connexins'. Trends in Neurosciences 28, no. 4 (April 2005): 188–95. https://doi.org/10.1016/j.tins.2005.02.006.
- Thi Thanh Huong Le et al., 'Efficient and Precise CRISPR/Cas9-Mediated MECP2 Modifications in Human-Induced Pluripotent Stem Cells', Frontiers in Genetics 10 (2 July 2019), https://doi.org/10.3389/fgene.2019.00625.
- Tillotson, Rebekah, Jim Selfridge, Martha V. Koerner, Kamal K. E. Gadalla, Jacky Guy, Dina De Sousa, Ralph D. Hector, Stuart R. Cobb, and Adrian Bird. 'Radically Truncated MeCP2 Rescues

Rett Syndrome-like Neurological Defects'. Nature 550, no. 7676 (October 2017): 398–401. https://doi.org/10.1038/nature24058.

- Tropea, Daniela, Emanuela Giacometti, Nathan R. Wilson, Caroline Beard, Cortina McCurry, Dong Dong Fu, Ruth Flannery, Rudolf Jaenisch, and Mriganka Sur. 'Partial Reversal of Rett Syndrome-like Symptoms in MeCP2 Mutant Mice'. Proceedings of the National Academy of Sciences of the United States of America 106, no. 6 (10 February 2009): 2029–34. https://doi.org/10.1073/pnas.0812394106.
- Tudor, Matthew, Schahram Akbarian, Richard Z. Chen, and Rudolf Jaenisch. 'Transcriptional Profiling of a Mouse Model for Rett Syndrome Reveals Subtle Transcriptional Changes in the Brain'. Proceedings of the National Academy of Sciences of the United States of America 99, no. 24 (26 November 2002): 15536–41. https://doi.org/10.1073/pnas.242566899.
- Turovsky, Egor, Anastassios Karagiannis, Ana Paula Abdala, and Alexander V. Gourine. 'Impaired CO2 Sensitivity of Astrocytes in a Mouse Model of Rett Syndrome'. The Journal of Physiology 593, no. 14 (15 July 2015): 3159–68. https://doi.org/10.1113/JP270369.
- Tzingounis, Anastassios V., and Jacques I. Wadiche. 'Glutamate Transporters: Confining Runaway Excitation by Shaping Synaptic Transmission'. Nature Reviews Neuroscience 8, no. 12 (December 2007): 935–47. https://doi.org/10.1038/nrn2274.
- Uemura, Atsumi, Takumi Takizawa, Wataru Ochiai, Makoto Yanagisawa, Kinichi Nakashima, and Tetsuya Taga. 'Cardiotrophin-Like Cytokine induces astrocyte differentiation of fetal neuroepithelial cells via activation of STAT3'. Cytokine 18, no. 1 (1 April 2002): 1–7. https://doi.org/10.1006/cyto.2002.1006.
- Ullian, E. M., S. K. Sapperstein, K. S. Christopherson, and B. A. Barres. 'Control of Synapse Number by Glia'. Science (New York, N.Y.) 291, no. 5504 (26 January 2001): 657–61. https://doi.org/10.1126/science.291.5504.657.
- Ure, Kerstin, Hui Lu, Wei Wang, Aya Ito-Ishida, Zhenyu Wu, Ling-Jie He, Yehezkel Sztainberg, Wu Chen, Jianrong Tang, and Huda Y. Zoghbi. 'Restoration of Mecp2 Expression in GABAergic Neurons Is Sufficient to Rescue Multiple Disease Features in a Mouse Model of Rett Syndrome'. ELife 5 (21 2016). https://doi.org/10.7554/eLife.14198.
- Uyeda, C. T., L. F. Eng, and A. Bignami. 'Immunological Study of the Glial Fibrillary Acidic Protein'. Brain Research 37, no. 1 (11 February 1972): 81–89. https://doi.org/10.1016/0006-8993(72)90347-2.
- Vacca, Marcella, Floriana Della Ragione, Francesco Scalabrì, and Maurizio D'Esposito. 'X Inactivation and Reactivation in X-Linked Diseases'. Seminars in Cell & Developmental Biology 56 (2016): 78–87. https://doi.org/10.1016/j.semcdb.2016.03.009.
- Vacca, Marcella, Kumar Parijat Tripathi, Luisa Speranza, Riccardo Aiese Cigliano, Francesco Scalabrì, Federico Marracino, Michele Madonna, et al. 'Effects of Mecp2 Loss of Function in Embryonic Cortical Neurons: A Bioinformatics Strategy to Sort out Non-Neuronal Cells Variability from Transcriptome Profiling'. BMC Bioinformatics 17 Suppl 2 (20 January 2016): 14. https://doi.org/10.1186/s12859-015-0859-7.
- Valente, Enza Maria, Rasim O. Rosti, Elizabeth Gibbs, and Joseph G. Gleeson. 'Primary Cilia in Neurodevelopmental Disorders'. Nature Reviews. Neurology 10, no. 1 (January 2014): 27–36. https://doi.org/10.1038/nrneurol.2013.247.
- Valerie Matagne et al., 'A Codon-Optimized Mecp2 Transgene Corrects Breathing Deficits and Improves Survival in a Mouse Model of Rett Syndrome', Neurobiology of Disease 99 (1 March 2017): 1–11, https://doi.org/10.1016/j.nbd.2016.12.009.
- Van Brocklyn, James R., and Joseph B. Williams. 'The Control of the Balance between Ceramide and Sphingosine-1-Phosphate by Sphingosine Kinase: Oxidative Stress and the Seesaw of Cell

Survival and Death'. Comparative Biochemistry and Physiology. Part B, Biochemistry & Molecular Biology 163, no. 1 (September 2012): 26–36. https://doi.org/10.1016/j.cbpb.2012.05.006.

- Van Esch, Hilde, Marijke Bauters, Jaakko Ignatius, Mieke Jansen, Martine Raynaud, Karen Hollanders, Dorien Lugtenberg, et al. 'Duplication of the MECP2 Region Is a Frequent Cause of Severe Mental Retardation and Progressive Neurological Symptoms in Males'. American Journal of Human Genetics 77, no. 3 (September 2005): 442–53. https://doi.org/10.1086/444549.
- Vashi, Neeti, and Monica J. Justice. 'Treating Rett Syndrome: From Mouse Models to Human Therapies'. Mammalian Genome 30, no. 5 (1 June 2019): 90–110. https://doi.org/10.1007/s00335-019-09793-5.
- Vaughn, James E., and Alan Peters. 'Electron Microscopy of the Early Postnatal Development of Fibrous Astrocytes'. American Journal of Anatomy 121, no. 1 (1967): 131–51. https://doi.org/10.1002/aja.1001210109.
- Verkhratsky, Alexei, and Maiken Nedergaard. 'Physiology of Astroglia'. Physiological Reviews 98, no. 1 (1 January 2018): 239–389. https://doi.org/10.1152/physrev.00042.2016.
- Verkhratsky, Alexei, and Maiken Nedergaard. 'The Homeostatic Astroglia Emerges from Evolutionary Specialization of Neural Cells'. Philosophical Transactions of the Royal Society B: Biological Sciences 371, no. 1700 (5 August 2016): 20150428. https://doi.org/10.1098/rstb.2015.0428.
- Volterra, Andrea, and Jacopo Meldolesi. 'Astrocytes, from Brain Glue to Communication Elements: The Revolution Continues'. Nature Reviews. Neuroscience 6, no. 8 (August 2005): 626–40. https://doi.org/10.1038/nrn1722.
- Wade, Paul A. 'Dynamic Regulation of DNA Methylation Coupled Transcriptional Repression: BDNF Regulation by MeCP2'. BioEssays: News and Reviews in Molecular, Cellular and Developmental Biology 26, no. 3 (March 2004): 217–20. https://doi.org/10.1002/bies.20018.
- Waller, Rachel, M. Nicola Woodroofe, Stephen B. Wharton, Paul G. Ince, Simona Francese, Paul R. Heath, Alex Cudzich-Madry, et al. 'Gene Expression Profiling of the Astrocyte Transcriptome in Multiple Sclerosis Normal Appearing White Matter Reveals a Neuroprotective Role'. Journal of Neuroimmunology 299 (15 October 2016): 139–46. https://doi.org/10.1016/j.jneuroim.2016.09.010.
- Walz, W. 'Controversy Surrounding the Existence of Discrete Functional Classes of Astrocytes in Adult Gray Matter'. Glia 31, no. 2 (August 2000): 95–103. https://doi.org/10.1002/1098-1136(200008)31:2<95::aid-glia10>3.0.co;2-6.
- Walz, Wolfgang, and Melody K Lang. 'Immunocytochemical Evidence for a Distinct GFAP-Negative Subpopulation of Astrocytes in the Adult Rat Hippocampus'. Neuroscience Letters 257, no. 3 (4 December 1998): 127–30. https://doi.org/10.1016/S0304-3940(98)00813-1.
- Wang, Hong, Shyue-an Chan, Michael Ogier, David Hellard, Qifang Wang, Corey Smith, and David M. Katz. 'Dysregulation of Brain-Derived Neurotrophic Factor Expression and Neurosecretory Function in Mecp2 Null Mice'. The Journal of Neuroscience: The Official Journal of the Society for Neuroscience 26, no. 42 (18 October 2006): 10911–15. https://doi.org/10.1523/JNEUROSCI.1810-06.2006.
- Wang, I-Ting J, Arith-Ruth S Reyes, and Zhaolan Zhou. 'Neuronal Morphology in MeCP2 Mouse Models Is Intrinsically Variable and Depends on Age, Cell Type, and Mecp2 Mutation'. Neurobiology of Disease 58 (October 2013): 3–12. https://doi.org/10.1016/j.nbd.2013.04.020.
- Wang, Jiaping, Qingping Zhang, Yan Chen, Shujie Yu, Xiru Wu, and Xinhua Bao. 'Rett and Rett-like Syndrome: Expanding the Genetic Spectrum to KIF1A and GRIN1 Gene'. Molecular Genetics & Genomic Medicine 7, no. 11 (11 September 2019). https://doi.org/10.1002/mgg3.968.
- Wilczynska, Katarzyna M., Sandeep K. Singh, Bret Adams, Lauren Bryan, Raj R. Rao, Kristoffer Valerie, Sarah Wright, Irene Griswold-Prenner, and Tomasz Kordula. 'Nuclear Factor I Isoforms

Regulate Gene Expression During the Differentiation of Human Neural Progenitors to Astrocytes'. STEM CELLS 27, no. 5 (2009): 1173–81. https://doi.org/10.1002/stem.35.

- Williams, Emily Cunningham, Xiaofen Zhong, Ahmed Mohamed, Ronghui Li, Yan Liu, Qiping Dong, Gene E. Ananiev, et al. 'Mutant Astrocytes Differentiated from Rett Syndrome Patients-Specific IPSCs Have Adverse Effects on Wild-Type Neurons'. Human Molecular Genetics 23, no. 11 (1 June 2014): 2968–80. https://doi.org/10.1093/hmg/ddu008.
- Wit, Joris de, and Anirvan Ghosh. 'Specification of Synaptic Connectivity by Cell Surface Interactions'. Nature Reviews. Neuroscience 17, no. 1 (January 2016): 22–35. https://doi.org/10.1038/nrn.2015.3.
- Wit, Nienke M. de, Sandra den Hoedt, Pilar Martinez-Martinez, Annemieke J. Rozemuller, Monique T. Mulder, and Helga E. de Vries. 'Astrocytic Ceramide as Possible Indicator of Neuroinflammation'. Journal of Neuroinflammation 16, no. 1 (25 February 2019): 48. https://doi.org/10.1186/s12974-019-1436-1.
- Witcher, Mark R., Sergei A. Kirov, and Kristen M. Harris. 'Plasticity of Perisynaptic Astroglia during Synaptogenesis in the Mature Rat Hippocampus'. Glia 55, no. 1 (2007): 13–23. https://doi.org/10.1002/glia.20415.
- Wonders, Carl P., and Stewart A. Anderson. 'The Origin and Specification of Cortical Interneurons'. Nature Reviews. Neuroscience 7, no. 9 (September 2006): 687–96. https://doi.org/10.1038/nrn1954.
- Wu, Yang, Weiwei Zhong, Ningren Cui, Christopher M. Johnson, Hao Xing, Shuang Zhang, and Chun Jiang. 'Characterization of Rett Syndrome-like Phenotypes in Mecp2-Knockout Rats'. Journal of Neurodevelopmental Disorders 8, no. 1 (16 June 2016): 23. https://doi.org/10.1186/s11689-016-9156-7.
- Wu, Yi, Sukhwinder Singh, Maria-Magdalena Georgescu, and Raymond B. Birge. 'A Role for Mer Tyrosine Kinase in Alphavbeta5 Integrin-Mediated Phagocytosis of Apoptotic Cells'. Journal of Cell Science 118, no. Pt 3 (1 February 2005): 539–53. https://doi.org/10.1242/jcs.01632.
- Xin Xu, Alan P. Kozikowski, and Lucas Pozzo-Miller, 'A Selective Histone Deacetylase-6 Inhibitor Improves BDNF Trafficking in Hippocampal Neurons from Mecp2 Knockout Mice: Implications for Rett Syndrome', Frontiers in Cellular Neuroscience 8 (2014): 68, https://doi.org/10.3389/fncel.2014.00068.
- Xing, LingYan, Tuo Yang, ShuSen Cui, and Gang Chen. 'Connexin Hemichannels in Astrocytes: Role in CNS Disorders'. Frontiers in Molecular Neuroscience 12 (2019). https://doi.org/10.3389/fnmol.2019.00023.
- Xu, Junyu, Nan Xiao, and Jun Xia. 'Thrombospondin 1 Accelerates Synaptogenesis in Hippocampal Neurons through Neuroligin 1'. Nature Neuroscience 13, no. 1 (January 2010): 22–24. https://doi.org/10.1038/nn.2459.
- Xu, Xin, Eric C. Miller, and Lucas Pozzo-Miller. 'Dendritic Spine Dysgenesis in Rett Syndrome'. Frontiers in Neuroanatomy 8 (2014): 97. https://doi.org/10.3389/fnana.2014.00097.
- Xu-Friedman MA, Harris KM, Regehr WG. Three-dimensional comparison of ultrastructural characteristics at depressing and facilitating synapses onto cerebellar Purkinje cells. *J Neurosci* 21: 6666–6672, 2001.
- Yang, Jiangyan, Evelyne Ruchti, Jean-Marie Petit, Pascal Jourdain, Gabriele Grenningloh, Igor Allaman, and Pierre J. Magistretti. 'Lactate Promotes Plasticity Gene Expression by Potentiating NMDA Signaling in Neurons'. Proceedings of the National Academy of Sciences 111, no. 33 (19 August 2014): 12228–33. https://doi.org/10.1073/pnas.1322912111.
- Yang, Yongjie, Svetlana Vidensky, Lin Jin, Chunfa Jie, Ileana Lorenzini, Miriam Frankl, and Jeffrey D. Rothstein. 'Molecular Comparison of GLT1+ and ALDH1L1+ Astrocytes in Vivo in Astroglial Reporter Mice'. Glia 59, no. 2 (2011): 200–207. https://doi.org/10.1002/glia.21089.

- Yasui, Dag H., Huichun Xu, Keith W. Dunaway, Janine M. Lasalle, Lee-Way Jin, and Izumi Maezawa. 'MeCP2 Modulates Gene Expression Pathways in Astrocytes'. Molecular Autism 4, no. 1 (25 January 2013): 3. https://doi.org/10.1186/2040-2392-4-3.
- Yasui, Tetsuro, Naohiro Uezono, Hideyuki Nakashima, Hirofumi Noguchi, Taito Matsuda, Tomoko Noda-Andoh, Hideyuki Okano, and Kinichi Nakashima. 'Hypoxia Epigenetically Confers Astrocytic Differentiation Potential on Human Pluripotent Cell-Derived Neural Precursor Cells'. Stem Cell Reports 8, no. 6 (6 June 2017): 1743–56. https://doi.org/10.1016/j.stemcr.2017.05.001.
- Young, Juan I., Eugene P. Hong, John C. Castle, Juan Crespo-Barreto, Aaron B. Bowman, Matthew F. Rose, Dongcheul Kang, et al. 'Regulation of RNA Splicing by the Methylation-Dependent Transcriptional Repressor Methyl-CpG Binding Protein 2'. Proceedings of the National Academy of Sciences 102, no. 49 (6 December 2005): 17551–58. https://doi.org/10.1073/pnas.0507856102.
- Yu, Xiaomeng, Nan Lu, and Zheng Zhou. 'Phagocytic Receptor CED-1 Initiates a Signaling Pathway for Degrading Engulfed Apoptotic Cells'. PLOS Biology 6, no. 3 (18 March 2008): e61. https://doi.org/10.1371/journal.pbio.0060061.
- Yu, Xinzhu, Anna M. W. Taylor, Jun Nagai, Peyman Golshani, Christopher J. Evans, Giovanni Coppola, and Baljit S. Khakh. 'Reducing Astrocyte Calcium Signaling In Vivo Alters Striatal Microcircuits and Causes Repetitive Behavior'. Neuron 99, no. 6 (19 2018): 1170-1187.e9. https://doi.org/10.1016/j.neuron.2018.08.015.
- Yu, Xinzhu, Jun Nagai, and Baljit S. Khakh. 'Improved Tools to Study Astrocytes'. Nature Reviews Neuroscience 21, no. 3 (March 2020): 121–38. https://doi.org/10.1038/s41583-020-0264-8.
- Zachariah, Robby M., Carl O. Olson, Chinelo Ezeonwuka, and Mojgan Rastegar. 'Novel MeCP2 Isoform-Specific Antibody Reveals the Endogenous MeCP2E1 Expression in Murine Brain, Primary Neurons and Astrocytes'. PloS One 7, no. 11 (2012): e49763. https://doi.org/10.1371/journal.pone.0049763.
- Zachariah, Robby Mathew, and Mojgan Rastegar. 'Linking Epigenetics to Human Disease and Rett Syndrome: The Emerging Novel and Challenging Concepts in MeCP2 Research'. Neural Plasticity 2012 (2012): 415825. https://doi.org/10.1155/2012/415825.
- Zanella, Sébastien, Saida Mebarek, Anne-Marie Lajard, Nathalie Picard, Mathias Dutschmann, and Gérard Hilaire. 'Oral Treatment with Desipramine Improves Breathing and Life Span in Rett Syndrome Mouse Model'. Respiratory Physiology & Neurobiology 160, no. 1 (1 January 2008): 116–21. https://doi.org/10.1016/j.resp.2007.08.009.
- Zeisel, Amit, Ana B. Muñoz-Manchado, Simone Codeluppi, Peter Lönnerberg, Gioele La Manno, Anna Juréus, Sueli Marques, et al. 'Cell Types in the Mouse Cortex and Hippocampus Revealed by Single-Cell RNA-Seq'. Science 347, no. 6226 (6 March 2015): 1138–42. https://doi.org/10.1126/science.aaa1934.
- Zeug, Andre, Franziska E. Müller, Stefanie Anders, Michel K. Herde, Daniel Minge, Evgeni Ponimaskin, and Christian Henneberger. 'Control of Astrocyte Morphology by Rho GTPases'. Brain Research Bulletin 136 (2018): 44–53. https://doi.org/10.1016/j.brainresbull.2017.05.003.
- Zhang, Xiaoli, Junda Su, Ningren Cui, Hongyu Gai, Zhongying Wu, and Chun Jiang. 'The Disruption of Central CO2 Chemosensitivity in a Mouse Model of Rett Syndrome'. American Journal of Physiology. Cell Physiology 301, no. 3 (September 2011): C729-738. https://doi.org/10.1152/ajpcell.00334.2010.
- Zhang, Ye, Kenian Chen, Steven A. Sloan, Mariko L. Bennett, Anja R. Scholze, Sean O'Keeffe, Hemali P. Phatnani, et al. 'An RNA-Sequencing Transcriptome and Splicing Database of Glia, Neurons, and Vascular Cells of the Cerebral Cortex'. The Journal of Neuroscience 34, no. 36 (3 September 2014): 11929–47. https://doi.org/10.1523/JNEUROSCI.1860-14.2014.

- Zhang, Yunjia, Mengmeng Chen, Zilong Qiu, Keping Hu, Warren McGee, Xiaoping Chen, Jianghong Liu, Li Zhu, and Jane Y. Wu. 'MiR-130a Regulates Neurite Outgrowth and Dendritic Spine Density by Targeting MeCP2'. Protein & Cell 7, no. 7 (2016): 489–500. https://doi.org/10.1007/s13238-016-0272-7.
- Zhou, Bin, Yun-Xia Zuo, and Ruo-Tian Jiang. 'Astrocyte Morphology: Diversity, Plasticity, and Role in Neurological Diseases'. CNS Neuroscience & Therapeutics 25, no. 6 (2019): 665–73. https://doi.org/10.1111/cns.13123.
- Zhou, Zhaolan, Elizabeth J. Hong, Sonia Cohen, Wen-Ning Zhao, Hsin-Yi Henry Ho, Lauren Schmidt, Wen G. Chen, et al. 'Brain-Specific Phosphorylation of MeCP2 Regulates Activity-Dependent Bdnf Transcription, Dendritic Growth, and Spine Maturation'. Neuron 52, no. 2 (19 October 2006): 255–69. https://doi.org/10.1016/j.neuron.2006.09.037.
- Zhou, Zheng, Erika Hartwieg, and H. Robert Horvitz. 'CED-1 Is a Transmembrane Receptor That Mediates Cell Corpse Engulfment in C. Elegans'. Cell 104, no. 1 (12 January 2001): 43–56. https://doi.org/10.1016/S0092-8674(01)00190-8.
- Zoghbi, Huda Y. 'Postnatal Neurodevelopmental Disorders: Meeting at the Synapse?' Science (New York, N.Y.) 302, no. 5646 (31 October 2003): 826–30. https://doi.org/10.1126/science.1089071.
- Zonta, Micaela, Annalisa Sebelin, Sara Gobbo, Tommaso Fellin, Tullio Pozzan, and Giorgio Carmignoto. 'Glutamate-Mediated Cytosolic Calcium Oscillations Regulate a Pulsatile Prostaglandin Release from Cultured Rat Astrocytes'. The Journal of Physiology 553, no. Pt 2 (1 December 2003): 407–14. https://doi.org/10.1113/jphysiol.2003.046706.
- Zorec, R., A. Verkhratsky, J. J. Rodríguez, and V. Parpura. 'Astrocytic Vesicles and Gliotransmitters: Slowness of Vesicular Release and Synaptobrevin2-Laden Vesicle Nanoarchitecture'. Neuroscience 323 (26 May 2016): 67–75. https://doi.org/10.1016/j.neuroscience.2015.02.033.